Geomorphology, Stratigraphy, and Paleohydrology of the Aeolis Dorsa region, Mars, with Insights from Modern and Ancient Terrestrial Analogs

A Dissertation Presented for the
Doctor of Philosophy
Degree
The University of Tennessee, Knoxville

Robert Eric Jacobsen II
December 2016

Copyright © 2016 by Robert Eric Jacobsen II
All rights reserved.

Dedication

How can I dedicate what has been prepared for me by my family, my friends, and my God? I offer this back to them with gratitude.

Acknowledgements

I find these words wanting and I attribute this wanting to the dissertation before you. This dissertation stands in the gap between planets, times, and research communities. It is liminal. Please know that this dissertation would not be possible without the individuals and organizations mentioned here and many others. This dissertation would have been too much for me to bear alone and much less satisfying on my own.

First, I'd like to acknowledge my advisor and friend Professor Devon Burr. Devon's gifts include, but are not limited to, patience, enthusiasm, and steadfastness. These gifts shepherded me here and shaped me into the geomorphologist I am today. I couldn't have done this without you, Devon. I'm so happy to share this with you and to know that we'll get to share this with others.

I am very grateful for Professor Chris Fedo. Chris sat me down in the middle of my third year, a time when I was struggling with major changes to my dissertation committee. Chris saw where I wanted to go, into the gap between Earth and Mars, ancient and modern, geomorphology and sedimentology. He directed me to Earth, and the works of Andrew Miall, to complement my knowledge of Martian fluvial geomorphology. Lively and sometimes heated discussions with Chris changed the way I think about Mars and the science of geology.

Many thanks are given to Professors Anna Szynkiewicz and Liem Tran for their interest and input throughout the course of this dissertation. Professors Jeff Moersch and Carol Harden were also helpful. Thanks to Professors Joshua Emery, Linda Kah, and Colin Sumrall for their interest and thought-provoking questions. I extend (warm Californian) thanks to Professor Sally Horn for all her encouragement and enthusiasm.

Although I applied to the University of Tennessee to study planetary geomorphology, I came to Knoxville because of the community of students in the Earth and Planetary Sciences Department. There was a family in EPS when I visited and I have been blessed to be part of that family. Sarah Drummond, Andrea Hughes, Kelsey Singer, Matt Chojnacki, Geoff Gilleaudeau, Brian Balta, and Christina Viviano-Beck were among the welcoming faces that invited me to Knoxville. I then joined the ranks with Chloe Beddingfield, Latisha Brengman, Richard Cartwright, Sheri Singerling, Arya Udry, and closely followed by Mike Lucas and Tim Diedesch. You guys are the best! Later came Nicole Lunning, Chris Tate, Derek Street, Kati and Tyler Ayers, Michael Gragg, Eric Maclennan, Ashley Manning-Berg, Rose Borden, Jason Muhlbauer, Emily Nield, Samantha Peel, Keenan Golder, Michael Phillips, Miles Henderson, Sarah Sheffield, Cameron Hughes, and Rachel Kronyak. You all made this worth it!

Graduate Teaching Assistantships from the Earth and Planetary Sciences Department, Research Assistantships from the Planetary Geosciences Institute and from the Tennessee Space Grant Consortium also made this dissertation possible. Funding for assistantships and travel to conferences was provided by NASA's Mars Fundamental Research Program and Mars Data Analysis Program, Planetary Geology Division of the Geological Society of America, the University of Tennessee College of Arts and Sciences, and the Earth and Planetary Sciences Department Discretionary Fund.

Many thanks are due to Corey Fortezzo, Trent Hare, and Jim Skinner of the USGS Astrogeology Branch for producing image data, answering questions about planetary geologic mapping, and their warm collegiality. I thank Ross Irwin, Laura Kerber, Edwin Kite, Ken Tanaka, Jim Zimbelman, Rebecca Williams, and the planetary geologic mapping community for insightful discussions throughout the course of this dissertation. I also thank Brett Eaton, Kory Konsoer, Caleb Fassett, and Tim Goudge for helpful discussions regarding the second chapter of this dissertation.

Outside of the Earth and Planetary Sciences Department, I have been welcomed into a family of students from around the world. My heart is full of thanks for Bridges International, Michael Henderson, Emily Ackerson, Jonathan and Li Yin Goode, Ba-Er Baer, Nan Chen, CeCe Ging, Terry and Rosann Douglass, John Wood, Mark and Janet Cockrum, Meg Cockrum, Justin Kaewnopparat, Akin Ola, Steven Shen, Nate Henry, Leah Henry, and Josie Henry, Ming and Yang Qi, Reza and Melika Ghahremani, Derek Koe, Sheng and Kay Wang, and many others. I thank God for Intervarsity's Graduate and Faculty Christian Fellowship, the Veritas Forum, Melanie and Julian Reese, Teresa Hooper, Janelle Coleman, Mark Gates, Jordan Baker, and Eliza Scott. Many from outside the University of Tennessee made this journey particularly rich and I thank God for Josiah and Caleb Glafenhein, Jake Felde, Chris Rowe, Rick Moore, Erik Johnson, Jeff Upshaw, Jon Cate, Dennis Schauer, Austin Womac, Laura Owen, Alyson Grimes, Julie Lamb, Anna McRhee, Greg & Shirley DelMoro, Ryan and Lisa Matthews, Keith and Shelly Percic, Kelsey Vaughn, Hannah Martin, Kristin Ponsonby, Misha Testerman, Noelle Harb, Vincent Charlow, Jonathan Foster, Doug Banister, Linda Hamilton, and Jill Branson. Finally, but no less gratefully, there are those that have loved and encouraged me from afar, my parents Bob and Georgia Jacobsen, Jimmy and Ariel Lowe, Nathan Bennett, Ben Goldeen, Lauren Serpa, Rachel Griffith, Al and Marcy Barrera, Amy Ryan, and many others.

Abstract

Ancient fluvial features on Mars evidence past episodes of hydrologic activity and paleoclimate conditions suitable for liquid water. The Aeolis Dorsa region preserves the most numerous and diverse assemblage of fluvial features yet observed on Mars and many of these features have experienced a history of burial, exhumation, and topographic inversion. This dissertation describes analyses of visual images and topography of Mars and complementary analyses of fluvial analogs on Earth. These analyses provide information about the styles of fluvial activity, magnitudes of paleodischarge, changes in slope, and inferences about Martian paleoclimate conditions. Results indicate that the Aeolis Dorsa deposits encapsulate a wet-to-dry hydrologic transition, characterized by decreasing geospatial extent and frequency of hydrologic events. This wet-to-dry transition mimics the history of hydrologic activity preserved in valley networks and alluvial fans elsewhere on Mars. Results from an analysis of the Quinn River, NV, a terrestrial analog fluvial channel, indicate that width-discharge relationships from hydraulic geometry yield more accurate and more precise estimates of discharge than previously applied width-discharge relationships from the Missouri River Basin. These more accurate width-discharge relationships from hydraulic geometry, when applied to Martian features, yield larger paleodischarge estimates for Noachian-Hesperian valley networks and smaller paleodischarges for Hesperian-Amazonian fluvial deposits than were previously estimated. These new paleodischarges increase the contrast between early and late episodes of hydrologic activity by an order of magnitude. Results from additional analyses of terrestrial analogs and the Aeolis Dorsa deposits reveal confounding factors associated with resistant channel banks and erosion. These factors increase the systematic uncertainty of terrestrial-based empirical relationships and increase the error associated with estimates of paleochannel width and paleodischarge. These results point to the importance of assessing the validity of applying terrestrial-based empirical relationships to Mars, and they suggest that changes in paleodischarge are equivocal explanations of major changes in fluvial geomorphology. Findings from the remote analyses presented in this dissertation, combined with results from many previous field investigations, emphasize the importance of coupling Martian and terrestrial investigations for elucidating paleohydraulic conditions and fluvial histories, both of which are important considerations in the evaluations of future rover landing sites.

Table of Contents

Introduction 1
References 2
Chapter I The Aeolis Dorsa, Mars, Analyzed with Insights from Terrestrial Analog Deposits, Encapsulate a History of Decreasing Hydrologic Activity 4
Abstract 5
Introduction 5
Background 7
Formation Model: Hydrologic Activity, Sedimentation, Preservation, & Exposure 7
Aeolis Dorsa: Regional Context and Formation 8
The Medusae Fossae Formation (MFF) 8
Fluvial and Alluvial Deposits on Earth and in Aeolis Dorsa 9
Synopsis of Formation and Questions about the Aeolis Dorsa 14
Hypotheses for History of Aeolis Dorsa 14
Methods 15
Part 1: Deriving Morphological Attributes from Terrestrial Deposits 15
Part 2: Geospatial Distribution of Alluvial and Fluvial Deposits 16
Part 3: Mapping of Sedimentary Units 16
Part 4: Stratigraphy of Local Areas 16
Results 17
Part 1: Geomorphic Attributes of Sedimentary Units and Environments 17
Part 2: Geospatial Distribution of Features in Aeolis Dorsa 21
Part 3: Geomorphological Mapping of Local Areas 22
Part 4: Stratigraphy of Local Areas 27
Discussion 32
Synthesis of Aeolis Dorsa History 32
Assessment of Hypotheses 34
Comparison with Martian Hydrologic History 35
Conclusions 36
Future Work 37
References 39

Appendix I 47
Chapter II Greater Contrast in Martian Hydrological History from More Accurate Estimates of Paleodischarge 80
Abstract 81
Introduction 81
Background 82
Correlative Width-Discharge Relationships 82
Causal Width-Discharge Relationships Based on Hydraulic Geometry 83
Comparison of Width-Discharge Relationships 84
Analysis 85
Results 86
Discussion 87
Conclusions 88
References 90
Appendix II 94
Chapter III Decreasing Paleodischarge in the Aeolis Dorsa Region, Mars, with Confounding Factors Suggested by Morphometry of Terrestrial Analog Channels 104
Abstract 105
Introduction 105
Background 107
Records of Decreasing Hydrologic Activity in Aeolis Dorsa and on Mars 107
Empirical Relationships for Estimating Paleodischarge 109
Empirical Relationships for Estimating Paleochannel Width 110
Analyses of Terrestrial Analog Channels to Assess Empirical Relationships 111
Methods 112
Morphometric Analysis of Terrestrial Analog Channels 112
Morphometric and Paleodischarge Analyses of Martian Fluvial Deposits 113
Results 113
Morphometric Results from Terrestrial Analog Channels 113
Morphometric and Paleodischarge Results from Aeolis Dorsa, Mars 114
Discussion 115
Anomalous Point Bar Radii and Implications for Martian Results 115

Erosion of Fluvial Deposits and Implications for Paleodischarge Estimates 116
Challenges of Interpretating Eroded Fluvial Environments 117
Conclusions 118
References 119
Appendix III 124
Conclusion 135
References 137
Vita 138

List of Tables

Table I-1. Alluvial fans classified by dynamics, process, & mud involvement..... 47
Table I-2. Morphological attributes of fluvial sedimentary units 48
Table I-3. Morphological attributes of alluvial sedimentary units..... 48
Table II-1. Applications of width-discharge relationships on Mars and Titan..... 94
Table II-2. Exponents of width-discharge relationships..... 97
Table III-1. Empirical relationships of estimating discharge and channel width 124

List of Figures

Figure I-1. Formation model for the Aeolis Dorsa deposits 49
Figure I-2. Regional context images of the Aeolis Dorsa, Mars 50
Figure I-3. Examples of flat features in the Aeolis Dorsa, Mars 51
Figure I-4. Ridge-and-swale topography of a modern point bar 52
Figure I-5. Examples of thin features in the Aeolis Dorsa, Mars 53
Figure I-6. Portion of Aeolis Serpens showing lateral ridges 54
Figure I-7. An example of a fan feature with radiating ridges 55
Figure I-8. Satellite image shows fluvial units, including point bars, of the Scalby Formation, exposed along the east coast of England 56
Figure I-9. Images and topography profiles of Type 1 flat features 57
Figure I-10. Inverted paleochannel located southwest of Green River, Utah, USA 58
Figure I-11. Alluvial fan, located near Dolomite, CA, showing morphology of debris flow deposits 59
Figure I-12. Morphology of fan ridges in Aeolis Dorsa 60
Figure I-13. Morphology of an ancient alluvial fan in Oman 61
Figure I-14. Fan feature in Area 45S 62
Figure I-15. Delineations of inverted features in Aeolis Dorsa 63
Figure I-16. Area 35 map 64
Figure I-17. Geomorphic units in Area 35 65
Figure I-18. Area 40 map 66
Figure I-19. Geomorphic units in Area 40 67
Figure I-20. Area 45N map 68
Figure I-21. Geomorphic units in Area 45N 69
Figure I-23. Geomorphic units in Area 45S 72
Figure I-24. Stratigraphic columns for mapped areas. 73
Figure I-25. Topographic profiles through Area 35 74
Figure I-26. Topographic profile through Area 40 76
Figure I-27. Topographic profile through Area 45N 77
Figure I-28. Topographic profile through Area 45S 78
Figure I-29. Martian geologic timescale and age-dates of major hydrologic features ... 79

Figure II-1. Martian fluvial landforms and analogous fluvial systems on Earth 99
Figure II-2. Discharge and width data used to derive empirical relationships 100
Figure II-3. The Quinn River and examples of channel width measurements 101
Figure II-4. Discharge estimates from correlative and causal width-discharge relationships 102
Figure II-5. Comparison of width-discharge relationships and the modeled bankfull discharge 103
Figure III-1: Regional context image for the Aeolis Dorsa deposits and locations of stacked fluvial deposits 125
Figure III-2: Stacked fluvial deposits include younger fluvial channel fills superimposed on top of older meander point bars 126
Figure III-3: Three terrestrial analog rivers from two fluvial systems provide a variety of scales and conditions to assess morphometric relationships 127
Figure III-4: Examples of morphometric measurements along the Quinn River, NV, and stacked deposits in Aeolis Dorsa. 128
Figure III-5: Results of morphometric analyses of terrestrial analogs 129
Figure III-6: Morphometric results of fluvial deposits in Aeolis Dorsa 130
Figure III-7: Results from paleodischarge analyses in Aeolis Dorsa 131
Figure III-8: Comparison of terrestrial analog and Martian deposits 132
Figure III-9: Comparison of meander bends along the Quinn River 133
Figure III-10: Directionality and symmetry of meandering fluvial deposits in the Aeolis Dorsa region 134

Introduction

Mars has a relatively cold and dry surface compared to Earth. However, the geomorphology of Mars suggests a wetter past. The transition from wet to dry surface conditions is most clearly evidenced by a change in the distribution of valley networks. The largest and most widespread valley networks extend to regional drainage divides suggesting an atmospheric source for fluvial runoff (Hynek and Phillips, 2003; Howard et al., 2005). Younger craters dissect the networks, and crater-size frequency distributions of those craters suggest the valley networks formed around the boundary between the Noachian and Hesperian Epochs (~3.7 Ga) (Howard et al., 2005; Fassett and Head, 2008). After this time, surface hydrology began to change as is evidenced by a reduction in the size, number, and geospatial distribution of the valley networks during the Late Hesperian and Early Amazonian (~3.0 Ga) (Fassett and Head, 2008; Hynek et al., 2010).

Valley networks, open-basin lakes, degraded crater rims, outflow channels, sedimentary fans and closed-basin lakes represent the global effects of a waning hydrologic system (Howard et al., 2005; Fassett and Head, 2008; Carr, 2012; Goudge et al., 2016). However, there are several issues with this straightforward wet-to-dry Mars. First, the wet-to-dry paradigm has not been examined at regional scales as would be necessary to reconcile differences between orbital observations and those of landed rovers (e.g., Milliken et al., 2010). Second, qualitative descriptions of surface conditions as either "wet" or "dry" are unhelpful for modeling ancient Martian climate and for evaluating the habitability of paleoenvironments (Kerber, 2015; Hynek, 2016). The lens through which we observe, interpret, and even quantify the paleohydrology of Mars is terrestrial (Williams et al., 2009). Therefore, our methods for quantifying "wet" and "dry" conditions must be reexamined within terrestrial systems comparable to ancient Martian environments. Finally, although climatically driven fluvial activity has virtually ceased on Mars, erosion and other surface modification processes have not (Burr et al., 2010; Lefort et al., 2012; Lefort et al., 2015). How erosive processes and other confounding variables affect our interpretations of fluvial history must be reconsidered.

This dissertation examines these issues through analyses of the Aeolis Dorsa region of Mars and complementary analyses of ancient and modern fluvial systems on Earth. The Aeolis Dorsa region of Mars contains numerous fluvial and alluvial deposits, many of which have experienced topographic inversion and appear in positive relief (Pain et al., 2007; Burr et al., 2009). Chapter 1 of this dissertation describes fluvial and alluvial deposits on Earth and how this information was applied to the geomorphology and stratigraphy of the Aeolis Dorsa deposits. This first investigation tests the regional consistency of the wet-to-dry hydrologic transition. Chapter 2 describes terrestrial-based empirical relationships used to quantify paleohydraulics on Mars. This second investigation demonstrates the accuracies and inaccuracies of these relationships through an analysis of a terrestrial analog channel (Jacobsen and Burr, 2016). Chapter 3 describes a major geomorphic change preserved in the stratigraphy of Aeolis Dorsa and how that change was examined through additional terrestrial-based empirical relationships. Results from analyses of terrestrial analog channels suggest confounding factors and erosion affect the interpretations of Martian fluvial features.

References

Burr, D.M., Enga, M.-T., Williams, R.M.E., Zimbelman, J.R., Howard, A.D., and Brennand, T.A., 2009, Pervasive aqueous paleoflow features in the Aeolis/Zephyria Plana region, Mars: Icarus, v. 200, no. 1, p. 52–76, doi: 10.1016/j.icarus.2008.10.014.

Burr, D.M., Williams, R.M.E., Wendell, K.D., Chojnacki, M., and Emery, J.P., 2010, Inverted fluvial features in the Aeolis/Zephyria Plana region, Mars: Formation mechanism and initial paleodischarge estimates: Journal of Geophysical Research: Planets, v. 115, no. E7, p. E07011, doi: 10.1029/2009JE003496.

Carr, M.H., 2012, The fluvial history of Mars: Philosophical Transactions of the Royal Society of London A: Mathematical, Physical and Engineering Sciences, v. 370, no. 1966, p. 2193–2215, doi: 10.1098/rsta.2011.0500.

Fassett, C.I., and Head, J.W., 2008, The timing of Martian valley network activity: Constraints from buffered crater counting: Icarus, v. 195, no. 1, p. 61–89, doi: 10.1016/j.icarus.2007.12.009.

Goudge, T.A., Fassett, C.I., Head, J.W., Mustard, J.F., and Aureli, K.L., 2016, Insights into surface runoff on early Mars from paleolake basin morphology and stratigraphy: Geology, p. G37734.1, doi: 10.1130/G37734.1.

Howard, A.D., Moore, J.M., and Irwin, R.P., 2005, An intense terminal epoch of widespread fluvial activity on early Mars: 1. Valley network incision and associated deposits: Journal of Geophysical Research: Planets, v. 110, no. E12, p. E12S14, doi: 10.1029/2005JE002459.

Hynek, B., 2016, Research Focus: The great climate paradox of ancient Mars: Geology, v. 44, no. 10, p. 879–880, doi: 10.1130/focus102016.1.

Hynek, B.M., Beach, M., and Hoke, M.R.T., 2010, Updated global map of Martian valley networks and implications for climate and hydrologic processes: Journal of Geophysical Research: Planets, v. 115, no. E9, p. E09008, doi: 10.1029/2009JE003548.

Hynek, B.M., and Phillips, R.J., 2003, New data reveal mature, integrated drainage systems on Mars indicative of past precipitation: Geology, v. 31, no. 9, p. 757–760, doi: 10.1130/G19607.1.

Jacobsen, R.E., and Burr, D.M., 2016, Greater contrast in Martian hydrological history from more accurate estimates of paleodischarge: Geophysical Research Letters, p. 2016GL070535, doi: 10.1002/2016GL070535.

Kerber, L., 2015, Geology and Atmospheric Science for Early Mars: Synthesis and Synergies, in *in* Lunar and Planetary Institute, Houston, p. Abstract #2946.

Lefort, A., Burr, D.M., Beyer, R.A., and Howard, A.D., 2012, Inverted fluvial features in the Aeolis-Zephyria Plana, western Medusae Fossae Formation, Mars: Evidence for post-formation modification: Journal of Geophysical Research: Planets, v. 117, no. E3, p. E03007, doi: 10.1029/2011JE004008.

Lefort, A., Burr, D.M., Nimmo, F., and Jacobsen, R.E., 2015, Channel slope reversal near the Martian dichotomy boundary: Testing tectonic hypotheses: Geomorphology, v. 240, p. 121–136, doi: 10.1016/j.geomorph.2014.09.028.

Milliken, R.E., Grotzinger, J.P., and Thomson, B.J., 2010, Paleoclimate of Mars as captured by the stratigraphic record in Gale Crater: Geophysical Research Letters, v. 37, no. 4, p. L04201, doi: 10.1029/2009GL041870.

Pain, C.F., Clarke, J.D.A., and Thomas, M., 2007, Inversion of relief on Mars: Icarus, v. 190, no. 2, p. 478–491, doi: 10.1016/j.icarus.2007.03.017.

Williams, R.M.E., Irwin III, R.P., and Zimbelman, J.R., 2009, Evaluation of paleohydrologic models for terrestrial inverted channels: Implications for application to martian sinuous ridges: Geomorphology, v. 107, no. 3–4, p. 300–315, doi: 10.1016/j.geomorph.2008.12.015.

Chapter I

The Aeolis Dorsa, Mars, Analyzed with Insights from Terrestrial Analog Deposits, Encapsulate a History of Decreasing Hydrologic Activity

This chapter is the peer-reviewed version of a manuscript by the same name submitted to the journal Geosphere in March of 2016 by Robert Jacobsen and Devon Burr. A shorter version of this manuscript will be resubmitted to Geosphere in December 2016. Robert Jacobsen collected the data, performed the analyses, and drafted this manuscript and figures. Devon Burr provided advice on the science and edited the manuscript and figures.

Abstract

The Aeolis Dorsa, Mars, include fluvial and alluvial features formed by hydrologic activity, associated sedimentation, preservation, exposure, and often topographic inversion. Review of the Aeolis Dorsa and terrestrial literature reveals questions about their sedimentary units. A comparison with terrestrial deposits indicates that flat, thin, and fan features of the Aeolis Dorsa are consistent with a variety of meandering fluvial deposits, fluvial channel fills, and alluvial fans, respectively. Delineations of these fluvial and alluvial deposits show distinct geospatial distributions, specifically, widespread meandering fluvial deposits and networks of wide channel fills, more limited and discontinuous thin channel fills, and scattered localized groups of alluvial fans. Mapping of four local areas reveals two regional heterogeneities of sedimentary units, both of which may be explained by clays in southeast Aeolis Dorsa: (1) meandering fluvial deposits form only in southeast Aeolis Dorsa, whereas networks of wide fluvial channel fills appear in the northwest; (2) debris flow deposits comprise alluvial fans in the southeast, and sheetflood and/or traction deposits comprise fans in the northwest. Stratigraphic columns of the four map areas show a regionally consistent transition from older fluvial to younger alluvial deposits, but the expression of this transition varies in the number and type of sedimentary units. The transition from meandering fluvial deposits and wide channel fills to alluvial fan deposits indicates decreasing frequency and localization of hydrology activity and changes in slope through time. These findings refine previous hypotheses for regional history and suggest the Aeolis Dorsa deposits encapsulate the Martian time period of climatically-driven run-off.

Introduction

The Aeolis Dorsa (plural, meaning ‘ridges of Aeolis’) are numerous sinuous ridges interpreted to be topographically inverted fluvial and alluvial deposits (e.g., Pain et al., 2007; Burr et al., 2009; Burr et al., 2010). These well-preserved and well-exposed deposits are products of interleaved hydrologic activity, concomitant sedimentation, aeolian processes, burial, and exhumation, along with subsequent modification by tectonic and/or collapse processes (e.g., Burr et al., 2009; Burr et al., 2010; Lefort et al., 2012; Matsubara et al., 2014; Kite et al., 2015a; Kite et al., 2015b; Lefort et al., 2015). Fluvial and alluvial landforms, including those preserved in the Aeolis Dorsa region, provide critical data for understanding the record of water on Mars (Burr et al., 2009; Carr 2012 and references therein). Other investigations in the Aeolis Dorsa region

suggest regional tectonic modifications along the dichotomy boundary (Lefort et al., 2012; Kite et al., 2015a; Lefort et al., 2015), relationships among obliquity, climate change, and cycles of deposition and erosion (Kite et al., 2015a), and the presence of a putative northern ocean (DiBiase et al., 2013). Thus, understanding the Aeolis Dorsa region provides information on a range of questions in Mars science.

Much of the current understanding of the Aeolis Dorsa deposits has relied on analyses of plan-view satellite images and topography of Mars, and on modern riverine landscapes and deposits on Earth for comparison. Terrestrial studies have described similarities between landforms on Earth and Mars, and used those similarities to infer ancient conditions and processes in the Aeolis Dorsa region (e.g., Pain et al., 2007; Williams et al., 2007; Burr et al., 2009; Burr et al., 2010; Lefort et al., 2012; DiBiase et al., 2013; Williams et al., 2013; Matsubara et al., 2014; Kite et al., 2015a). Use of ancient terrestrial deposits as analogs acknowledges geologic time as an essential control on geomorphic modifications. Because of these modifications, active landforms on Earth may not provide robust analogs for ancient deposits on Mars. Thus, use of ancient sedimentary deposits on Earth and their morphological attributes may provide more specific insights into the sedimentary environments of the Aeolis Dorsa.

Building on this previous work, the investigation presented here consists of four parts. First, we revisit the origins of the Aeolis Dorsa and introduce some questions about the sedimentary units they represent. We address these questions by examining ancient deposits on Earth and identifying their morphologic attributes. Then, we compare these terrestrial-based attributes with the morphologies of the Aeolis Dorsa deposits. Results of this comparison provide more specific interpretations of the sedimentary units and hydrologic conditions that formed the Aeolis Dorsa deposits.

The remaining three parts of this investigation rely on the terrestrial-based morphologic attributes to enable testing of two hypotheses about the stratigraphic and hydrologic history of Aeolis Dorsa. In the second part of this investigation, we delineate the various fluvial and alluvial features in the Aeolis Dorsa region to show their locations and extents. In the third part of this investigation, we map four local areas, identify sedimentary units, and interpret their formative processes based upon the terrestrial-based geomorphic attributes. In the fourth part of this investigation, we analyze and correlate strata among the four local areas. Stratigraphic columns allow us to examine and document changes in sedimentary environments and hydrologic conditions through time. In our discussion, we synthesize the results from the preceding four parts, assess the proposed hypotheses, and compare the synoptic history of Aeolis Dorsa with the overall history of valley networks and alluvial fans on Mars (e.g., Carr and Head 2010; Hynek et al. 2010). Finally, we conclude with the key findings from each part of this investigation and suggest future opportunities for research.

Background

Formation Model: Hydrologic Activity, Sedimentation, Preservation, and Exposure

The Aeolis Dorsa deposits are the results of four processes: hydrologic activity, concomitant sedimentation, preservation, and subaerial exposure (Figure I-1). Here, we describe these processes generally and cite terrestrial examples (e.g., Pain and Oilier, 1995). In the next section, we explain how this formation model applies to the Aeolis Dorsa. Reviewing these formation processes is essential for proper analysis of Aeolis Dorsa history and identification of knowledge gaps in that history. Whether on Earth or Mars, plan view analyses require each of these four formation processes. If ancient fluvial and alluvial deposits do not undergo preservation and subaerial exposure, they might still be identifiable in cross section, e.g., by a field geologist or rover, but identification would not be possible by remote sensing. For example, the Mars Exploration Rover analyzed sediments exposed in crater walls of Meridiani Planum and identified evaporates, traction fluvial deposits, and aeolian deposits, which suggested a playa sedimentary environment (Grotzinger et al., 2005). However, this environment was not inferred by remote sensing prior to landing (Golombek et al., 2003).

First, the formation model requires a climate favorable for hydrologic activity, which may be sourced from precipitation run-off or groundwater seepage. Sedimentation may occur in tandem with this hydrologic activity. A sufficient supply of sediment under transport-limited conditions is necessary for sedimentation, without which sedimentary units, such as point bars, will not form (Figure I-1a). Continued sedimentation leads to aggradation of the channel bed and the formation of a channel fill (Figure I-1b) (Gibling, 2006), which then must be preserved from erosive processes.

Preservation processes represent the second step in the model and include burial and/or induration. Preservation against erosion (e.g., fluvial erosion, aeolian abrasion, and impact cratering) is necessary to retain sedimentary units and morphologies. On Earth, burial by other alluvial deposits, marine sediments, or infilling of channels and valleys with lava shields the underlying deposits from erosive processes (e.g., Maizels, 1990; Williams et al., 2007; Burr et al. 2010). Induration preserves fluvial and alluvial deposits from erosion during subsequent exposure. Without sufficient induration, deposits may be heavily eroded and indiscernible in satellite images (Lucchitta et al., 2011). Types of induration include in-channel deposition of a gravel lag or geochemical cementation of channel deposits (e.g., Pain and Oilier, 1995; Burr et al., 2010 and references therein). On Earth, primary induration by gravel lags occurs on steep slopes and forms discontinuous induration (Osterkamp and Toy, 1994). Geochemical cementation may occur through evaporation of near-surface groundwater (McLaren, 2004; Williams et al., 2013) or through precipitation from groundwater after burial (Maizels, 1990; Williams et al., 2007).

The final step, exposure of deposits to satellite imaging, requires erosive processes, such as fluvial erosion or aeolian abrasion, that remove the surrounding landscape or – in cases of burial – the overburden (Maizels, 1990; Brookes, 2003). Differential erosion of the surrounding landscape leads to topographic inversion of the fluvial or alluvial deposits (Pain and Oilier, 1995; Williams et al., 2007).

Aeolis Dorsa: Regional Context and Formation

The processes included in the four-step model illustrated in Figure I-1 have been inferred for the formation of the Aeolis Dorsa deposits (e.g., Pain et al., 2007; Williams et al., 2007; Burr et al., 2009; Burr et al., 2010). Hydrologic activity in the Aeolis Dorsa region may have been produced by orographic precipitation and subsequent run-off (Burr et al., 2009; Kite et al., 2013). The Aeolis Dorsa region, located near the Mars equator, is in the transitional zone (Tanaka et al., 2014) between the southern highlands and northern lowlands (Figure I-2A). The topographic gradient in this area has been suggested to be favorable to orographic precipitation (Burr et al., 2009), as occurs, for example, in simulations of snowfall over valley networks (Scanlon et al., 2013). The possibility of hydrologic activity via snowmelt is supported by simulations that show higher pressures and temperatures at lower elevations along the equator, e.g., at Aeolis Dorsa and Gale Crater (Kite et al., 2013).

The Medusae Fossae Formation (MFF)

The remaining processes in the formation of the Aeolis Dorsa – sedimentation, preservation, and exposure – are inferred from properties and features of the Medusae Fossae Formation (MFF). The MFF is an extensive, multi-lobed (Figure I-2A), layered deposit that is hypothesized to be of aeolian and/or pyroclastic origins (e.g., Ward, 1979; Scott and Tanaka, 1982; Shultz and Lutz, 1988; Hynek et al., 2003; Mandt et al., 2008; Mandt et al., 2009; Kerber and Head, 2010; de Silva et al., 2010; Kerber et al., 2011; Kite et al., 2015a). Remnant deposits of the MFF appear as far east as Tharsis and possibly as far west as Gale Crater (Figure I-2A) (e.g., Bradley et al., 2002; Hynek et al., 2003; Harrison et al., 2010; Zimbelman and Scheidt, 2012). Analyses of satellite images and topography suggest an average thickness of several hundred meters, a maximum thickness of a couple kilometers, and layers with thicknesses of less than a meter to over a hundred meters (e.g., Scott and Tanaka, 1982; Bradley et al., 2002; Zimbelman and Griffin, 2010; Kite et al., 2015a). These observations suggest that the MFF has undergone numerous episodes of widespread deposition (Bradley et al., 2002; Mandt et al., 2008; Kerber et al., 2011). The Aeolis Dorsa coincide, nearly entirely, with mapped units of the MFF (Figure I-2A) (Burr et al., 2009; Zimbelman and Griffin, 2010; Zimbelman and Scheidt, 2012). This coincidence of the Aeolis Dorsa and the MFF deposits suggests that the MFF supplies substantial quantities of sediment (i.e., transport-limited conditions) necessary for the formation of fluvial sedimentary units (e.g., point bars) and aggradation of channel beds leading to the formation of channel fills.

Within the context of the MFF, preservation, the next process in the formation model (Figure I-1), was likely accomplished in two ways, burial and cementation (Burr et al., 2010). MFF deposits are observed around and on top of fluvial and alluvial deposits, demonstrating that the deposits have experienced burial (e.g., Burr et al., 2009; Burr et al., 2010). Preservation of sedimentary textures and enhanced thermal inertia of sinuous features suggest geochemical cementation of the Aeolis Dorsa deposits (Burr et al., 2010). However, the delivery mechanism, timing, and composition of the cement(s) are unknown (Burr et al., 2010). The possible volcanic origin of the MFF (e.g., Ward, 1979;

Scott and Tanaka, 1982; Mandt et al., 2008; Kerber and Head, 2010; de Silva et al., 2010) suggests volcanic solutes, such as silica, iron, and sulfate, could form silcrete, ferricrete, and gypcrete cements, respectively, when precipitated from an aqueous solution (Pain and Oilier, 1995; Pain et al., 2007; Burr et al., 2010). Cementation of the Aeolis Dorsa deposits by salts is also possible (Pain et al., 2007), and is consistent with a regional enhancement of chlorine, measured by gamma-ray spectroscopy, that is largely coincident with the MFF (Keller et al., 2006; Kerber et al., 2011). However, remote spectroscopic constraints on the composition(s) of these possible cements are limited by regional dust (Ruff and Christensen, 2002), which obstructs observations of the underlying deposits at near-infrared wavelengths.

Exposure, the final process of the formation model, involved exhumation and topographic inversion (Figure I-1). Exposure is inferred to have resulted from aeolian processes, such as erosion and deflation (e.g., Burr et al., 2009; Burr et al., 2010). The pervasive aeolian erosion is indicated by yardangs, which are seen throughout the Aeolis Dorsa region and MFF (Ward, 1979; Scott and Tanaka, 1982; Mandt et al., 2009; Zimbelman and Griffin, 2010). Yardangs are elongate ridges sculpted by aeolian abrasion (de Silva et al., 2010). Yardang formation requires material induration, either by welding or cementation, followed by aeolian abrasion (de Silva et al., 2010). Yardang orientation is parallel to the direction of aeolian abrasion (de Silva et al., 2010) and therefore may be used as a proxy of paleo-wind direction (Mandt et al., 2009). The morphometry of MFF yardangs are comparable to yardangs formed in terrestrial deposits of volcanic ash (Scott and Tanaka, 1982; Mandt et al., 2008; Mandt et al., 2009; de Silva et al., 2010).

Fluvial and Alluvial Deposits on Earth and in Aeolis Dorsa

Here, we summarize previous observations and interpretations of the Aeolis Dorsa landforms and deposits. Following previous investigators (Burr et al., 2009), we describe the Aeolis Dorsa features within a (revised) classification scheme derived from width and cross-sectional shape. Comparing the morphologies of Aeolis Dorsa deposits with ancient fluvial and alluvial deposits on Earth suggests new questions about the sedimentary units preserved in Aeolis Dorsa.

Fluvial Origins of Flat Features

Flat features have broad flat upper surfaces with widths on the order of several hundred meters to a few kilometers (e.g., Burr et al., 2009), although low-order and eroded examples may be narrower. Flat features vary from having no discernable relief (Figure I-3A) up to several tens of meters of relief (Figure I-3B). From previous observations (Burr et al., 2009; Zimbelman and Griffin, 2010), we distinguish two sub-classes of flat features: Type 1 flat features have semi-concentric, curved ridges on their upper surfaces (e.g., Figures I-3A & I-3B), and Type 2 features have nondescript or plain upper surfaces (e.g., Figure I-3C).

Based on morphological similarities to active meander floodplains on Earth, the semi-concentric, curved ridges of Type 1 features were initially interpreted as point bars

(e.g., Figure I-3B; Burr et al., 2009; Zimbelman and Griffin, 2010), which may also be called "scroll bars" (e.g., Gibling and Rust, 1993; Burr et al., 2009). Since then, the topographic profiles of some Type 1 features (i.e., Figure I-3A) have been interpreted as laterally aggrading fluvial channel beds, i.e., lateral migration of a meandering fluvial channel and simultaneous aggradation of the channel bed (Matsubara et al., 2014). While examples of modern and ancient point bars on Earth are common, laterally aggrading fluvial channels are less common because they are limited to high-strength floodplains or areas with valley confinement (e.g., Gibling and Rust, 1990; Gibling, 2006). Furthermore, laterally aggrading channel beds are unusual in that younger channel fill or floodplain sediments usually cover channel beds. The following information about meandering fluvial environments on Earth highlights the importance of critically analyzing the sedimentary units of deposits on Mars and suggests a topographic criterion for distinguishing point bars and channel beds for Type 1 features.

Point bars are fundamental sedimentary units (i.e., architectural elements) of meandering fluvial channels (Miall, 2010). On Earth, point bars form through lateral accretion of sediment in a direction perpendicular to the direction of channel flow. Flow momentum and channel curvature increase flow velocity, channel depth, and erosion along the (outer) cut bank. Flow build-up along the cut bank leads to a helical secondary current that deposits sediment on the inclined surfaces of the inner bank (Gibling and Rust, 1993; Howard, 2009). These flow mechanics form channels with low width-to-depth ratios, which require structurally stable channel banks, such as those with rooted plants (Davies and Gibling, 2010), cohesive silts and clays, or possibly floodplains with permafrost or geochemical cements (Howard, 2009; Matsubara et al., 2014).

Deposits of channel beds differ from point bars in terms of their sedimentology, structure, and topography. Channel beds often include the coarsest fraction of transported sediment and form bars within the channel that appear as trough cross-beds in cross-section (Miall, 2010). Through deposition by oblique secondary currents, point bars comprise finer fractions of transported sediment and appear as lateral accretion sets in cross-section (Davies and Gibling, 2010; Miall, 2010). Channel beds and point bars are also topographically distinct, in that point bars form above channel bed deposits (Figure I-4). On Earth, recent point bars have elevations that decrease from the interior of the meander bend to the exterior (Profile C-C' in Figure I-4), and most of the elevation change occurs between the youngest point bar and the channel bed. Also, point bars have surfaces with ridges and swales that have little change in relative elevation (Profile C-C' in Figure I-4; see also Gibling and Rust, 1993; Ielpi and Ghinassi, 2014).

The elevations of curved, semi-concentric ridges in Aeolis Dorsa, specifically those in Figure I-3A, have been qualitatively described (Matsubara et al., 2014) to increase from the interior of the meander bend to the exterior. That is, the exterior of the meander bend (e.g., arrow in Figures I-3A) was described as topographically higher than the area that the bend surrounds (Matsubara et al., 2014). Increasing elevations from the interior of the meander bend to the exterior is consistent with the topography of laterally aggrading channel-bed deposits (e.g., Page & Nanson, 1996). An interpretation of laterally aggrading channel beds requires an explanation for the lack of adjacent point bars, which for these features was posited to result from subsequent erosion (Matsubara

et al., 2014). This topographic comparison, supplemented by geomorphic attributes of recent point bars on Earth, demonstrates the utility of sedimentary analogs for distinguishing various deposits, in this case, channel beds from point bars. An inspection of ancient point bars on Earth, rather than the modern examples (Figure I-4), is needed to identify attributes for a more robust interpretation of Type 1 features in Aeolis Dorsa.

Type 2 flat features have nondescript upper surfaces, lacking the semi-concentric ridges of Type 1 flat features, and are more linear and less broad than the Type 1 features (e.g., Figure I-3C). Type 1 & 2 features may appear conjoined within the same ridge network, which suggests that, despite their texture and morphological differences, the two types of flat features may have similar origins. However, the specific sedimentary unit represented by Type 2 has not been inferred in previous investigations, and this information is need for an interpretation of a specific fluvial sedimentary environment.

Fluvial Origins of Thin Features

Thin features are narrower in plan view than flat features, with widths on the order of tens of meters, and have either sharp medial crests (Burr et al., 2009; Zimbelman and Griffin, 2010) or in some cases flat upper surfaces (Figure I-5). Thin features are the most sinuous ridges in Aeolis Dorsa, with sinuosity values (i.e., ratios of landform length to straight end-to-end length) up to ~2 (Burr et al., 2010), although they may also be much straighter (e.g., Figure I-5A). Some thin features appear stratigraphically stacked above flat features (e.g., Figure I-5B) (Burr et al., 2009; Zimbelman and Griffin, 2010). Based on their coincidence above some inferred meander deposits (i.e., Type 1 flat features) and their high sinuosities, thin features were interpreted as inverted channel beds of meandering fluvial channels (Burr et al., 2009; Burr et al., 2010; Zimbelman and Griffin, 2010), but presumably where either point bars did not form adjacent to the channel or the former point bars were not preserved. The interpretations of thin features as inverted channel beds were used to justify the use of morphometry in support of paleohydraulic calculations. For example, the widths of some thin features were taken to be the widths of the former fluvial channels and, with terrestrial-based empirical relationships, were used to estimate paleodischarge values (Burr et al., 2010; Kite et al., 2015b). Therefore, accurate interpretation of the fluvial sedimentary unit(s) is important because their dimensions influence paleodischarge estimates.

As with the interpretation of some Type 1 flat features as laterally aggrading channel beds, the interpretation of thin features as fluvial channel beds implies that the channel beds are preferentially exposed in the rock record. However, such exposure would be unusual because younger sediments, most commonly channel fills, usually cover the original channel beds (Gibling, 2006). Therefore, an examination of ancient channel fills may provide insights for the reinterpretation of thin features and suggest attributes indicative of the channel dimensions needed for paleohydraulic analyses.

Fluvial channel fills are the most common sedimentary unit representing the dimensions – including width and depth – of the original fluvial channel (Gibling, 2006). The channel fill, like a cast, is created by sediment accumulation within a single fluvial channel (i.e., the mold). As a result, the width and thickness of a channel fill preserves the active channel dimensions, which are the parameters needed for paleohydraulic

analyses. Fixed-channel fluvial environments, such as megafans (Cuevas Martinez et al., 2010), high-strength floodplains (Gibling and Rust, 1990), or aeolian settings (Jones and Blakey, 1997) are dominated by avulsion (Gibling, 2006). During avulsion, the active channel moves away from older deposits and effectively leaves channel fills intact. In contrast, meandering and braided fluvial channels tend to migrate across their floodplains, forming an amalgamation of multiple smaller channel deposits. The result is a channel deposit that is integrated over time and space and so misrepresents the original channel dimensions.

Channel fill deposits from fixed-channel and migrating-channel environments may be distinguished by their width-to-thickness ratios (W/T) (Gibling, 2006). Because of the amalgamation of their deposits, braided fluvial environments have W/T ratios of 50 to greater than 1000 (e.g., Miall and Jones, 2003; Gibling, 2006) and meandering fluvial environments have overlapping, though smaller, ratios of 30 to 250 (e.g., Smith, 1987; Gibling, 2006). Fixed channels produce channel fills with W/T ratios of 5 to 100, which are similar to width-to-depth ratios of active fluvial channels (Gibling, 2006). An inspection of ancient channel fills with low W/T ratios on Earth is needed to identify their geomorphic attributes. These attributes, when used to interpret the thin features of Aeolis Dorsa, may either support the previous interpretation of thins as channel beds or help reinterpret what (if any) remains of the ancient channel widths. This information, in turn, can be used for future paleohydraulic analyses.

Aeolis Serpens

This sinuous feature, centrally located in the topographically low region between Aeolis Planum and Zephyria Planum, is ~600 km long and tens to hundreds of meters wide. Aeolis Serpens has multiple branches and exhibits variable cross-sectional shapes, including medial troughs and twin lateral ridges (Figure I-6) (Burr et al., 2009; Lefort et al., 2012; Williams et al., 2013). The characteristics of Aeolis Serpens were interpreted to be consistent with fluvial channel deposits that have been variably indurated along their margins by geochemical cements (Williams et al., 2013). Examples of such landforms are found in the Atacama Desert (Lefort et al., 2012) and in Australia (Williams et al., 2013). The moderate sinuosity of Aeolis Serpens was interpreted as evidence of a meandering fluvial channel, but neither point bars nor evidence of lateral migration were observed (Williams et al., 2013).

Alluvial Origins of Fan Features

Fan features radiate and descend from apices, some of which connect to branching networks of ridges (Figure I-7) (Burr et al., 2009). The inverted ridges that comprise fan features bifurcate in the downslope direction. Most fan apices border the interior margins of Aeolis and Zephyria Plana (Figure I-2B) (Burr et al., 2009; Kite et al., 2015a). Based on morphology, topography, and network relationships, fan features are interpreted as deposits of alluvial fans (Burr et al., 2009; Kite et al., 2015a). On Earth, a variety of sedimentological processes form alluvial fans (Blair and McPherson, 2009), some of which are reflected in the geomorphologic attributes of their deposits (Table I-1).

Requirements of alluvial fan formation are topographic relief, accumulation of weathered sediment, intermittent hydrologic activity, and loss of flow confinement (Blair and McPherson, 2009; Stock, 2013). Alluvial fans are found in both arid and humid climates (Kochel and Johnson, 1984; Evans, 1991; Blair and McPherson, 1994; Saito and Oguchi, 2005; Stock, 2013). Climate is relevant to fan formation because of temperature, which affects weathering rates, and the frequency of precipitation events. Precipitation must be infrequent enough to allow accumulation of weathered sediment, and intense or "flashy" enough to initiate erosion by overland flow or hillslope failure (Blair and McPherson, 2009). Thus, alluvial fan deposits provide information about ancient climate, but only with respect to its effect on weathering and intermittency of hydrologic activity (Blair and McPherson, 2009).

Two types of flow dynamics are involved in the formation of alluvial fans (Table I-1). In inertial sedimentary processes, flow velocity has more influence on flow dynamics than the effect of gravity (i.e., Froude ≥ 1). In traction sedimentary processes, the effect of gravity has greater influence than flow velocity (i.e., Froude < 1).

Inertial processes begin as hillslope failures in mountain catchments and form many different deposits. Fan catchments with appreciable mud and weathered sediments produce debris flows (Blair and McPherson, 1998; Blair, 1999). Mud lowers hillslope permeability and increases hydrostatic pore pressure in the shallow subsurface, leading to hillslope failure, cohesion of flow, and poorly shorted, massive deposits (Blair, 1999). Debris flow deposits consist of boulder-rich levees and distal lobes with relatively steep slopes ($\geq 2°$), thicknesses up to a few meters, and widths of up to100 meters (e.g., Blair and McPherson, 1994; Blair and McPherson, 1998). Debris flow levees are composed of boulders and other coarse materials, which are rafted during transport, concentrated at the head of the surge, and then sheared from the lateral edges of the flow by contact with the channel margins. Lobes form where the debris flow extends down-fan beyond the confinement of the levees and expands laterally (Blair and McPherson, 1994).

Inertial sedimentary processes also occur in catchments with low mud content. Slopes with lower mud content have greater permeability and so require greater amounts of water infiltration for hillslope failures (Blair, 1999). Because of this greater water-to-sediment ratio, subsequent flows are driven by fluid-gravity interactions, such as sheetfloods (Blair, 2000). Sheetfloods are unconfined inertial sedimentary processes (Table I-1), which produce deposits of imbricated gravels, antidunes, and laminated sands that are several meters wide and several centimeters thick (Blair, 1987; Blair, 1999). Sheetflood deposits are not readily apparent in plan view because their low relief (cf. Blair, 1999).

Alluvial fans also form through traction sedimentary processes (Stock, 2013). Traction processes include bed load and suspended load, which are commonly associated with fluvial environments. On alluvial fans, these processes form imbricated gravels and bedform slip faces appearing as trough cross-beds in cross-section (Kochel, 1990; Maizels, 1990; Stock et al., 2007). An inspection of alluvial fan deposits on Earth is needed to identify the plan view geomorphic attributes of the various deposits described above. Applying these attributes to the Aeolis Dorsa may help identify specific alluvial sedimentary units and suggest alluvial processes in Aeolis Dorsa.

Synopsis of Formation and Questions about the Aeolis Dorsa

Background information suggests this synopsis for the formation of the Aeolis Dorsa deposits:

1. Hydrologic activity in the Aeolis Dorsa region may have been sourced from orographic precipitation and snowmelt run-off (Burr et al., 2009; Kite et al., 2013).

2. Sedimentation, preservation, and surficial exposure of fluvial and alluvial deposits may be explained by repeated deposition and subsequent erosion of the Medusae Fossae Formation (MFF). Deposits are preserved through widespread burial and geochemical cementation (Burr et al., 2010). Also, the MFF has experienced aeolian abrasion, which exhumes, exposes, and topographically inverts deposits (Burr et al., 2010; de Silva et al., 2010).

3. The hydrologic history of Aeolis Dorsa is represented by several deposits, including (i) fluvial deposits of flat features, (ii) fluvial deposits of thin features, (iii) the inverted paleochannel Aeolis Serpens, and (iv) alluvial deposits of fan features.

However, information from terrestrial deposits suggests several questions about the ancient conditions and sedimentary units of the Aeolis Dorsa:

1. Are topographic profiles of Type 1 flat features consistent with meandering fluvial deposits, such as laterally aggrading channel beds? Is there variety in the topography of Type 1 flat features that would suggest preservation of multiple types of meandering fluvial deposits (e.g., laterally aggrading channel beds and point bars)?

2. What sedimentary units comprise Type 2 flat features (e.g., Figure I-3C) and what sedimentary environment do they represent?

3. Are thin features consistent with fluvial channel beds or channel fills? What, if any, dimensions of the former channel have been preserved and may be used in future paleodischarge analyses?

4. What sedimentary units comprise fan features (e.g., Figure I-7)? What primary processes and formation conditions do these units suggest?

Hypotheses for History of Aeolis Dorsa

The fluvial and alluvial deposits of the Aeolis Dorsa region are rich data for studying the history of hydrology on Mars (Burr et al., 2009; Kite et al., 2015a). The Martian global history shows an early transition from widespread runoff to localize and intermittent runoff (Carr and Head, 2010; Hynek et al., 2010; Carr, 2012), as evidenced by the distribution of valley networks and alluvial fans (e.g., Hynek et al., 2010; Grant

and Wilson, 2011). Stratigraphy of the Aeolis Dorsa has also shown similar changes, specifically from fluvial deposits to alluvial fans with individual units and unconformities representing 10^6 to 10^8 years (Kite et al., 2015a). Analyses of select fluvial features show decreases in feature width and wavelength, relative to stratigraphic age, suggesting a decrease in paleodischarge through time (Kite et al., 2015b). We summarize these changes as (1) a regional transition from fluvial to alluvial deposits, and (2) a regional decrease in hydrologic activity through time. These two regional changes are two hypotheses that we will test in this investigation through regional delineations by feature type and local analyses of sedimentary units and stratigraphy. Addressing the aforementioned questions about sedimentary units will enable us to test these hypotheses with higher specificity than previous analyses. Through this work, we will elucidate local processes that accompanied the climatic and hydrologic changes in the Aeolis Dorsa region.

Methods

Part 1: Deriving Morphological Attributes from Terrestrial Deposits

Our plan-view inspection of alluvial and fluvial deposits on Earth uses high-resolution satellite images and data from published in-situ analyzes of these terrestrial deposits. The examined satellite images have comparable resolutions to images of the Aeolis Dorsa deposits (i.e., one to several meters per pixel). Terrestrial plan view images are accessible from Google© Earth software, or their data providers, and the National Agriculture Imagery Program.

We focus on morphologies at scales of meters to tens of meters, which are comparable to the sizes of sedimentary units indicative of fluvial and alluvial environments (i.e., architectural units; see Miall, 2006). Morphologic attributes of these terrestrial deposits will be compared with the morphologies of Aeolis Dorsa features and used to interpret their sedimentary units and environments. Tables will summarize the morphologic attributes of sedimentary units, the sedimentary environments where the units may form, and any hydrologic, sedimentologic, or topographic conditions implied by the sedimentary units.

We focus this analysis on terrestrial examples of sedimentary environments that are inferred in the Aeolis Dorsa region. Our analysis includes meandering fluvial channels (Burr et al., 2009; Howard, 2009; Matsubara et al., 2014), single-thread fluvial channels (Burr et al., 2009; Burr et al., 2010), and alluvial fans (Burr et al., 2009; Kite et al., 2015a). A single deposit in Aeolis Dorsa has been interpreted as a delta (DiBiase et al., 2013), but this interpretation relies on a flow direction that is opposite the modern slope and inconsistent with all other results from the Aeolis Dorsa region (Burr et al., 2009; Burr et al., 2010; Zimbelman and Griffin, 2010; Lefort et al., 2012; Williams et al., 2013; Matsubara et al., 2014; Kite et al., 2015a; Lefort et al., 2015; Kite et al., 2015b). In view of these inconsistencies and a lack of other potential deltas in Aeolis Dorsa, we do not study deltaic deposits here.

Part 2: Geospatial Distribution of Alluvial and Fluvial Deposits

Testing the two hypotheses for the history of hydrologic activity in Aeolis Dorsa requires knowing the geospatial distribution of preserved features in Aeolis Dorsa. Therefore, we examine a mosaic of 83 images from the Context Camera (CTX, 6 m/pixel) (Malin et al., 2007) largely covering the area adjacent to and between Aeolis and Zephyria Plana (Figure I-2A), and use ArcMap software to delineate shapefile polylines through the center of features. Features are classified as flat, thin, or fan features, or Aeolis Serpens based on their morphologies, which were described in the Background.

Part 3: Mapping of Sedimentary Units

To augment the geospatial distribution of part 2 with information about sedimentary units, we map sedimentary units in four local areas shown in Figure I-2A. Numbers identifying local areas correspond to Table 1 in Burr et al. (2009). These local areas are chosen for mapping because of their good exposure and stratigraphic stacking of flat features, thin feature, fan features, and Aeolis Serpens. These areas also provide a spatially distributed sampling of deposits in both the northern and southern portions of the Aeolis Dorsa region. Our interpretations of fluvial and alluvial sedimentary units and environments are based on the geomorphological attributes derived from inspection of terrestrial analogs (i.e., part 1). Based on previous investigations of the Aeolis Dorsa region and surrounding regions, we interpret yardangs as deposits of MFF that have been abraded by paleo-winds (e.g., de Silva et al., 2010) and cratered plains with wrinkle ridges as lavas (Kerber and Head, 2010, and references therein). Using ArcMap software, we map these fluvial, alluvial, volcanic, and aeolian units as they appear in the CTX mosaic, which serves as our base map. Where available, visual images and stereo-pair DTMs from the High Resolution Imaging Science Experiment (HiRISE, 0.3 m/pixel) (McEwen et al., 2007) were examined in order to distinguish specific sedimentary units (e.g., point bars or laterally aggrading channel beds).

Part 4: Stratigraphy of Local Areas

To understand how sedimentary units and environments changed through time in local areas, and to infer how sedimentary units changed throughout the region, we then derive the stratigraphy of the four map areas from part 3. The relationship between sedimentary units and time is presented in four stratigraphic columns, one for each local area. We derive stratigraphic columns from a combination of plan view observations and topographic analyses. Plan view observations of CTX and HiRISE images give evidence of superposition, crosscutting, and embayment relationships of mapped units that indicate the relative order of units in stratigraphic columns. Analyses of topographic profiles are used to infer thicknesses of units in stratigraphic columns. Topographic data include point and gridded data from the Mars Orbiter Laser Altimeter (MOLA) (Smith et al., 2001), three digital terrain models (DTMs) derived from CTX stereo-image pairs using Ames Stereo Pipeline (Moratto et al., 2010), and two DTMs derived from HiRISE stereo-image pairs using BAE SOCET SET (Kirk et al., 2008). Units with covered or otherwise

unobservable upper and/or lower contacts are given broken and jagged contacts in stratigraphic columns. Without observations in cross-section, it is not possible to know the exact thicknesses of fluvial units; therefore, we estimate thicknesses of fluvial units from width to thickness (W/T) ratios of ancient terrestrial deposits (Gibling, 2006). Although a similar W/T ratio has not been demonstrated on Mars, we use it as a reasonable means of separating fluvial deposits from substrate material in stratigraphic columns. We posit flat and thin features to have W/T ratios of 30, which is consistent with meandering and fixed-channel fluvial environments (Gibling, 2006). Like the terrestrial-based morphologic attributes for interpreting sedimentary units, use of this W/T ratio increases the specificity of our interpretations compared to previous investigations of the Aeolis Dorsa. Where sinuous ridge relief is greater than the inferred thickness, we assume the lower portion of the ridge to be a deposit of MFF, suggesting that it was the substrate of fluvial activity. Lithostratigraphic correlations among the four local areas are based on similar geomorphology (e.g., thin features are correlated) or sedimentology (e.g., meander fluvial deposits are correlated). Correlated stratigraphic columns are used to interpret any spatial heterogeneity and temporal change of sedimentary environments in the Aeolis Dorsa region.

Results

Part 1: Geomorphic Attributes of Sedimentary Units and Environments

Inspection of satellite images, in conjunction with in-situ analyses published by previous investigators, provides geomorphic attributes of fluvial and alluvial sedimentary units, as described below. These geomorphic attributes, their implications for sedimentary environments, and uncertainties are summarized in Tables I-2 and I-3.

Ancient Point Bars in Satellite Images

Ancient point bars exposed in the plan view perspective have been identified in Argentina (Foix et al., 2012), Egypt (Brookes, 2003), England (Ielpi and Ghinassi, 2014), Nova Scotia (Gibling and Rust, 1993), South Africa (Smith, 1987), Spain (Donselaar and Overeem, 2008), and Texas (Edwards et al., 1983). The examples identified in England are exhumed point bars from the Jurassic Scalby Formation near Scarborough, England (Nami, 1976; Ielpi and Ghinassi, 2014) and we focus on these examples because the same satellite images that were used as a base map for mapping in-situ observations (Ielpi and Ghinassi, 2014) are available and used here in our remote inspection, providing a common frame of reference.

In the plan view satellite images (Figure I-8), ancient point bars appear as semi-concentric ridges and swales. Two sets of semi-concentric ridges are shown in Figure I-8A, and are labeled with numbers 1 and 2 in the interpreted map in Figure I-8B. Photographs of the outcrop (see Figures 4e and 5a of Ielpi and Ghinassi, 2014) show these ancient and exhumed point bars to be topographically above channel deposits and show relatively level elevations for the ridges and swales, consistent with observations of modern point bars (Figure I-4). Mapping and field observations of grain sizes,

superposition, and dip directions suggest that point bars are adjacent to younger channel fills (Ielpi and Ghinassi, 2014). However, these channel-fill deposits and the relative ages of units are not apparent in our observations of satellite images, either because of high illumination angles producing low shadow widths, and/or because of low albedo contrast between point bars and channel-fill deposits (Figure I-8A). Based on this plan view examination, semi-concentric ridges and swales with relatively level elevations are a reliable morphological attribute of ancient point bars (Table I-2). However, interpretations of relative age (i.e., older vs. younger point bars) and adjacent fluvial units (i.e. channel fills) may require in-situ analyses, such as observations in three dimensions (Miall and Jones, 2003; Ielpi and Ghinassi, 2014).

With the relatively level topography of semi-concentric ridges and swales as an attribute of these exhumed point bars (Figure I-8), and the slightly decreasing topography of ridges and swales of modern point bars (Figure I-4), we now compare these topographic profiles with profiles of deposits in the Aeolis Dorsa region. A portion of the HiRISE image in Figure I-3B and a topographic profile show multiple, meter-scale, semi-concentric ridges and swales on the upper surface of a Type 1 flat feature (Figure I-9B). The Martian semi-concentric ridges in Figure I-9B are like the modern point bars along the Quinn River (Figure I-4) and the exhumed point bar deposits of the Jurassic Scalby Formation (Figure I-8), in that their elevations are within 1 to 2 meters of each other and do not increase toward the exterior of the meandering bend. Similarities of relative topography and plan view morphology of the modern terrestrial, ancient terrestrial, and Martian deposits support previous interpretations (e.g., Burr et al., 2009; Burr et al., 2010) that such Type 1 flat features exhibiting topographically level ridges and swales are point bars. However, as previously described, the topography of other Type 1 features (Figure I-9A), which show elevations of ridges and swales increasing towards the bend exterior, is not consistent with point bars and more consistent with laterally aggrading channel beds of a meandering fluvial channel (Matsubara et al., 2014). Thus, there are various types of meandering fluvial deposits – laterally aggrading channel beds and point bars – and topography offers a method to distinguish these different sedimentary units.

Ancient Channel Fills in Satellite Images

The plan view morphology of channel fills is apparent in large inverted fluvial deposits located southwest of Green River, Utah (Figure I-10). These inverted paleochannels are composed of Lower Cretaceous Cedar Mountain Formation (Harris, 1980), and have been studied as terrestrial analogs (Williams et al., 2007; Williams et al., 2009). Architectural elements composing these inverted paleochannels include massive, well-graded channel fills with W/T ratios of 5 to 28 (Harris, 1980). In plan view images, these channel fills have relatively flat upper surfaces and steep sides (Figure I-10).

Previous analyses identified point bars next to the channel fills and were used to interpret a meandering fluvial environment for most of the inverted deposits (Harris, 1980; Williams et al., 2007; Williams et al., 2009). However, in our plan view analysis of satellite images, semi-concentric ridges were not apparent (Figure I-10A) at locations previously mapped as point bars (Figure I-10B) (Harris, 1980). As a result, an inference

of point bars and a meandering fluvial environment on the basis of plan view morphology alone would not be possible here, although this inference might be possible with increased image resolution and/or albedo contrast between point bars and channel fills. Thus, from plan view observations alone, deposits with flat nondescript upper surfaces are consistent with channel fills, but they may be indistinguishable from adjacent point bars (Table I-2). Without additional facies information, the specific fluvial environment (e.g., meandering fluvial, high-strength floodplain) of channel fills is equivocal (Table I-2).

The featureless and nondescript upper surfaces of the channel-fill deposits in Utah are also apparent in the Type 2 flat features of Aeolis Dorsa (e.g., Figure I-3C). Based on similar nondescript upper surfaces and steep sides, we infer Type 2 flat features to be fluvial channel fills. It is possible that some Type 2 flat features contain point bars, but like the example in Utah, those point bars may be eroded, small, or otherwise unapparent. The possibility of unapparent point bars along the margins of Type 2 flat features contributes additional uncertainty to any measurement of apparent channel fill width.

In addition to the Type 2 flat features, some thin features in Aeolis Dorsa (e.g., Figures I-5) also have flat nondescript upper surfaces. Thus, based on this shared attribute of a flat nondescript upper surface, we also interpret thin features to be fluvial channel fills. Alternatively, these nondescript thin features could be interpreted as fluvial channel beds, but, because younger sediments, namely, channel fill, usually cover channel beds, we suggest that channel fill is a more reasonable explanation for such thin features.

Thin features that exhibit medial crests, rather than flat upper surfaces, may be explained as channel fills that have been eroded along their margins (cf. Burr et al., 2010). Thus, thin features with sharp medial crest, and those showing evidence for having their widths eroded (Burr et al., 2010), do not preserve original channel width for paleohydraulic analyses. However, thin features or portions of thin features with flat upper surfaces may preserve original channel widths, suitable for paleohydraulic analyses.

Alluvial Fan Deposits in Satellite Images

In this section, we describe the attributes of sedimentary units on two different types of alluvial fans, specifically debris flow units on the Dolomite Fan, CA and inverted channel fills of an exhumed Pliocene megafan in Oman. We compare morphologic attributes of the terrestrial examples with the morphologies of fans in the Aeolis Dorsa region to infer possible sedimentary units and formation processes.

The Dolomite Fan is the one active feature that we inspect for morphologic attributes. Although the aim of this work was to examine ancient deposits, our literature search did not reveal any documented examples of ancient debris flow fans exposed in plan view. We posit poor preservation or poor exposure as possible explanations for the lack of apparent debris-flow dominated alluvial fans.

The Dolomite alluvial fan, located 8 km east of Lone Pine, CA, displays morphologies of relatively old and young debris flow deposits (Blair and McPherson, 1998). In satellite images (Figure I-11), deposits of a flow in 1984 appear light grey,

whereas older deposits are brown, attributed to desert varnish (Blair and McPherson, 1998). Although no age was determined for the older deposits (Blair and McPherson, 1998), the contrast between the relatively bright, young deposits and darker, old deposits highlights the intermittency of hydrologic activity leading to fan accumulation (Beaty, 1970; Blair and McPherson, 1994; Blair and McPherson, 1998). The fan deposits consist of debris flow levees paired with downslope debris flow lobes. Individual debris flow lobes are difficult to distinguish because of their low relief (Figure I-11). However, levee ridges are apparent, especially for older deposits. Enhanced relief of older ridges is attributed to the winnowing of fine-grained material from the fan surface by secondary flows (Blair and McPherson, 1998). Thus, narrow parallel ridges on fans are consistent with debris flow levees, and lobes at fan termini are consistent with debris flow lobes (Table I-3) (Blair and McPherson, 1998; Blair and McPherson, 2009). Because debris flows require a significant mud fraction, the identification of debris flow levees and lobes in plan view images implies intermittent fluid flow with appreciable mud content eroded from catchments (Table I-3).

Geomorphic attributes of the debris flow deposits of the Dolomite fan are apparent on fans in the southern Aeolis Dorsa region (Figure I-12). Debris flow levees are suggested by the morphology of twin parallel ridges on a large fan (Figure I-12A). Elsewhere in southern Aeolis Dorsa, small channels connect to lobate features (Figure I-12B), which are interpreted to be debris flow lobes based on their plan view morphologic similarity to terrestrial debris flow lobes (Figure I-11; Table I-3). Analysis of these deposits supports previous interpretations of fan-shaped features as alluvial fans (e.g., Burr et al., 2009; Kite et al., 2015a). Identification of debris flow deposits in the Aeolis Dorsa region suggests, more specifically, that certain fans formed by inertial sedimentary processes and intermittent hydrologic activity with appreciable mud.

In the Sharqiya, Oman, Pliocene-Early Pleistocene alluvial fan deposits have been topographically inverted to form numerous sinuous ridges (Maizels, 1987; Maizels, 1990). Mapping and analysis of two large fan systems reveal that most ridges contain meter-scale, finning-upward, trough cross-bedded layers of sand and gravel, interpreted to be traction deposits (Maizels, 1990). The Omani alluvial fan deposits are multigenerational, appearing as stacked ridges (Figure I-13C). These stacked ridges exhibit various states of preservation, depending on the size of the original deposit and amount of induration by calcite cement (Maizels, 1990). Ridges I, II, and III are cut by modern wadis and gullies appear along ridge margins (Figure I-13C). Erosion has narrowed the ridges, especially ridge II. Furthermore, ridges iv & v have been eroded so much that they are indistinguishable from ridges I and III, respectively (Figure I-13C), suggesting uncertainty in the interpretation of generations from plan view examination alone.

The plan view morphologies of fan deposits in the northwest Aeolis Dorsa are consistent with the attributes of sheetflood deposits and traction deposits (Table I-3). The fan feature in Figure I-14 serves as an example. Fan ridges on the left have attributes similar to traction deposits, but fan ridges on the right are similar to both traction deposits and sheetflood deposits (Table I-3). Further analyses of terrestrial alluvial fan deposits

may help to identify unique morphologic attributes that distinguish sheetflood and traction deposits.

This examination of terrestrial alluvial fan deposits and comparison with fan features in Aeolis Dorsa suggests multiple sedimentary units of alluvial fans in Aeolis Dorsa, specifically debris flow levees, debris flow lobes, sheetflood deposits and/or traction deposits. This analysis provides more detailed descriptions of fans than previous investigations (e.g., Burr et al., 2009; Kite et al., 2015a), and suggests that they formed by heterogeneous processes: debris flow, sheetfloods, and/or traction flows.

Part 2: Geospatial Distribution of Features in Aeolis Dorsa

Locations of flat features, thin features, fan features, and Aeolis Serpens are shown in Figure I-15. Approximately 1600 individual features were delineated in the Aeolis Dorsa region. This number is an order of magnitude larger than a previously published total (Burr et al., 2009). This increase is largely explained by a different method for counting the features, as well as improved data coverage. The previous total (Burr et al., 2009) is the summation of individual areas that contain one or more features (e.g., networks of features). The total presented here represents the number of individual features, including features that form "links" of individual networks. Additionally, in superpositional examples (previously 'multilevel features' in Burr et al., 2009; e.g., Figure I-5B), the superposed thin features and their underlying flat features are counted separately. Also, in the previous total (Burr et al., 2009), areas were largely defined by data coverage. Since then, improved data coverage and resolution allow for counting all features.

Flat features are the most numerous, accounting for nearly two thirds of all features, and are the most broadly distributed across Aeolis Dorsa (Figure I-15A). They are found around the margins and lower elevations interior to the Aeolis and Zephyria Plana, with particular concentrations in the northwest, southwest, and southeast. Thin features are the second most abundant feature type (Figure I-15B). They are often found near and generally cluster in the same locations as networks of flat features, and may be superposed on individual flat features (e.g., Figure I-5B). However, thin features are less widespread than flat features and rarely form networks (Figure I-15B). Where thin features do form networks, they often exhibit braid-like patterns, in which individual thins bifurcate and reconnect with each other. Fan features have a limited geospatial distribution, and are often clustered at locations in the northwest and the southeast along the topographic margins of Aeolis Planum and Zephyria Planum (Figure I-15C). Aeolis Serpens, the longest feature, makes a southeast-northwest traverse through the broad topographic low between Aeolis and Zephyria Plana (Figure I-15D).

In summary, this analysis shows that the four types of fluvial and alluvial deposits in Aeolis Dorsa have distinctive geospatial distributions: flat features are widespread along the low interior margins of the two plana; thin are less widespread and found at slightly higher elevations; fan features are found at higher and more limited locations along the topographic margins, and Aeolis Serpens is the most prominent feature in the topographic low of central Aeolis Dorsa. Results of mapping four local areas – part

three, described next – suggest the sedimentary units representing these distinct geospatial distributions. Stratigraphic columns of the four local areas – part four – suggest the relative ages and changes through time of these geospatial distributions.

Part 3: Geomorphological Mapping of Local Areas

Results from mapping four local areas suggest that morphologies of the Aeolis Dorsa deposits are consistent with terrestrial morphologies for meander point bars, laterally aggrading channel beds, fluvial channel fills, and alluvial fans. Here we describe how specific fluvial and alluvial units have geospatial heterogeneities between northwest and southeast Aeolis Dorsa. Deposits of meandering fluvial environments, i.e., point bars and laterally aggrading channel beds, only appear in southeastern Aeolis Dorsa. Areas in northwestern Aeolis Dorsa contain fluvial deposits, specifically networks of fluvial channel fills, but no evidence of meandering. Debris flow deposits on alluvial fans only appear in the southeastern Aeolis Dorsa, whereas alluvial fans in the northwest exhibit only traction and/or sheetflood deposits. Adjacent to the fluvial and alluvial deposits are units of lava, MFF, and yardangs. Areas covered by craters, impact ejecta, or aeolian materials were not divided into units and are not shaded by a unit color in map figures. We first describe the southeastern mapping areas of Aeolis Dorsa (Areas 35 and 40) and then the northwestern areas of Aeolis Dorsa (Areas 45N and 45S) so that similarities and differences between adjacent areas and separate regions of Aeolis Dorsa are apparent (see Figures I-2 and I-15E for area locations).

Map of Area 35

Area 35 is adjacent to the eastern margin of Zephyria Planum, which appears in the northeast corner of the Area 35 map (Figure I-16). Type 2 flat features form a network along the margin of Zephyria Planum (Figure I-17A). We interpret these features to be fluvial channel fills based on their morphology of flat, nondescript upper surfaces, which are similar to terrestrial channel fill deposits (Table I-2). This network of fluvial channel fills connects to wide Type 1 flat features in central and eastern portions of Area 35 (Figure I-16). An example of the topography of this Type 1 flat feature shows meter-scale ridges and swales (Figure I-17B), whose horizontality is consistent with the topography of terrestrial meander point bars (Table I-2). However, these inferred point bar ridges exhibit qualitatively sharper crests than those on Earth (cf. Figure I-4) or elsewhere in Aeolis Dorsa (cf. Figure I-9B), possibly a result of enhanced aeolian abrasion and/or impact cratering. These point bars indicate regular supplies of water and sediment during formation, and stable channel banks.

Thin features have alternating flat upper surfaces and sharp-crests (Figure I-17B). We interpret these features as fluvial channel fills based on their similarity to terrestrial channel fills (Table I-2). These fluvial channel fills indicate hydrologic activity and sedimentation. However, point bars or other deposits associated with channel fills are not observed. It is not clear whether the absence of these meander deposits is due to lack of formation, e.g., poor floodplain development or stability, a lack of preservation, or that

they are unapparent in satellite images, similar to the terrestrial meander point bars adjacent to fluvial channel fills in Utah (Figure I-10).

Mounds have rough upper surfaces (Figure I-17C) and appear next to fluvial deposits (Figure I-16). Mound morphology is unlike the linear and sinuous morphologies of fluvial deposits and yardangs and suggests some other mode of deposition (e.g., air fall) and/or subsequent modification.

Fans features appear in the northwest and southwest portions of the area map (Figure I-16) and near mound-unit outcrops (Figure I-17C). Fan ridges radiate from fan apices (Figure I-17C) and have flat upper surfaces (Figure I-12A), which are consistent with traction deposits (Table I-3). Twin-parallel ridges are also present (Figure I-12A & I-17C), consistent with debris flow levees (Table I-3). These alluvial fan deposits indicate distributary flow away from the apex, infrequent hydrologic activity, and a loss of channel confinement. The debris flow deposits also indicate inertial sedimentary processes in the presence of mud (Table I-3). Each distributary alluvial fan is connected to a network that lies close to the margin of Zephyria Planum (Figure I-16). Ridges of these networks converge toward the apices of fans. We interpret these as paired tributary networks and distributary fans, which are most consistent with an alluvial fan system.

Yardangs appear throughout Area 35 (Figures I-16 & I-17A) and represent deposition of MFF. The northeast-southwest orientations of these yardangs suggest aeolian abrasion by a northeast-southwest paleo-wind in this local area (Figure I-16).

In summary, Area 35 contains (a) Zephyria Planum, (b) networks of fluvial channel fills connected to point bar deposits, (c) thin fluvial channel fills, (d) a unit of mounds, (e) alluvial fans with debris flow levees and traction deposits, and (f) yardangs of MFF. The fluvial and alluvial deposits preserved here represent distinct sedimentary environments. The meandering fluvial environments represented by point bar deposits required recurring, relatively steady hydrologic activity, stable floodplains, and relatively low slopes to form. In contrast, the alluvial fan deposits required infrequent, relatively flashy hydrologic activity, appreciable mud to initiate debris flows, an elevated slope relative to the depositional slopes of the fluvial deposits, and loss of channel confinement, such as at a topographic escarpment.

Map of Area 40

Area 40 is in southern Aeolis Dorsa, approximate 100 km southwest of Area 35 (Figures I-2 and I-15E). Area 40 is situated in a relative flat region but closer to the current location of the global dichotomy boundary (Figure I-15E).

Within this region, we distinguish two units of flat features (i.e., unit I and unit II) that are separated geospatially within the local mapping area (Figure I-18). We shade unit I purple in our mapping to distinguish it from unit II, which is shaded blue. Flat features unit I forms well-connected, sub-parallel networks of Type 2 flat features (Figure I-19A) in the eastern portion of Area 40. Although some of these flat features approach the widths of thin features, we classify them based on their network connections to relatively wide ridges (>100 m). We interpret the sub-parallel networks in eastern Area 40 as networks of fluvial channel fill based on their morphology (Table I-2), which can be seen in the largest ridges (Figure I-19A). We suggest these networks connect in the

subsurface with wide Type 1 flat features (Figure I-19B) in the northern and northwestern portions of Area 40 (i.e., they are partially covered by the mounds unit, described later). The Type 1 flat feature of unit I has meter-scale ridges and swales (profile B-B' in Figure I-19B), consistent with the topography of terrestrial meander point bar deposits (Table I-2), although it has irregular ridge amplitude, which may result from erosion by aeolian abrasion.

Flat features unit II has dendritic-like networks of Type 2 flat features in the southern portion of Area 40 (Figure I-18). We interpret these southern ridge networks as networks of fluvial channel fill (Table I-2). Channel fill networks in the previous Area 35 (Figure I-16) are more similar (e.g. wider junction angles) to the networks of unit II than the networks of unit I (Figure I-18). We, therefore, matched the blue color shade of unit II in Area 40 with the blue color of the fluvial networks in Area 35. The networks of fluvial channel fills on unit II in Area 40 connect to Type 1 flat features in the northwestern portion of Area 40 (Figure I-18). The morphology and topography of these Type 1 flat features has been previously shown in Figures I-4A and I-9A. As previously described in the results section on meander deposits, the topography of this Type 1 feature (Figure I-9A) is more consistent with laterally aggrading channel beds of a meandering fluvial channel, rather than meander point bar deposits because ridge elevation increases towards the exterior of the meander bend (Figure I-9A).

Thus, Area 40 has two units of flat features (unit I and unit II), each with networks of fluvial channel fills (Type 2 flat features) that connect to fluvial meander deposits (i.e., point bars in unit I, laterally aggrading channel beds in unit II). These meander fluvial deposits indicate regular supplies of water and sediment during formation, and stable floodplains to maintain meander dynamics.

Thin features appear on top of meander deposits in the northwestern portion of Area 40 (Figure I-19C). As in Area 35, we interpret these features as fluvial channel fills superposed on the fluvial meander deposits.

A mounds unit obscures flat features across the middle of Area 40 (Figure I-18). The mounds unit also has many sinuous troughs, some of which connect to lobes (Figure I-12B & I-19D). These lobes have irregular textures on their upper surfaces (Figure I-19D), which are unlike terrestrial debris flow lobes that have smooth surfaces (Figure I-11). The widths of these lobes increase away from the termini of troughs (Figure I-12B & I-19D). This morphology is most consistent will formation by alluvial processes, such as loss of flow confinement and lateral expansion during deposition. For these reasons, we interpret these troughs and lobes as alluvial channels and debris flow lobes, respectively. The formation of these deposits requires infrequent hydrologic activity, involvement of mud, and loss of channel confinement.

In summary, Area 40 preserves (a) two units of fluvial channel fills and meander fluvial deposits, (b) a separate unit of thin fluvial channel fills, and (c) a mounds unit with (d) incised channels and debris flow lobes. The fluvial and alluvial deposits in Area 40, like Area 35, represent distinct sedimentary environments with implicit differences in the frequency of hydrologic activity and paleotopography.

Map of Area 45N

Area 45N is the northern of the two areas in northwest Aeolis Dorsa, located to the east of Aeolis Planum (Figure I-15E). A cratered unit is exposed in the northwest corner of the mapping area (Figure I-20). This unit has smooth surfaces between craters, and a wrinkle ridge (Figure I-21A), both of which are consistent with features on lava plains north of Aeolis Dorsa (Kerber and Head, 2010 and references therein). An impact crater with an atypical morphology, similar to craters formed in the MFF (Kerber and Head, 2010), is superposed on this lava plains unit (Figure I-21A) indicating that the MFF previously extended over this area.

A unit of yardangs with northwest-southeast orientations is found next to the cratered unit. This unit indicates a period of MFF deposition and aeolian abrasion by a NW-SE paleo-wind (cf. de Silva et al., 2010). Dashed lines through the yardangs unit (e.g., south of the cratered unit) represent boundaries between possible sub-units of yardangs. These sub-units may suggest multiple episodes of MFF deposition; however, we do not investigate these sub-units further (e.g., through comparative morphometry) because they do not represent a change in sedimentary environment.

A third unit has Type 2 flat features with widths of a couple hundred meters (Figure I-21B) and morphologies consistent with fluvial channel fills (Table I-2). These fluvial channel fills converge eastward into a large fluvial deposit (Figure I-20) that is covered by another unit of NW-SE yardangs (Figure I-21C). Thin features superpose both the individual fluvial channel fills (Figure I-21B) and the large fluvial deposit (Figure I-21C). These thin features have flat upper surfaces, consistent with fluvial channel fills (Table I-2), and indicate a second episode of hydrologic activity and sedimentation.

In the northeastern portion of Area 45N (Figure I-20), the deposit with wide channel fills connects with Aeolis Serpens. The fluvial deposits in Area 45N, including Aeolis Serpens, are sinuous along some of their lengths (Figure I-21D), but do not show evidence for lateral migration, i.e., meandering or floodplain formation. Therefore, we interpret these features as evidence of hydrologic activity and sedimentation, but we cannot discern evidence of fluvial meandering with a regular hydrologic regime and stable floodplains (Table I-2).

A plateau unit appears in the eastern portion of Area 45N, adjacent to units of flat features and fan features (Figure I-20). One fan feature connects to the plateau (Figure I-21E), which likely represents the host material for this fan. In contrast, several fan networks on the west side of Area 45N are surrounded by yardangs (Figure I-20), which suggests that the MFF represents the host material for alluvial fan sedimentation in this location. Fan features in Area 45N form ridges and wide deposits with flat upper surfaces (Figure I-21E), which are consistent with sheetflood and/or traction deposits (Table I-3). Fan deposits in Area 45N exhibit neither debris flow levees nor lobes, which were apparent on fans in southern Aeolis Dorsa (Figures I-12, I-17C, and I-19D).

In summary, Area 45N preserves (a) cratered lava plains, (b) yardangs of MFF, (c) wide fluvial channel fills that amalgamate to form a large indurated deposit that in turn surrounds (d) Aeolis Serpens, (e) thin fluvial channel fills that superpose these wider channel fills, (f) a plateau unit, and (g) alluvial fans consisting of sheetflood and/or

traction deposits. Fluvial units in Area 45N do not show evidence of lateral migration, i.e., meandering, but are consistent with fluvial channel fills. Also, alluvial fans in Area 45N do not consist of debris flow deposits, and so do not imply the presence of mud in the catchment.

Map of Area 45S

Area 45S is the southern of two areas in northwest Aeolis Dorsa, located along the eastern margin of Aeolis Planum (Figure I-15E). Portions of Aeolis Planum appear in the southwestern corner of the mapping area (Figure I-22). In the northeast corner of the mapping area is a cratered unit with smooth surface texture between the craters and a wrinkle ridge (Figure I-23A). As in Area 45N, we interpret this unit as lava.

A large portion of Area 45S, including flat and thin features, is covered by yardangs of MFF with NW-SE orientations. These features indicate deposition of MFF followed by induration and then aeolian abrasion from a NW-SE paleo-wind. Like Area 45N, possible sub-units of yardangs were observed in Area 45S. These sub-units are delineated with dashed lines in the area map (Figure I-22) and may represent multiple deposits of MFF.

Flat features have nondescript upper surfaces (Figure I-23B), similar to the upper surfaces of terrestrial channel fills (Table I-2), but no evidence of meander deposits was observed. These fluvial channel fills form a network of ridges that connect in the northeast corner of the mapping area (Figure I-22).

Thin features have sharp crests rather than flat upper surfaces (Figure I-23C). We attribute the sharp-crest morphology to aeolian abrasion, which is evident in this area by the numerous yardangs. The sharp-crest morphologies of these thin features are consistent with eroded fluvial channel fills. As in all the other local mapping areas, these thin fluvial channel fills also appear on top of the fluvial deposits of flat features (Figure I-22).

The multiple morphologies of alluvial fan ridges in Area 45S have been previously shown in Figure I-14. Fan ridges may be up to a couple 100 meters wide with flat upper surfaces consistent with sheetflood deposits (Table I-3), or thin with sinuous patterns consistent with traction (Table I-3). However, no pairs of parallel ridges, indicative of debris flow deposits, were observed in Area 45S. Alluvial fans in Area 45S are connected to small, ridges (light pink units in Figure I-22). More extensive networks, as observed in other areas, have presumably been eroded.

In summary, Area 45S has (a) Aeolis Planum, (b) a cratered lava unit, (c) many yardangs of MFF, (d) wide fluvial channel fills that form a network, (e) thin superposing fluvial channel fills, and (f) alluvial fans of sheetflood and/or traction deposits. Similar to Area45N, fluvial channel fills in Area 45S show no evidence for meandering. Also, alluvial fans in Area 45S, like Area 45N, consist of sheetflood and/or traction deposits, but no evidence for debris flow deposits.

Part 4: Stratigraphy of Local Areas

Derivation and correlation of stratigraphic columns from these four local areas suggest that the preserved history of sedimentary environments in Aeolis Dorsa is regionally consistent, but also that it is locally varied. Stratigraphic columns (Figure I-24) show that the deposits of flat features, including meandering deposits and channel fills, represent the first episode of hydrologic activity and sedimentation in Aeolis Dorsa. This history is locally varied in that one area (Area 40) preserves two units of flat features, specifically meandering fluvial deposits, but other areas (Areas 35, 45N & 45S) exhibit only one unit of fluvial deposits. Stratigraphic columns generally show that the unit forming thin fluvial channel fills represents a subsequent episode of hydrologic activity and sedimentation and that the formation of alluvial fans was the last-preserved episode of hydrologic activity and sedimentation. This history is locally varied in that deposition of the mounds unit, which was limited to southeastern Aeolis Dorsa, preceded the alluvial deposits. Deposits of MFF occurred throughout the region, with a final episode of MFF deposition and yardang formation in Area 35. To elucidate this regionally consistent but locally varied history, we present our observations and interpretations in column order, from stratigraphically lowest to highest (Figure I-24). The width-to-thicknesses ratio of 30 for fluvial deposits (Gibling, 2006) was assumed to infer unit thicknesses based on measurements of unit widths, which are given in the text below.

Strata of Area 35

From our mapping of Area 35 described above, we identified 6 separate units (Figure I-16), which we examine in order to derive the stratigraphic column shown in Figure I-24. Zephyria Planum appears in the northeast corner of Figure I-16. The topographic profile A-A' is drawn across Area 35 and shows Zephyria Planum to be the highest local unit (Figure I-25), approximately 200 meters higher than the adjacent drainage network unit. The drainage network unit in profile A-A' (Figure I-25) and the network of fluvial channel fills (Figure I-17A) form near the topographic high of Zephyria Planum and slope down and away from the planum scarp. We postulate that Zephyria Planum once extended further towards the southwest and was in contact with the network of fluvial channel fills and the drainage network unit, but has since experienced cliff-retreat towards the northeast, perhaps in response to the hydrologic activity that formed the networks. If this postulate is accurate, it would suggest that Zephyria Planum is the oldest unit in Area 35 because it was in place prior to fluvial and alluvial activity. Therefore, we place the Zephyria Planum unit at the bottom of the stratigraphic column (Figure I-24), but give it jagged contacts because its thickness and relationship with other units are uncertain.

Fluvial deposits of flat features are the oldest fluvial deposits in Area 35 as indicated by superposition relationships. Figures I-17A and I-17B and the topographic profile B-B' in Figure I-25 show that thin fluvial channel fills stack on top of the flat channel fill and point bar deposits. The widths of these point bars and channel fills are up to 1 km. This width suggests a proportionate thickness, based on our posited W/T ratio of 30, of approximately 33 meters. However, the average relief of these fluvial deposits

is on the order of 100 meters, suggesting that the bottom 67 meters of material is MFF. Therefore, we place a 33-meter thick, flat features unit beneath other fluvial and alluvial units in the stratigraphic column for Area 35 and add 67 meters of MFF beneath the flat features unit (Figure I-24). Because this unit shows point bars on its upper surface (Figure I-17B), cross-stratification symbology is shown at the top of the unit in the column to indicate lateral accretion sets.

Thin fluvial channel fills above the flat feature unit indicate that the unit of thin fluvial channel fills is younger (Figure I-17A, I-17B, and Profile B-B' in Figure I-25). The average width of thin channel fills is ~60 meters, suggesting a proportionate deposit thickness of 2 meters. These thin channel fills have reliefs of approximately 25 meters, suggesting that the bottom 23 meters of material is MFF that acted as the substrate for fluvial activity and sedimentation. Therefore, we place a 2-meter thick, fluvial channel fill unit and 23-meter thick, unit of MFF above the flat features unit in the stratigraphic column of Area 35 (Figure I-24).

The mounds unit appears next to and is cut by the alluvial fans unit (Figure I-17C) indicating that the mounds are older relative to the fans. The topographic profile C-C' was drawn over a mound and plotted on the profile A-A' for comparison (Figure I-25). Profile C-C' shows the mounds unit has at least 50 meters of relief. We place the mounds unit below the alluvial fans unit in the stratigraphic column, but place a broken contact between the mounds unit and the unit of thin channel fills because no indication of relative age was observed in Area 35 (Figure I-24).

Alluvial fans have thicknesses of at least 50 meters, as shown in topographic profiles A-A' and B-B' (Figure I-25). Therefore, in the stratigraphic column, we place a 50-meter thick, alluvial fan unit on top of the mounds unit and separate the units with an erosional unconformity (Figure I-24). This unconformity is suggested by the cross-cutting relationship between the mounds and fans, which, in order to form, had to erode through portions of the mounds unit. Based on these erosional and cross-cutting relationships, we also infer that portions of the mound unit compose the alluvial fan sediment and add that material (i.e., brown clasts) to the stratigraphic unit (Figure I-24).

Yardangs are stacked on top of alluvial fans and also appear in the space between inverted fluvial deposits (Figures I-16 and I-17A). These relationships indicate that yardangs have the youngest relative age and formed after the topographic inversion of fluvial deposits. Yardangs have an average thickness of ~25 meters (Figure I-25). Therefore, we place a 25-meter thick, yardang unit on top of the alluvial fan in the stratigraphic column (Figure I-24). We add arrows to the right of the stratigraphic unit to indicate the direction (NE-SW) of the paleo-wind that abraded the yardangs.

Strata of Area 40

Mapping of Area 40 identified 5 units (Figure I-18), which we examine to derive the stratigraphic column shown in Figure I-24. Flat features unit I includes fluvial channel fills with an average width of ~300 meters (Figures I-19A). This width suggests channel fills are 10 meters thick, so we assign unit I a thickness of 10 meters in the stratigraphic column of Area 40 (Figure I-24). Meandering fluvial deposits of unit I appear in the northern and northwestern portions of Area 40 (Figures I-18 & I-19B).

Here, the lower contact, and therefore the underlying unit, is not apparent, but thicknesses are suggested to be greater than 10 meters based on widths of more than 1 kilometer (Figure I-18). Therefore, we give flat features unit I a jagged lower contact in the stratigraphic column to indicate a minimum thickness of 10 meters (Figure I-24).

Meander fluvial deposits of flat features unit II have widths up to ~1.5 kilometers (Figure I-18), suggesting maximum thickness of 50 meters. Also, the two large reaches of unit II separate and reconnect in the northwestern corner of Area 40, suggesting that unit II cuts through unit I. Therefore, we place a 50-meter thick unit of flat feature unit II above unit I in the stratigraphic column for Area 40 (Figure I-24).

The topographic profile A-A' is drawn over several units in Area 40 (Figure I-26) and shows that the relief of thin fluvial channel fills is ~10 meters. The average width of thin fluvial channel fills is approximately 50 meters (Figure I-19C), suggesting that the deposit is approximately 2 meters thick. Therefore, we place a 2-meter thick, fluvial channel fill unit and 8-meter thick unit of MFF above flat features unit II in the stratigraphic column (Figure I-24).

Mapping of the mounds unit in Area 40 (Figure I-18) suggests that it covers fluvial units, including flat features unit I and II, and the thin channel fills unit. Therefore, we place the mounds unit over other fluvial units in the stratigraphic column for Area 40 (Figure I-24). The topographic profile A-A' (Figure I-26) shows that the relief of the mounds unit is ~150 meters above flat features unit I, but this relief varies as exhibited by many knobs in Area 40. Without observations in cross-section, the orientation of the contact between the mounds unit and the underlying fluvial units is uncertain. Therefore, we place a 150-meter thick, mounds unit in the stratigraphic column of Area 40, but add a jagged lower contact to indicate an uncertain thickness (Figure I-24).

Troughs and lobes in Area 40 are evidence of erosion and alluvial sedimentation, largely occurring within the mounds unit (Figures I-12B, I-18 and I-19D). The topographic profile A-A' shows the debris flow lobes to be approximately 15 meters thick (Figure I-26). Lobe material was likely derived from the mounds unit during trough erosion suggesting an erosional unconformity between the debris flow lobes and the underlying mounds unit. We place 15-meter thick alluvial unit, composed of mounds material (i.e., brown clasts), at the top of the stratigraphic column for Area 40 (Figure I-24).

The lithology and order of units in Area 40 is consistent with those in Area 35, but the units are not equal in number or thicknesses (Figure I-28). Both locations have fluvial, alluvial, and mounds units. Also, in stratigraphic order, the mounds unit separates fluvial units from alluvial units in both areas. Area 40 differs from Area 35 in that it has two units (I & II) of flat features, while Area 35 only has one. All three of these flat feature units preserve meandering fluvial deposits.

Strata of Area 45N

We examine the stratigraphy of the 7 mapped units in Area 45N (Figure I-20) to derive the stratigraphic column in Figure I-24. The cratered lava unit (Figure I-21A), is exposed in the northwest corner of the mapping area (Figure I-20) and is the

topographically lowest unit, as shown in the topographic profile A-A' (Figure I-27). The topography of the cratered lava suggests that it is flat lying and may project beneath other units in the area. However, we give the cratered lava unit jagged contacts in the stratigraphic column because we cannot confirm the nature of these subsurface contacts and the lateral extent of this unit.

The plateau unit appears in the eastern portion of Area 45N (Figure I-20) and is older than fluvial and alluvial units based on superposition and embayment relationships. Flat and thin fluvial channel fills (Figures I-21B and I-21C) appear to converge towards the plateau unit in southern Area 45N (Figure I-20). From southern Area 45N, these fluvial channel fills form a wide deposit that extends to the north and then to the east, possibly wrapping around the plateau unit. Based on this geospatial arrangement, we infer that the wide deposit of fluvial channel fills embays (i.e., on-laps) the plateau unit. This inference implies that the plateau unit is older than fluvial units in Area 45N. Also, the drainage network unit of an alluvial fan superposes and crosscuts the plateau unit (Figure I-21E) indicating that the plateau unit is older. Therefore, we place the plateau unit below fluvial and alluvial units (Figure I-24), but also give it jagged edges because these subsurface interpretations are uncertain.

Fluvial channel fills of flat features have reliefs of 200 and 150 meters on either end of topographic profile A-A' (Figure I-27). This relief represents thick deposits, some of which are the fluvial channel fill observed at the surface. The remaining deposits are interpreted to be one or multiple units of MFF that forms yardangs throughout the area. The fluvial channel fills in southwestern Area 45N have widths up to ~750 meters (Figure I-21B), which suggests a maximum deposit thickness of 25 meters. These fluvial channel fills converge into a deposit up to ~7 km wide (Figure I-21B and I-21C). A single channel of this width would imply a unit thickness of approximately 230 meters. However, we interpret this wide deposit to be an amalgamation of the much smaller fluvial channel fills rather than a single channel (Figure I-21C). Therefore, assuming the same 750-m width for all the amalgamated fluvial channel fills, we place a 25-meter fluvial channel fill unit above a 125-meter-thick MFF unit in the stratigraphic column (Figure I-24). We also give the MFF unit jagged lower contacts to indicate a minimum thickness and uncertain contact with the plateau unit.

Aeolis Serpens appears in the northeast corner of Area 45N (Figure I-21D) and is covered twice by the topographic profile A-A' (Figure I-27). The profile shows that Aeolis Serpens has approximately ~25 meters of relief. Measurements of width indicate that Aeolis Serpens has an average width of 500 meters, suggesting a thickness of approximately 16 meters. Therefore, we place a 16-meter thick unit for Aeolis Serpens underlain by a 9-meter thick unit of MFF in the stratigraphic column for Area 45N (Figure I-24).

Thin fluvial channel fills in southern Area 45N (Figures I-20, I-21B, and I-21C) have average widths of 60 meters, which suggest a thickness of 2 meters. The resolution of MOLA topography is not sufficient to resolve the relief of these fluvial channel fills. We assume a relief of 10 meters, based on the reliefs of similar thin fluvial channel fills resolved in the topographic profile in Area 40 (Figure I-26). The relative ages of thin fluvial channel fills and Aeolis Serpens are unknown without superposition or cross-

cutting relationships. We posit an 8-meter thick MFF unit beneath a 2-meter thick thin channel fill unit in the stratigraphic column. We give the channel fill unit a jagged lower contact with Aeolis Serpens to indicate that this relationship is not known. Rather than thin channel fills forming before Aeolis Serpens, we prefer the interpretation that the paleochannel Aeolis Serpens came after the flat features unit, as is shown in Figure 24. This preferred interpretation is based on the regional extent of Aeolis Serpens with a high degree of continuity along its length (Figure I-15D), suggesting an episode of widespread and perhaps through-flowing hydrologic activity (Williams et al., 2013). Such hydrologic activity is similar to that implied by flat features (Figure I-15A) and unlike that implied by thin features, which appear discontinuous throughout Aeolis Dorsa (Figure I-15B).

One alluvial fan and corresponding drainage network appear in eastern Area 45N (Figure I-20) and are in contact with the plateau unit. The topographic profile A-A' suggests that the alluvial fan is ~100 meter higher than the fluvial channel fills (Figure I-27). The relief along the profile that covers the fan suggests a fan thickness of only 40 meters, implying that the remaining 60 meters is some other material beneath the fan. We suggest that this material is another unit of MFF deposited over the fluvial channel fills and then covered by the alluvial fan. This second deposit of MFF would explain the origins of the yardangs that cover fluvial channel fills (Figure I-21C). Based on this inference, we place a 60 meter-thick unit of MFF beneath a 40-meter thick, unit of the alluvial fan unit in the stratigraphic column for Area 45N (Figure I-24). In the stratigraphic column, we do not give the alluvial clasts a color because fans in Area 45N are comprised of either sheetfloods or traction deposits, which do not require the presence of mud (Table I-1).

Strata of Area 45S

We examine the stratigraphy of 6 mapped units in Area 45S (Figure I-22) to derive the stratigraphic column in Figure I-24. Like Area 45N, Area 45S also has a cratered lava unit (Figure I-23A). The topographic profile in Figure I-28 shows that these lava plains are the topographically lowest unit. Therefore, we place this unit at the bottom of the stratigraphic column, suggesting that all other units (e.g., MFF) have been emplaced on to these lava plains. However, we give this unit jagged contacts because its thickness and lateral extent are uncertain.

Aeolis Planum in Area 45S does not contact any fluvial or alluvial units. However, remnants of drainage networks are connected to fan apices (Figure I-22) and are oriented towards Aeolis Planum (i.e., in a northeast-southwest direction), suggesting that larger, now eroded, drainage networks may have extended towards and been in contact with Aeolis Planum. Like Zephyria Planum in Area 35, we interpret the current position of Aeolis Planum to be the product of cliff-retreat towards the southwest. Based on this interpretation, we place Aeolis Planum beneath alluvial and fluvial units in the stratigraphic column, but give it jagged edges since its thickness and relationships with the MFF and cratered units are uncertain.

Yardangs of MFF comprise a large portion of Area 45S (Figure I-22). From examination of the CTX mosaic and topographic profile of Area 45S, we interpret at least

three separate units of MFF based on observations of strata interleaved with fluvial and alluvial units.

Fluvial channel fills of flat features form networks in Area 45S. The topographic profile shows that channel fills have reliefs on the order of 200 meters (Figure I-28) and an average width of ~450 meters. These dimensions suggest an average thickness of 15 meters for the fluvial deposit and 185 meters of MFF to account for the remaining relief. This underlying deposit represents the first unit of MFF, which likely forms yardangs in lower elevations of Area 45S. Based on these interpretations, we place a 185-meter thick, MFF unit beneath a 15-meter thick, fluvial channel fill unit in the stratigraphic column (Figure I-24). The MFF unit has a jagged lower contact because the nature of the contact with Aeolis Planum is uncertain.

Thin fluvial channel fills are discontinuous in Area 45S (Figure I-22), but have reliefs on the order of 10 meters and an average with of ~45 meters, suggesting an average fill thickness of 3 meters (Figure I-28). Therefore, in the stratigraphic column for Area 45S (Figure I-24), we place a 7-meter thick unit of MFF beneath a 3-meter thick unit of thin fluvial channel fill. This underlying deposit represents the second unit of MFF, which may also form yardangs in the areas adjacent to (Figure I-23C) and on top of fluvial channel fills (Figure I-23B).

Alluvial fans appear in the southern and northwestern portions of Area 45S (Figure I-22). The topographic profile shows the top of the alluvial fan is ~200 meters above the fluvial units (Figure I-28). The relief along the profile that covers the fan suggests a fan thickness of only 80 meters, implying that the remaining 120 meters is some other material beneath the fan. Therefore, we place a 120-meter thick unit of MFF, beneath an 80-meter thick alluvial fan unit (Figure I-24).

In summary, the stratigraphic columns for Areas 45N and 45S are mutually consistent, but not uniform, much like the regional stratigraphy of Aeolis Dorsa. For both areas, their hydrologic histories begin with large networks of fluvial channel fills, which eventually transition to discontinuous thin channel fills, and finally alluvial fans. This transition is also consistent with the stratigraphic columns of Areas 35 and 40 in southeastern Aeolis Dorsa, which show the same relative sequence of units (Figure I-24). However, these stratigraphic columns are not uniform in that Area 45S is nearly twice as thick as other areas. This greater thickness may be due to a larger amount of exhumation and erosion, which are suggested by the prevalent yardangs.

Discussion

Synthesis of Aeolis Dorsa History

The preceding results provide insightful information about the history of Aeolis Dorsa. Area maps and stratigraphic columns (i.e., parts 3 and 4 of the investigation) suggest four units predate fluvial deposits in Aeolis Dorsa: Zephyria Planum, the plateau unit, the cratered lava plains unit, and Aeolis Planum (Figure I-24). Stratigraphic relationships among these pre-fluvial units are unclear from our results, but we suggest two scenarios. In the first scenario, the cratered unit projects beneath Aeolis Planum in

Areas 45S and 45N, indicating an older age for the cratered unit. This first scenario is consistent with the results of radar analyses over northern plains lavas and Zephyria Planum, showing a horizontal reflector projecting beneath the MFF (Watters et al., 2003; Carter et al., 2009). However, the presence of a similar radar reflector has not been demonstrated for areas near Aeolis Planum. In the second scenario, the cratered unit embays Aeolis Planum, indicating a younger age for the cratered unit. This second scenario has been documented for Hesperian-age lavas north of Area 45N (Kerber and Head, 2010). However, embayment is not apparent in our mapping areas.

Synthesis of stratigraphic columns is consistent with a regional transition from fluvial to alluvial processes. Maps and stratigraphic columns suggest four different fluvial units: two units (I and II) of fluvial deposits, Aeolis Serpens, and thin fluvial channel fills. Two units of flat features were mapped in Area 40, suggesting this area in southeastern Aeolis Dorsa preserves a rich history of hydrologic activity and sedimentation. In all cases, the fluvial units are beneath, and therefore predate, the alluvial units.

Within this regionally consistent transition, our application of terrestrial-based attributes (i.e., part 1) to the four mapping areas indicates geospatial heterogeneity of sedimentary units. This geospatial heterogeneity is represented in that meandering fluvial deposits are found only in southeastern Aeolis Dorsa (Figure I-24). Overall, these deposits imply regular supplies of fluid and sediment. We propose that higher elevations in southern Aeolis Dorsa were more favorable for stable channel banks, and therefore meandering channels. Higher elevations in southern Aeolis Dorsa may have favored orographic precipitation (Burr et al., 2009; cf. Scanlon et al., 2013), weathering, and greater yield of cohesive sediments, i.e., clays, needed for bank stabilization (cf. Matsubara et al., 2014).

Aeolis Serpens is an unusually long and continuous fluvial deposit oriented southeast-to-northwest across Aeolis Dorsa (Figure I-15D). Aeolis Serpens appears to connect with fluvial channel fills in Area 45N, but we did not observe connections between Aeolis Serpens and fluvial units in southern Aeolis Dorsa. Therefore, it is unclear whether Aeolis Serpens is a separate deposit that formed after the flat features unit (Figure I-24) or if Aeolis Serpens is part of the northernmost extension of the widespread fluvial deposits in southern Aeolis Dorsa (Kite et al., 2015a).

Maps and stratigraphic columns of each area show fluvial channel fills of thin features. We interpret these thin fluvial channel fills as the last-preserved episode of fluvial activity and sedimentation (Figure I-24). Fluvial activity and sedimentation may have occurred after the formation of thin channel fills, but cementation and/or burial processes (Figure I-1) were insufficient at preserving such deposits. Delineations throughout Aeolis Dorsa (Figure I-15B) suggest that this last-preserved episode formed discontinuous deposits that were less widespread than the older fluvial deposits of flat features (Figure I-15A).

Superposition and cross-cutting relationships in Areas 35 and 40 suggest that the mounds unit formed after the fluvial deposits and before the alluvial fans. We interpret the mounds unit as an extensive deposit in southern Aeolis Dorsa that hosted later alluvial fans. Our mapping implies either that deposition of this unit was confined to the southern

Aeolis Dorsa or that the unit was preferentially eroded in the north. Distinguishing between these two possibilities requires a more extensive mapping and characterization of the mounds unit.

Alluvial fans appear in each local area and represent the final episodes of hydrologic activity in Aeolis Dorsa. Whereas older fluvial deposits of flat features imply regular hydrologic activity over low slopes, alluvial fans imply intermittent hydrologic activity in areas with enhanced relief. Thus, this stratigraphic change from fluvial to alluvial deposit implies changes in both climate and topography. Tectonic activity, such as normal faulting along the interior margins of Aeolis and Zephyria Plana, is one viable cause of enhanced relief later in the history of the Aeolis Dorsa region.

Interpretation of alluvial deposits in light of terrestrial analogs suggests geospatial heterogeneity of the alluvial deposits. Specifically, only fans of southeast Aeolis Dorsa exhibit debris flow morphologies, whereas fans in northwest Aeolis Dorsa exhibit sheetflood or traction deposits (Figure I-24). The interpretation of debris flow deposits implies that mud was present in southeastern Aeolis Dorsa. The coincidence of debris flow deposits with the mounds unit suggests that mud may have been sourced from the mounds unit (Figure I-24).

Involvement of mud in these southeastern alluvial deposits is consistent with our interpretation of more cohesive material, i.e., clays, required to form meandering fluvial deposits in southeastern areas. As with the meandering fluvial deposits, we suggest that higher elevations in southeastern Aeolis Dorsa were favorable for orographic precipitation (cf. Scanlon et al., 2013), weathering, and involvement of mud in alluvial processes. In comparison, the relative dearth of meandering fluvial deposits and lack of evidence for debris flow fans in northwestern Aeolis Dorsa may suggest that these lower elevations did not experience such clay-production.

The youngest unit mapped in Aeolis Dorsa is a unit of yardangs located in Area 35 (Figure I-24). This unit represents a deposit of MFF and aeolian abrasion by a paleo-wind with a northeast-southwest orientation. Maps and stratigraphic columns (Figure I-24) indicate that yardangs of MFF are interleaved with fluvial and alluvial deposits throughout Aeolis Dorsa, showing that widespread sedimentation and subsequent aeolian abrasion represent a significant part of the regional history.

Assessment of Hypotheses

Previous analyses of fluvial and alluvial strata in Aeolis Dorsa examined units and unconformities at regional scales, resulting in the hypotheses that the Aeolis Dorsa region experienced (1) a regional transition from fluvial to alluvial deposits (Kite et al., 2015a) and (2) a decrease in hydrologic activity through time (Kite et al., 2015b). These findings, which then formed the hypotheses for our work, are largely supported by our results. Whereas the previous analyses considered regional scales, we applied a complementary approach, using terrestrial analogs and analyses at local scales. Our local analyses identified specific fluvial and alluvial sedimentary units and heterogeneities in the processes that form the Aeolis Dorsa deposits. Analyses of these sedimentary units and their stratigraphy imply a decrease in hydrologic activity through time. Specifically,

the transition from meandering fluvial and channel fills to alluvial fans implies a change in the frequency of hydrologic activity, from frequent to intermittent. Thus, the overall findings of our analysis are consistent with those of the previous research (Kite et al., 2015a; 2015b).

Compared to the previous work, these results effectively increased the specificity of conditions and processes active in the Aeolis Dorsa region. While the overall findings of our analysis are consistent with those of the previous research (Kite et al., 2015a; Kite et al., 2015b), there are some differences. For example, our flat features unit 1, flat features unit 2, Aeolis Serpens, and the thin features unit compose one unit (R-1) in the previous analysis of stratigraphy (Kite et al., 2015a). Also, additional mapping of the mounds unit, beyond our local areas, suggests that the unit contains fluvial deposits (unit R-2 of Kite et al., 2015). These fluvial deposits are younger and less widespread than the deposits that compose flat features, suggesting that this additional information does not change the overall history of decreasing frequency and geospatial extent of hydrologic activity in Aeolis Dorsa. We attribute these differences to the particular methods used to elucidate the history of Aeolis Dorsa, i.e., regional verses local analyses.

Comparison with Martian Hydrologic History

The relative ages and geospatial distributions of fluvial deposits and alluvial fans in Aeolis Dorsa is remarkably similar to the timing and distribution of valley networks and alluvial fans on Mars. Overly simplistic descriptions of ancient Mars as either 'wet' or 'dry' can be rendered in more specific terms of geospatial distribution, frequency, and duration of hydrologic activity over time (Figure I-29). Valley networks throughout the southern highlands preserve widespread and frequent (perhaps seasonally controlled) hydrologic activity during the Late Noachian-Early Hesperian transition (Howard et al., 2005; Fassett and Head, 2008; Barnhart et al., 2009; Hynek et al., 2010). They include valley networks near Aeolis Dorsa, such as Al-Qahira Vallis, which has been dated to between 3.7 and 3.5 Ga (Fassett and Head, 2008). Some valley networks of this period are connected to large alluvial fans within craters (Fassett and Head, 2005; Moore and Howard, 2005; Williams et al., 2011).

Later, during the Late Hesperian and Early Amazonian, valley networks were fewer in number and generally limited to plateaus around Valles Marineris, the flanks of some volcanoes, and the margins of the Hellas Basin (Mangold et al., 2004; Fassett and Head, 2008; Hynek et al., 2010). Furthermore, local and regional analyses of alluvial fans suggest shorter durations of hydrologic activity relative to older fans, consistent with infrequent episodes of run-off during the Late Hesperian and Early Amazonian (Grant and Wilson, 2011; Williams et al., 2011; Hauber et al., 2013; Parsons et al., 2013).

Based on these observations of fluvial networks and alluvial fans distributed across Mars, we suggest that the Aeolis Dorsa deposits encapsulate the Martian hydrologic timeline. Older, widespread fluvial deposits in Aeolis Dorsa are consistent with climatic episodes of hydrologic activity that formed widespread valley networks in the southern highlands during the Noachian-Hesperian transition. Localization of

hydrologic activity and the formation of alluvial fans in Aeolis Dorsa are consistent with the distribution of alluvial fans in craters during the Hesperian and Amazonian epochs.

Conclusions

1. Inspection of fluvial and alluvial deposits in the rock record on Earth, and the observable geomorphic attributes derived therefrom, elucidate specific sedimentary units and support previous interpretations of sedimentary environments in the Aeolis Dorsa region. Terrestrial point bar deposits remain level or decrease slightly in elevation towards the exterior of a meander bend, whereas laterally aggrading channel deposits increase, so that topography of these deposits, if not eroded or overlain by other material, can be used to distinguish these two types of deposits. On this basis, we find that the relatively level topography of semi-concentric ridges on some Martian flat features (Type 1) is indicative of point bars laid down by meandering rivers, whereas instances where semi-concentric ridge topography increases from interior to exterior of channel bends is more consistent with a laterally aggrading channel bed. Based on similarities to an example in Utah, flat features with nondescript upper surfaces lacking semi-concentric ridges (Type 2) are consistent with fluvial channel fills. Thus, we here divide flat features into two subgroups that encompass three different fluvial sedimentary units: point bars, laterally aggrading channel bed, and channel fills. Thin features are also consistent with fluvial channel fills, although narrower than flat features. Based on analyses of terrestrial channel fills (Gibling, 2006), the widths of these pre-eroded channel fills represent former active channel widths, and so can be used in paleohydraulic analyses. Alluvial fans in Aeolis Dorsa have deposits with levees and lobes, which are consistent with terrestrial debris flow deposits and imply formation in the presence of mud. Morphologies of other fan deposits are consistent with sheetflood deposits or traction deposits, which do not require the presence of mud during formation.

2. Fluvial and alluvial deposits have distinct geospatial distributions in Aeolis Dorsa. Deposits consistent with point bars and broad fluvial channel fills are widespread. Thin fluvial channel fills are less widely distributed than either the meandering fluvial deposits or the broad channel fills. Alluvial fans are most limited in their distribution, found interior to the topographic margins of Aeolis and Zephyria Plana.

3. Maps of local areas show fluvial units, alluvial units, cratered lava units, and units of MFF that have been emplaced, indurated, and modified by aeolian processes to form yardangs. Heterogeneities of fluvial and alluvial units exist between northwest and southeast Aeolis Dorsa. First, meandering fluvial deposits, i.e., point bars and laterally aggrading channel beds, only appear in southeast Aeolis Dorsa (i.e., Area 35 and 40) and are not observed in northwest Aeolis Dorsa (i.e., Area 45N and 45S). Areas in northwest Aeolis Dorsa only preserve networks of

fluvial channel fills. Second, alluvial fans with debris flow levees and lobes only form in southeast Aeolis Dorsa, whereas fans in northwest Aeolis Dorsa are consistent with traction and/or sheetflood deposits. Appreciable clays in the southeast Aeolis Dorsa may explain these heterogeneities in processes and resultant sedimentary units. More abundant clays may have provided sufficient bank cohesion to maintain meandering of fluvial channels (cf. Matsubara et al., 2015) and would have been necessary to initiate debris flow processes (Table I-3; cf. Blair, 1999). Enhanced orographic precipitation and weathering proximal to the Highland-Lowland Boundary is one plausible explanation for this inferred relative abundance of clays in southeast Aeolis Dorsa. This explanation is consistent with previous atmospheric modeling, which predicts enhance snowmelt at this location (Kite et al., 2013).

4. Stratigraphic columns of local areas show a regionally consistent but locally varied fluvial and alluvial history. Across the Aeolis Dorsa region, stratigraphic units show a transition from networks of meandering fluvial deposits and broad fluvial channel fills, to intermediate thin fluvial channel fills, and finally alluvial fan deposits of debris flows, sheetfloods, and/or traction deposits. This stratigraphy implies i) a decrease in the frequency of hydrologic activity and ii) a late increase in topographic relief, as would be formed by tectonic faulting. However, while the regional stratigraphy is broadly consistent, it is not spatially uniform. That is, the same type and number of fluvial and alluvial units do not appear in each mapping area.

5. Coupling the geospatial distributions of deposits (conclusion 2) with the stratigraphy of deposits (conclusion 4) implies that the geospatial distribution of deposits in Aeolis Dorsa decreased over time. This decrease is represented by the transition from older widespread fluvial deposits to the geospatially-localized alluvial fans. Also, coupling the types of sedimentary units (conclusion 3) with stratigraphy (conclusion 4) implies that the history of Aeolis Dorsa transitioned from frequent episodes of hydrologic activity in fluvial sedimentary environments to localized, intermittent, and "flashy" episodes of hydrologic activity in alluvial sedimentary environments.

The hydrologic history of Aeolis Dorsa, its transition from predominately fluvial to alluvial deposits and decrease in geospatial distribution, are largely similar to the hydrologic timeline for Mars. While these similarities suggest the Aeolis Dorsa deposits are like other features on Mars, the Aeolis Dorsa region stands unique in preserving a diversity and abundance of exhumed fluvial and alluvial deposits (e.g., Burr et al., 2009; Kite et al., 2015a) that encapsulate the global hydrologic history of Mars.

Future Work

Previous analyses have examined the paleohydrology of certain features in Aeolis Dorsa (Burr et al., 2010; Williams et al., 2013) or well-exposed stratigraphic logs (Kite et

al., 2015b), but knowledge of sedimentary environment is critical for valid paleohydraulic analyses and proper inference of initial channel dimensions (e.g., width and depth). The stratigraphy of sedimentary environments presented here will be augmented with a "hydro-stratigraphy" of paleodischarge estimates, derived from models (e.g., terrestrial-based form-discharge relationships) that are appropriate to the sedimentary environment of each stratigraphic unit.

A time-stratigraphic maximum age of the fluvial deposits in Aeolis Dorsa is essential for augmenting the fluvial history of Mars with the record of Aeolis Dorsa. A maximum age for the fluvial and alluvial deposits may be found through a more thorough geologic mapping of possible basement and host units in regions surrounding the Aeolis Dorsa, like lava plains to the north (Figure I-2A) (Tanaka et al., 2003; Kerber and Head, 2010) or Aeolis Mensae to the east (Figure I-2B) (Irwin et al., 2004). Geologic mapping and stratigraphic correlations in these areas may benefit from, and may mutually benefit, the in-situ investigation of geologic history, sedimentary environments, and habitability at Gale Crater (e.g., Grotzinger et al., 2014).

The terrestrial-based geomorphological attributes presented here might serve other locations that have evidence for substantial hydrologic activity (e.g., Eberswalde crater). However, the criteria are by no means comprehensive and should be refined and augmented with additional plan view examples of ancient terrestrial deposits (e.g., ancient deltas). Also, further examinations of sheetflood and traction deposits on terrestrial alluvial fans are necessary to identify geomorphic attributes that distinguish these deposits in plan view satellite images.

Alluvial fan deposits in southeast and northwest Aeolis Dorsa imply late formation of relatively steep slopes, possibly formed by tectonic activity. The cause and structure of tectonic activity in Aeolis Dorsa may be associated with regional compression and the formation of reverse faults, or regional extension and the formation of normal faults, or both. Analyses of inferred tectonic features, such as wrinkle ridges within Aeolis Dorsa and rectilinear troughs in Aeolis Mensae, may suggest the type of relief-forming deformation in southeast and northwest Aeolis Dorsa.

Although preliminary spectral analyses have shown that regional dust coverage effectively obscures observations in near-infrared wavelengths, an in-depth analysis of high-resolution CRISM images has not been performed. If possible, spectroscopy analyses should examine the Aeolis Dorsa region for weathered materials, which are needed to explain meandering fluvial deposits and debris flow deposits.

References

Barnhart, C.J., Howard, A.D., and Moore, J.M., 2009, Long-term precipitation and late-stage valley network formation: Landform simulations of Parana Basin, Mars: Journal of Geophysical Research: Planets, v. 114, no. E1, p. E01003, doi: 10.1029/2008JE003122.

Beaty, C.B., 1970, Age and estimated rate of accumulation of an alluvial fan, White Mountains, California, U.S.A: American Journal of Science, v. 268, no. 1, p. 50–77, doi: 10.2475/ajs.268.1.50.

Blair, T.C., 1987, Sedimentary Processes, Vertical Stratification Sequences, and Geomorphology of the Roaring River Alluvial Fan, Rocky Mountain National Park, Colorado: Journal of Sedimentary Research, v. 57, no. 1, p. 1–18, doi: 10.1306/212F8A8A-2B24-11D7-8648000102C1865D.

Blair, T.C., 1999, Cause of dominance by sheetflood vs. debris-flow processes on two adjoining alluvial fans, Death Valley, California: Sedimentology, v. 46, no. 6, p. 1015–1028, doi: 10.1046/j.1365-3091.1999.00261.x.

Blair, T.C., 2000, Sedimentology and progressive tectonic unconformities of the sheetflood-dominated Hell's Gate alluvial fan, Death Valley, California: Sedimentary Geology, v. 132, p. 233-262, doi: 10.1016/S0037-0738(00)00010-5.

Blair, T.C., and McPherson, J.G., 1994, Alluvial fans and their natural distinction from rivers based on morphology, hydraulic processes, sedimentary processes, and facies assemblages; discussion and reply: Journal of Sedimentary Research, v. 65, p. 706–711, doi: 10.1306/D42681B2-2B26-11D7-8648000102C1865D.

Blair, T.C., and McPherson, J.G., 2009, Processes and Forms of Alluvial Fans, *in* Parsons, D.A.J. and Abrahams, A.D., eds., Geomorphology of Desert Environments: Springer, Netherlands, p. 413–467.

Blair, T.C., and McPherson, J.G., 1998, Recent debris-flow processes and resultant form and facies of the Dolomite alluvial fan, Owens Valley, California: Journal of Sedimentary Research, v. 68, no. 5, p. 800–818, doi: 10.2110/jsr.68.800.

Bradley, B.A., Sakimoto, S.E.H., Frey, H., and Zimbelman, J.R., 2002, Medusae Fossae Formation: New perspectives from Mars Global Surveyor: Journal of Geophysical Research: Planets, v. 107, no. E8, p. 2–1, doi: 10.1029/2001JE001537.

Brookes, I.A., 2003, Palaeofluvial estimates from exhumed meander scrolls, Taref Formation (Turonian), Dakhla Region, Western Desert, Egypt: Cretaceous Research, v. 24, no. 2, p. 97–104, doi: 10.1016/S0195-6671(03)00033-8.

Burr, D.M., Enga, M.-T., Williams, R.M.E., Zimbelman, J.R., Howard, A.D., and Brennand, T.A., 2009, Pervasive aqueous paleoflow features in the Aeolis/Zephyria Plana region, Mars: Icarus, v. 200, no. 1, p. 52–76, doi: 10.1016/j.icarus.2008.10.014.

Burr, D.M., Williams, R.M.E., Wendell, K.D., Chojnacki, M., and Emery, J.P., 2010, Inverted fluvial features in the Aeolis/Zephyria Plana region, Mars: Formation mechanism and initial paleodischarge estimates: Journal of Geophysical Research: Planets, v. 115, no. E7, p. E07011, doi: 10.1029/2009JE003496.

Carr, M.H., 2012, The fluvial history of Mars: Philosophical Transactions of the Royal Society of London A: Mathematical, Physical and Engineering Sciences, v. 370, no. 1966, p. 2193-2215, doi: 10.1098/rsta.2011.0500.

Carr, M.H., and Head, J.W., 2010, Geologic history of Mars: Earth and Planetary Science Letters, v. 294, no. 3–4, p. 185–203, doi: 10.1016/j.epsl.2009.06.042.

Carter, L.M., Campbell, B.A., Watters, T.R., Phillips, R.J., et al., 2009, Shallow radar (SHARAD) sounding observations of the Medusae Fossae Formation, Mars: Icarus, v. 199, no. 2, p. 295–302, doi: 10.1016/j.icarus.2008.10.007.

Cuevas Martinez, J.L., Cabrera Perez, L., Marcuello, A., Arbues Cazo, P., Marzo Carpio, M., and Bellmunt, F., 2010, Exhumed channel sandstone networks within fluvial fan deposits from the Oligo- Miocene Caspe Formation, South- east Ebro Basin (North- east Spain): Sedimentology, v. 57, no. 1, p. 162–189, doi: 10.1111/j.1365-3091.2009.01096.x.

Davies, N.S., and Gibling, M.R., 2010, Paleozoic vegetation and the Siluro-Devonian rise of fluvial lateral accretion sets: Geology, v. 38, no. 1, p. 51–54, doi: 10.1130/G30443.1.

DiBiase, R.A., Limaye, A.B., Scheingross, J.S., Fischer, W.W., and Lamb, M.P., 2013, Deltaic deposits at Aeolis Dorsa: Sedimentary evidence for a standing body of water on the northern plains of Mars: Journal of Geophysical Research: Planets, v. 118, no. 6, p. 1285–1302, doi: 10.1002/jgre.20100.

Donselaar, M.E., and Overeem, I., 2008, Connectivity of fluvial point-bar deposits: An example from the Miocene Huesca fluvial fan, Ebro Basin, Spain: AAPG Bulletin, v. 92, no. 9, p. 1109–1129, doi: 10.1306/04180807079.

Edwards, M.B., Eriksson, K.A., and Kier, R.S., 1983, Paleochannel Geometry and Flow Patterns Determined from Exhumed Permian Point Bars in North-central Texas: Journal of Sedimentary Research, v. 53, no. 4, p. 1261–1270, doi: 10.1306/212F835A-2B24-11D7-8648000102C1865D.

Evans, J.E., 1991, Facies Relationships, Alluvial Architecture, and Paleohydrology of a Paleogene, Humid-tropical Alluvial-fan System: Chumstick Formation, Washington State, U.S.A.: Journal of Sedimentary Research, v. 61, no. 5, p. 732–755, doi: 10.1306/D42677C1-2B26-11D7-8648000102C1865D.

Fassett, C.I., and Head, J.W., 2005, Fluvial sedimentary deposits on Mars: Ancient deltas in a crater lake in the Nili Fossae region: Geophysical Research Letters, v. 32, no. 14, p. L14201, doi: 10.1029/2005GL023456.

Fassett, C.I., and Head, J.W., 2008, The timing of martian valley network activity: Constraints from buffered crater counting: Icarus, v. 195, no. 1, p. 61–89, doi: 10.1016/j.icarus.2007.12.009.

Foix, N., Allard, J.O., Paredes, J.M., and Giacosa, R.E., 2012, Fluvial styles, palaeohydrology and modern analogues of an exhumed, Cretaceous fluvial system: Cerro Barcino Formation, Cañadón Asfalto Basin, Argentina: Cretaceous Research, v. 34, p. 298–307, doi: 10.1016/j.cretres.2011.11.010.

Gibling, M.R., 2006, Width and Thickness of Fluvial Channel Bodies and Valley Fills in the Geological Record: A Literature Compilation and Classification: Journal of Sedimentary Research, v. 76, no. 5, p. 731–770, doi: 10.2110/jsr.2006.060.

Gibling, M., and Rust, B., 1993, Alluvial ridge-and-swale topography: a case study from the Morien Group of Atlantic Canada, *in* Marzo, C., and Puigdefábregas, C., eds., Alluvial sedimentation: Oxford, UK, Blackwell, p. 133–150, doi: 10.1002/9781444303995.ch11.

Gibling, M.R., and Rust, B.R., 1990, Ribbon sandstones in the Pennsylvanian Waddens Cove Formation, Sydney Basin, Atlantic Canada: the influence of siliceous duricrusts on channel- body geometry: Sedimentology, v. 37, no. 1, p. 45–66, doi: 10.1111/j.1365-3091.1990.tb01982.x.

Golombek, M.P., Grant, J.A., Parker, T.J., et al., 2003, Selection of the Mars Exploration Rover landing sites: Journal of Geophysical Research: Planets, v. 108, no. E12, p. 8072, doi: 10.1029/2003JE002074.

Grant, J.A., and Wilson, S.A., 2011, Late alluvial fan formation in southern Margaritifer Terra, Mars: Geophysical Research Letters, v. 38, no. 8, p. L08201, doi: 10.1029/2011GL046844.

Greeley, R., and Guest, J.E., 1987, Geologic map of the eastern equatorial region of Mars: U.S. Geological Survey, IMAP 1802-B, scale 1:15,000,000.

Grotzinger, J.P., Arvidson, R.E., Bell III, J.F., et al., 2005, Stratigraphy and sedimentology of a dry to wet eolian depositional system, Burns formation, Meridiani Planum, Mars: Earth and Planetary Science Letters, v. 240, no. 1, p. 11–72, doi: 10.1016/j.epsl.2005.09.039.

Grotzinger, J.P., Sumner, D.Y., Kah, L.C., et al., 2014, A Habitable Fluvio-Lacustrine Environment at Yellowknife Bay, Gale Crater, Mars: Science, v. 343, no. 6169, p. 1242777, doi: 10.1126/science.1242777.

Harris, D.R., 1980, Exhumed paleochannels in the Lower Cretaceous Cedar Mountain Formation near Green River, Utah: Brigham Young University Geology Studies, v. 27, p. 51–66.

Harrison, S.K., Balme, M.R., Hagermann, A., Murray, J.B., and Muller, J.-P., 2010, Mapping Medusae Fossae Formation materials in the southern highlands of Mars: Icarus, v. 209, no. 2, p. 405–415, doi: 10.1016/j.icarus.2010.04.016.

Hauber, E., Platz, T., Reiss, D., Le Deit, L., Kleinhans, M.G., Marra, W.A., de Haas, T., and Carbonneau, P., 2013, Asynchronous formation of Hesperian and Amazonian-aged deltas on Mars and implications for climate: Journal of Geophysical Research: Planets, v. 118, no. 7, p. 1529–1544, doi: 10.1002/jgre.20107.

Howard, A.D., 2009, How to make a meandering river: Proceedings of the National Academy of Sciences, v. 106, no. 41, p. 17245–17246, doi: 10.1073/pnas.0910005106.

Howard, A.D., Moore, J.M., and Irwin, R.P., 2005, An intense terminal epoch of widespread fluvial activity on early Mars: 1. Valley network incision and associated deposits: Journal of Geophysical Research: Planets, v. 110, no. E12, p. E12S14, doi: 10.1029/2005JE002459.

Hynek, B.M., Beach, M., and Hoke, M.R.T., 2010, Updated global map of Martian valley networks and implications for climate and hydrologic processes: Journal of Geophysical Research: Planets, v. 115, no. E9, p. E09008, doi: 10.1029/2009JE003548.

Hynek, B.M., Phillips, R.J., and Arvidson, R.E., 2003, Explosive volcanism in the Tharsis region: Global evidence in the Martian geologic record: Journal of Geophysical Research: Planets, v. 108, no. E9, p. 5111, doi: 10.1029/2003JE002062.
Ielpi, A., and Ghinassi, M., 2014, Planform architecture, stratigraphic signature and morphodynamics of an exhumed Jurassic meander plain (Scalby Formation, Yorkshire, UK): Sedimentology, v. 61, no. 7, p. 1923–1960, doi: 10.1111/sed.12122.
Irwin, R.P., Watters, T.R., Howard, A.D., and Zimbelman, J.R., 2004, Sedimentary resurfacing and fretted terrain development along the crustal dichotomy boundary, Aeolis Mensae, Mars: Journal of Geophysical Research (Planets), v. 109, p. E09011, doi: 10.1029/2004JE002248.
Jones, L.S., and Blakey, R.C., 1997, Eolian-fluvial interaction in the Page Sandstone (Middle Jurassic) in south-central Utah, USA—a case study of erg-margin processes: Sedimentary Geology, v. 109, no. 1, p. 181–198, doi:10.1016/S0037-0738(96)00044-9.
Keller, J.M., Boynton, W.V., Karunatillake, S., et al., 2006, Equatorial and midlatitude distribution of chlorine measured by Mars Odyssey GRS: Journal of Geophysical Research: Planets, v. 111, no. E3, p. E03S08, doi: 10.1029/2006JE002679.
Kerber, L., and Head, J.W., 2010, The age of the Medusae Fossae Formation: Evidence of Hesperian emplacement from crater morphology, stratigraphy, and ancient lava contacts: Icarus, v. 206, no. 2, p. 669–684, doi: 10.1016/j.icarus.2009.10.001.
Kerber, L., Head, J.W., Madeleine, J.-B., Forget, F., and Wilson, L., 2011, The dispersal of pyroclasts from Apollinaris Patera, Mars: Implications for the origin of the Medusae Fossae Formation: Icarus, v. 216, no. 1, p. 212–220, doi: 10.1016/j.icarus.2011.07.035.
Kirk, R.L., Howington-Kraus, E., Rosiek, M.R., Anderson, J.A., et al., 2008, Ultrahigh resolution topographic mapping of Mars with MRO HiRISE stereo images: Meter-scale slopes of candidate Phoenix landing sites: Journal of Geophysical Research (Planets), v. 113, p. E00A24, doi: 10.1029/2007JE003000.
Kite, E.S., Halevy, I., Kahre, M.A., Wolff, M.J., and Manga, M., 2013, Seasonal melting and the formation of sedimentary rocks on Mars, with predictions for the Gale Crater mound: Icarus, v. 223, no. 1, p. 181–210, doi: 10.1016/j.icarus.2012.11.034.
Kite, E.S., Howard, A.D., Lucas, A.S., Armstrong, J.C., Aharonson, O., and Lamb, M.P., 2015a, Stratigraphy of Aeolis Dorsa, Mars: Stratigraphic context of the great river deposits: Icarus, v. 253, p. 223–242, doi: 10.1016/j.icarus.2015.03.007.
Kite, E.S., Howard, A.D., Lucas, A., and Lewis, K.W., 2015b, Resolving the era of river-forming climates on Mars using stratigraphic logs of river-deposit dimensions: Earth and Planetary Science Letters, v. 420, p. 55–65, doi: 10.1016/j.epsl.2015.03.019.
Kochel, R.C., 1990, Humid fans of the Appalachian Mountains, *in* Rachocki, A., and Church, M.A., eds., Alluvial Fans: A Field Approach: Wiley, New York, p. 109–129.
Kochel, R.C., and Johnson, R.A., 1984, Geomorphology and Sedimentology of Humid-Temperate Alluvial Fans, Central Virginia, *in*, Koster, E.H., and Steel, R.J., eds., Sedimentology of Gravels and Conglomerates: Canadian Society of Petroleum Geologist, Calgary, Memoir 10, p. 109–122.

Lefort, A., Burr, D.M., Beyer, R.A., and Howard, A.D., 2012, Inverted fluvial features in the Aeolis-Zephyria Plana, western Medusae Fossae Formation, Mars: Evidence for post-formation modification: Journal of Geophysical Research: Planets, v. 117, no. E3, p. E03007, doi: 10.1029/2011JE004008.

Lefort, A., Burr, D.M., Nimmo, F., and Jacobsen, R.E., 2015, Channel slope reversal near the Martian dichotomy boundary: Testing tectonic hypotheses: Geomorphology, v. 240, p. 121–136, doi: 10.1016/j.geomorph.2014.09.028.

Lucchitta, I., Holm, R.F., and Lucchitta, B.K., 2011, A Miocene river in northern Arizona and its implications for the Colorado River and Grand Canyon: GSA Today, v. 21, p. 4–10, doi: 10.1130/G119A.1.

Maizels, J.K., 1987, Plio-Pleistocene raised channel systems of the western Sharqiya (Wahiba), Oman: Geological Society, London, Special Publications, v. 35, no. 1, p. 31–50, doi: 10.1144/GSL.SP.1987.035.01.04.

Maizels, J., 1990, Raised channel systems as indicators of palaeohydrologic change: a case study from Oman: Palaeogeography, Palaeoclimatology, Palaeoecology, v. 76, no. 3–4, p. 241–277, doi: 10.1016/0031-0182(90)90115-N.

Malin, M.C., Bell, J.F., Cantor, B.A., et al., 2007, Context Camera Investigation on board the Mars Reconnaissance Orbiter: Journal of Geophysical Research: Planets, v. 112, no. E5, p. E05S04, doi: 10.1029/2006JE002808.

Mandt, K.E., de Silva, S.L., Zimbelman, J.R., and Crown, D.A., 2008, Origin of the Medusae Fossae Formation, Mars: Insights from a synoptic approach: Journal of Geophysical Research: Planets, v. 113, no. E12, p. E12011, doi: 10.1029/2008JE003076.

Mandt, K., Silva, S. de, Zimbelman, J., and Wyrick, D., 2009, Distinct erosional progressions in the Medusae Fossae Formation, Mars, indicate contrasting environmental conditions: Icarus, v. 204, no. 2, p. 471–477, doi: 10.1016/j.icarus.2009.06.031.

Mangold, N., Quantin, C., Ansan, V., Delacourt, C., and Allemand, P., 2004, Evidence for Precipitation on Mars from Dendritic Valleys in the Valles Marineris Area: Science, v. 305, no. 5680, p. 78–81, doi: 10.1126/science.1097549.

Matsubara, Y., Howard, A.D., Burr, D.M., Williams, R.M.E., Dietrich, W.E., and Moore, J.M., 2014, River meandering on Earth and Mars: A comparative study of Aeolis Dorsa meanders, Mars and possible terrestrial analogs of the Usuktuk River, AK, and the Quinn River, NV: Geomorphology, v. 240, p. 102–120, doi: 10.1016/j.geomorph.2014.08.031.

McEwen, A.S., Eliason, E.M., Bergstrom, J.W., Bridges, N.T., et al., 2007, Mars Reconnaissance Orbiter's High Resolution Imaging Science Experiment (HiRISE): Journal of Geophysical Research: Planets, v. 112, no. E5, p. E05S02, doi: 10.1029/2005JE002605.

McLaren, S., 2004, Characteristics, evolution and distribution of Quaternary channel calcretes, southern Jordan: Earth Surface Processes and Landforms, v. 29, no. 12, p. 1487–1507, doi: 10.1002/esp.1135.

Miall, A., 1996, The Geology of Fluvial Deposits: Sedimentary Facies, Basin Analysis, and Petroleum Geology: Springer Berlin Heidelberg, 582 p.

Miall, A., 2010, Alluvial Deposits, *in* Dalrymple, R.W. and James, N.P. eds., Facies models 4: Geological Association of Canada, St. John's, Nfld, p. 105–138.
Miall, A.D., and Jones, B.G., 2003, Fluvial Architecture of the Hawkesbury Sandstone (Triassic), Near Sydney, Australia: Journal of Sedimentary Research, v. 73, no. 4, p. 531–545.
Moore, J.M., and Howard, A.D., 2005, Large alluvial fans on Mars: Journal of Geophysical Research: Planets, v. 110, no. E4, p. E04005, doi: 10.1029/2004JE002352.
Moratto, Z.M., Broxton, M.J., Beyer, R.A., Lundy, M., and Husmann, K., 2010, Ames Stereo Pipeline, NASA's Open Source Automated Stereogrammetry Software: Houston, Texas, Lunar and Planetary Institute, Lunar and Planetary Science XXXXI, abstract 2364.
Morgan, A.M., Howard, A.D., Hobley, D.E.J., Moore, J.M., Dietrich, W.E., Williams, R.M.E., Burr, D.M., Grant, J.A., Wilson, S.A., and Matsubara, Y., 2014, Sedimentology and climatic environment of alluvial fans in the martian Saheki crater and a comparison with terrestrial fans in the Atacama Desert: Icarus, v. 229, p. 131–156, doi: 10.1016/j.icarus.2013.11.007.
Nami, M., 1976, An exhumed Jurassic meander belt from Yorkshire, England: Geological Magazine, v. 113, no. 01, p. 47–52, doi: 10.1017/S0016756800043004.
Osterkamp, W.R., and Toy, T.J., 1994, The healing of disturbed hillslopes by gully gravure: Geological Society of America Bulletin, v. 106, no. 10, p. 1233–1241, doi: 10.1130/0016-7606(1994)106<1233:THODHB>2.3.CO;2.
Page, K.J., and Nanson, G.C., 1996, Stratigraphic architecture resulting from Late Quaternary evolution of the Riverine Plain, south-eastern Australia: Sedimentology, v. 43, p. 927-945, doi: 10.1111/j.1365-3091.1996.tb01512.x.
Pain, C.F., Clarke, J.D.A., and Thomas, M., 2007, Inversion of relief on Mars: Icarus, v. 190, no. 2, p. 478–491, doi: 10.1016/j.icarus.2007.03.017.
Pain, C.F., and Oilier, C.D., 1995, Inversion of relief — a component of landscape evolution: Geomorphology, v. 12, no. 2, p. 151–165, doi: 10.1016/0169-555X(94)00084-5.
Parsons, R.A., Moore, J.M., and Howard, A.D., 2013, Evidence for a short period of hydrologic activity in Newton crater, Mars, near the Hesperian-Amazonian transition: Journal of Geophysical Research: Planets, v. 118, no. 5, p. 1082–1093, doi: 10.1002/jgre.20088.
Ruff, S.W., and Christensen, P.R., 2002, Bright and dark regions on Mars: Particle size and mineralogical characteristics based on Thermal Emission Spectrometer data: Journal of Geophysical Research: Planets, v. 107, no. E12, p. 5119, doi: 10.1029/2001JE001580.
Scanlon, K.E., Head, J.W., Madeleine, J.-B., Wordsworth, R.D., and Forget, F., 2013, Orographic precipitation in valley network headwaters: Constraints on the ancient Martian atmosphere: Geophysical Research Letters, v. 40, no. 16, p. 4182–4187, doi: 10.1002/grl.50687.
Schultz, P.H., and Lutz, A.B., 1988, Polar wandering of Mars: Icarus, v. 73, no. 1, p. 91–141, doi: 10.1016/0019-1035(88)90087-5.

Scott, D.H., and Tanaka, K.L., 1986, Geologic map of the western equatorial region of Mars: U.S. Geological Survey, IMAP 1802-A, scale 1:15,000,000.
Scott, D.H., and Tanaka, K.L., 1982, Ignimbrites of Amazonis Planitia Region of Mars: Journal of Geophysical Research: Solid Earth, v. 87, no. B2, p. 1179–1190, doi: 10.1029/JB087iB02p01179.
Saito, K., and Oguchi, T., 2005, Slope of alluvial fans in humid regions of Japan, Taiwan and the Philippines: Geomorphology, v. 70, p. 147-162, doi: 10.1016/j.geomorph.2005.04.006.
de Silva, S.L., Bailey, J.E., Mandt, K.E., and Viramonte, J.M., 2010, Yardangs in terrestrial ignimbrites: Synergistic remote and field observations on Earth with applications to Mars: Planetary and Space Science, v. 58, no. 4, p. 459–471, doi: 10.1016/j.pss.2009.10.002.
Smith, R.M.H., 1987, Morphology and Depositional History of Exhumed Permian Point Bars in the Southwestern Karoo, South Africa: Journal of Sedimentary Research, v. 57, no. 1, p. 19–29, doi: 10.1306/212F8A8F-2B24-11D7-8648000102C1865D.
Smith, D.E., Zuber, M.T., Frey, H.V., Garvin, J.B., Head, J.W., et al., 2001, Mars Orbiter Laser Altimeter: Experiment summary after the first year of global mapping of Mars: Journal of Geophysical Research: Planets, v. 106, no. E10, p. 23689–23722, doi: 10.1029/2000JE001364.
Stock, J.D., 2013, 9.23 Waters Divided: A History of Alluvial Fan Research and a View of Its Future, in Shroder, J.F. ed., Treatise on Geomorphology, Academic Press, San Diego, p. 413–458.
Stock, J.D., Schmidt, K.M., and Miller, D.M., 2008, Controls on alluvial fan long-profiles: Geological Society of America Bulletin, v. 120, no. 5-6, p. 619–640, doi: 10.1130/B26208.1.
Tanaka, K.L., Skinner, J.A., Dohm, J.M., Irwin III, R.P., Kolb, E.J., Fortezzo, C.M., Platz, T., Michael, G.G., and Hare, T.M., 2014, Geologic Map of Mars: U.S. Geological Survey Scientific Investigations Map 3292, scale 1:20,000,000, 1 sheet, 43 p. text, http://dx.doi.org/10.3133/sim3292.
Tanaka, K.L., Skinner, J.A., Hare, T.M., Joyal, T., and Wenker, A., 2003, Resurfacing history of the northern plains of Mars based on geologic mapping of Mars Global Surveyor data: Journal of Geophysical Research (Planets), v. 108, p. 8043, doi: 10.1029/2002JE001908.
Ward, A.W., 1979, Yardangs on Mars - Evidence of recent wind erosion: Journal of Geophysical Research, v. 84, p. 8147–8166, doi: 10.1029/JB084iB14p08147.
Watters, T.R., Campbell, B., Carter, L., et al., 2007, Radar Sounding of the Medusae Fossae Formation Mars: Equatorial Ice or Dry, Low-Density Deposits? Science, v. 318, no. 5853, p. 1125–1128, doi: 10.1126/science.1148112.
Williams, R.M., Chidsey Jr, T.C., and Eby, D.E., 2007, Exhumed paleochannels in central Utah—Analogs for raised curvilinear features on Mars, *in* Willis, G.C., Hylland, M.D., Clark, D.L., Chidsey Jr., T.C., eds., Central Utah: Diverse Geology of a Dynamic Landscape: Utah Geological Association, Salt Lake City, vol. 36., p. 221–235.

Williams, R.M.E., Rogers, A.D., Chojnacki, M., Boyce, J., Seelos, K.D., Hardgrove, C., and Chuang, F., 2011, Evidence for episodic alluvial fan formation in far western Terra Tyrrhena, Mars: Icarus, v. 211, no. 1, p. 222–237, doi: 10.1016/j.icarus.2010.10.001.

Williams, R.M.E., Irwin III, R.P., Burr, D.M., Harrison, T., and McClelland, P., 2013, Variability in martian sinuous ridge form: Case study of Aeolis Serpens in the Aeolis Dorsa, Mars, and insight from the Mirackina paleoriver, South Australia: Icarus, v. 225, no. 1, p. 308–324, doi: 10.1016/j.icarus.2013.03.016.

Williams, R.M.E., Irwin III, R.P., and Zimbelman, J.R., 2009, Evaluation of paleohydrologic models for terrestrial inverted channels: Implications for application to martian sinuous ridges: Geomorphology, v. 107, no. 3–4, p. 300–315, doi: 10.1016/j.geomorph.2008.12.015.

Zimbelman, J.R., and Griffin, L.J., 2010, HiRISE images of yardangs and sinuous ridges in the lower member of the Medusae Fossae Formation, Mars: Icarus, v. 205, no. 1, p. 198–210, doi: 10.1016/j.icarus.2009.04.003.

Zimbelman, J.R., and Scheidt, S.P., 2012, Hesperian Age for Western Medusae Fossae Formation, Mars: Science, v. 336, no. 6089, p. 1683–1683, doi: 10.1126/science.1221094.

Appendix I

Table I-1. Alluvial fans classified by dynamics, process, & mud involvement.

Dynamics	Inertial (Fr ≥ 1)		Traction (Fr < 1)
Primary process	debris flow	sheetflood	bedload & suspension
Mud involvement	yes	no	no
Units & structures	• channel levees • terminal lobes • massive deposits	• antidunes • plane laminations • imbrication	• channel fills • cross bedding • imbrication
Modern examples visible in satellite images	• Dolomite fan, CA • Warm Spring fan, CA • Blue Ridge fans, VA	• Anvil Spring fan, CA • Hell's Gate fan, CA • Roaring R. fan, CO	• Hanaupah fan, CA • Kiso river fan, Japan • Shenandoah fans, VA
Ancient examples	N/A*		• Sharqiya fans, Oman

Note: See citations in text for reference to specific modern and ancient fans. *Our inspection of the literature found no examples of ancient debris-flow or sheetflood deposits apparent in satellite images.

Table I-2. Morphological attributes of fluvial sedimentary units

Sedimentary unit, attributes	Environment (*implications*)	Uncertainty of unit interpretation
Point bars		
Semi-concentric ridges with meter-scale spacing and relatively level ridge and swale elevations (Fig. I-8)	Meandering fluvial (*stable channel banks, regular hydrologic activity and associated sedimentation*)	Number of generations of point bars and their relative ages; unclear boundaries with adjacent channel fills and floodplain fines
Channel fill		
Nondescript/featureless surface lacking surface textures; straight to sinuous pattern (Fig. I-10)	Polygenetic deposits of meandering fluvial, mixed aeolian-fluvial, megafan, or high-strength floodplain environments	Narrowing of original channel width by erosion; may be difficult to distinguish from adjacent point bars

Table I-3. Morphological attributes of alluvial sedimentary units

Sedimentary unit, attributes	Environment (*implications*)	Uncertainty of unit interpretation
Debris flow levees		
Parallel ridges that extend from fan apex, often cross-cutting other ridges (Fig. I-11)	Alluvial fan of inertial sedimentary deposits (*topographic relief, intermittent hydrologic activity, involvement of mud*)	Relative history of deposits, associated debris flow lobes may not be apparent
Debris flow lobe		
Lobate mass at the terminus of an incised channel (Fig. I-11)	*same as above*	Low relief of deposit may obscure number of lobes
Sheetflood deposit		
Wide, low sinuosity deposits with low relief	Alluvial fan of inertial sedimentary deposits (*topographic relief, intermittent hydrology*)	Low relief of deposit may obscure deposit in plan view
Traction deposits		
Straight or sinuous deposits extending from fan apex, may have flat surfaces or crests depending on erosion (Fig. I-13)	Alluvial fan of traction sedimentary deposits (*topographic relief, intermittent hydrology*)	Narrowing of channel width

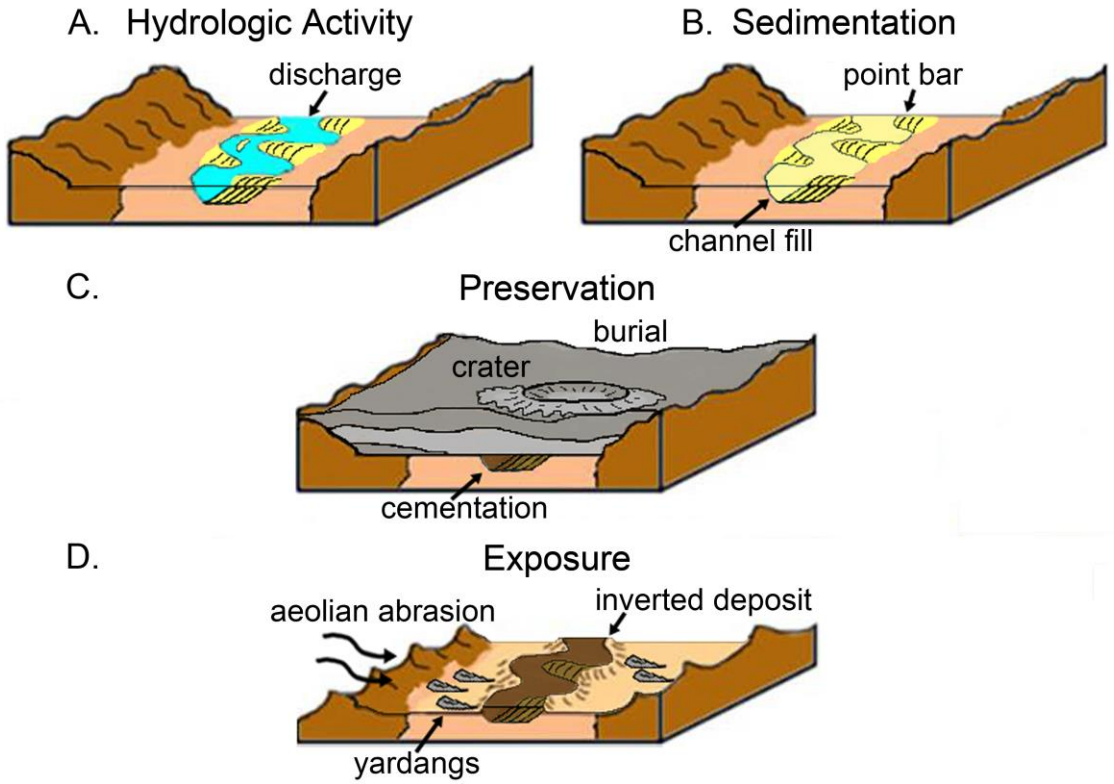

Figure I-1. Model illustrating the four processes required for plan-view detection and analysis of ancient fluvial deposits, and our schematic formation model of the Aeolis Dorsa deposits (adapted from Williams et al., 2007; Burr et al., 2009). Diagrams show segment of larger fluvial system. In the first part, precipitation and run-off lead to **(A)** hydrologic activity, transport of sediment, and formation of sedimentary units (e.g., point bars). **(B)** Concomitant sedimentation under transport-limited conditions leads to aggradation of the channel bed and the formation of a channel fill. In the next part, **(C)** preservation processes protect these sedimentary units from erosion, e.g., impact comminution. Cementation may occur either during hydrologic activity via evaporation or after hydrologic activity via precipitation from groundwater. In the final part, **(D)** deposits are exposed to plan view observation through exhumation, e.g., by aeolian abrasion. Topographically inverted deposits form when erosion removes the antecedent floodplain. Remnants of overburden may appear as yardangs.

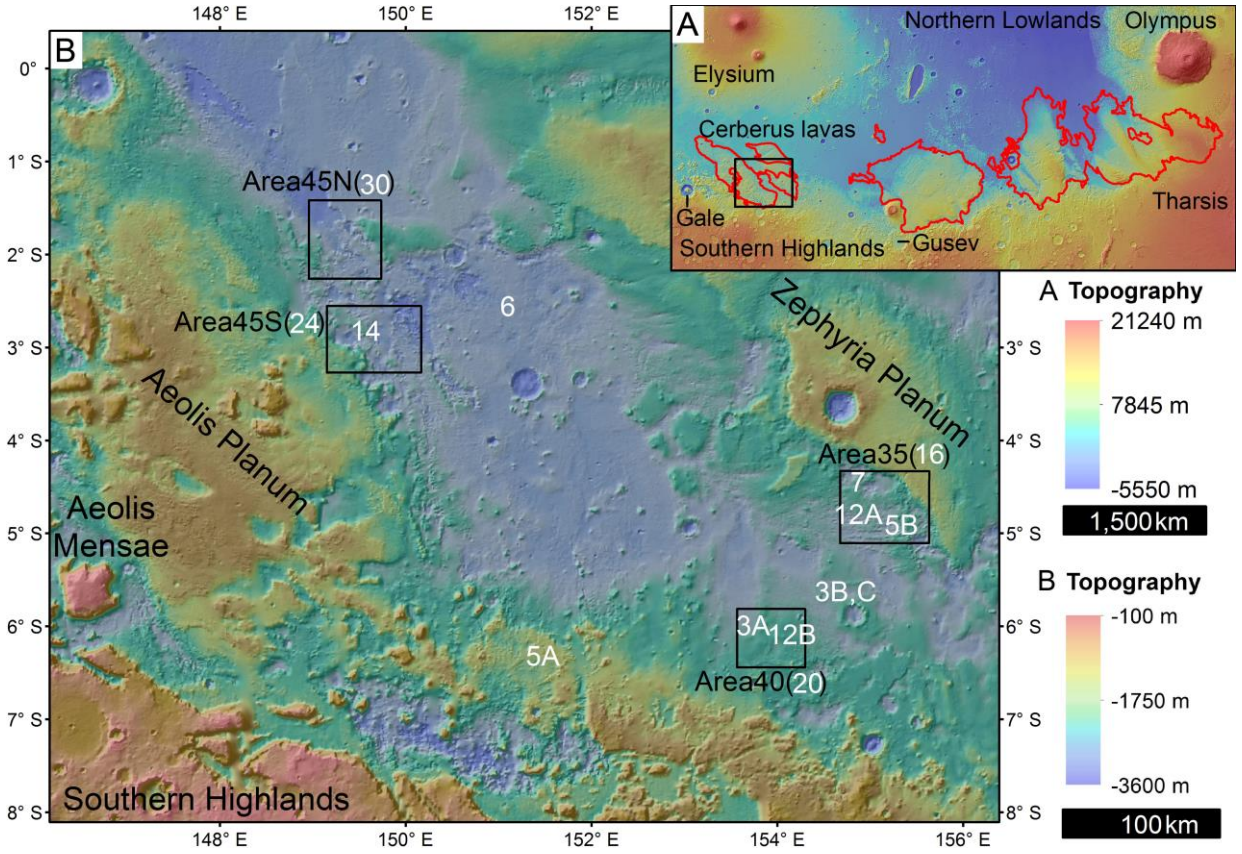

Figure I-2. (A) Context image: Topographic color and hillshade of the western equatorial region of Mars. Red outline is the mapped extent of the Medusae Fossae Formation (Scott and Tanaka, 1986; Greely and Guest, 1987), although outlying deposits have a wider distribution (Bradley et al., 2002; Harrison et al., 2010). Black box corresponds to the extent of (B). **(B)** Topographic color and hillshade of the Aeolis Dorsa region. These data show the central low between the regional highs of Aeolis Planum, Zephyria Planum, and the Southern Highlands. White alphanumeric identifiers correspond to the locations of subsequent figures. Both images are derived from Mars Orbiter Laser Altimeter data (Smith et al., 2001).

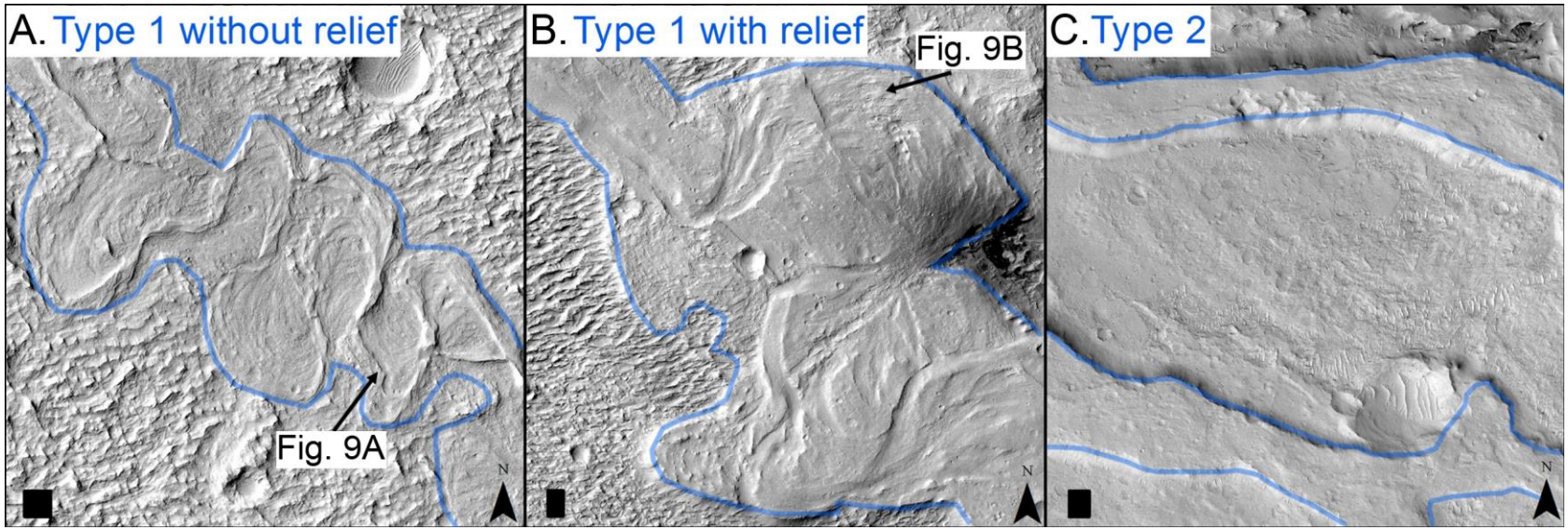

Figure I-3. Examples of flat features in Aeolis Dorsa. Blue lines outline flat features. Scale bars in lower left corners are 100 m wide, chevrons point north, and illumination is from the northwest. **(A & B)** Type 1 flat features have upper surfaces with semi-concentric curved ridges. Topographies of the curved ridges of (A) and (B) are described in the text, though both have been interpreted as deposits of meandering fluvial channels (Burr et al., 2009; Howard, 2009; Matsubara et al., 2014). **(C)** Type 2 flat features show relatively featureless or nondescript upper surfaces, lacking the semi-concentric ridges of Type 1 flat features. The specific fluvial units of Type 2 features have not been proposed previously, and are proposed here to be channel fills.

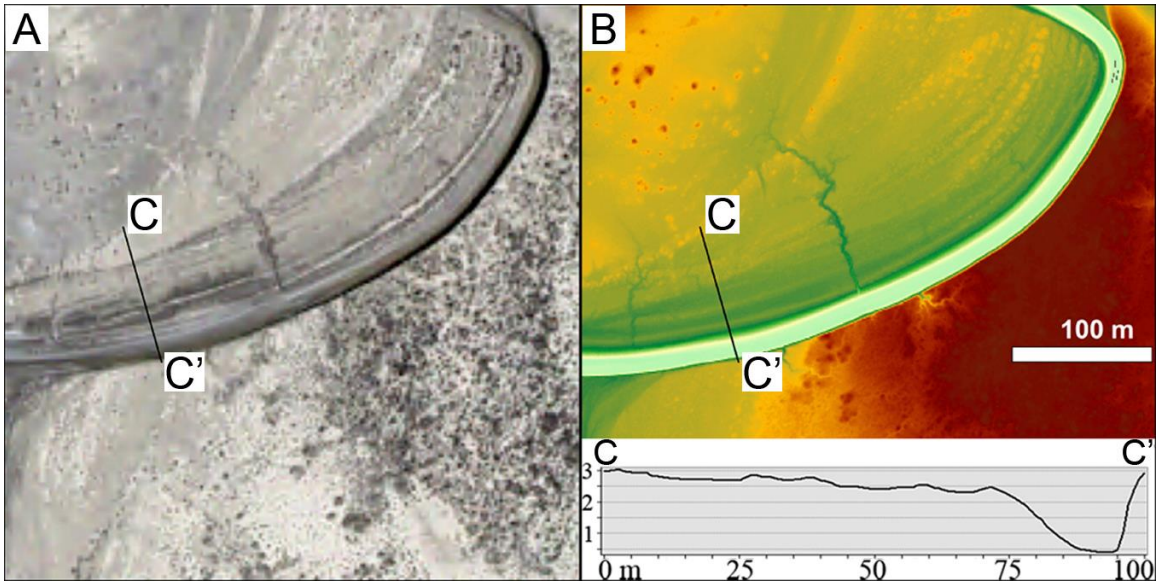

Figure I-4. **(A)** Visual image of the Quinn River, NV, USA, accessible from the National Agriculture Imagery Program. Image shows the desert environment with limited scrub vegetation and clay-rich cohesive channel banks, which were found to be a possible mechanism for promoting fluvial meandering on Mars (Matsubara et al., 2014). **(B)** Topographic color scheme is from LiDAR data of the Quinn River made by the National Center for Airborne Laser Mapping and available online (http://dx.doi.org/10.5069/G98G8HMJ). Elevation range is approximately 5 meters; reds are high and cyan is low. Topographic profile C-C' is drawn from the interior of the meander bend, with ridge-and-swale topography of the point bars, to the adjacent Quinn River channel. The ridges and swales are topographically above any channel deposits.

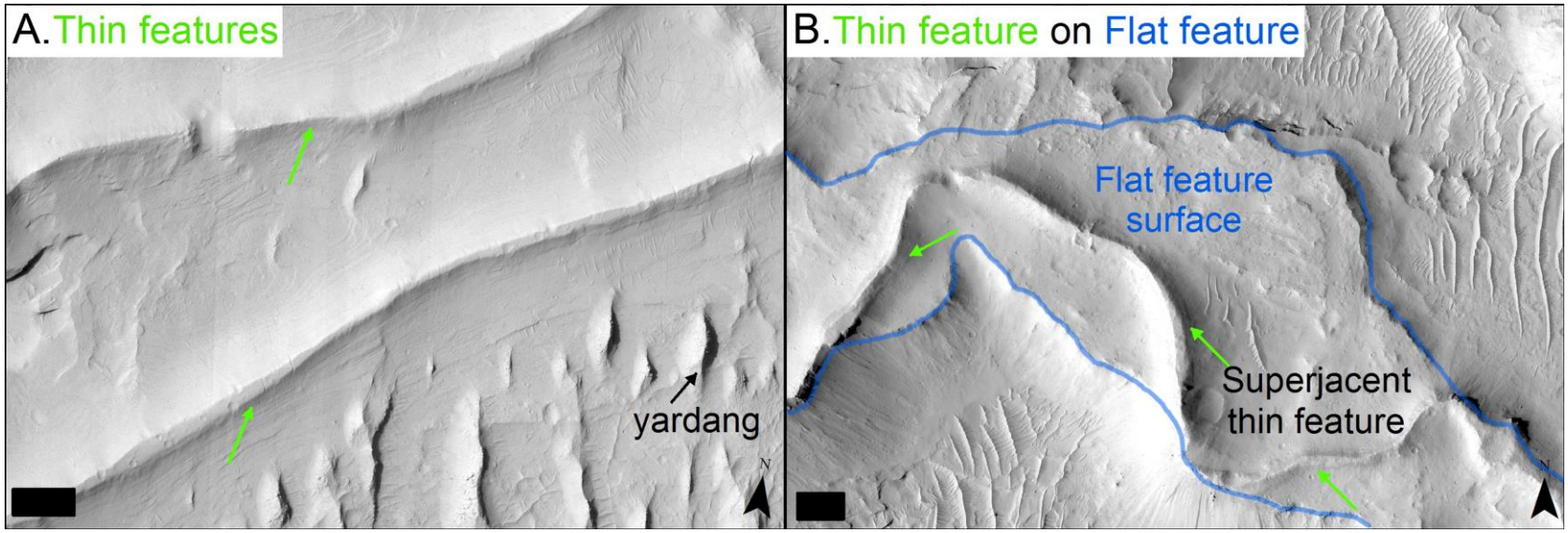

Figure I-5. Examples of thin features in Aeolis Dorsa. Scale bars in lower left corners are 100 m wide, chevrons point north, and illumination is from the northwest. **(A)** Relatively straight thin features may have sharp crests and/or flat topped cross-sectional profiles. **(B)** A thin feature situated on top of a flat feature.

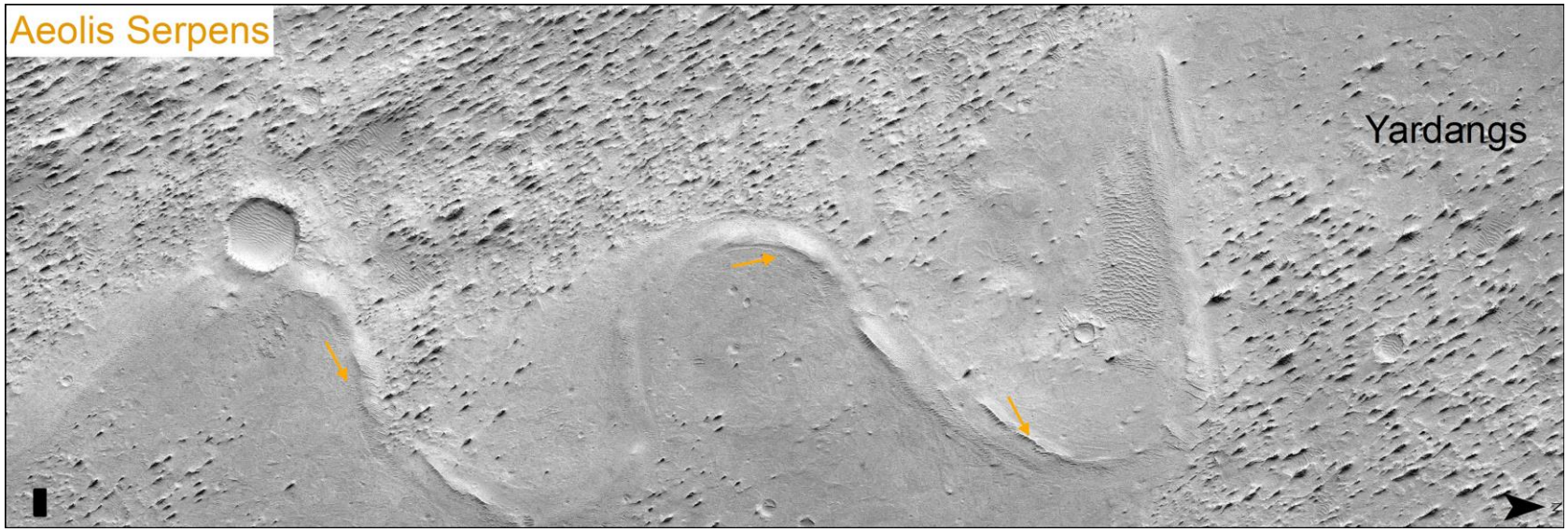

Figure I-6. Portion of Aeolis Serpens showing lateral ridges (orange arrows) along its length. Scale bar in lower left corner is 100 m wide, chevron points north, and illumination is from the northwest.

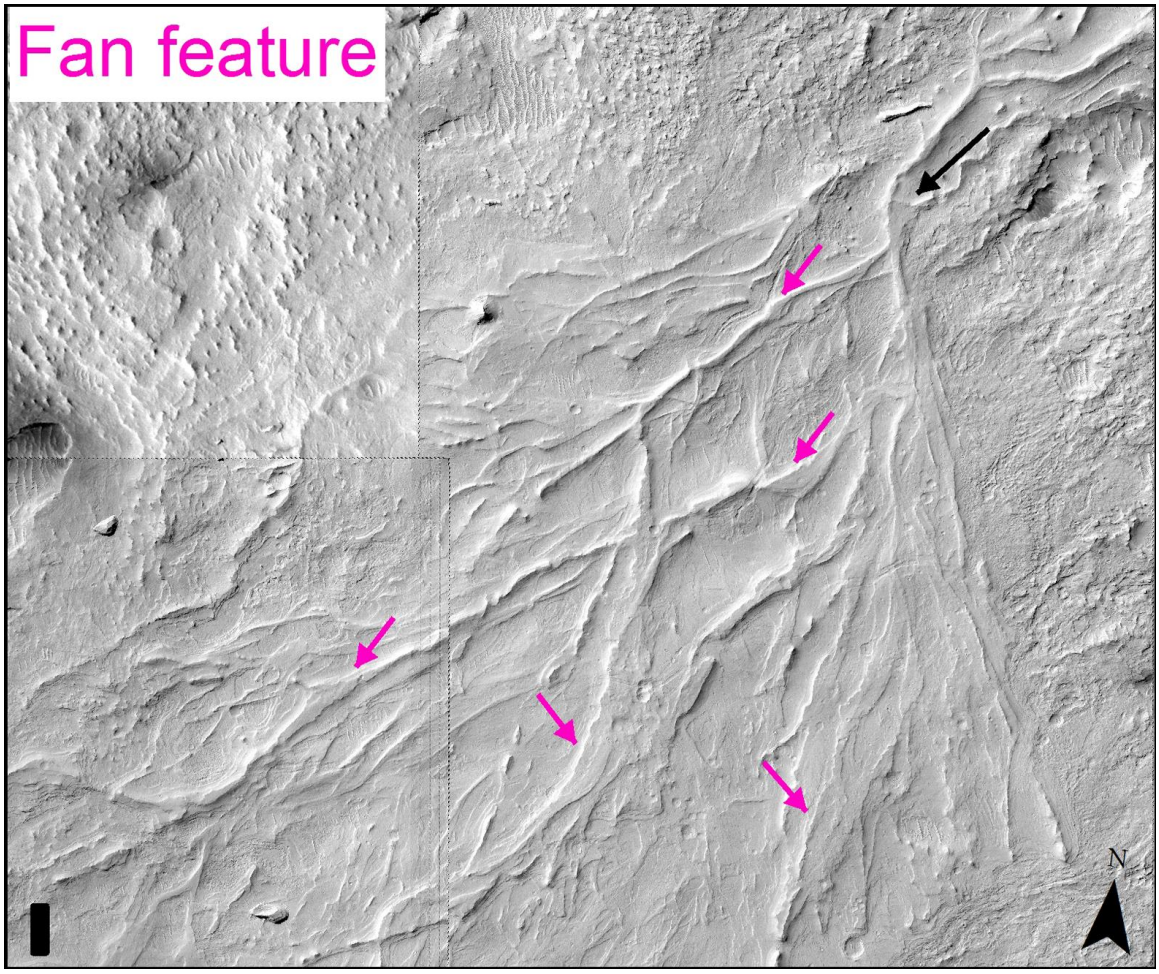

Figure I-7. An example of a fan feature with radiating ridges (pink arrows), which have been interpreted as alluvial fan deposits (e.g., Burr et al., 2009; Kite et al., 2015a). Black arrow in the upper right points downslope from the fan head/apex. Scale bar in lower left corner is 100 m wide, chevron points north, and illumination is from the northwest.

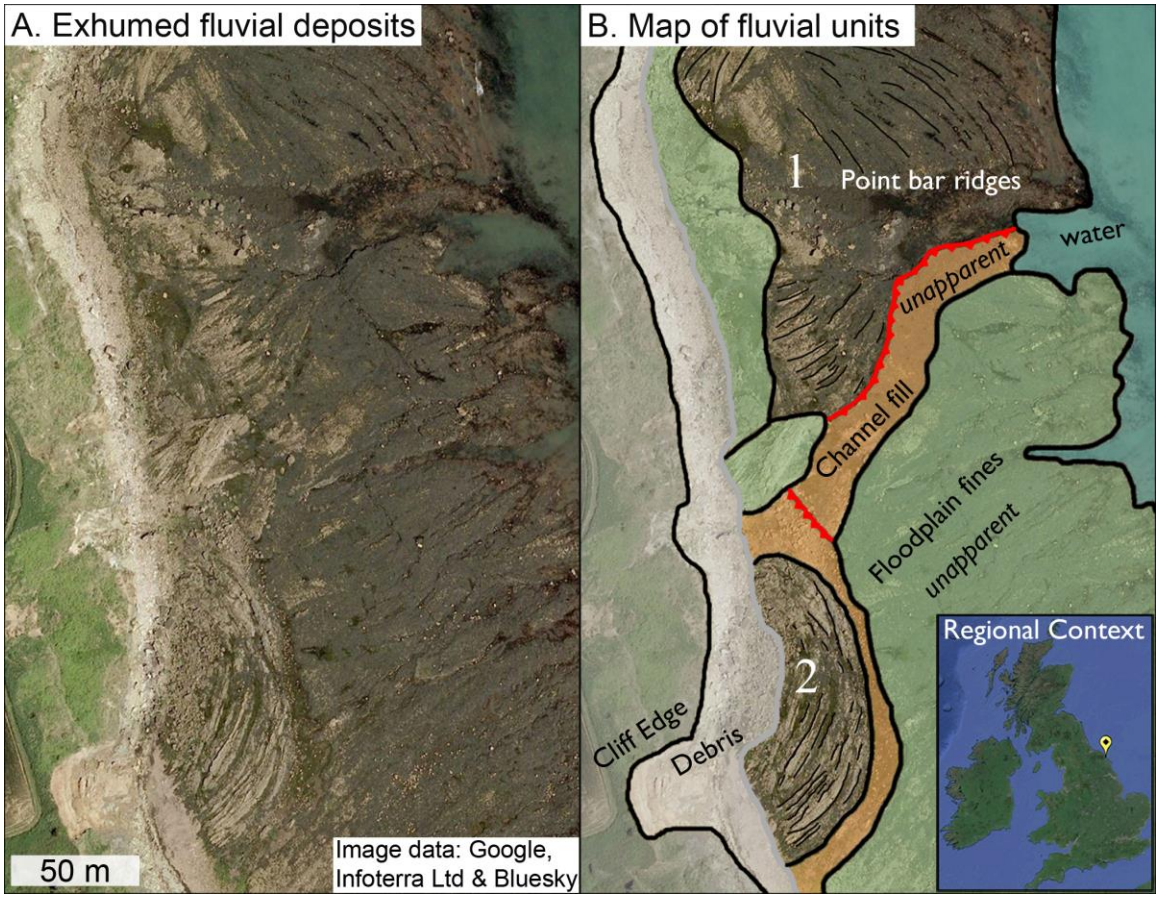

Figure I-8. **(A)** Satellite image shows fluvial units, including point bars, of the Scalby Fm., exposed along the east coast of England, near 54.325 N, 0.420 W. **(B)** Map showing interpreted units in (A). Sets of point bars are apparent as semi-concentric ridges and swales and are labeled with numbers 1 and 2. The southern portion of point bar set 1 and the majority of point bar set 2 appear at least level with or above the adjacent channel deposits. However, channel fills and relative ages of units (red lines, arrows toward younger units), which are distinguishable in-situ, are not apparent in the satellite image. Mapping of units and relative ages are adapted from mapping with in-situ data by Ielpi and Ghinassi (2014), their Figure 2.

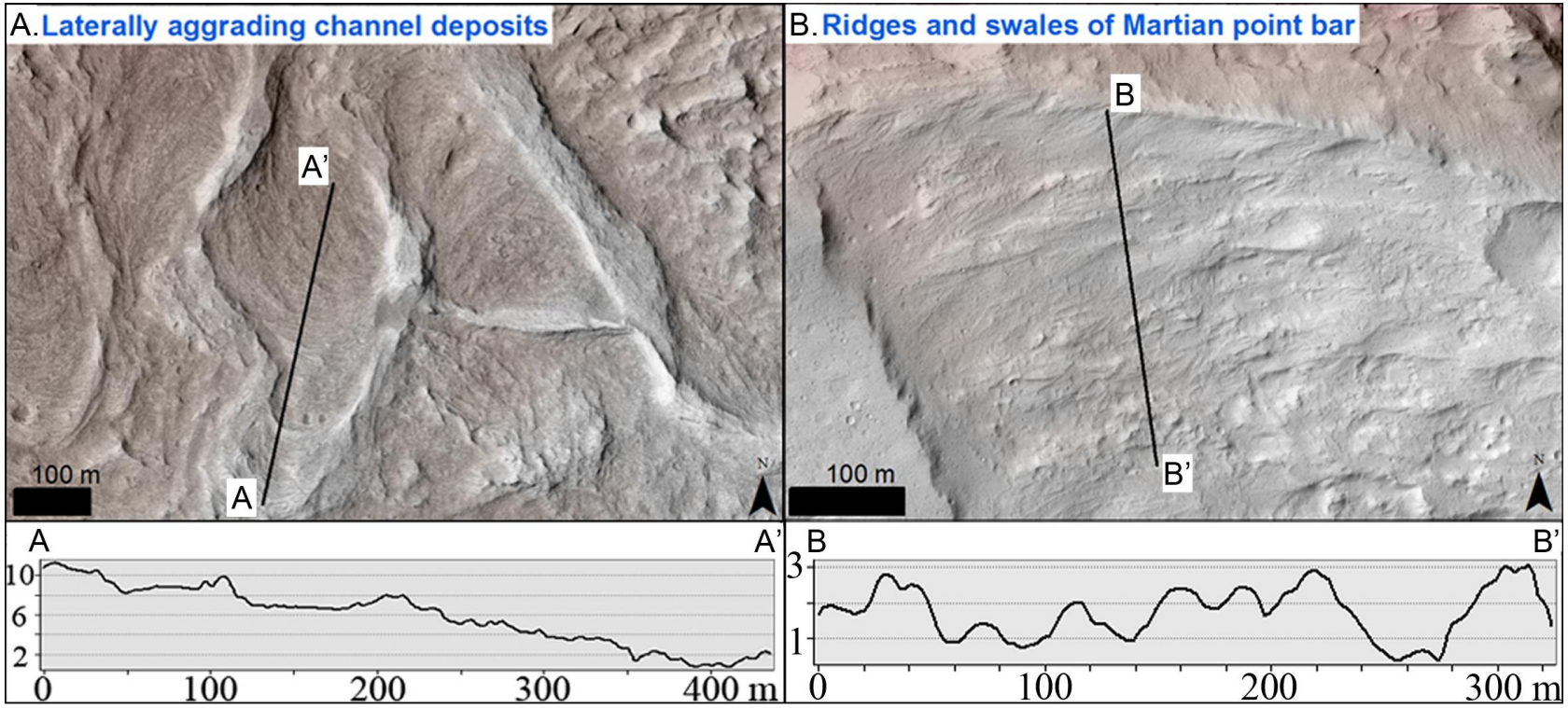

Figure I-9. Images and topographies of Type 1 flat features in Figures I-3A and I-3B. Topography and color for each image are from HiRISE DTMs. (A) Profile A-A' shows a 12-meter increase in elevation from interior (A') to exterior (A) of the meander bend. This trend has been interpreted as the topographic expression of laterally aggrading channel-bed deposits and presumed erosion of any point bars (Matsubara et al., 2014). (B) Profile B-B' differs in that meter-scale ridges and swales maintain a relatively level trend across the meander bend. The trend of Profile B-B' is more consistent with observations of ridges and swales on terrestrial point bars (Table I-1).

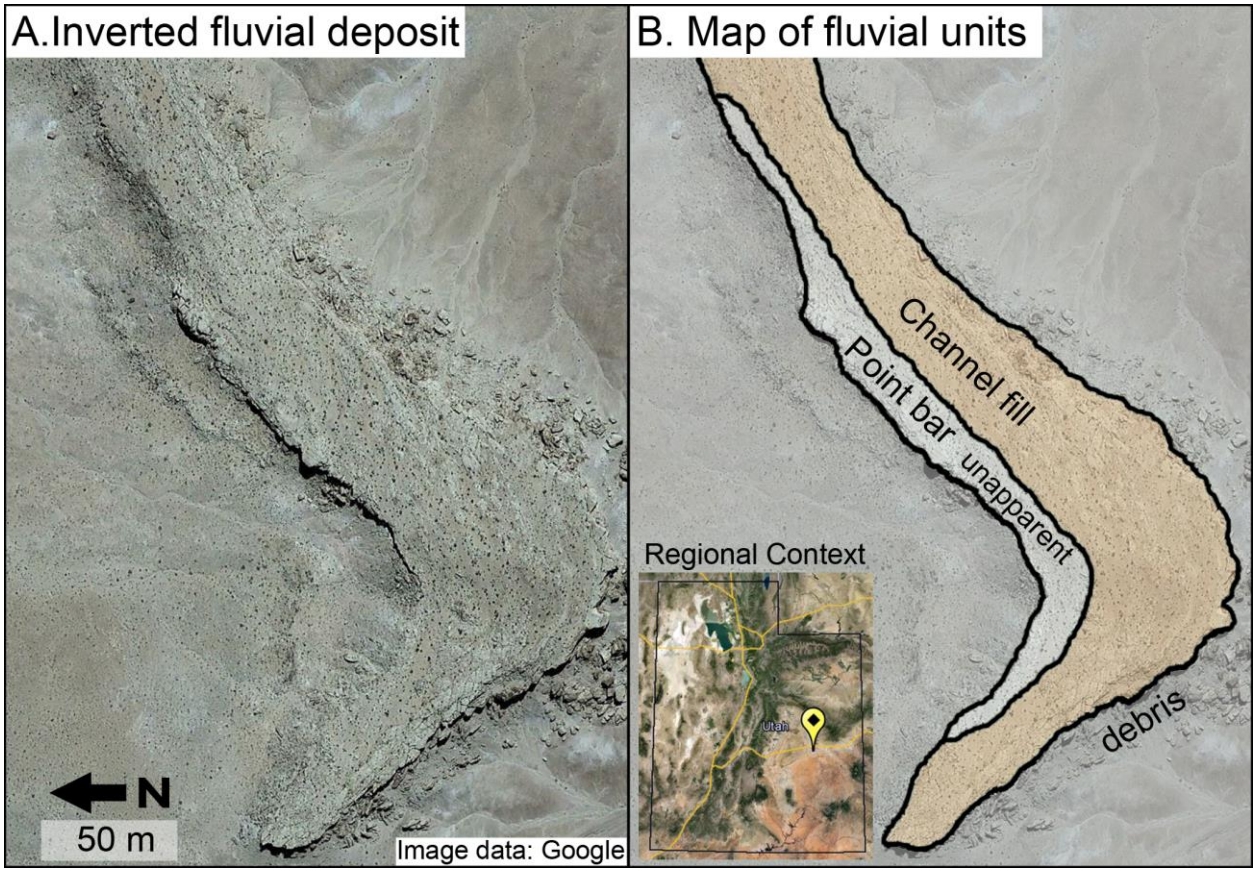

Figure I-10. (A) Inverted paleochannel southwest of Green River, Utah, USA, at 38.886 N, 110.305 W. The inverted deposit is largely composed of channel fill, which has steep sides and a flat but generally nondescript or featureless upper surface at the meter-scale resolution of the image. **(B)** Map showing interpreted units in (A). Neither the semi-concentric ridges of the point bar nor the boundary between the bar and channel fill are apparent in (A). Unit boundaries in (B) were adapted from mapping by Harris (1980), his Figure 6.

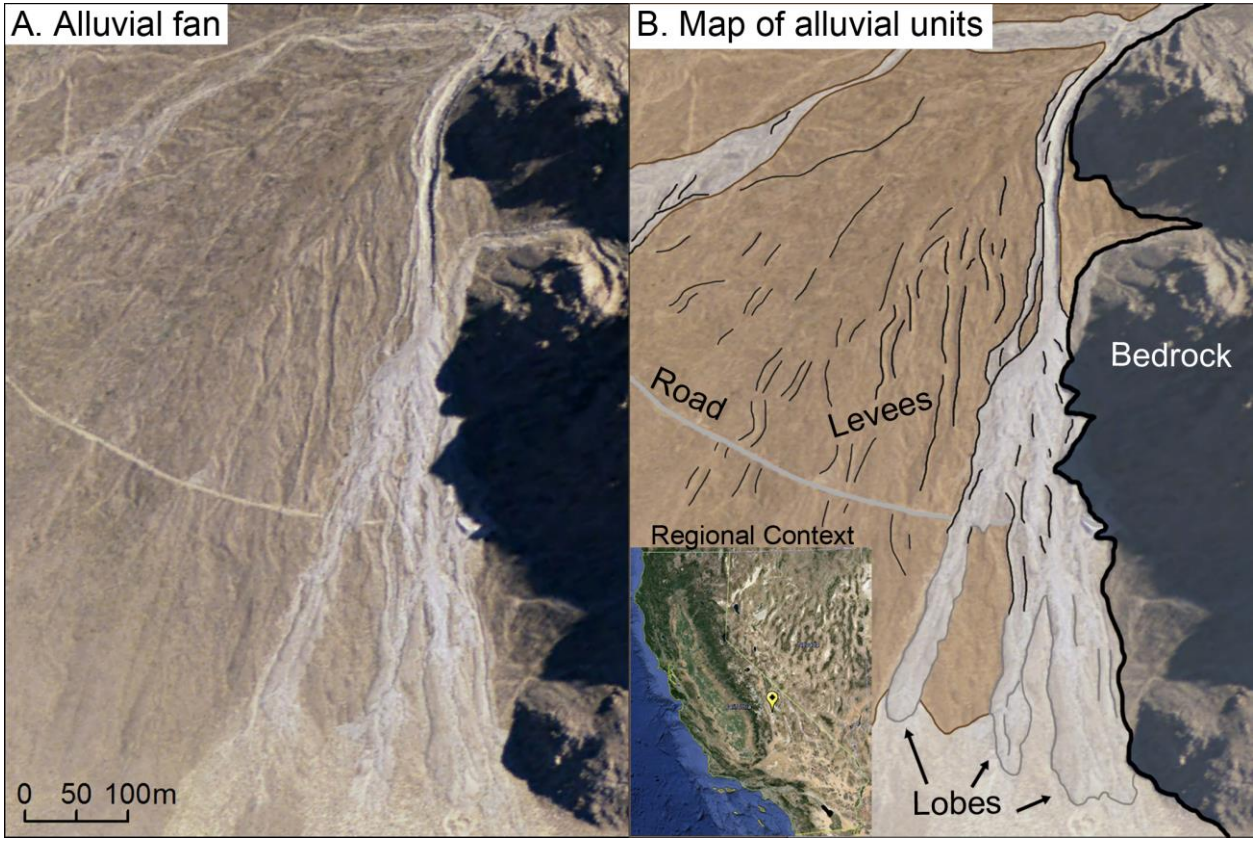

Figure I-11. (A) National Agriculture Imagery Program image of the Dolomite alluvial fan, located near Dolomite, CA, USA, near 36.60 N, 117.97 W. Deposits of a 1984 debris flow have higher albedo than older deposits, whose lower albedo is attributed to desert varnish (Blair and McPherson, 1998). **(B)** Map showing interpreted units in (A). Black lines are debris flow levees and the relief of older levees is enhanced by secondary winnowing processes (Blair and McPherson, 1998). Low-relief margins of debris flow lobes are not readily apparent. Mapping of these units was adapted from mapping by Blair and McPherson (1998), their Figure 4.

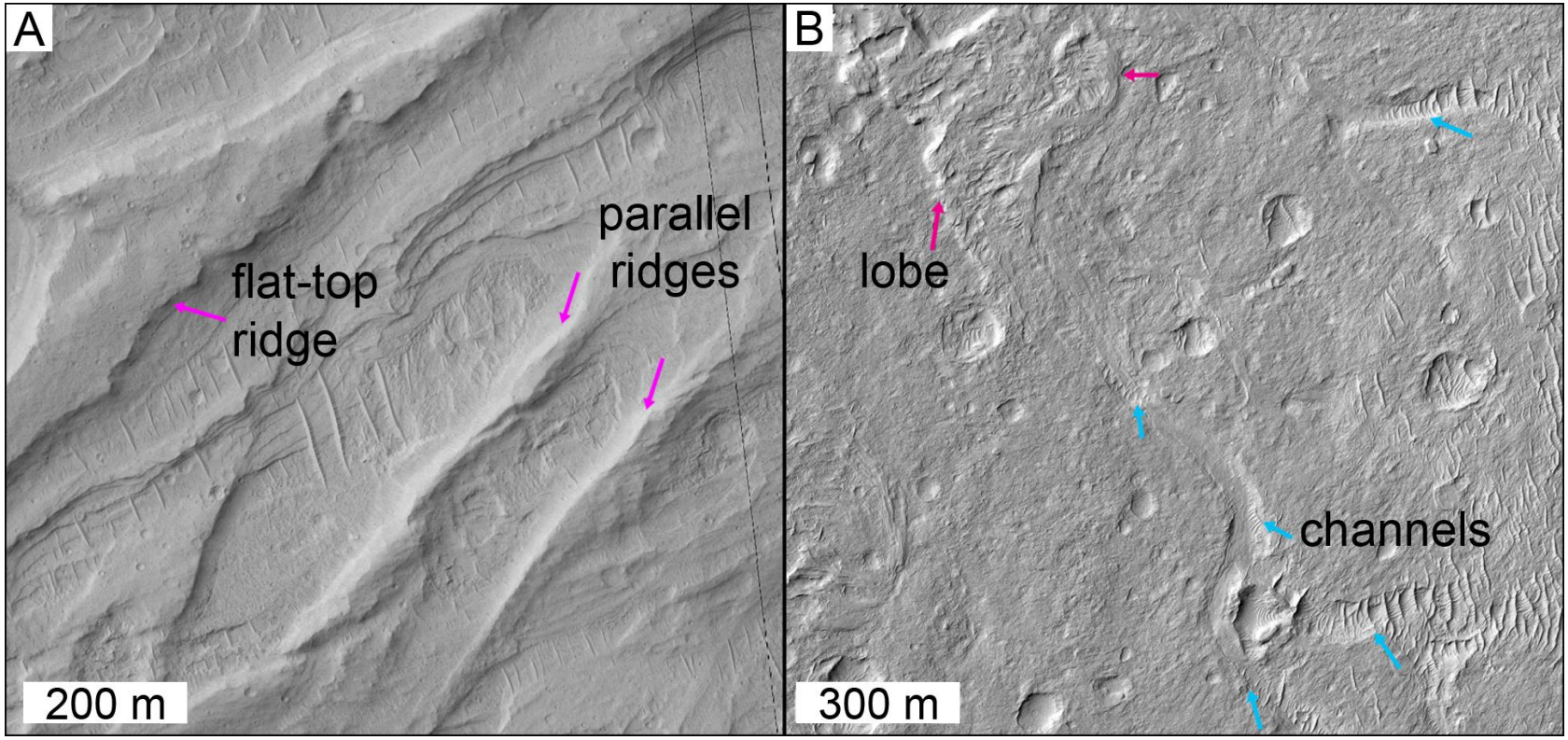

Figure I-12. (A) Portion of HiRISE image (ESP_035468_1755) showing two morphologies of fan ridges. See mapping in Figure I-16 for context. The parallel ridges on the right of (A) are interpreted to be debris flow levees (Table I-3). The ridge with a flat upper surface is consistent with the morphology of an inverted traction deposit (Table I-3). **(B)** Portion of HiRISE image (ESP_019104_1740) showing a lobate feature (pink arrows) interpreted to be a debris flow lobe at the end of an incised channel (blue arrows). See mapping in Figure I-20 for context.

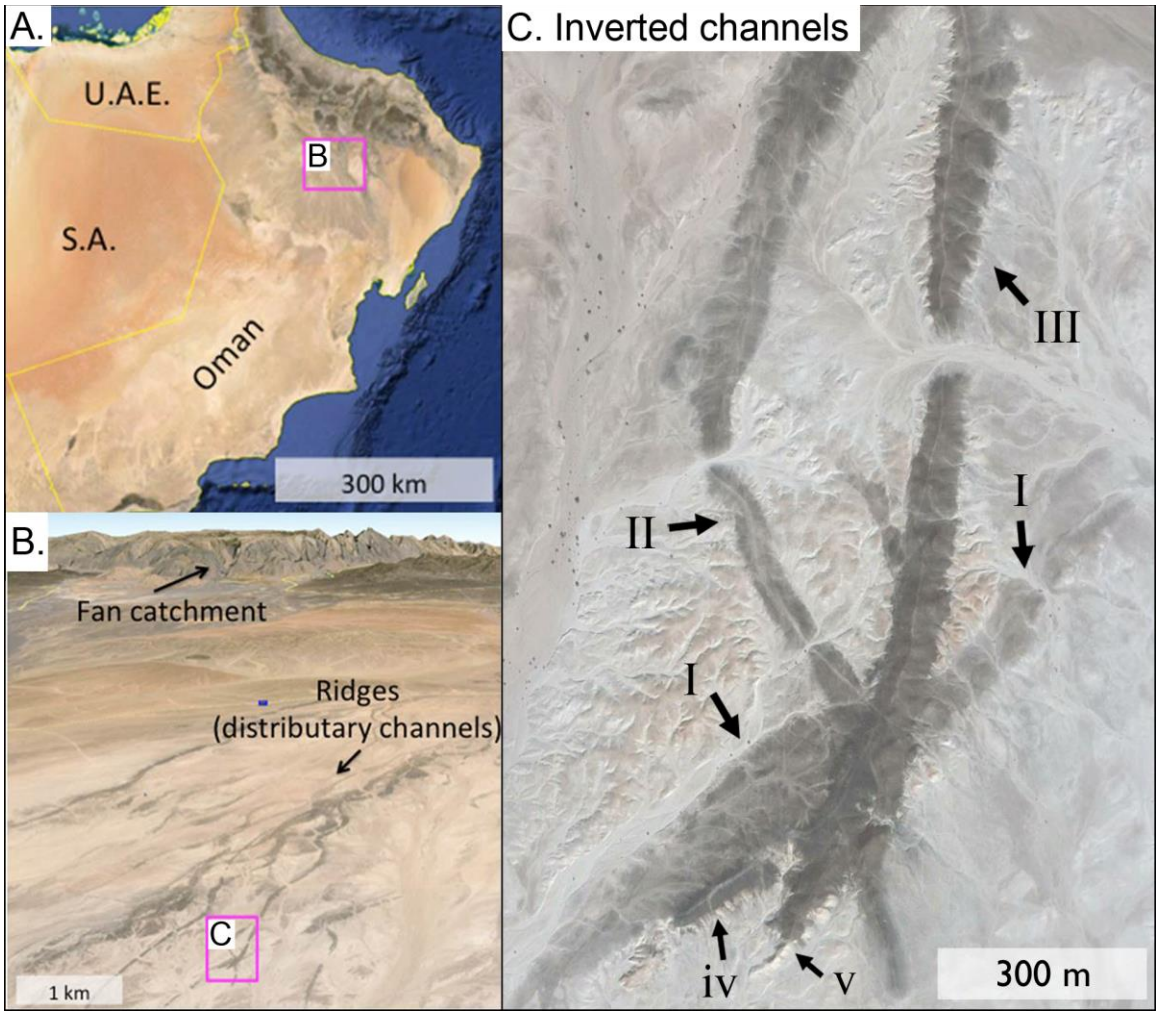

Figure I-13. Satellite images showing the **(A)** regional setting and **(B)** oblique perspective of an ancient alluvial fan in the Sharqiya, Oman. Image (B) shows the location of the Pliocene fan catchment and modern inverted distributary channels. Location of image **(C)** is near 22.26 N, 57.82 E. Image (C) shows three generations of channels, labeled I, II, and III, from oldest to youngest. However, two additional deposits, labeled iv and v, were also identified by Maizels (1990) but are not distinguishable from ridges I and III, respectively, in this plan view examination. Data are from Google, Landsat, US Dept. of State Geographer, and DigitalGlobe.

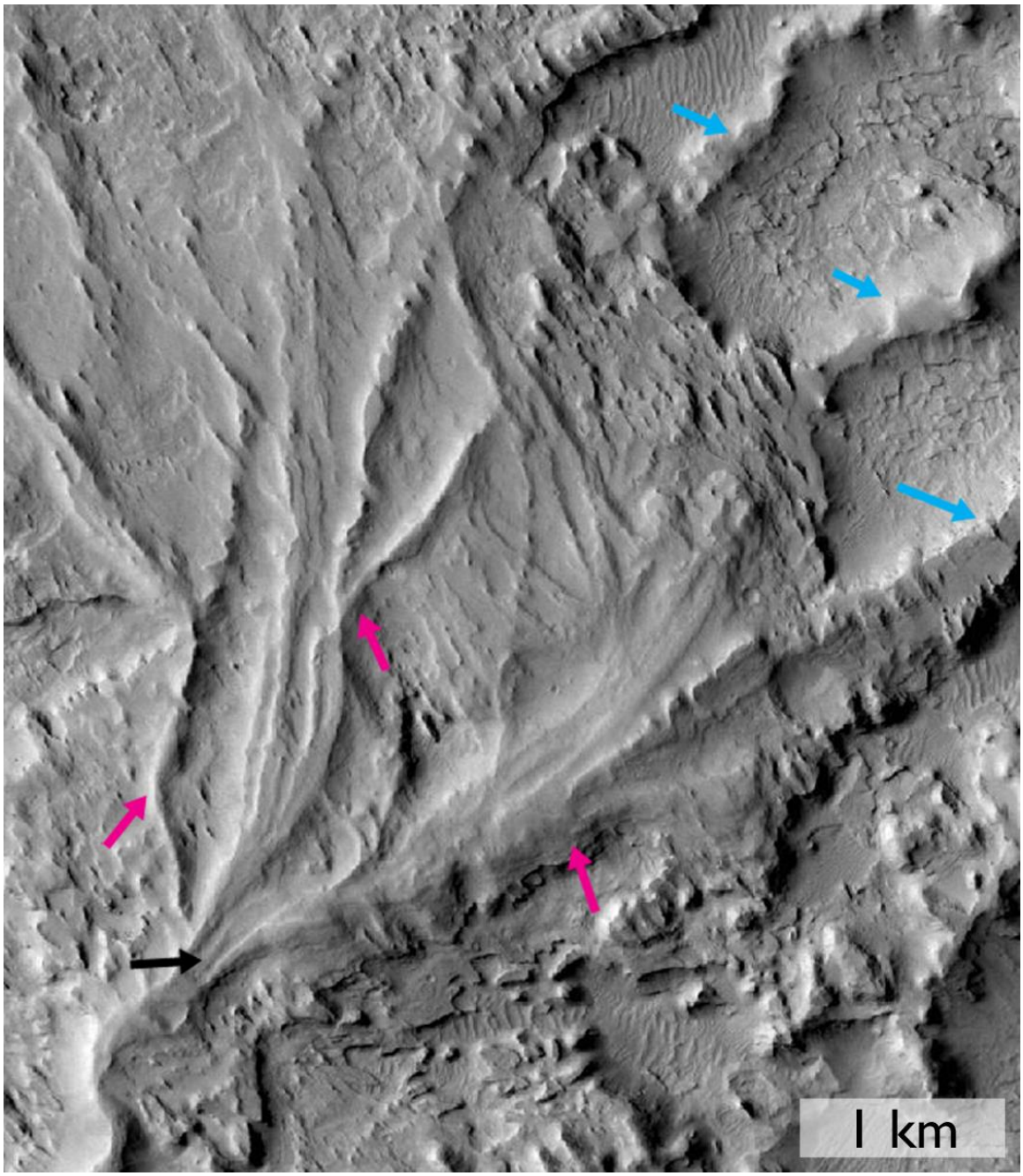

Figure I-14. A portion of the CTX mosaic showing a fan feature in Area 45S with different morphologies of fan ridges (pink arrows). Three sets of fan ridges diverge from the fan apex (black arrow). Fan ridges on the left are thin with sinuous patterns, consistent with traction deposits (Table I-3). Fan ridges on the right are straighter and wider than ridges on the left, suggesting that they may be either traction deposits or sheetflood deposits (Table I-3). The fan feature is stacked above flat features (blue arrows). See mapping in Figure I-22 for context.

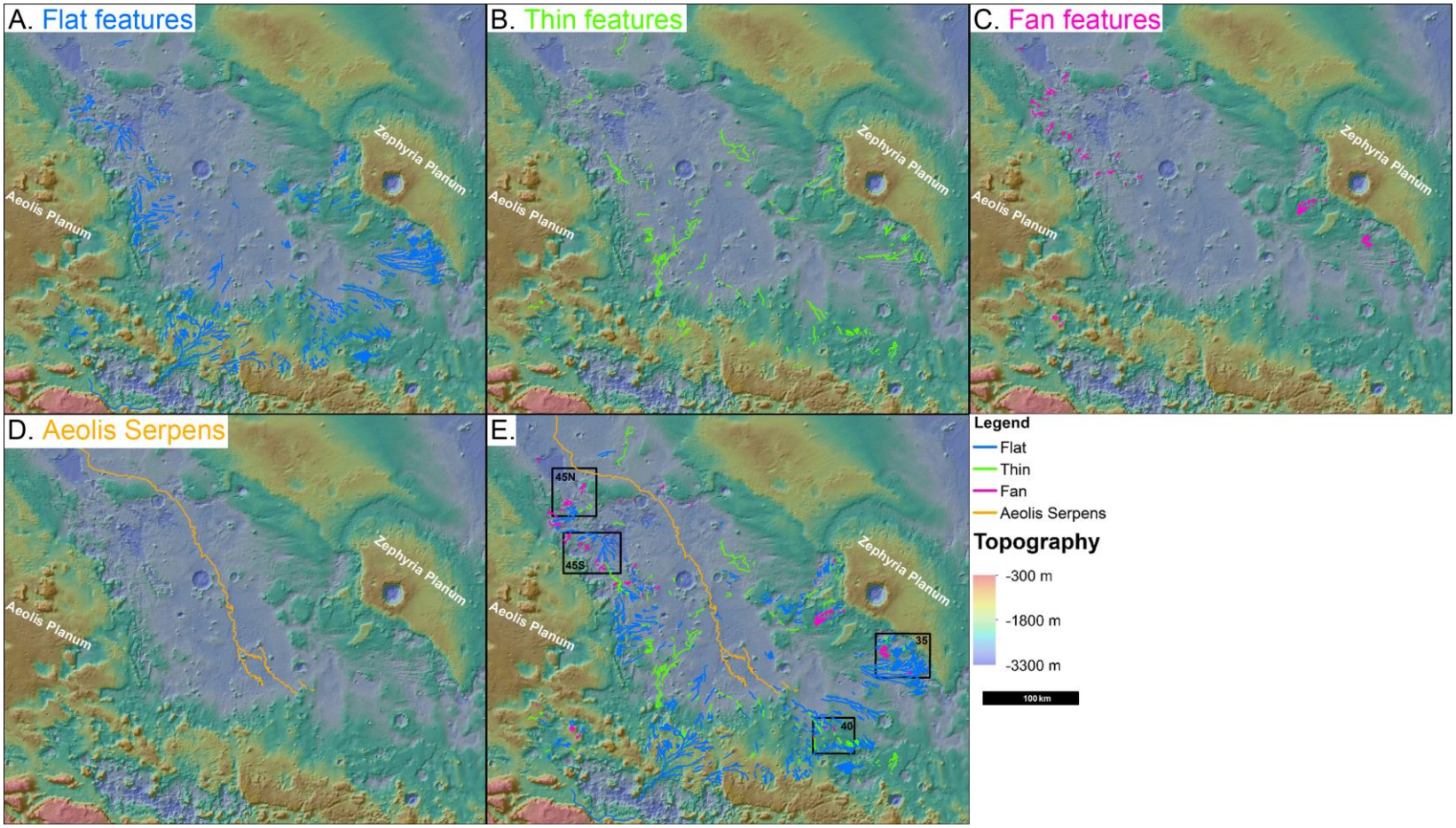

Figure I-15. Delineations of over 1600 features displayed over topographic shaded relief and colors, derived from Mars Orbiter Laser Altimeter data (Smith et al., 2001). Flat features **(A)**, thin features **(B)**, fan features **(C)**, and Aeolis Serpens **(D)** have different geospatial distributions and patterns, but most features are oriented towards the topographic low between Aeolis Planum and Zephyria Planum. All features are shown **(E)**, along with the four local areas, numbered and outlined in black.

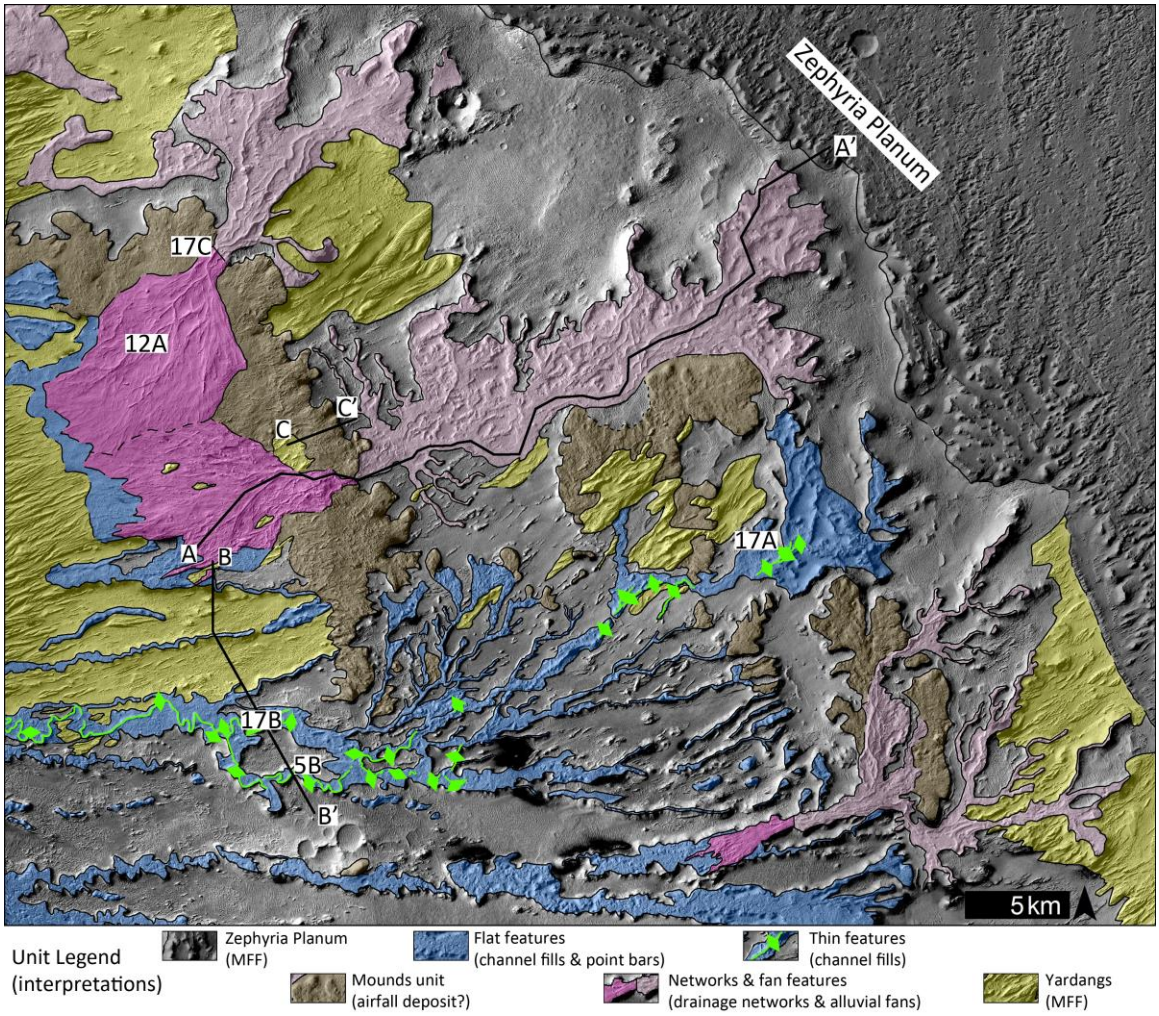

Figure I-16. Area 35 mapped with 7 units, as they appear in the CTX mosaic. Green lines with diamonds delineate fluvial channel fills (i.e., thin features). The drainage network unit (light pink) and alluvial fan unit (dark pink) are interpreted to form an alluvial system, with respective tributary and distributary components. Numbered locations correspond to figure locations. Letters correspond to the ends of topographic profiles derived from CTX stereo DTMs (Figure I-25).

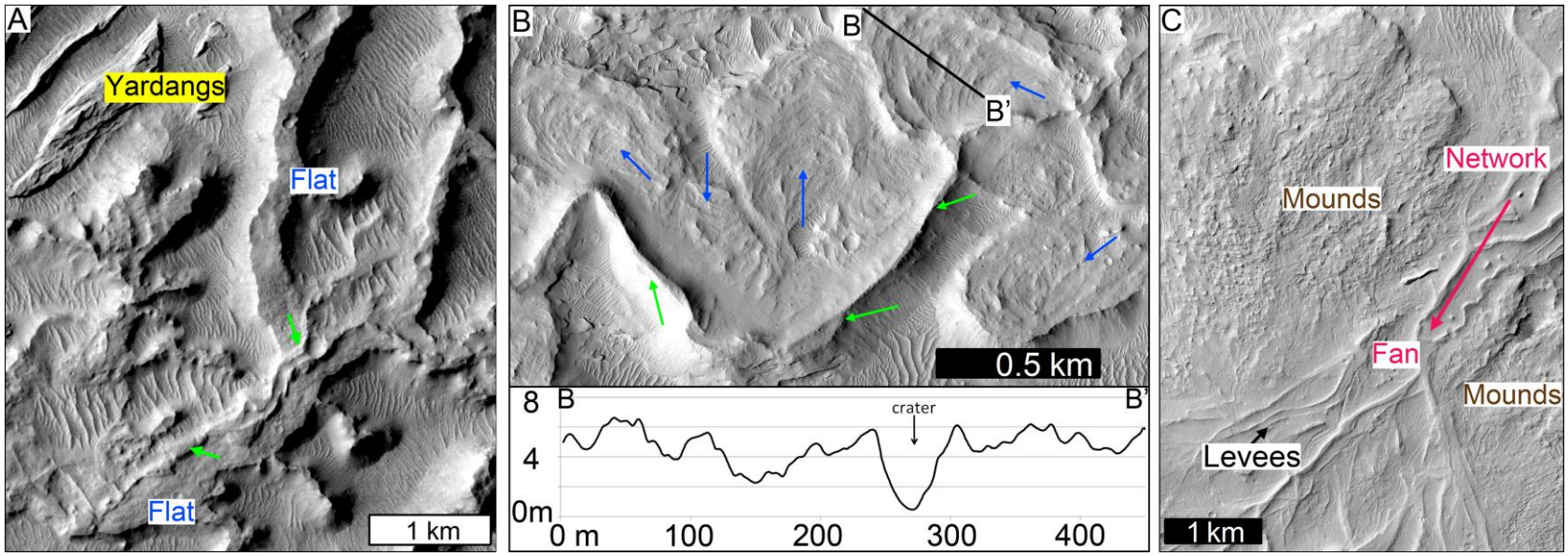

Figure I-17. Examples of geomorphological units in Area 35. **(A)** Networked Type 2 flat features have nondescript upper surfaces consistent with the morphology of fluvial channel fills (Table I-2). A thin feature (green arrows) is stacked on top of the network and is interpreted as a second fluvial channel fill. Yardangs of MFF have NW-SE orientations, suggesting aeolian abrasion by a NW-SE paleo-wind. **(B)** Portion of HiRISE image (PSP_009623_1755) and corresponding DTM profile B-B' show locations of a Type 1 flat feature with meter-scale ridges and swales (blue arrows). The relatively consistent elevations of these ridges and swales are similar to terrestrial meander point bars (Table I-2). A thin feature with both flat-top and sharp-crested sections (green arrows) is stacked on top of the point bar deposit and is consistent with the morphology of fluvial channel fills (Table I-2). This stacking relationship of thin fluvial channel fills above wide fluvial deposits is also shown in Figures I-5B. **(C)** A portion of HiRISE image (ESP_035468_1755) shows the rough surface of the mounds unit, which is adjacent to and cut by ridges of the alluvial fan unit (pink arrow). Here and farther downslope (Figure I-12A), this fan shows parallel ridges, which are similar to the morphology of debris flow levees (Table I-3).

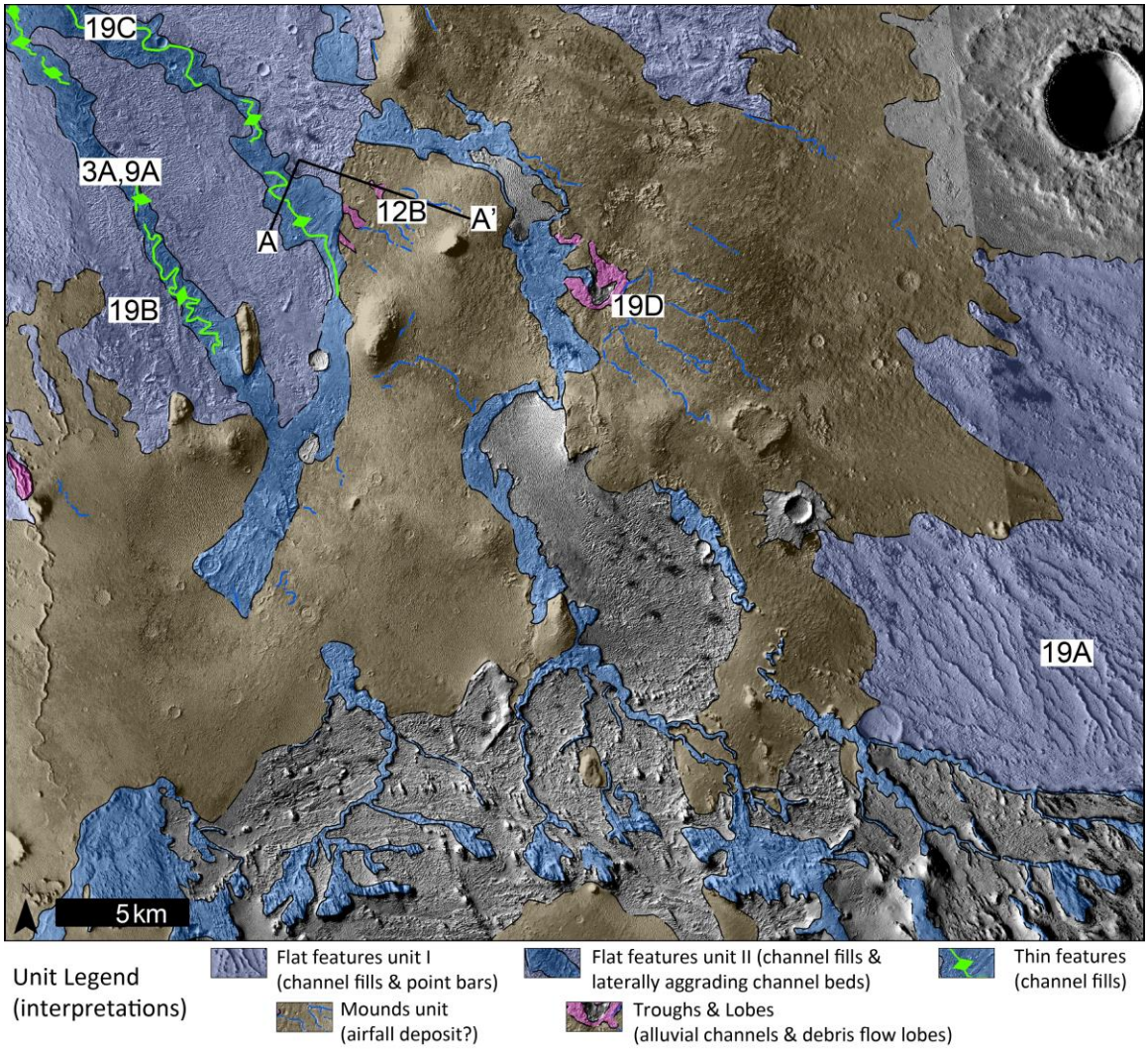

Figure I-18. Area 40 mapped with 5 units, as they appear in the CTX mosaic. Thin blue delineations represent sinuous troughs, some of which connect to lobes (shaded pink). We interpret the coincidence of these troughs and lobes as alluvial channels and debris flow lobes, respectively. Grey areas are undivided units of craters, impact ejecta, and aeolian material. Letters correspond to the ends of topographic profiles derived from CTX stereo DTMs (Figure I-26).

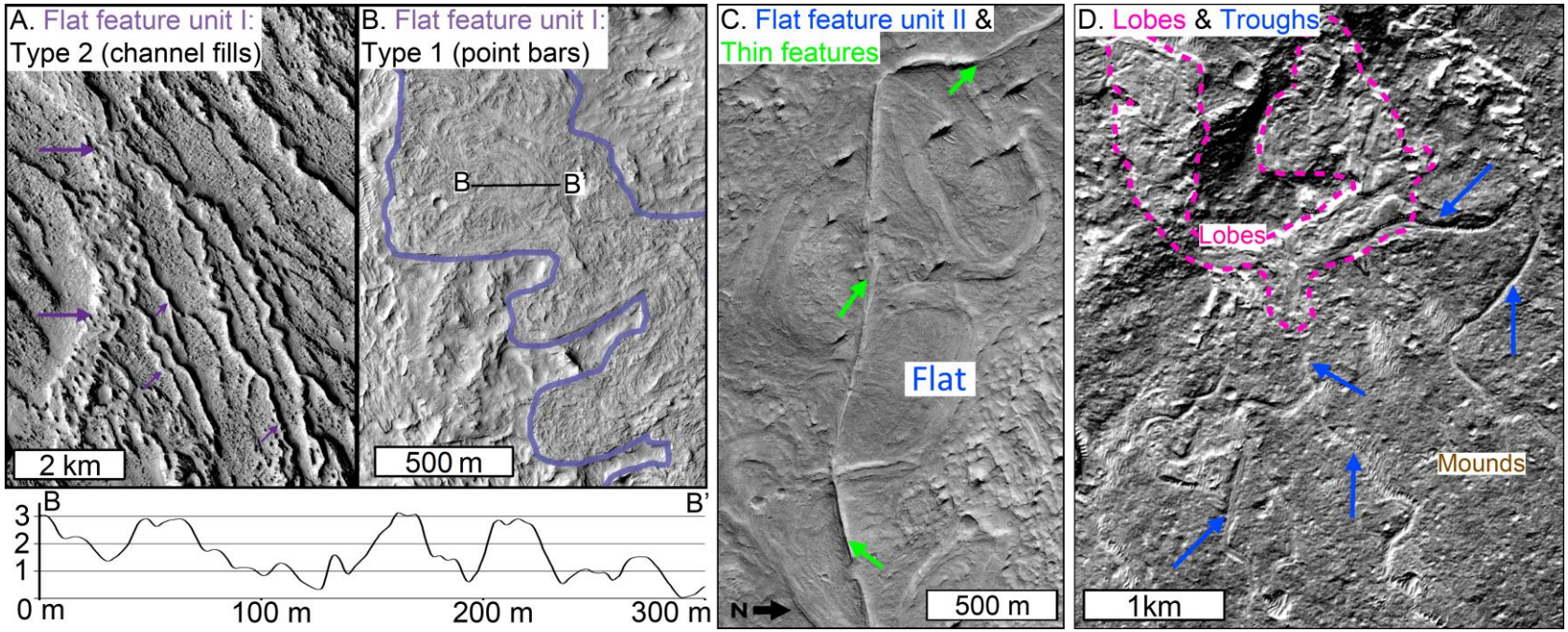

Figure I-19. Examples of geomorphological units in Area 40. **(A)** Type 2 flat features form sub-parallel networks of ridges. The largest ridges in these networks are several hundred meters wide, consistent with flat feature morphology. Based on their relatively nondescript upper surfaces lacking semi-concentric ridges, these networks are interpreted as many interconnect fluvial channel fills (Table I-2). **(B)** Portion of HiRISE image (PSP_006683_1740) shows a Type 1 flat feature. HiRISE DTM profile B-B' shows that the upper surface of this feature has meter-scale ridges and swales, consistent with the topography of meander point bar deposits (Table I-2). **(C)** A thin feature (green arrows) appears above a Type 1 flat feature of unit II. The thin features in this area have some sections with flat upper surfaces, but are mostly sharp-crested, likely shaped by aeolian abrasion. These flat upper surfaces are consistent with the morphologies of fluvial channel fills (Table I-2). **(D)** Sinuous troughs (blue arrows) appear in the mounds unit and are connected to lobes (pink dashed outline) as is shown in Figure I-12B. The troughs and lobes are interpreted as alluvial channels and debris flow deposits, respectively, based on their morphological similarity to terrestrial deposits (Table I-3).

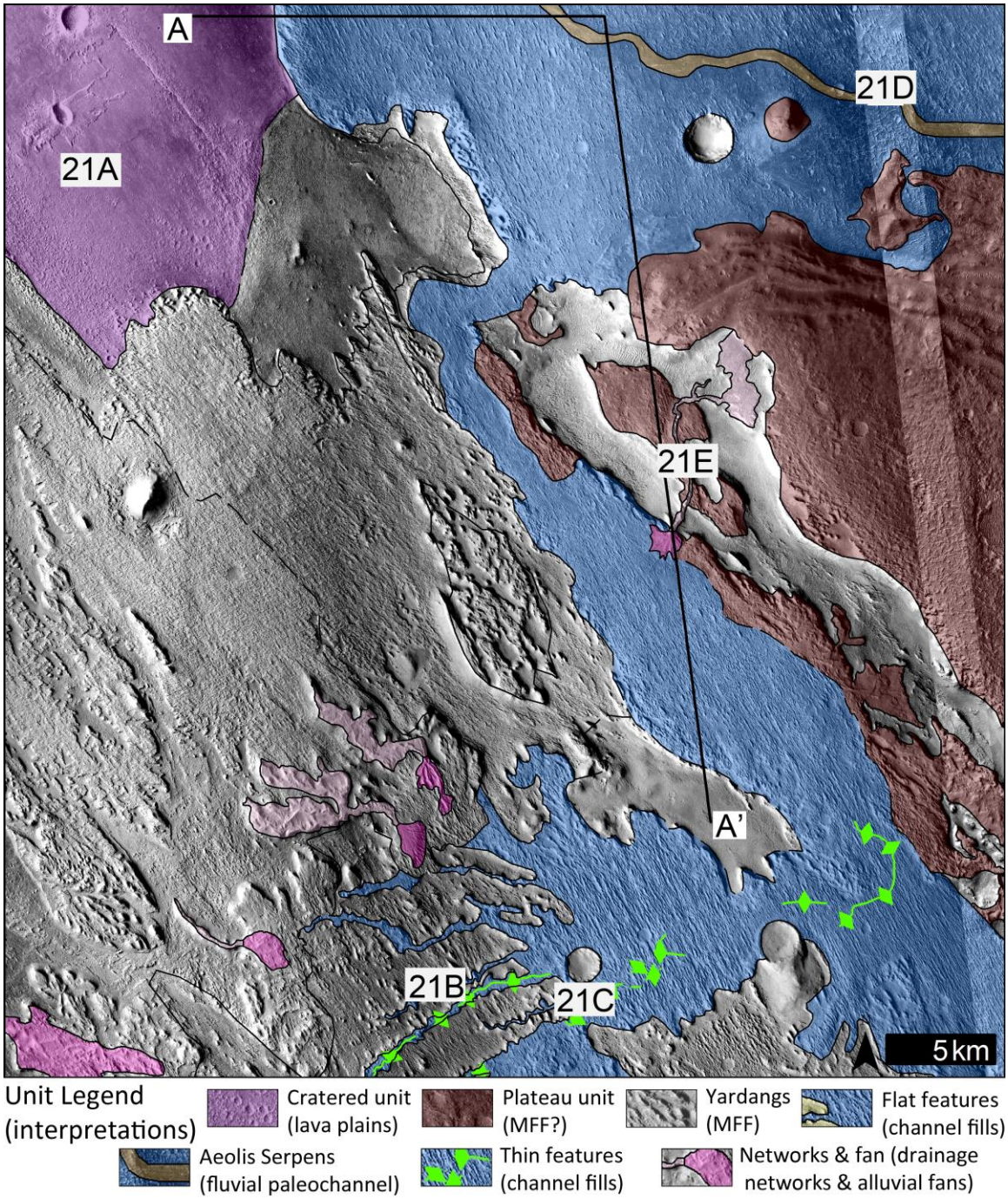

Figure I-20. Area 45N mapped with 7 units, as they appear in the CTX mosaic. Dashed lines through the unit of yardangs (e.g., south of the cratered unit) delineate boundaries between possible sub-units of MFF. Letters correspond to the ends of topographic profiles derived from CTX stereo DTMs (Figure I-27).

Figure I-21. Examples of geomorphological units in Area 45N. **(A)** The cratered unit has smooth surfaces between many small craters and a wrinkle ridge. Similar feature are also found on Hesperian and Amazonian lavas north of Aeolis Dorsa (Kerber and Head, 2010 and references therein). **(B)** Type 2 flat features have nondescript upper surfaces that we interpret as fluvial channel fills (Table I-2). The fluvial channel fill at the bottom of the image has a thin feature (green arrow) on its upper surface, suggesting the formation of a superposing thin fluvial channel fill. These ridges connect eastward (to Figure I-21C) and form a large deposit with three units. **(C)** Three units of the large deposit are fluvial channel fills of flat features (blue outlines), thin superposing channel fills (green arrows), and NW-SE yardangs. **(D)** In this map area, Aeolis Serpens exhibits twin lateral ridges (orange arrows). **(E)** Fan and network units appear adjacent to the plateau unit. The ridge connecting the network and the fan is surrounded by high-standing material. We interpret this material as remnant portions of the plateau unit, the original source area which has eroded away from the fan. The fan is small and consists of wide and flat ridges that are morphologically consistent with sheetflood and/or traction deposits (Table I-3).

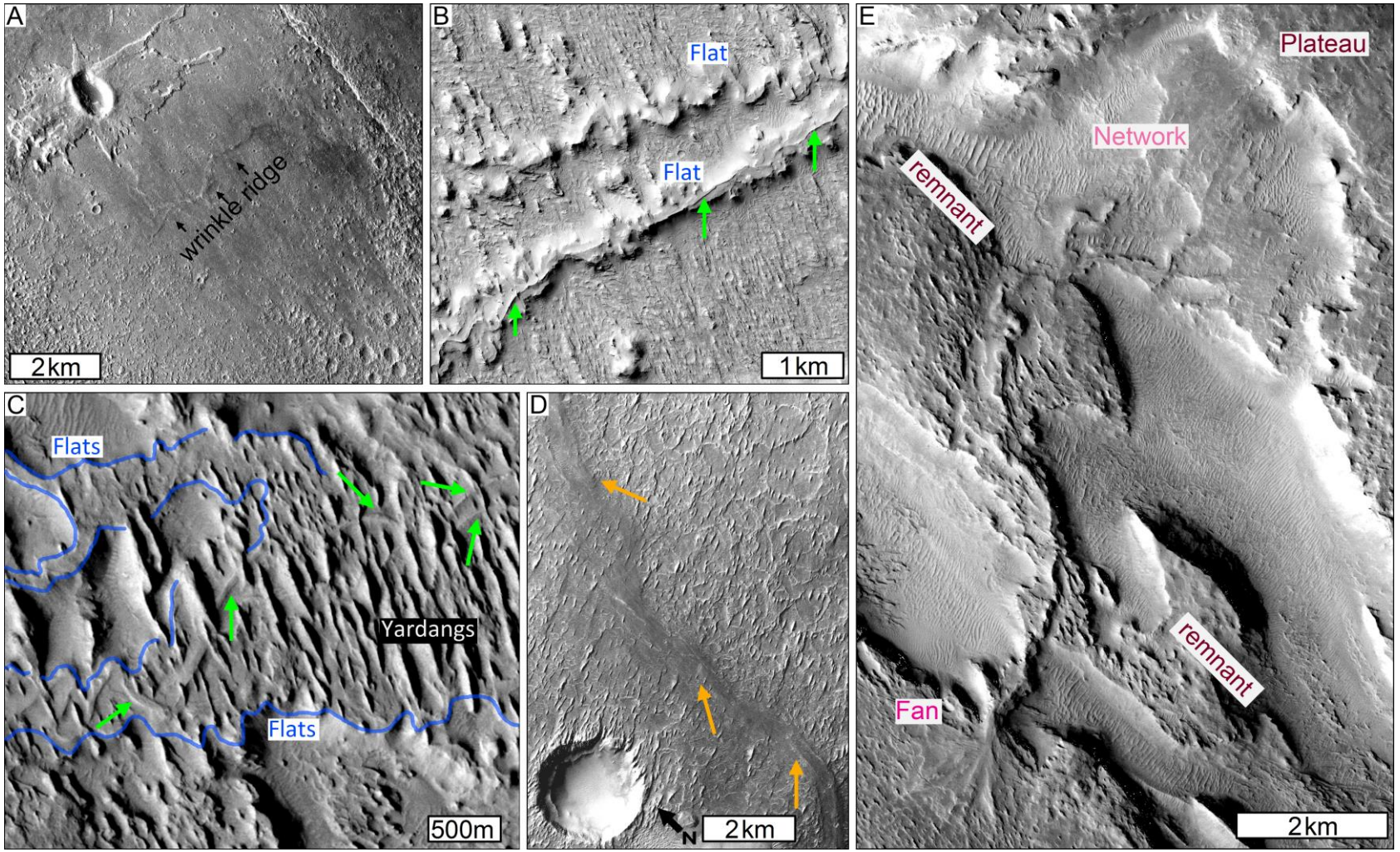
A
wrinkle ridge
2km
B
Flat
Flat
1km
C
Flats
Yardangs
Flats
500m
D
N
2km
E
Plateau
Network
remnant
remnant
Fan
2km

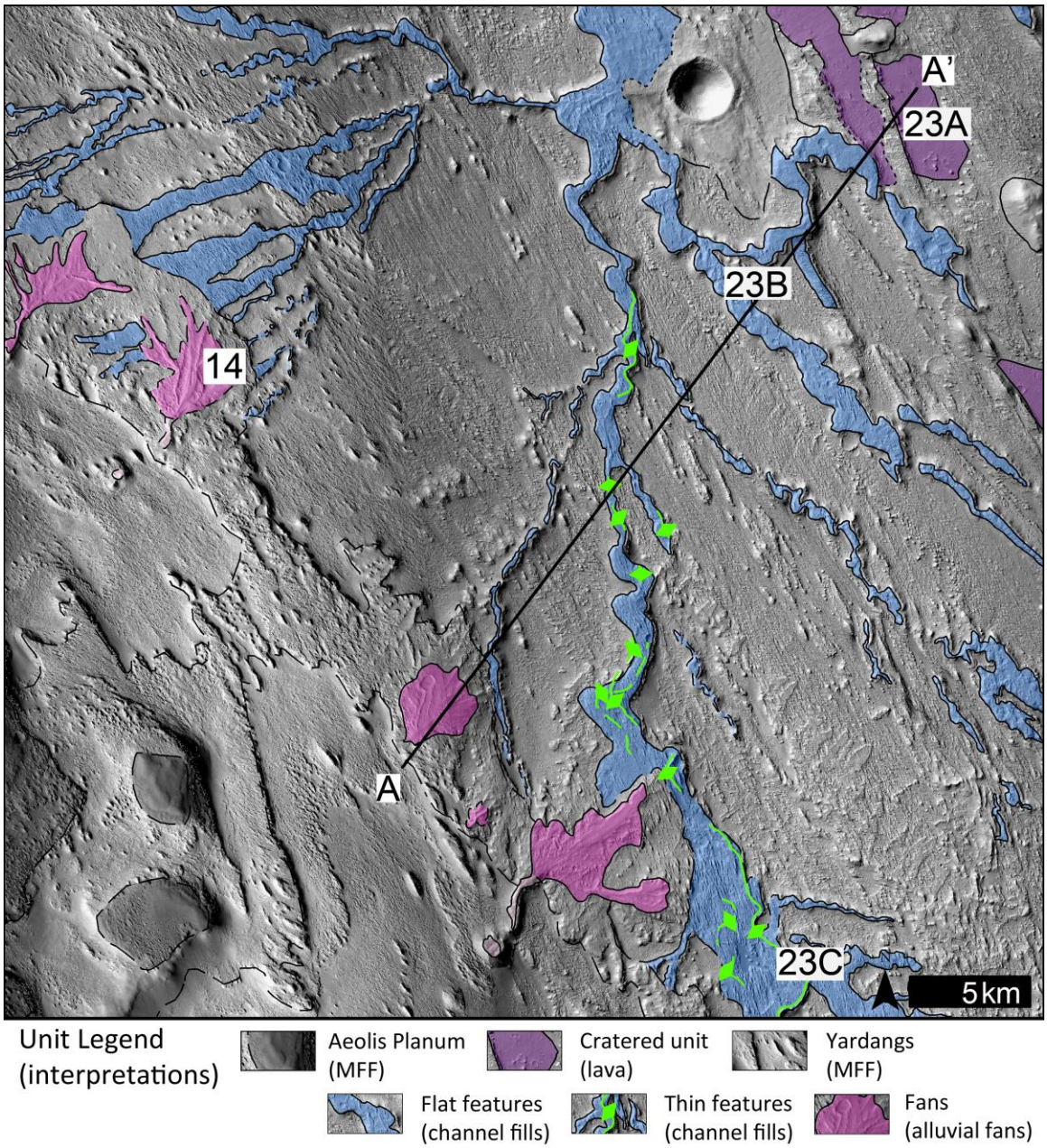

Figure I-22. Mapping of Area 45S suggests 6 units as they appear in the CTX mosaic. Dark grey unit in the southwest corner corresponds to the eastern margin of Aeolis Planum (Figure I-15E). Dashed lines around yardangs mark boundaries between possible sub-units of MFF. Letters correspond to the ends of topographic profiles derived from CTX stereo DTMs (Figure I-28).

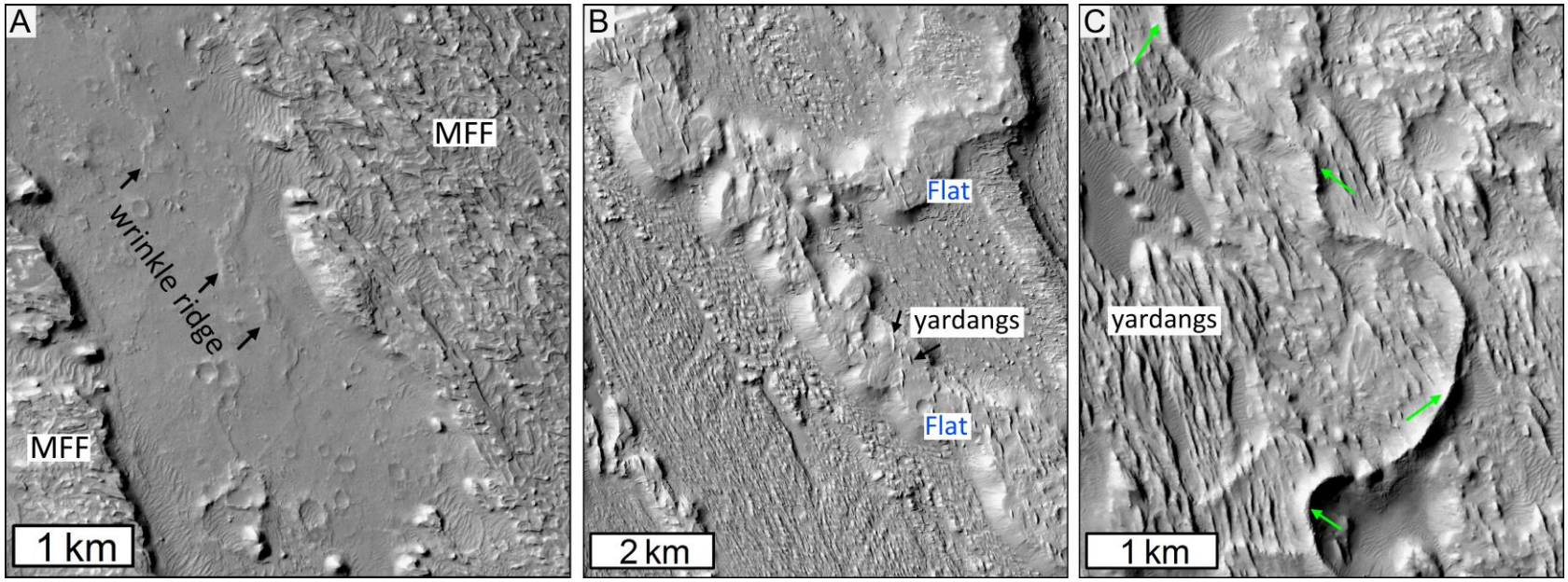

Figure I-23. Examples of geomorphological units in Area 45S. **(A)** A cratered unit appears between units of MFF, forming crude yardangs with northwest-southeast orientations. The cratered unit has a smooth surface texture between many small craters and a wrinkle ridge. As for Area 45N (Figure I-21A), we interpret the cratered unit as lava based on similar textures and features observed north of Aeolis Dorsa (cf. Kerber and Head, 2010). **(B)** Type 2 flat features are consistent with fluvial channel fills based on their flat, nondescript upper surfaces (Table I-2). Yardangs with northwest-southeast orientations appear on the upper surfaces of fluvial channel fills, similar to Area 45N (Figure I-21C). **(C)** This thin feature has sharp crests (green arrows), which would suggest the formation of a fluvial channel fill (Table I-2). The pervasive yardangs in Area 45S suggest that aeolian abrasion has been an effective erosional process in this area. Aeolian abrasion of thin features may explain the formation of sharp crests along thin features, and degradation of flat upper surfaces in this area.

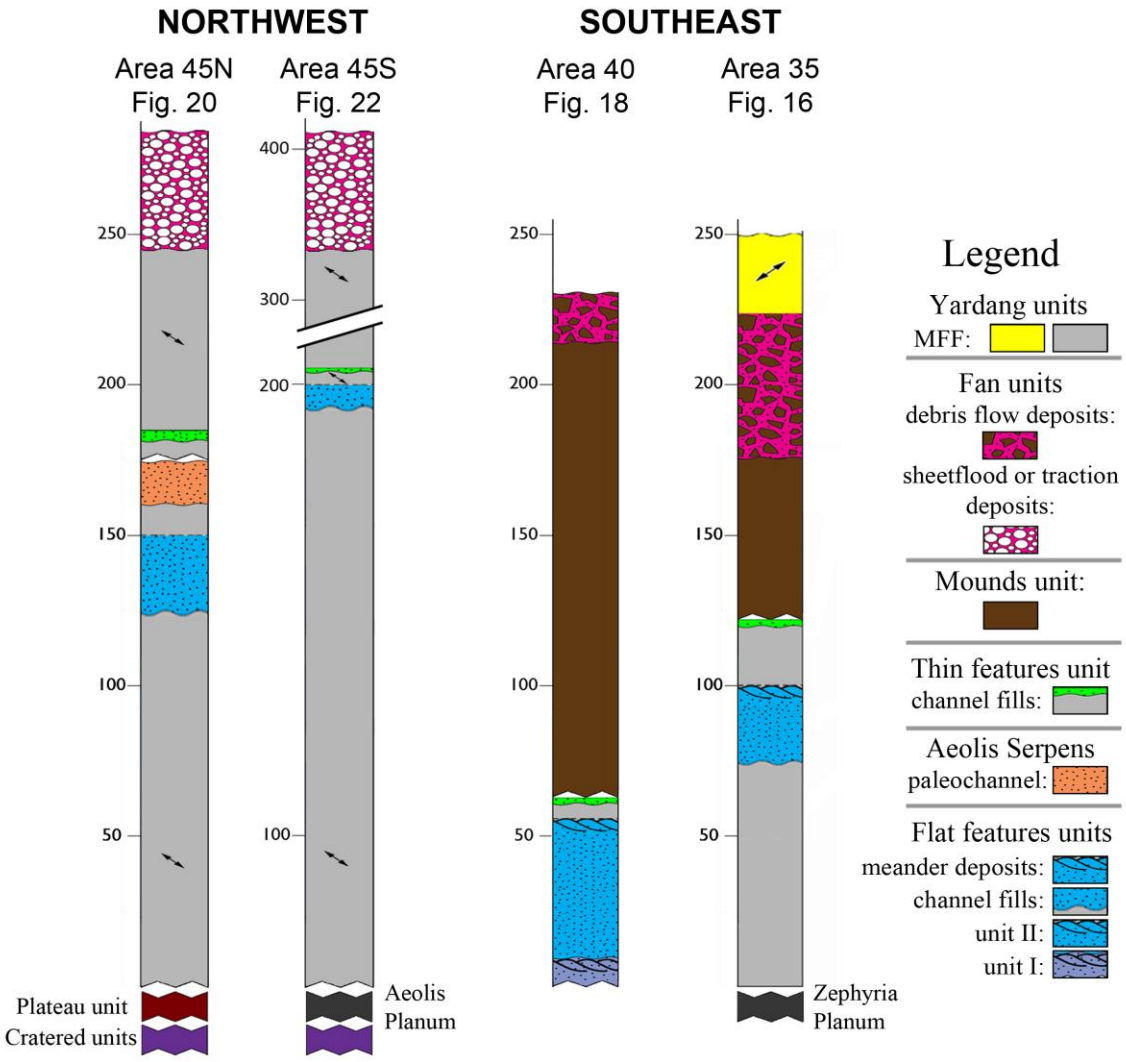

Figure I-24. Stratigraphic columns for the four map areas. Area locations are shown in Figures I-2 & I-15E. Unit names and annotations for specific sedimentary units appear in the legend. Unit colors in stratigraphic columns match unit colors in local area maps (maps figure numbers above columns). Broken and jagged contacts between units represent an uncertain stratigraphic relationship and unit thickness, both of which are explained in the text. Bimodal arrows in units indicate the orientations of yardangs. Note the change in scale for Area 45S relative to the other areas.

Figure I-25. Topographic profiles through Area 35 (Figure I-16). Profile A-A' shows the relationships among Zephyria Planum, alluvial fan, and drainage network units. Hypotheses for the undulations along profile A-A' include settling or faulting (Lefort et al., 2013). Profile B-B' shows the topography over fluvial, alluvial, yardang units, and the underlying MFF. Profile C-C' is shown on the diagram for profile A-A' in order to compare the mound and the adjacent alluvial fan, which cuts the mounds unit (Figure I-17C).

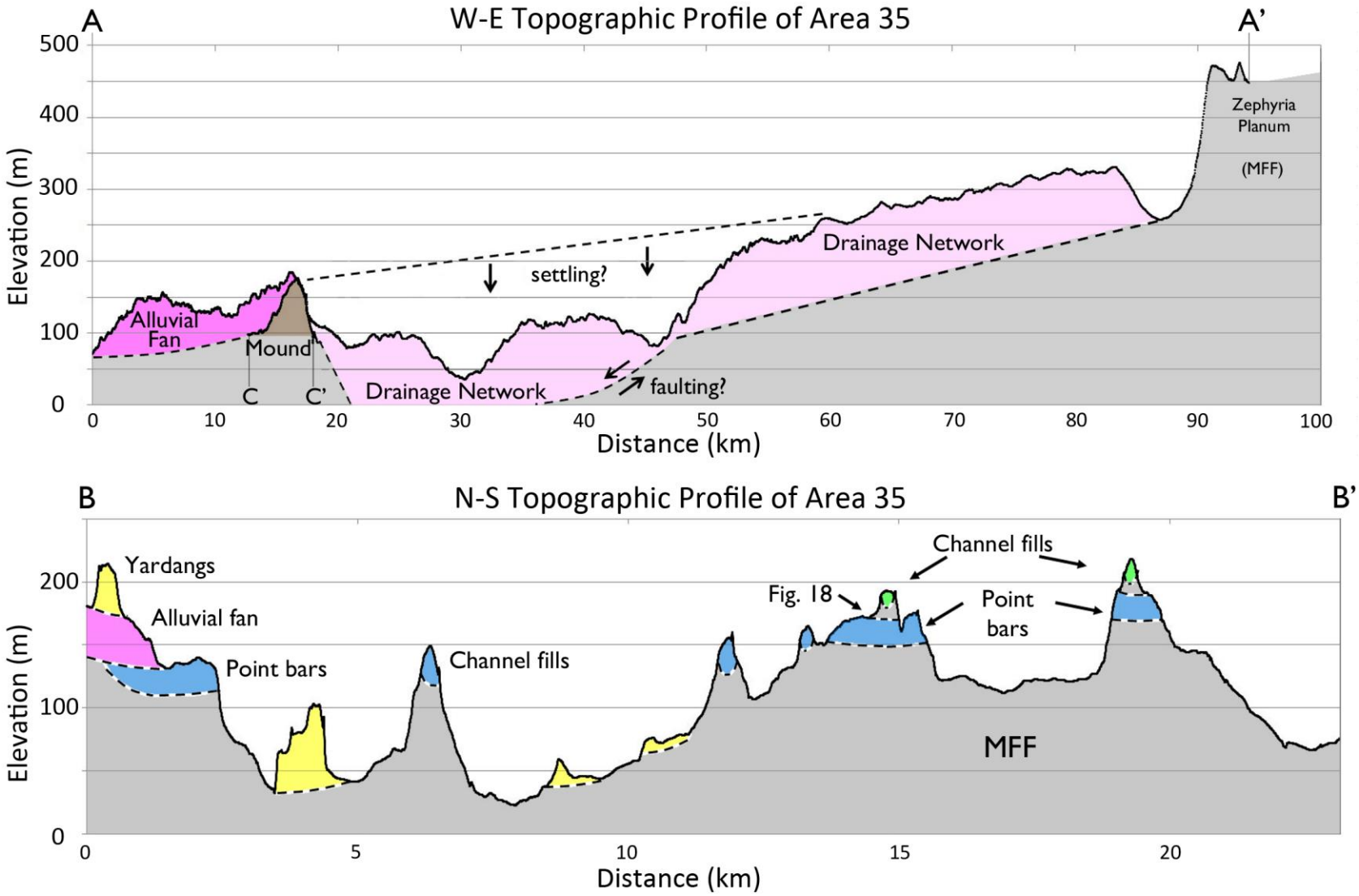
A
W-E Topographic Profile of Area 35
A'
Elevation (m)
500
400
300
200
100
0
Zephyria
Planum
(MFF)
Drainage Network
settling?
Alluvial
Fan
Mound
C
C'
Drainage Network
faulting?
0
10
20
30
40
50
60
70
80
90
100
Distance (km)
B
N-S Topographic Profile of Area 35
B'
Channel fills
Yardangs
Fig. 18
Point
bars
Alluvial fan
Point bars
Channel fills
MFF
Elevation (m)
200
100
0
0
5
10
15
20
Distance (km)

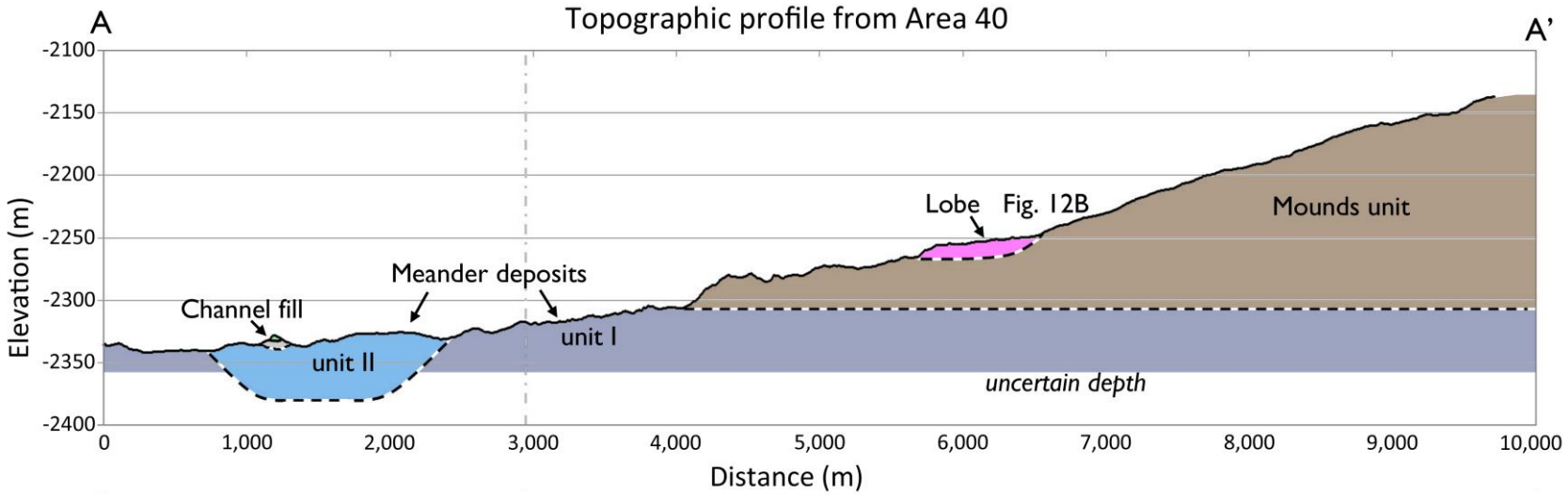

Figure I-26. Topographic profile in Area 40 (Figure I-18). Profile A-A' from a CTX stereo DEM shows the topography and inferred stratal geometries of units in this area. Vertical gray line marks the near right-angle turn in profile heading.

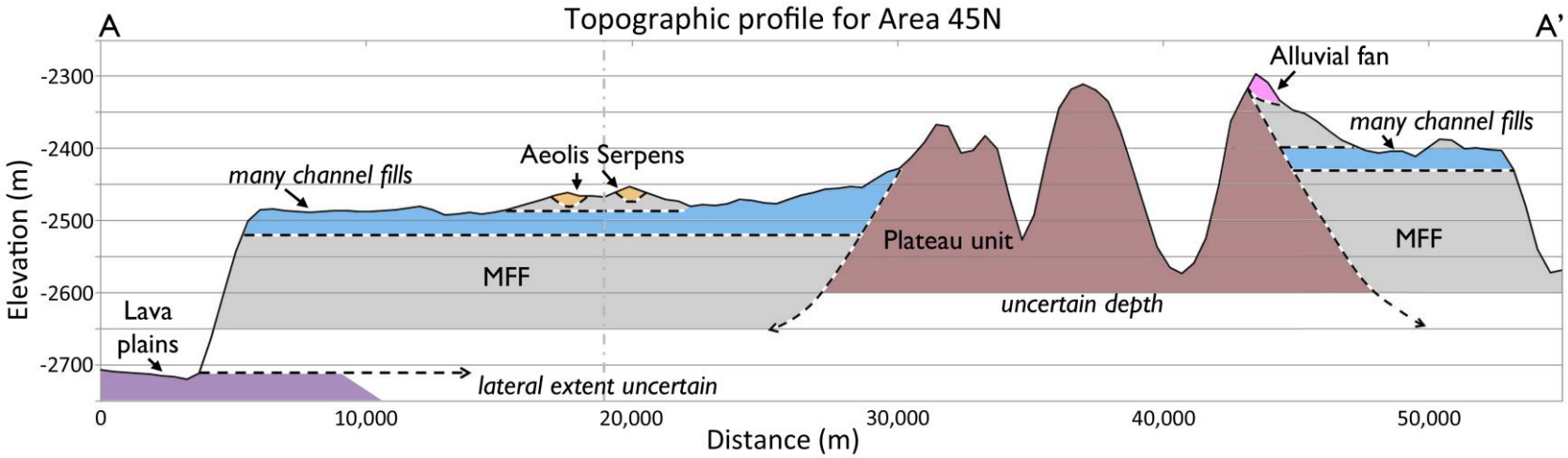

Figure I-27. Topographic profile through Area 45N (Figure I-20). Profile A-A' from MOLA gridded DEM shows the surface topography and inferred subsurface relationships of units. Vertical gray line marks the right turn in profile heading towards the south.

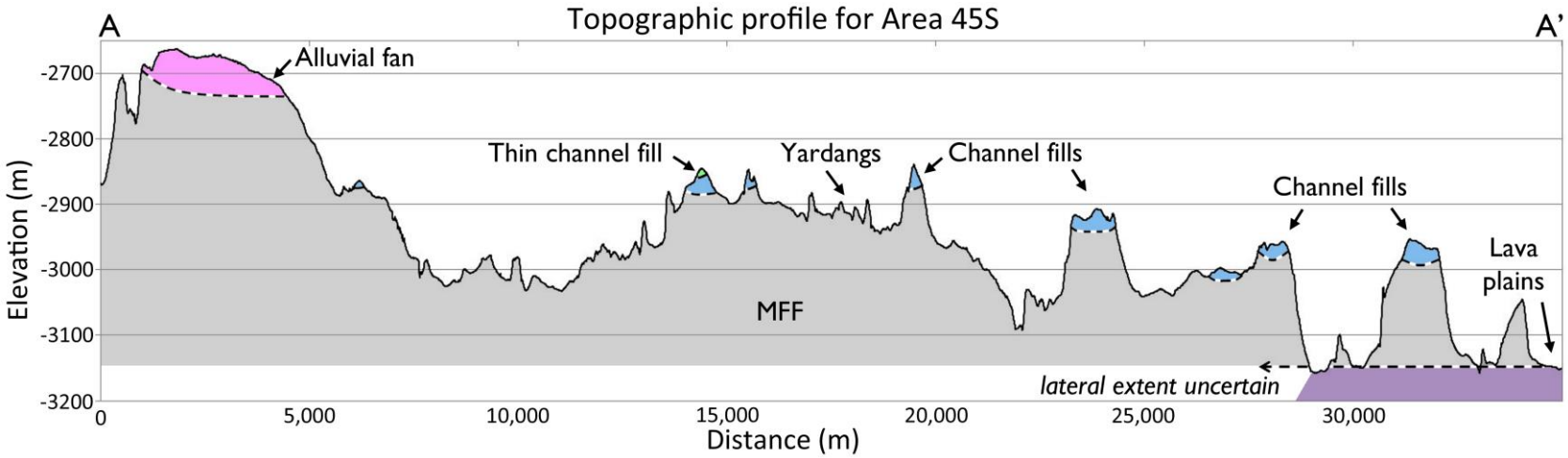

Figure I-28. Topographic profile through Area 45S (Figure I-22). Profile A-A' from a CTX DTM shows the topography of units in Area 45S.

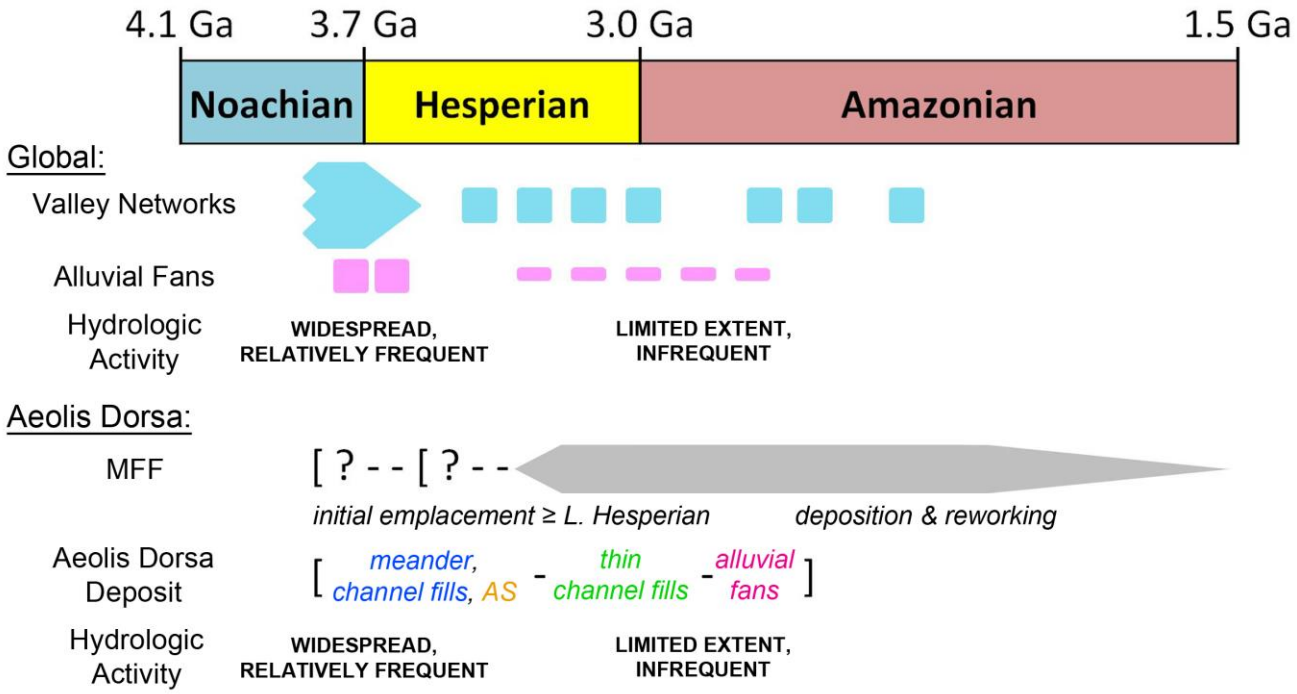

Figure I-29. Portion of the Martian geologic timescale and age-dates of major hydrologic features, which suggest an overall Noachian to Amazonian, "wet-to-dry" hydrological transition (Carr and Head, 2010). These wet and dry conditions are described in terms of the frequency of hydrologic activity and the geospatial extend of that activity. Hydrologic activity during the Late Noachian formed extensive valley networks throughout the southern highlands (Hynek et al., 2010). By the Late Amazonian, hydrologic activity was intermittent and limited to the formation of networks on volcanoes (Fassett and Head, 2008) and alluvial fans within craters (Parsons et al., 2013). Initial emplacement of the MFF occur during the Late Hesperian or earlier (Kerber and Head, 2010), suggesting that the initial episode of hydrologic activity and sedimentation that formed the earliest Aeolis Dorsa deposits may have occurred during the Noachian-Hesperian transition or sometime during the Hesperian. The last-preserved episode of hydrologic activity has not been age dated, but may have occurred as late as the Amazonian, similar to alluvial fans elsewhere on Mars (Grant and Wilson, 2011). Timeline adapted from Carr and Head (2010), their Figure 1.

Chapter II

Greater Contrast in Martian Hydrological History from More Accurate Estimates of Paleodischarge

This chapter is a reformatted version of the manuscript published in the journal Geophysical Research Letters:

Jacobsen, R. E., and D. M. Burr (2016), Greater contrast in Martian hydrological history from more accurate estimates of paleodischarge, Geophys. Res. Lett., 43, doi:10.1002/2016GL070535.

Robert Jacobsen collected the data, performed the analyses, and drafted the manuscript and figures. Devon Burr provided advice on the science and edited the manuscript and figures.

Abstract

Correlative width-discharge relationships from the Missouri River Basin are commonly used to estimate fluvial paleodischarge on Mars. However, hydraulic geometry provides alternative, and causal, width-discharge relationships derived from broader samples of channels, including those in reduced-gravity (submarine) environments. Comparison of these relationships implies that causal relationships from hydraulic geometry should yield more accurate and more precise discharge estimates. Our remote analysis of a Martian-terrestrial analog channel, combined with in-situ discharge data, substantiates this implication. Applied to Martian features, these results imply paleodischarges of interior channels of Noachian-Hesperian (~3.7 Ga) valley networks have been underestimated by a factor of several, whereas paleodischarges for smaller fluvial deposits of the Late Hesperian-Early Amazonian (~3.0 Ga) have been overestimated. Thus, these new paleodischarges significantly magnify the contrast between early and late Martian hydrologic activity. Width-discharge relationships from hydraulic geometry represent validated tools for quantifying fluvial input near candidate landing sites of upcoming missions.

Introduction

Valley networks, paleolakes, and diverse sedimentary deposits on Mars evidence ancient climates with precipitation leading to channelized runoff, which has been quantified as paleodischarge [*Fassett and Head*, 2005; *Irwin et al.*, 2005a, 2015; *Burr et al.*, 2010; *Williams and Weitz*, 2014; *von Paris et al.*, 2015]. Estimates of paleodischarge have been used in landscape evolution models with implications for the frequency and duration of ancient precipitation [e.g., *Howard*, 2007; *Hoke et al.*, 2014]. Paleodischarge is, therefore, a critical variable linking Martian geomorphology with specific paleoclimate conditions. Paleodischarge has also been used to characterize the fluvial input of ancient deltaic and lacustrine environments, which have been considered as possible sites of future landed rovers [*Fassett and Head*, 2005; *Williams and Weitz*, 2014; *Irwin et al.*, 2015; *Golombek et al.*, 2016].

Empirical relationships for estimating paleodischarge rely on an oversimplification that fluvial discharge controls dimensions of fluvial channels and their deposits. In reality, fluvial channels are shaped by multiple independent variables, including discharge, slope, sediment load, and flow resistance, which are accounted for in physical formulae (i.e., Chézy-Manning, Darcy-Weisbach) [*Knighton*, 1998]. However, on Mars, many of these variables are either not preserved or cannot be reliably estimated. Without knowledge of these variables, empirical width-discharge relationships between discharge and one planform variable – most commonly width – have been essential tools for estimating paleodischarges of Martian paleochannels (Figure II-1a) [e.g., *Irwin et al.*, 2005a; *von Paris et al.*, 2015], fluvial deposits (Figure II-1b) [e.g., *Burr et al.*, 2010], and some putative channels on Titan [*Jaumann et al.*, 2008]. Table II-1 lists previous applications of width-discharge relationships.

Other empirical relationships, derived from hydraulic geometry, relate discharge to its three component variables, width, depth, and velocity [*Leopold and Maddock*, 1953]. Hydraulic geometry relationships have been used extensively in terrestrial geomorphology and ecohydrology, and to make orbital-scale predictions of regional fluvial discharge [e.g., *Eaton*, 2013; *Gleason and Smith*, 2014]. Hydraulic geometry relationships between width and discharge may be algebraically rearranged to solve for discharge, and thus, provide alternative width-discharge relationships for estimating paleodischarge on Mars. However, the relative accuracy of these two types of empirical relationships, particularly for application to Mars, is not known.

In this paper, we compare the rationale, data, and derivation these two types of width-discharge relationships. We then apply both types of relationships to a Martian analog channel for which discharge is known. We compare the resultant discharge estimates with the known discharge to evaluate relative accuracies and precisions of these two types of relationships. Lastly, we apply our findings to Martian features to assess any differences from previous paleodischarge estimates.

Background

Correlative width-discharge relationships

Width-discharge relationships used to estimate paleodischarge on Mars were derived from terrestrial discharge records and measurements of planform dimensions, including width, wavelength, and radius of curvature [*Williams*, 1988; *Wharton*, 1995]. The width-discharge relationship most commonly used on Mars (Table II-1) was derived from 252 channels in the Missouri River Basin (MRB),

$$Q_{2yr} = 1.9W_{ac}^{1.22} \qquad (2.1),$$

where Q_{2yr} is the discharge that recurs every two years, calculated from a distribution of annual peak discharges, and W_{ac} is the active channel width, defined as the distance between opposing breaks in bank slope [*Osterkamp and Hedman*, 1982]. The two-year discharge and the distribution of annual peak discharges, in general, are largely

determined by climate, variability of precipitation, and the hydrologic response of an individual watershed [*Rosbjerg et al.*, 2013], whereas the active channel width is largely determined by bank strength and the extent of bank vegetation [*Osterkamp and Hedman*, 1982]. Therefore, variables of width and discharge in equation (2.1) have no known causal relationship and are correlative. The standard error of relationship (2.1) is 109% or 0.41 log units, reflecting the large scatter of width-discharge data (Figure II-2) and the systematic uncertainty involved with estimating discharge. Discharge and width data (Figure II-2) used to derive correlative relationship (2.1) were sampled from channels comprising a spectrum of bed and bank sediment (i.e., clays to cobbles), but mostly include channels with sandy beds and banks (96 of 252 channels) and channels <90 meters wide (237 of 252 channels) [*Osterkamp and Hedman*, 1982].

In most cases, the correlative relationship (2.1) has been scaled in extraterrestrial applications to account for the putative effect of lower gravity relative to Earth [*Irwin et al.*, 2005a; *Jaumann et al.*, 2008; *Williams et al.*, 2009; *Burr et al.*, 2010]. Applying the most commonly used scale factor for Mars (0.76; see Table II-1) to relationship (2.1) yields

$$Q = 1.44W^{1.22} \qquad (2.2),$$

where Q represents a formative discharge, with no specific recurrence interval, and W is the width between edges of the preserved channel or deposit [e.g., *Irwin et al.*, 2005a; *Burr et al.*, 2010]. However, scaling relationship (2.1), and others (Table II-1), for differences in gravity may not be necessary based on analyses of submarine channels (Figure II-1c), which flow in reduced-gravity environments [*Konsoer et al.*, 2013]. Analyses of submarine channels show that reduced gravity lowers the driving force, forming steeper channel slopes relative to terrestrial river channels, but empirical relationships for submarine channels are similar to hydraulic geometry relationships of terrestrial channels [*Konsoer et al.*, 2013].

Causal width-discharge relationships based on hydraulic geometry

Whereas analysis of MRB data provides correlative width-discharge relationships, hydraulic geometry and algebraic inversion yield causal width-discharge relationships. Hydraulic geometry is of two types. At-a-station hydraulic geometry quantifies flow dimensions and velocity as functions of rising and falling discharge at a gauge station [*Leopold and Maddock*, 1953; *Eaton*, 2013]. Downstream hydraulic geometry uses data from multiple locations along the fluvial system to derive three relationships describing how channel width, depth, and velocity change relative to a 'channel-forming' discharge, commonly taken to be the bankfull discharge or the flow filling the channel cross-section [*Williams*, 1978; *Andrews*, 1980; *Knighton*, 1998; *Eaton*, 2013]. Therefore, hydraulic geometry relationships reflect some degree of causation because they use the same formative process to relate flow and channel variables [*Williams*, 1978; *Andrews*, 1980; *Knighton*, 1998; *Eaton*, 2013]. Causal hydraulic geometry data of fluvial channels (Figure II-2) form remarkably consistent trends over several orders of magnitude of

discharge and width, across a wide range of median grain sizes (<0.062 mm to >25 mm), bank strengths, and sedimentary environments [*Eaton*, 2013; *Konsoer et al.*, 2013; *Gleason and Smith*, 2014]. Two datasets (Figure II-2) of bankfull discharge and width were previously used to derive hydraulic geometry relationships, namely,

$$W_{bf} = 3.35Q_{bf}^{0.536} \qquad (2.3)$$

and

$$W_{bf} = 3.73Q_{bf}^{0.524} \qquad (2.4),$$

where Q_{bf} is the bankfull discharge and W_{bf} is the bankfull width. Associated with these relationships are previously reported depth-discharge and velocity-discharge relationships (Appendix II). The standard error of relationship (2.3) is 0.29 log units [*Eaton*, 2013]; the standard error of relationship (2.4) was not reported [*Konsoer et al.*, 2013].

In order to derive discharge from width, relationships (2.3) and (2.4) may be algebraically rearranged by taking the inverse, which is a valid transformation of relationships derived from data with low variation (i.e., high correlation coefficients) [*Williams and Troutman*, 1987]. Algebraic inversion of causal hydraulic geometry relationships (2.3) and (2.4) yields

$$Q = 0.10W^{1.866} \qquad (2.5)$$

and

$$Q = 0.08W^{1.908} \qquad (2.6),$$

respectively. Relationship (2.5) has been used to estimate paleodischarge of Martian fluvial deposits, but, like relationship (2.2), was scaled for the putative effect of gravity [*Kite et al.*, 2015].

Comparison of width-discharge relationships

Causal width-discharge relationships from hydraulic geometry and correlative width-discharge relationships from MRB data have similar structures and oversimplifications of channel processes. However, these empirical relationships also have several critical differences primarily related to their causal and correlative variables, respectively.

Hydraulic geometry and MRB data are composed of different types of discharge and widths variables, which produce an offset between these two datasets. The first difference is from sampling different types of discharge variables. Commonly, the two-year discharge is greater than the bankfull discharge, which has been shown to have a recurrence interval around 1.5 years [*Williams*, 1978; *Andrews*, 1980; *Knighton*, 1998; *Eaton*, 2013]. Use of the greater two-year discharge instead of the bankfull discharge

increases discharge values in MRB data (i.e., MRB data plot to the right of hydraulic geometry data in Figure II-2). Conversely, active channel width is less than bankfull width [*Osterkamp and Hedman*, 1982]. Therefore, MRB data also plot lower than hydraulic geometry data (Figure II-2).

Offset MRB data affect the derivation of coefficients and exponents, which are poor descriptions of fluvial channels worldwide. The exponent (1.22) of MRB width-discharge relationship (2.1) and the large value of its algebraic inverse ($1.22^{-1} = 0.82$, i.e., the exponent if width were a function of discharge) imply that changes in discharge are accommodated, nearly entirely, by changes in flow width. In comparison, the exponents of hydraulic geometry relationships (2.3) and (2.4) have lower values (~0.5), which imply that changes in discharge are also accommodated by changes in depth and velocity. These hydraulic geometry exponents are constrained by unity with depth-discharge and velocity-discharge relationships (Supporting Information) and are consistent with the range (0.3-0.6) of exponents derived in many hydraulic geometry studies [e.g., *Leopold and Maddock*, 1953; *Knighton*, 1998; *Eaton*, 2013; *Konsoer et al.*, 2013; *Gleason and Smith*, 2014].

Another difference is the selection of explanatory and predicted variables, which affect the exponents of the derived relationships. Derivation of hydraulic geometry relationships (2.3) and (2.4) yielding exponents ~0.5 used discharge as the explanatory variable and channel width as the predicted variable. This selection accurately reflects causation in fluvial systems because discharge is an independent variable and width is a dependent variable. In contrast, derivation of the MRB relationship (2.1) with an exponent of 1.22 used width as the explanatory variable and discharge as the predicted variable. The effect of the selected variables on the derived exponent is apparent from a least-squares regression of the MRB data, but with discharge as the explanatory variable and width as the predicted variable. This reanalysis yields an exponent of 0.58, which is similar to the exponents of the hydraulic relationships and many other hydraulic geometry studies [e.g., *Leopold and Maddock*, 1953; *Knighton*, 1998; *Gleason and Smith*, 2014]. For comparison, the algebraic inverse of this exponent ($0.58^{-1} = 1.72$, i.e., the exponent if discharge were a function of width) is dissimilar from the exponent (1.22) of the original width-discharge relationship (2.1). This comparison (expanded upon in the Supporting Information) suggests that the exponent of relationship (2.1) is the result of sampling correlative variables (i.e., two-year discharge and active channel width) and selection of explanatory and predictor variables that are not consistent with causation in fluvial systems.

Analysis

Although applying multiple correlative width-discharge relationships is the conventional approach for constraining paleodischarge on Mars [e.g., *Williams et al.*, 2009; *Burr et al.*, 2010; *Irwin et al.*, 2015], the above comparison indicates that causal width-discharge relationships from hydraulic geometry provide rational and potentially more robust alternatives. Here, we compare the accuracies of correlative (MRB) width-discharge relationships and of causal (hydraulic geometry) width-discharge relationships

and elucidate which relationship(s) should be applied to Mars for estimating paleodischarge.

The Aeolis Dorsa of Mars include numerous inverted fluvial deposits (e.g., Figure II-1b), some of which were formed by meandering fluvial channels [*Burr et al.*, 2009, 2010; *Matsubara et al.*, 2014]. Meandering rivers on Earth with minimally-vegetated floodplains provide possible analogs for the Aeolis Dorsa [*Matsubara et al.*, 2014]. The Quinn River, NV, (Figure II-1d) actively meanders without appreciable vegetation, exhibits striking plan view similarities to the Aeolis Dorsa, and affords robust data of plan view dimensions and discharge [*Matsubara and Howard*, 2014; *Matsubara et al.*, 2014]. Characteristics of the Quinn River floodplain that enable meandering include abundant paleo-lacustrine clays, and such clays have been identified elsewhere on Mars [e.g., *Williams and Weitz*, 2014].

We conducted a remote hydraulic analysis of the Quinn River. This remote analysis mimics paleohydraulic analyses of Martian paleochannels, but has the advantage of well-preserved channel morphology, exposure, and field observations of relevant variables. Previous *in-situ* observations of channel flow at ~75% bankfull stage and complementary modeling of bankfull conditions provide values of bankfull discharge and width, as 11.9 m^3s^{-1} and 20 meters, respectively [*Matsubara and Howard*, 2014]. Estimates of the two-year discharge (Q_{2yr}) are not possible for the Quinn River because of limited gauge records along the Quinn and in northwest Nevada, in general [*Thomas et al.*, 1997; *Matsubara and Howard*, 2014]. Therefore, we compare estimated discharges with the modeled bankfull discharge (11.9 m^3s^{-1}) of the Quinn River. As discussed above, the two-year discharge is expected to be greater than the bankfull discharge with a 1.5-year recurrence interval. Therefore, the two-year discharge value derived from relationship (2.1) may overestimate bankfull discharge of the Quinn River.

Remote measurements of channel width were made by examining visual images with 1-m spatial resolution provided by the National Agriculture Imagery Program (Figure II-1d) and airborne LiDAR topography with 1-m spatial resolution provided by the National Center for Airborne Laser Mapping (Figure II-3). Along relatively straight channel reaches, we measured bankfull width as the distance between breaks in opposing banks. Along meander bends, we measured bankfull width as the distance between the cut bank and the crest of the innermost point bar (Figure II-3). Measurements were taken approximately every half-kilometer. Average width was coupled with the correlative width-discharge relationship (2.1) from the MRB and the causal width-discharge relationships (2.5) and (2.6) from hydraulic geometry relationships to estimate discharge. Discharge estimates were then compared with the previously reported value. Standard errors of relationships (2.1) and (2.5) were used to calculate 95% prediction intervals (P.I.), which represent the precision of each relationship at the average channel width.

Results

We found an average bankfull channel width of 15 meters (n=44, s.d.=3.5m). Coupled with relationship (2.1), this width yields a discharge estimate of 52 m^3s^{-1} (95% P.I. of 8 – 342 m^3s^{-1}). Coupling the average width of the Quinn River with relationship

(2.5) yields 16 m^3s^{-1} (95% P.I. of 4 – 60 m^3s^{-1}) and relationship (2.6) yields 14 m^3s^{-1}. Comparing these discharge estimates (Figure II-4) to previously reported field observations and modeling of bankfull discharge (11.9 m^3s^{-1}) shows that the correlative width-discharge relationship (2.1) overestimates discharge for the Quinn River by a factor of ~4. It is uncertain how much this overestimate derives from relationship (2.1) estimating the two-year discharge, rather than the bankfull discharge. Estimates from the causal width-discharge relationships (2.5) and (2.6) are more accurate, overestimating discharge by a factor of <2 (Figure II-4).

Discussion

Accurate measurement of channel width is critical in the use of width-discharge relationships because they rely on one dimension to estimate paleodischarge. Previous field observations and bankfull flow modeling suggest a bankfull width of 20 meters, which is greater than the average width of our remote measurements (15 m, $\sigma = 3.5$). Our systematic measurements may underestimate bankfull width as flows may expand along portions of the channel without point bars or at chute cutoffs (Figure II-3). Preservation or modification of original widths on Mars may be detected by comparative morphometry of fluvial planform dimensions [*Burr et al.*, 2010] and by identification of specific in-channel sedimentary units, such as channel fills [*Jacobsen and Burr*, 2015].

Accurate estimates of paleodischarge are critical to a range of investigations in Mars science including quantitative modeling of sedimentary deposition, landscape evolution, and paleoclimate [*Howard*, 2007; *Hoke et al.*, 2014; *von Paris et al.*, 2015]. Although the accuracy or precision of paleodischarge estimates cannot be verified from Martian data, the correlative width-discharge relationship (2.1) from the MRB and others have been assumed to be accurate to within an order of magnitude [*Irwin et al.*, 2005a; *Williams et al.*, 2009] and the results presented here support that order-of-magnitude accuracy. However, a comparison of precision (Figure II-4) shows the prediction interval of relationship (2.1) covers three orders of magnitude and is ~5 times greater than the prediction interval of relationship (2.5).

Based on results from the Quinn River, the more accurate and more precise discharge estimates from algebraically inverted hydraulic geometry relationships indicate the potential for improved paleodischarge estimates for the Aeolis Dorsa deposits. Previous paleodischarge estimates were made by coupling the scaled width-discharge relationship (2.2) with measurements of width [*Irwin et al.*, 2005a, 2015; *Burr et al.*, 2010; *Williams and Weitz*, 2014]. A comparison of empirical relationships (Figure II-5) shows that for widths <60 meters, the scaled width-discharge relationship (2.2) overestimates discharge by a factor of ~2, relative to estimates from relationships (2.5) and (2.6). Previous overestimation of discharges for smaller channels is particularly relevant to younger Martian paleochannels and deposits that formed in the Late Hesperian and Early Amazonian (3.0 Ga) (Table II-1).

Conversely, the comparison of relationships (Figure II-5) also shows that for widths >60 meters, the scaled width-discharge relationship (2.2) underestimates discharge. For example, the inverted channel deposit in Figure II-1b was measured to be

106 meters wide and yielded paleodischarges between 350 and 429 m^3s^{-1} (95% P.I. of 65 – 2,821 m^3s^{-1}) when coupled with scaled width-discharge relationship (2.2) [*Burr et al.*, 2010]. This same width, coupled with causal width-discharge relationship (2.5), yields an estimate of 601 m^3s^{-1} (95% P.I. of 158 – 2,286 m^3s^{-1}). For a second example, the interior channel shown in Figure II-1a was measured to be 380 meters wide, which when coupled with the scaled width-discharge relationship (2.2) yielded a paleodischarge of ~2,000 m^3s^{-1} [*Irwin et al.*, 2005a] (95% P.I. of 306 – 13,394 m^3s^{-1}). However, applying causal width-discharge relationship (2.5) to this channel width yields an estimate of ~6,500 m^3s^{-1} (95% P.I. of 1,713 – 24,767 m^3s^{-1}), a +320% differential. Interior channels of valley networks largely formed during the Noachian-Hesperian transition (3.7 Ga) [*Fassett and Head*, 2008] and have widths up to ~1 km [*Irwin et al.*, 2005a], which would have differential paleodischarge values of ~+600%. Thus, these more accurate paleodischarge estimates collectively increase the contrast of hydrologic activity between early and late periods of Martian hydrologic activity [*Fassett and Head*, 2008] by up to an order of magnitude (Table II-1) and are consistent with the hydrologic record of Martian crater lakes [*Goudge et al.*, 2016].

The applicability of width-discharge relationships from hydraulic geometry to valley-network interior channels is less certain than for the Aeolis Dorsa because the substrate of these channels, whether bedrock, alluvium, or mixed, remains an open question. Large variations between smooth and stepped longitudinal profiles and the relationship between width and drainage area suggest channel substrates may be diverse [*Matsubara et al.*, 2013; *Penido et al.*, 2013]. Simplified hydraulic geometry relationships for bedrock channels have similar exponents as relationships for alluvial channel [*Montgomery and Gran*, 2001; *Finnegan et al.*, 2005], implying that the hydraulic geometry relationships used here are applicable to valley-network interior channels for a variety of substrates. Channels and deposits of alluvial fans and deltas are not necessarily amenable to these hydraulic geometry relationships because fluvial channels fundamentally differ in terms of flow and sediment dynamics [*e.g., Blair and McPherson*, 1994]. Thus, further analysis of hydraulic geometry in diverse terrestrial analogs is needed for improved accuracy in paleodischarge estimates for Martian alluvial fans and deltas.

Conclusions

Data from the MRB used to derive the width-discharge correlation most commonly applied to Mars are fundamentally different from the widely sampled data used to derive causal hydraulic geometry relationships. Our analysis shows that width-discharge relationships from hydraulic geometry are more accurate and more precise at estimating discharge for a Martian-terrestrial analog river than the width-discharge correlation from the MRB. Paleodischarge estimates using causal width-discharge relationships from hydraulic geometry imply that the early Martian climate produced larger channelized discharges, which places new constraints on models for ancient climate, its evolution, and its influence on Martian geomorphology [*Howard*, 2007; *Hoke et al.*, 2014; *von Paris et al.*, 2015; *Goudge et al.*, 2016]. More accurate estimates of

paleodischarge help refine scientific hypotheses of paleo-environments (e.g., lacustrine) that are critical for the evaluation of candidate landing sites for upcoming rover missions, including the Mars 2020 rover [*Fassett and Head*, 2005; *Williams and Weitz*, 2014; *Irwin et al.*, 2015; *Golombek et al.*, 2016].

References

Andrews, E. D. (1980), Effective and bankfull discharges of streams in the Yampa River basin, Colorado and Wyoming, *J. Hydrol.*, *46*(3–4), 311–330, doi:10.1016/0022-1694(80)90084-0.

Baratti, E., M. Pajola, S. Rossato, C. Mangili, M. Coradini, A. Montanari, and K. McBride (2015), Hydraulic modeling of the tributary and the outlet of a Martian paleolake located in the Memnonia quadrangle, *J. Geophys. Res. Planets*, *120*(10), 2015JE004812, doi:10.1002/2015JE004812.

Blair, T. C., and J. G. McPherson (1994), Alluvial fans and their natural distinction from rivers based on morphology, hydraulic processes, sedimentary processes, and facies assemblages; discussion and reply, *J. Sediment. Res.*, *65*, 706–711, doi:10.1306/D42681B2-2B26-11D7-8648000102C1865D.

Burr, D. M., M.-T. Enga, R. M. E. Williams, J. R. Zimbelman, A. D. Howard, and T. A. Brennand (2009), Pervasive aqueous paleoflow features in the Aeolis/Zephyria Plana region, Mars, *Icarus*, *200*(1), 52–76, doi:10.1016/j.icarus.2008.10.014.

Burr, D. M., R. M. E. Williams, K. D. Wendell, M. Chojnacki, and J. P. Emery (2010), Inverted fluvial features in the Aeolis/Zephyria Plana region, Mars: Formation mechanism and initial paleodischarge estimates, *J. Geophys. Res. Planets*, *115*(E7), E07011, doi:10.1029/2009JE003496.

Burr, D. M., Jacobsen, R. E. and Lefort, A. (2016), Thermal Detection of an Extensive Buried Fluvial Unit in the Aeolis Dorsa Region, Medusae Fossae Formation, Mars, *Lunar Planet. Sci.*, XXXXVII, Abstract 1392.

Eaton, B. C. (2013), 9.18 Hydraulic Geometry: Empirical Investigations and Theoretical Approaches, in *Treatise on Geomorphology*, edited by J. F. Shroder, pp. 313–329, Academic Press, San Diego.

Fassett, C. I., and J. W. Head (2005), Fluvial sedimentary deposits on Mars: Ancient deltas in a crater lake in the Nili Fossae region, *Geophys. Res. Lett.*, *32*(14), L14201, doi:10.1029/2005GL023456.

Fassett, C. I., and J. W. Head (2008), The timing of martian valley network activity: Constraints from buffered crater counting, *Icarus*, *195*(1), 61–89, doi:10.1016/j.icarus.2007.12.009.

Finnegan, N. J., G. Roe, D. R. Montgomery, and B. Hallet (2005), Controls on the channel width of rivers: Implications for modeling fluvial incision of bedrock, *Geology*, *33*(3), 229–232, doi:10.1130/G21171.1.

Gleason, C. J., and L. C. Smith (2014), Toward global mapping of river discharge using satellite images and at-many-stations hydraulic geometry, *Proc. Natl. Acad. Sci.*, *111*(13), 4788–4791, doi:10.1073/pnas.1317606111.

Golombek, M. P., J. A. Grant, K. A. Farley, K. Williford, A. Chen, R. E. Otero, and J. W. Ashley (2016), Downselection of Landing Sites Proposed for the Mars 2020 Rover Mission, *Lunar Planet. Sci.*, XXXXVII, Abstract 2324.

Goudge, T. A., C. I. Fassett, J. W. Head, J. F. Mustard, and K. L. Aureli (2016), Insights into surface runoff on early Mars from paleolake basin morphology and stratigraphy, *Geology*, G37734.1, doi:10.1130/G37734.1.

Hoke, M. R. T., B. M. Hynek, G. Di Achille, and E. W. H. Hutton (2014), The effects of sediment supply and concentrations on the formation timescale of martian deltas, *Icarus*, *228*, 1–12, doi:10.1016/j.icarus.2013.09.017.

Howard, A. D., J. M. Moore, and R. P. Irwin (2005), An intense terminal epoch of widespread fluvial activity on early Mars: 1. Valley network incision and associated deposits, *J. Geophys. Res. Planets*, *110*(E12), E12S14, doi:10.1029/2005JE002459.

Howard, A. D., Moore, J. M., Dietrich, W. E. and Perron, J. T. (2008) Martian Gullies: Morphometric Properties and Flow Characteristics, *Lunar Planet. Sci.*, XXXIX, Abstract 1619.

Howard, A. D., and J. M. Moore (2011), Late Hesperian to early Amazonian midlatitude Martian valleys: Evidence from Newton and Gorgonum basins, *J. Geophys. Res. Planets*, *116*(E5), E05003, doi:10.1029/2010JE003782.

Howard, A. D. (2007), Simulating the development of Martian highland landscapes through the interaction of impact cratering, fluvial erosion, and variable hydrologic forcing, *Geomorphology*, *91*(3–4), 332–363, doi:10.1016/j.geomorph.2007.04.017.

Irwin, R. P., K. W. Lewis, A. D. Howard, and J. A. Grant (2015), Paleohydrology of Eberswalde crater, Mars, *Geomorphology*, *240*, 83–101, doi:10.1016/j.geomorph.2014.10.012.

Irwin, R. P., R. A. Craddock, and A. D. Howard (2005a), Interior channels in Martian valley networks: Discharge and runoff production, *Geology*, *33*(6), 489–492, doi:10.1130/G21333.1.

Irwin, R. P., A. D. Howard, R. A. Craddock, and J. M. Moore (2005b), An intense terminal epoch of widespread fluvial activity on early Mars: 2. Increased runoff and paleolake development, *J. Geophys. Res. Planets*, *110*(E12), E12S15, doi:10.1029/2005JE002460.

Jacobsen, R. E., and D. M. Burr (2015), Wet-to-Dry Hydrological Transition Encapsulated in Fluvial Stratigraphy of Aeolis Dorsa, Mars, *Lunar Planet. Sci.*, XXXXVI, Abstract 1011.

Jaumann, R. et al. (2008), Fluvial erosion and post-erosional processes on Titan, *Icarus*, *197*(2), 526–538, doi:10.1016/j.icarus.2008.06.002.

Kite, E. S., A. D. Howard, A. Lucas, and K. W. Lewis (2015), Resolving the era of river-forming climates on Mars using stratigraphic logs of river-deposit dimensions, *Earth Planet. Sci. Lett.*, *420*, 55–65, doi:10.1016/j.epsl.2015.03.019.

Knighton, D. (1998), *Fluvial forms and processes: a new perspective*, pp. 383, Hodder Arnold, London.

Konsoer, K., J. Zinger, and G. Parker (2013), Bankfull hydraulic geometry of submarine channels created by turbidity currents: Relations between bankfull channel characteristics and formative flow discharge, *J. Geophys. Res. Earth Surf.*, *118*(1), 216–228, doi:10.1029/2012JF002422.

Leopold, L. B., and T. Maddock (1953), *The hydraulic geometry of stream channels and some physiographic implications*, Professional Paper 252, United States Geological Survey, Washington, D. C.

Malaska, M. et al. (2011), High-Volume Meandering Channels in Titan's South Polar Region, *Lunar Planet. Sci.*, XXXXII, Abstract 1562.

Matsubara, Y., A. D. Howard, and J. P. Gochenour (2013), Hydrology of early Mars: Valley network incision, *Journal of Geophysical Research: Planets*, *118*(6), 1365–1387, doi:10.1002/jgre.20081.

Matsubara, Y., and A. D. Howard (2014), Modeling planform evolution of a mud-dominated meandering river: Quinn River, Nevada, USA, *Earth Surf. Process. Landf.*, *39*(10), 1365–1377, doi:10.1002/esp.3588.

Matsubara, Y., A. D. Howard, D. M. Burr, R. M. E. Williams, W. E. Dietrich, and J. M. Moore (2014), River meandering on Earth and Mars: A comparative study of Aeolis Dorsa meanders, Mars and possible terrestrial analogs of the Usuktuk River, AK, and the Quinn River, NV, *Geomorphology*, doi:10.1016/j.geomorph.2014.08.031.

Montgomery, D. R., and K. B. Gran (2001), Downstream variations in the width of bedrock channels, *Water Resour. Res.*, *37*(6), 1841–1846, doi:10.1029/2000WR900393.

Osterkamp, W. R., and E. R. Hedman (1982), *Perennial-streamflow characteristics related to channel geometry and sediment in Missouri River basin*, Professional Paper 1242, United States Geological Survey, Washington, D. C.

von Paris, P., A. Petau, J. L. Grenfell, E. Hauber, D. Breuer, R. Jaumann, H. Rauer, and D. Tirsch (2015), Estimating precipitation on early Mars using a radiative-convective model of the atmosphere and comparison with inferred runoff from geomorphology, *Planet. Space Sci.*, *105*, 133–147, doi:10.1016/j.pss.2014.11.018.

Penido, J. C., C. I. Fassett, and S. M. Som (2013), Scaling relationships and concavity of small valley networks on Mars, *Planetary and Space Science*, *75*, 105–116, doi:10.1016/j.pss.2012.09.009.

Petau, A., Tirsch, D. & Jaumann, J. (2012), Geomorphological Analysis of Mass Balances of Martian Valley Networks in Western Terra Sirenum, *Lunar Planet. Sci.*, XXXXIII, Abstract 1834.

Petau, A. et al. (2013), Constraints on Atmospheric Precipitation during the Noachian-Hesperian Boundary on Early Mars from Valley Network Discharge and Runoff, *Eur. Planet. Sci. Congr.*, Abstract 659.

Peel, S. E., and C. I. Fassett (2013), Valleys in pit craters on Mars: Characteristics, distribution, and formation mechanisms, *Icarus*, *225*(1), 272–282, doi:10.1016/j.icarus.2013.03.031

Rosbjerg, D. et al. (2013), Prediction of floods in ungauged basins, in *Runoff Prediction in Ungauged Basins*, Cambridge University Press.

Thomas, B. E., H. W. Hjalmarson, and S. D. Waltemeyer (1997), *Methods for estimating magnitude and frequency of floods in the southwestern United States*, Water Supply Paper, USGS Numbered Series, U.S. Geological Survey, Denver, CO.

Warton, D. I., I. J. Wright, D. S. Falster, and M. Westoby (2006), Bivariate line- fitting methods for allometry, *Biological Reviews*, *81*(2), 259–291, doi:10.1017/S1464793106007007.

Wharton, G. (1995), The channel-geometry method: Guidelines and applications, *Earth Surf. Process. Landf.*, *20*(7), 649–660, doi:10.1002/esp.3290200707.

Williams, G. P. (1978), Bank-full discharge of rivers, *Water Resour. Res.*, *14*(6), 1141–1154, doi:10.1029/WR014i006p01141.

Williams, G. P. (1988), Paleofluvial estimates from dimensions of former channels and meanders, in *Flood Geomorpholology*, John Wiley Sons, New York.
Williams, G. P., and B. M. Troutman (1987), Algebraic manipulation of equations of best-fit straight lines, in *Use and abuse of statistical methods in the earth sciences*, vol. 1, pp. 129–141, Oxford University Press, New York, New York.
Williams, R. M. E., and C. M. Weitz (2014), Reconstructing the aqueous history within the southwestern Melas basin, Mars: Clues from stratigraphic and morphometric analyses of fans, *Icarus*, *242*, 19–37, doi:10.1016/j.icarus.2014.06.030.
Williams, R. M. E., R. P. Irwin III, and J. R. Zimbelman (2009), Evaluation of paleohydrologic models for terrestrial inverted channels: Implications for application to martian sinuous ridges, *Geomorphology*, *107*(3–4), 300–315, doi:10.1016/j.geomorph.2008.12.015.
Williams, R. M. E., R. P. Irwin III, D. M. Burr, T. Harrison, and P. McClelland (2013), Variability in martian sinuous ridge form: Case study of Aeolis Serpens in the Aeolis Dorsa, Mars, and insight from the Mirackina paleoriver, South Australia, *Icarus*, *225*(1), 308–324, doi:10.1016/j.icarus.2013.03.016.
Zimbelman, J. R., and S. P. Scheidt (2012), Hesperian Age for Western Medusae Fossae Formation, Mars, *Science*, *336*(6089), 1683–1683, doi:10.1126/science.1221094.

Appendix II

Table II-1. Applications of Width-Discharge Relationships on Mars and Titan

Ref.	Features	Width-discharge relationship	Scale Factor	Widths (m)	Reported Discharges[§] (m^3s^{-1})	New Discharges[§] (m^3s^{-1})	Differential
Late Noachian-Early Hesperian, Mars:							
1	paleochannel	$Q=1.9W^{1.22}$	0.76	90 - 10^3	350 - 6,600 (53 - 44,000)	440 - 40,000 (120 - $1.5x10^5$)	+130%, +600%
2	paleochannel	$Q=1.9W^{1.22}$	0.74	19 - 840	50 - 5,200 (8 - 34,000)	24 - 29,000 (6 - $1.1x10^5$)	-48%, +560%
3	paleochannel	$Q=1.9W^{1.22}$	0.76	475 - 728	2,660 - 4,480 (403 - 29,600)	9,880 - 21,900 (2,600 - 83,300)	+371%, +489%
4	paleochannel	$Q=1.9W^{1.22}$	0.74	67 - 819	237 - 5,020 (36 - 33,300)	256 - 27,300 (67 - 104,000)	+105%, +528%
5	paleochannel	$Q=1.9W^{1.22}$	0.76	150	650 (99 - 4,300)	1,100 (300 - 4,400)	+170%
6	paleochannel	$Q=1.9W^{1.22}$	0.74	183.6	809 (123 - 5,369)	1,676 (440 - 6,374)	+208%
7	deltaic deposits	$Q=1.9W^{1.22}$	0.76	50 - 100	170 - 400 (26 - 2,600)	150 - 540 (39 - 2,100)	-87%, +135%
8	paleochannel	$Q=1.9W^{1.22}$	0.74	142	591 (90 - 3,920)	1,040 (273 - 3,950)	+175%
9	paleochannel*	$Q=1.9W^{1.22}$	0.62	390 ± 120	1,700 (260 - 11,000)	6,840 (1800 - 26,000)	+401%
4	paleochannel	$Q=0.027W^{1.71}$	0.67	67 - 819	24 - 1726 (6 - 7,230)	n/a[#]	n/a[#]
Late Hesperian-Amazonian, Mars:							
10	fluvial deposits	$Q=1.9W^{1.22}$	0.62 or 0.76	48 - 106	162 - 427 (25 - 2,810)	137 - 601 (36 – 2,290)	-84%, +136%
11	paleochannel	$Q=1.9W^{1.22}$	0.63	30 - 55	76 - 159 (11 - 1,050)	57 - 176 (15 - 672)	-75%, +111%
12	paleochannel	$Q=1.9W^{1.22}$	0.76	20 - 100	50 - 400 (8 - 3,000)	30 - 500 (7 - 2,000)	-48%, +140%
13	delta deposits	$Q=1.9W^{1.22}$	0.68	75	250 (35 - 1,500)	315 (83 - 1,200)	+126%
14	delta deposits	$Q=1.9W^{1.22}$	0.62	50 - 130	140 - 450 (21 - 3,000)	150 - 880 (39 - 3,300)	+110%, +200%
15	gullies	$Q=1.9W^{1.22}$	n/a	5.7	16 (2 - 100)	2.6 (<1 - 10)	-16%
10	fluvial deposits	$Q=0.027W^{1.71}$	0.68	48 - 106	14 – 53	n/a[#]	n/a[#]
13	delta deposits	$Q=0.027W^{1.71}$	0.68	75	30	n/a[#]	n/a[#]
Titan:							
16	channel/valley	$Q=0.027W^{1.71}$	0.441	10 - 1,000	<1 - 1,600	n/a[#]	n/a[#]
17	channel/valley	$Q=0.027W^{1.71}$	0.441	2.3 - 4 km	6,800 - 16,600	n/a[#]	n/a[#]

Table II-1. Cont.

[§]Ranges shown in parentheses are the 95% prediction intervals for ranges of estimated paleodischarges.

*The area with this paleochannel has a minimum age of Late Hesperian [*Zimbelman and Scheidt*, 2012], but stratigraphic analyses suggest this area likely from during the Late Noachian or Early Hesperian [*Burr et al.*, 2016].

[#]These estimates were derived from a correlation for daily discharge, which are incomparable with estimates from causal relationships for bankfull discharge. Thus, no new discharges or differentials were derived.

Data and estimates of paleodischarge of Late Noachian-Early Hesperian Martian features, Late Hesperian-Amazonian Martian features, and two features on Saturn's moon, Titan. We show previously reported minimum and maximum widths and corresponding discharge estimates based on the width-discharge correlation from the Missouri River Basin. New discharge estimates use hydraulic geometry relationship (2.5). Prediction intervals covering several orders of magnitude correspond to the lower limit of the smallest discharge estimate and upper limit of the highest discharge estimate. Differential values are the ratios of the minimum and maximum new discharges to the minimum and maximum reported discharges multiplied by 100. Differences between previously reported and new paleodischarge estimates are partly explained by the scale factor, which was previously applied to account for a putative effect of reduced gravity on Mars, but not applied in the new paleodischarge estimates because of similarities in hydraulic geometry for terrestrial and submarine channels [*Konsoer et al.*, 2013]. Late Noachian-Early Hesperian features show a wide range of differential values, several of which are >500%, whereas Late Hesperian-Amazonian features have differential percentages close to reported estimates (100%) or less. These differentially are related to size differences between Noachian-Hesperian and Hesperian-Amazonian features. References are listed below.

1. *Irwin et al.*, 2005a
2. *Petau et al.*, 2013
3. *Baratti et al.*, 2015
4. *von Paris et al.*, 2015
5. *Irwin et al.*, 2005b
6. *Howard et al.*, 2005
7. *Fassett and Head*, 2005
8. *Petau et al.*, 2012
9. *Williams et al.*, 2013
10. *Burr et al.*, 2010
11. *Howard and Moore*, 2011
12. *Peel and Fassett*, 2013
13. *Williams and Weitz*, 2014
14. *Irwin et al.*, 2015
15. *Howard et al.*, 2008
16. *Jaumann et al.*, 2008
17. *Malaska et al.*, 2011

Previously reported hydraulic geometry relationships

Hydraulic geometry relationships (2.3) and (2.4) in the main text show discharge-width equations that were constrained by continuity with depth-discharge and velocity-discharge equations [*Eaton*, 2013; *Konsoer et al.*, 2013], based on the equality of discharge (Q) to the product of its component variables, width (W), depth (d), and flow velocity (*v*):

$$Q = Wdv.$$

Regression of discharge with width, depth, and velocity produces three power-law hydraulic geometry relationships [*Eaton*, 2013].

$$W = aQ^b$$
$$d = cQ^f$$
$$v = kQ^m$$

To maintain continuity, relationship exponents must sum to 1 and relationship coefficients must multiply to 1 [*Leopold and Maddock*, 1953].

$$b + f + m = 1$$
$$a \cdot c \cdot k = 1$$

Hydraulic geometry relationship (2.4)

$$W = 3.73Q^{0.524}$$

was derived along with the depth-discharge and velocity-discharge relationships

$$d = 0.26Q^{0.427}$$
$$v = 1.02Q^{0.05},$$

in which the exponents sum to unity and the coefficients multiple to approximately unity [*Konsoer et al.*, 2013]. Disunity among these coefficients may be the result of rounding or an increase in parameter uncertainty through incorporation of submarine channel data [*Konsoer et al.*, 2013].

Hydraulic geometry relationship (2.3)

$$W = 3.35Q^{0.536}$$

was derived along with the depth-discharge relationship

$d = 0.305Q^{0.384}$,

but no velocity-discharge relationship was reported [*Eaton*, 2013]. Based on continuity, the velocity-discharge relationship would have an exponent of ~0.08 and a coefficient of ~.979, both of which are consistent with other hydraulic geometry studies [*Leopold and Maddock*, 1953; *Knighton*, 1998; *Gleason and Smith*, 2014].

Selection of explanatory and predicted variables in deriving width-discharge relationships

A critical component of width-discharge relationships is the exponent used to calculate (paleo)discharge from a measure of channel width. Here we describe different analyses and the effect of selecting explanatory and predicted variables on the derived exponent.

The effect of variable selection on exponents is presented through a comparison of causal derivations (i.e., discharge as explanatory variable, Q→W) and correlative derivations (i.e., width as explanatory variable, W→Q), shown in Table II-2. The algebraic inverse (^-1) of an exponent may be taken to compare exponents derived from different explanatory variables. In Table II-2, the first and fourth columns of exponents describe width as a function of discharge (e.g., causal relationships, hydraulic geometry). The second and third columns of exponents (grey in Table II-2) describe discharge as a function of width (e.g., width-discharge relationships).

Table II-2. Effect of explanatory variable on exponents of width-discharge relationships

	Causal		**Correlative**	
Data & Analysis Type	Q→W	(Q→W)^-1	W → Q	(W→Q)^-1
Missouri River Basin data:				
Ordinary least squares	0.58	1.72	1.11	0.90
Structural Analysis	0.60	1.67	1.22	0.82
Major axis	0.67	1.49	1.49	0.67
Hydraulic Geometry data:				
Relationship (2.3)	0.536	1.866	n/a	n/a
Relationship (2.4)	0.524	1.908	n/a	n/a

^-1 refers to taking the inverse of the derived exponent in the column to the left.

The effect of variable selection is particularly significant in ordinary least squares regression, which only accounts for error in the predicted variable and not the explanatory variable. In Table II-2, a causal derivation with discharge as the explanatory variable and width as the predicted variable (Q→W) yields an exponent of 0.58, whereas a correlative derivation yields an exponent of 1.11. As described above, algebraic inverses are taken to compare exponents. The exponent 0.58 from ordinary least squares regression following a causal selection of variables is consistent with hydraulic geometry exponents (~0.5) from relationships (2.3) and (2.4). However, the comparable exponent

of 1.11 (1.11^-1 = 0.90) from a correlative selection of variables is unlike hydraulic geometry exponents. This is also true for comparable exponents in the second and third columns that describe discharge as a function of width (i.e., width-discharge relationships).

The effect of variable selection is less significant in structural analysis, which was the type of analysis used in the original derivation of relationship (2.1) from the Missouri River Basin [*Osterkamp and Hedman*, 1982]. Structural analysis accounts for error in both the explanatory and predicted variables based on the ratio of error variance of discharges to error variance of widths. As in the ordinary least-squares example, selection of explanatory and predicted variables affects the derived exponent of the relationship. The original structural analysis of MRB data used a correlative selection of variables and derived the exponent 1.22 [*Osterkamp and Hedman*, 1982], which has a corresponding inverse of 0.82. These exponents (1.22 & 0.82) differ from the exponents 1.67 and 0.60 derived from a causal selection of variables.

Major axis regression eliminates the effect of the explanatory and predicted variables implying that either variable (an independent or dependent variable) may be taken as the explanatory variable and the same exponent will be derived. Major axis regression minimizes the sum of squares perpendicular to the line [*Warton et al.*, 2006]. Major axis regression was performed on the MRB data with a causal selection of variables and yielded an exponent of 0.67. This is the same exponent derived from a correlative selection of variables. This exponent is unlike the exponents of hydraulic geometry relationships possibly because it is a regression between correlative data (i.e., active channel width and two-year discharge).

From this comparison, we see that causal selection of explanatory and predicted variables is critical for ordinary least squares and structural analysis, and any algebraic inversion of relationships. Correlative selection of variables leads to exponents that poorly describe the relationship between flow and width and are inconsistent with the range of exponents (0.3-0.6) observed from many studies of hydraulic geometry [*Leopold and Maddock*, 1953; *Knighton*, 1998; *Eaton*, 2013; *Konsoer et al.*, 2013; *Gleason and Smith*, 2014].

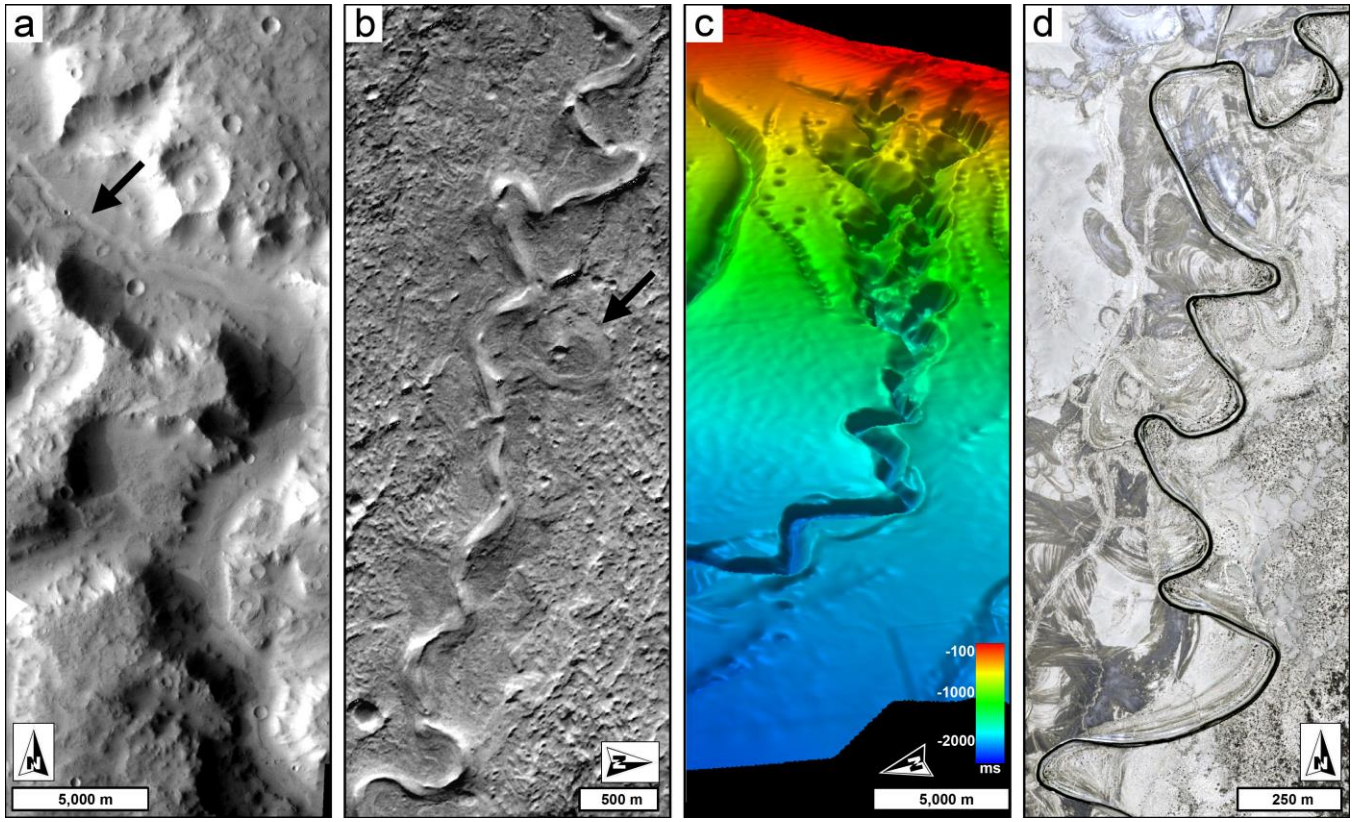

Figure II-1. Martian fluvial landforms and analogous fluvial systems on Earth. Paleodischarge estimates for **(a)** Martian interior channels (arrow) [*Irwin et al.*, 2005] and **(b)** inverted fluvial deposits have been scaled for a putative effect of reduced gravity on Mars relative to Earth. Analysis of **(c)** submarine channels, which experience reduced gravity, suggests scaling is unnecessary. **(d)** Quinn River, NV, meanders in the virtual absence of vegetation and is therefore analogous to (b) Martian meander deposits (arrow). Image information: (a) THEMIS image V05876001, 2.95°S, 126.35°E; (b) CTX image B21_017759_1746_XN, 5.61°S, 154.30°E; (c) seismic image by Zane Jobe, Visual Seismic Atlas, 1.5°N, 9.25°E; (d) planview image, 41.19°N, 118.74°W.

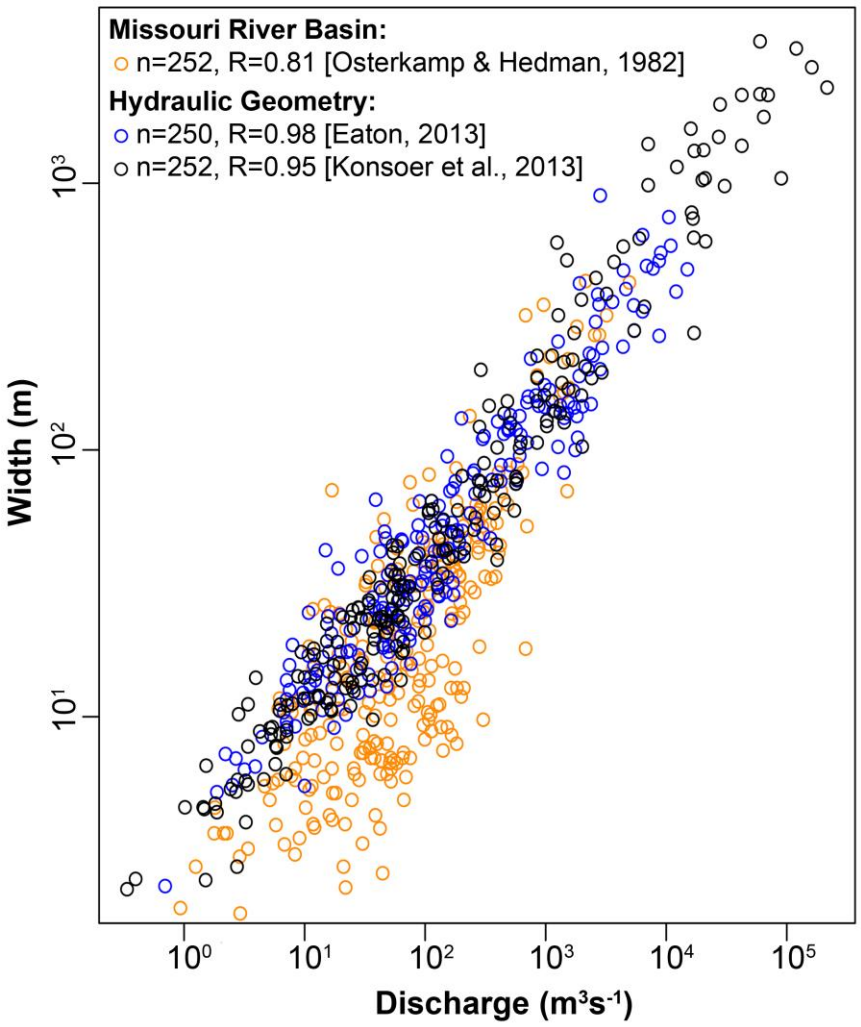

Figure II-2. Discharge and width data used to derive empirical relationships. Missouri River Basin data (orange circles) are active channel widths (W_{ac}) and discharges with two-year recurrence intervals (Q_{2yr}). Hydraulic geometry data (blue and black circles) are bankfull widths (W_{bf}) and bankfull discharges (Q_{bf}) from four continents, comprising a wide range of median grain sizes (<0.062 mm to >25 mm), terrestrial environments, and bank strengths. These broadly sampled hydraulic geometry data show a tighter correlation (R≥0.95) than the data from the Missouri River Basin (R=0.81).

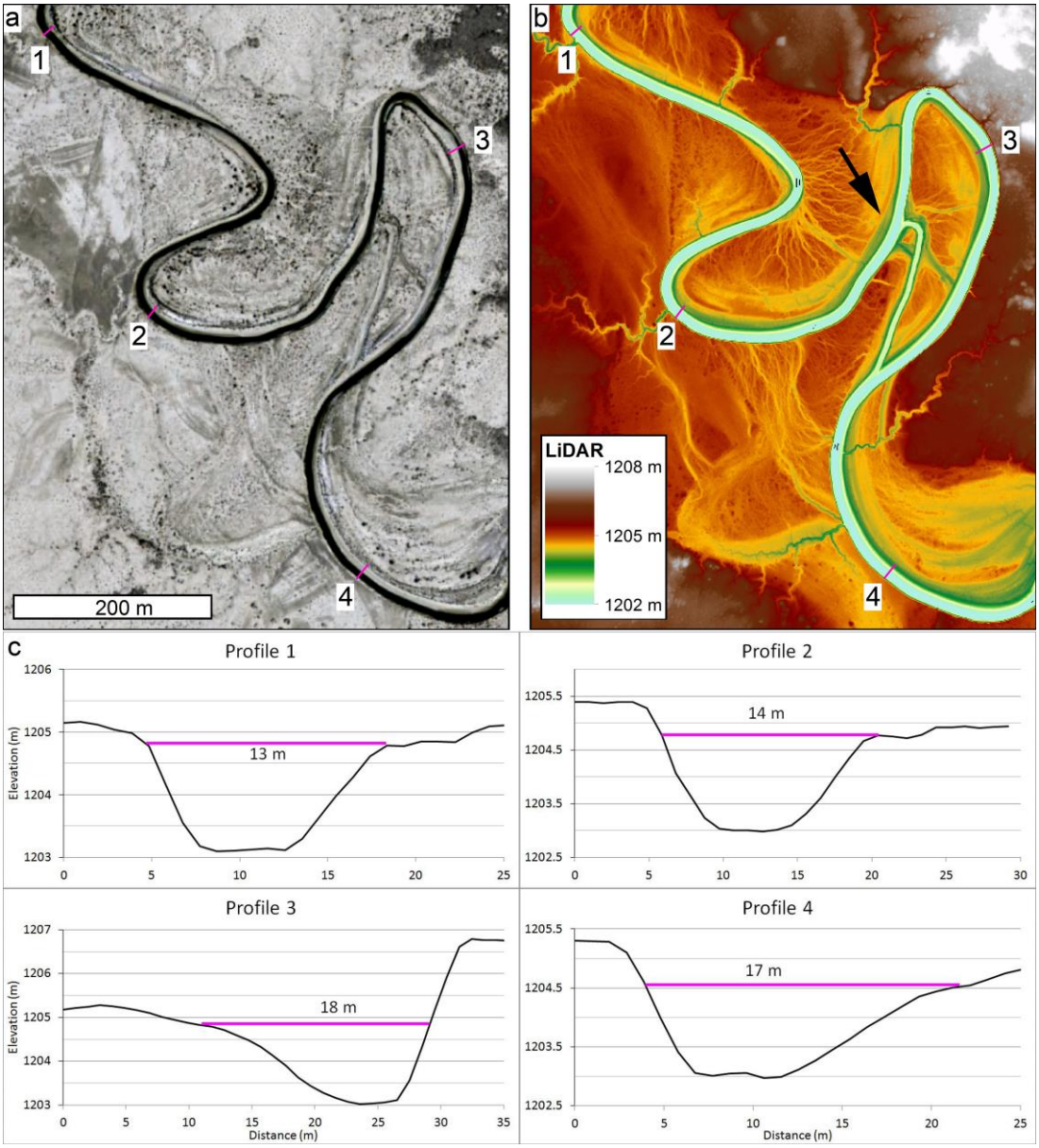

Figure II-3. Plan view data of a portion of the Quinn River with example channel width measurements and corresponding topographic profiles. **(a)** Visual image illustrates the collection of width measurements taken every ~500 meters, near bend apices. **(b)** LiDAR topographic data show that between width measurements, such as at the meander inflection point (arrow), the channel widens and forms a chute cutoff. This variation in width along channel length explains the difference between the previous estimate of bankfull width (20 meters) and the average remote estimate found here (15 meters, σ = 3.2). **(c)** Topographic profiles with measurements of channel widths (pink lines) show how the bankfull width data collected here correspond to the crests of the innermost point bars.

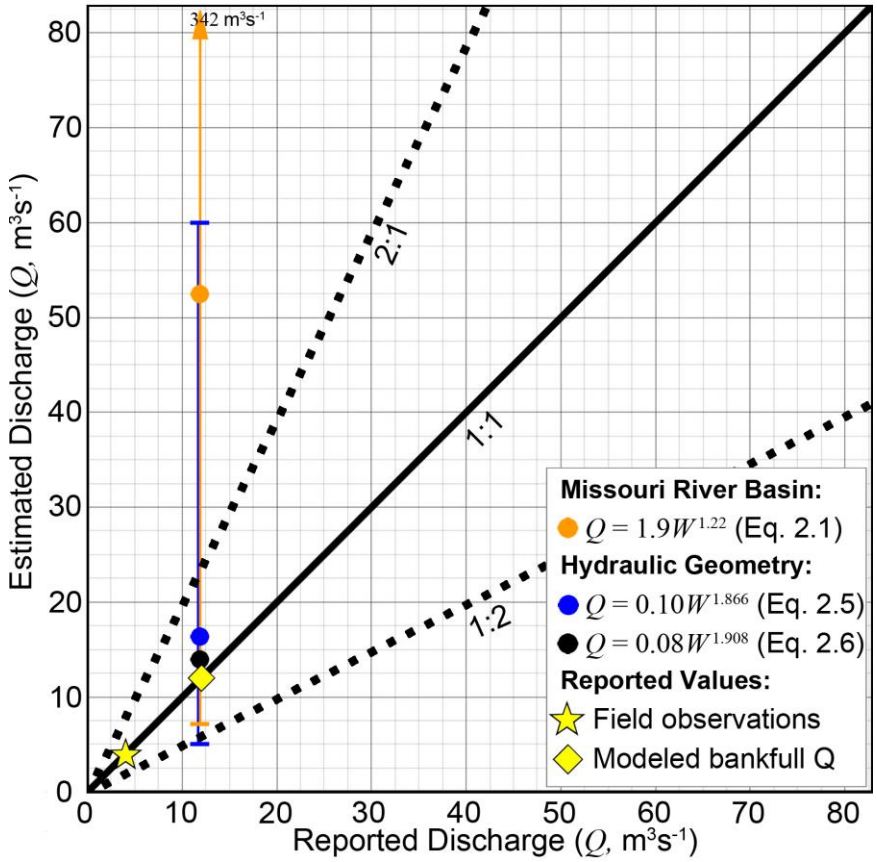

Figure II-4. Evaluation of discharge estimates from correlative (MRB) and causal (hydraulic geometry) width-discharge relationships. Reported values of discharge for Quinn River are from modeling of bankfull conditions and field observations of ~75% bankfull flow [*Matsubara and Howard*, 2014]. Brackets on discharge estimates correspond to 95% prediction intervals for relationships (2.1) and (2.5) at the average bankfull width of the Quinn River (15 m).

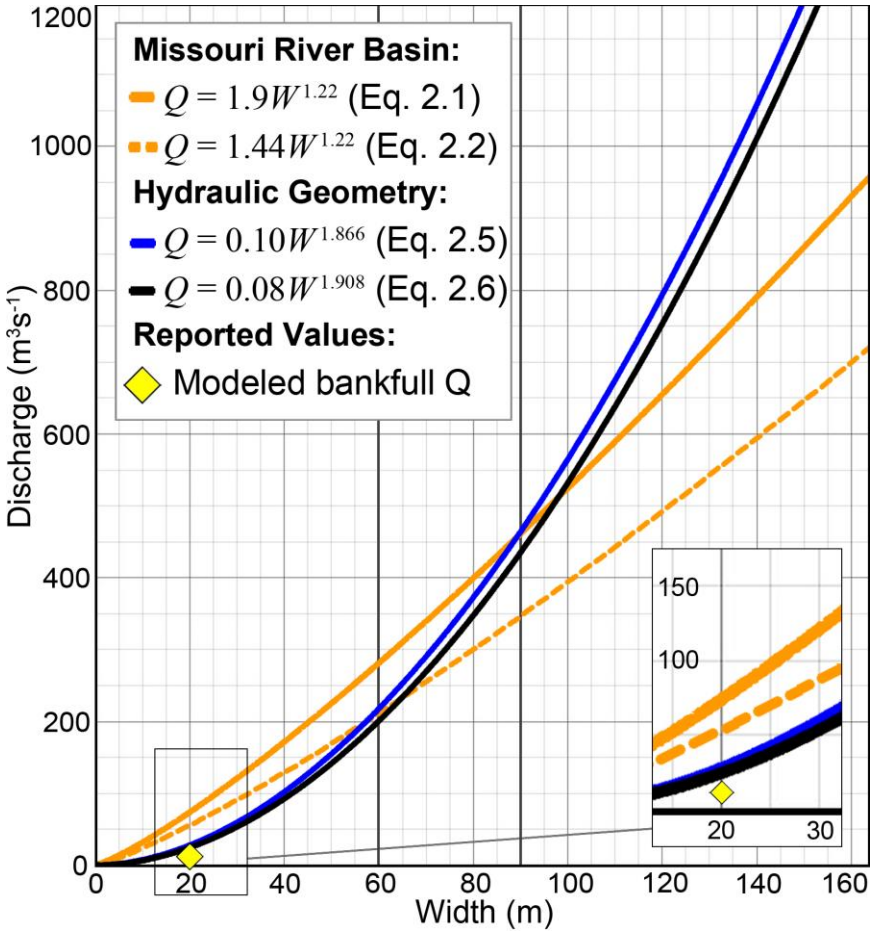

Figure II-5. Comparison of width-discharge relationships and the modeled bankfull discharge. Correlative width-discharge curves (2.1) and (2.2) from the MRB (orange) are shown both with scaling for the putative effect of gravity (dashed curve) and without scaling (solid curve). Width-discharge relationships (2.5) and (2.6) from hydraulic geometry cross these MRB relationships at ~60 meters and ~90 meters width, respectively. Discharge and width values of the Quinn River (diamond) are more consistent with relationships (2.5) and (2.6) than relationships (2.1) and (2.2), which overestimate discharge at smaller widths and underestimate discharge at larger widths.

Chapter III

A History of Decreasing Paleodischarge in the Aeolis Dorsa Region, Mars, with Confounding Factors Suggested by Morphometry of Terrestrial Analog Channels

This chapter is a reformatted version of a manuscript to be submitted to a peer-reviewed journal by Robert Jacobsen and Devon Burr. Robert Jacobsen collected the data, performed the analyses, and drafted the manuscript and figures. Devon Burr provided advice on the science and edited the manuscript and figures.

Abstract

Major changes in geomorphology with time-stratigraphic age suggest decreasing hydrologic activity across Mars and in the Aeolis Dorsa region. Paleochannel widths have been used extensively for paleodischarge analyses and to quantify the inference of decreasing hydrologic activity. Where fluvial landforms do not preserve paleochannel widths, other landform dimensions may be used to derive widths. In the Aeolis Dorsa region, for example, evaluating potential changes in paleodischarge from channel fill deposits overlying meander point bars requires knowing the consistency of measured widths in comparison to widths derived from point bar curvature. To assess this consistency, we analyzed the relationship between channel width and the radius of curvature of point bar ridges in three terrestrial analog fluvial channels. Results of our analysis support a consistent relationship between radii and width, but anomalously high and low radii suggest confounding factors associated with resistant channel banks and high sediment loads, respectively, and yield erroneous estimates of channel width from the morphometric relationship. Paleochannel widths and paleodischarges for the Aeolis Dorsa deposits decrease from an older meandering fluvial unit to a younger unit of fluvial channel fills. However, a confounding factor observed in the terrestrial analysis, namely heterogeneously resistant channel banks, are inferred for the older meandering fluvial deposits, suggesting that paleochannel widths and paleodischarges for this older stratum may be overestimated. Furthermore, high wavelength-to-width ratios indicate widths of younger fluvial channel fills have been eroded, leading to underestimation of width and paleodischarge, and exaggeration of the hydraulic contrast between older and younger units. These findings demonstrate the importance of terrestrial analog studies for revealing the effects of confounding factors and the challenges of analyzing eroded fluvial environments that are morphologically and stratigraphically similar to some proposed rover landing sites.

Introduction

The Aeolis Dorsa region of Mars (Figure III-1) preserves diverse paleochannels and ancient fluvial deposits, including meander point bars and channel fills, that are stratigraphically stacked and topographically inverted (Figure III-2) (Burr et al., 2009; Jacobsen and Burr, 2015; Kite et al., 2015a). The geomorphology, sedimentary environments, and stratigraphy of this region support a hypothesis of decreasing hydrologic activity, in terms of quantity, frequency, and geospatial extent (Jacobsen and Burr, 2015; Kite et al., 2015b; Burr et al., 2016). This regional history of decreasing hydrologic activity encapsulates the Martian global history of climatically driven runoff

evidenced by valley networks and paleolakes, which are more widespread and integrated during the Noachian-Hesperian transition (3.7 Ga), but less widespread and isolated during the Late Hesperian and Amazonian epochs (3.0 Ga) (e.g., Fassett and Head, 2008; Goudge et al., 2016). The stacked fluvial deposits in the Aeolis Dorsa region offer a unique opportunity to test this global paradigm of hydrologic change at local and regional scales.

Hydrologic change may be assessed through analyzing changes in paleodischarge. Quantifying paleodischarge is an essential part of understanding the geologic evolution of Mars because paleodischarge is commonly used in models linking paleoclimate and geomorphology (Howard, 2007; Parsons et al., 2013; Hoke et al., 2014). Paleodischarge analyses of Martian fluvial features commonly use terrestrial-based empirical relationships, which relate a dimension of channel width or channel wavelength to an estimate of flow discharge (Williams, 1988; and references therein). These empirical relationships have also been scaled to account for a putative effect of reduced gravity on Mars, relative to Earth (Irwin et al., 2005; Williams et al., 2009; Burr et al., 2010; Jacobsen and Burr, 2016a).

These terrestrial-based empirical relationships were derived from large samples of fluvial *channels*. In contrast, the fluvial features observed on Mars are often *deposits*. The deposits in the Aeolis Dorsa region include not only channel fills, but also meander point bars (Figure III-2d) that formed next to fluvial channels (Matsubara et al., 2014; Jacobsen and Burr, 2015). This variety of morphologies requires multiple empirical relationships that are appropriate for each type of preserved fluvial deposit. Thus, whereas analyzing paleodischarge in the Aeolis Dorsa region is desirable for quantifying the changes in hydrology with time (Kite et al., 2015b), diverse techniques must be used, and the relative consistency of these diverse techniques must be known.

We use two types of empirical relationships to analyze paleodischarge in the Aeolis Dorsa region. The first type is a terrestrial-based width-discharge relationship that estimates paleodischarge from a measure of paleochannel width (Eaton, 2013; Kite et al., 2015b; Jacobsen and Burr, 2016a). Causal width-discharge relationships from hydraulic geometry have been validated for Martian fluvial features through an analysis of a terrestrial analog channel (Jacobsen and Burr, 2016a). This technique is used to estimate paleodischarge from the younger (overlying) strata of fluvial channel fills (Figure III-2c). The second type of empirical relationship is a terrestrial-based morphometric relationship that estimates channel width from a measure of channel radius of curvature (Williams, 1988; Williams et al., 2013; Irwin et al., 2015). This technique is used to estimate paleochannel width from the radii of curvature of the older (underlying) strata of fluvial meanders (Figure III-2d). As in the first technique, we then couple estimates of paleochannel width and width-discharge relationships to estimate paleodischarge for the older strata.

The valid intercomparison of the paleodischarge values derived from these two different techniques requires the validation of the morphometric relationship between channel radius of curvature and channel width. For this validation, we analyze three terrestrial analog channels and compare estimates of width derived from the radii of curvature relationship with estimates of widths derived from direct measurement of the

channel width. Assessing the accuracy of the morphometric relationship through analyses of terrestrial analog channels continues a robust practice of validating terrestrial-based empirical relationships – and discerning systematic errors in these relationships – before applying empirical relationships to Mars (Jacobsen and Burr, 2016a). Analyses of terrestrial analogs provide validated tools for paleodischarge analyses in regions with diverse fluvial deposits. Such regions include Hadriacus Cavi, Arabia Terra, and NW Hellas (Barton et al., 2016; Davis et al., 2016; Gullikson et al., 2016) and candidate rover landing sites, including Jezero crater, Ebersewalde crater, and SW Melas Chasma (Fassett and Head, 2005; Williams and Weitz, 2014; Irwin et al., 2015; Golombek et al., 2016).

Background

Records of decreasing hydrologic activity in Aeolis Dorsa and on Mars

The Aeolis Dorsa region (Figure III-1b) includes of order a couple thousand fluvial features that are shallowly buried, exhumed, and/or topographically inverted (Pain et al., 2007; Burr et al., 2009; Jacobsen and Burr, 2015; Burr et al., 2016). Preservation and exposure of these fluvial features may be effects of the Medusae Fossae Formation (MFF) (Scott and Tanaka, 1986; Greeley and Guest, 1987; Burr et al., 2009), which has most recently been mapped as part of Amazonian-Hesperian and Hesperian transition units (Tanaka et al., 2014). The MFF is an equatorially extensive, layered deposit of volcaniclastic and/or aeolian sediment with a complex history of deposition and reworking (Scott and Tanaka, 1982; Schultz and Lutz, 1988; Mandt et al., 2008; Kerber and Head, 2010). Extensive burial of the Aeolis Dorsa fluvial deposits during the emplacement of the MFF may have shielded these deposits from erosion by impact cratering (Jacobsen and Burr, 2015). Some fluvial features would eventually be exhumed through extensive aeolian abrasion, which is evidenced by numerous yardangs throughout the region (Ward, 1979; Mandt et al., 2009; de Silva et al., 2010; Zimbelman and Griffin, 2010). Observations of stratigraphy and crater size-frequency distributions suggest the MFF was initially emplaced in the Aeolis Dorsa region during or before the Late Hesperian (Kerber and Head, 2010; Zimbelman and Scheidt, 2012).

The Late-Hesperian minimum initial emplacement age of the MFF suggests the Aeolis Dorsa deposits coincide with a period of waning hydrologic activity. Widespread peak hydrologic activity occurred during the formation of valley networks around the Late Noachian to Early Hesperian transition (3.7 Ga) (Howard et al., 2005; Fassett and Head, 2008). Hydrologic activity was significantly less during the formation of younger, less widespread alluvial sediments deposited within craters during the Late Hesperian to Early Amazonian (3.0 Ga) (Fassett and Head, 2008; Parsons et al., 2013; Grant et al., 2014).

The stratigraphy in the Aeolis Dorsa region suggests that this region encapsulates the global trend of decreasing hydrologic activity (Jacobsen and Burr, 2015; Kite et al., 2015a; Kite et al., 2015b). Beginning with the stratigraphically oldest unit, nighttime thermal infrared images show many bright, sinuous branches connecting with a large bright unit in the topographic low between Aeolis Planum and Zephyria Planum (Figure

III-1b). This large branching, thermally bright unit has been interpreted to represent shallowly buried, indurated fluvial sediments (Burr et al., 2016). These buried fluvial sediments represent the most extensive fluvial deposit in the Aeolis Dorsa region and may have formed during the peak of hydrologic activity around the Noachian-Hesperian transition (Burr et al., 2016). The feature Aeolis Serpens is several hundred kilometers long, has variable ridge morphology along its length, and multiple branches at its southern portion (Figure III-1b). Through examination of multiple terrestrial analogs, which also show variable ridge morphology, Aeolis Serpens has been interpreted as an inverted paleochannel (Lefort et al., 2012; Williams et al., 2013). Aeolis Serpens is inferred to be stratigraphically younger than the shallowly buried, thermally-bright fluvial unit because some branches of Aeolis Serpens appear above the thermally-bright fluvial unit (Burr et al., 2016). Local geologic mapping and regional stratigraphic correlations suggest widespread meandering fluvial deposits formed in southeast Aeolis Dorsa (Figure III-1b) (Jacobsen and Burr, 2015; Kite et al., 2015a). Topographic analyses of meandering fluvial deposits show profiles with either ridge-and-swales, consistent with the topography of meander point bars, or ascending topographic profiles that are consistent with laterally aggrading channel beds. These diverse meandering fluvial deposits suggest regular supplies of flow and sediment, and stable channel banks to maintain meander dynamics (Jacobsen and Burr, 2016b).

Thin sinuous ridges and fans are distinct from the older fluvial units described above. These thin ridges are interpreted to be inverted fluvial channel fills based on the plan-view similarity of their flat, non-descript upper surfaces (Figure III-2c), similar to those of inverted channel fills on Earth (Williams et al., 2007; Burr et al., 2009; Jacobsen and Burr, 2015). Sinuous channel fills appear stratigraphically stacked on top of the older unit of meander fluvial deposits (Figure III-2) and suggest a change in fluvial style (i.e., from an actively meandering channel to a weakly or non-meandering sinuous channel) or a change in preservation (i.e., induration and preservation of point bar sediments in the lower stratum and preservation of channel fill in the upper stratum). Regionally, thin fluvial channel fills form discontinuous networks that are less extensive than the older networks of meandering fluvial deposits (Figure III-1b) and suggest a decrease in the geospatial extent of hydrologic activity over time (Jacobsen and Burr, 2015). Alluvial fans are the stratigraphically youngest deposits and least geospatially extensive features in Aeolis Dorsa (Figure III-1b) (Jacobsen and Burr, 2015; Kite et al., 2015a). These alluvial deposits imply relatively late relief-forming tectonic activity and infrequent and isolated episodes of hydrologic activity, particularly in northwest and southeast Aeolis Dorsa (Figure III-1b). In summary, the hydrologic history of Aeolis Dorsa begins with the formation of a large thermally-bright fluvial unit, followed by the formation of Aeolis Serpens and widespread meandering fluvial deposits. At this point, regional hydrology transitions to thin and discontinuous fluvial channel fills, and finally alluvial fans (Jacobsen and Burr, 2015; Kite et al., 2015a; Burr et al., 2016).

In order to link the sedimentologic and geomorphologic changes in Aeolis Dorsa with changes in paleoclimate, terrestrial-based empirical relationships have been used to quantify paleodischarge (Burr et al., 2010; Williams et al., 2013; Kite et al., 2015b). These empirical relationships estimate discharge from a measure of channel width or

wavelength (Osterkamp and Hedman, 1982; Williams, 1988; Williams et al., 2009). These relationships have been scaled for a putative effect of reduced gravity on Mars relative to Earth (Irwin et al., 2005; Burr et al., 2010), although such scaling may be inappropriate for these empirical relationships (Konsoer et al., 2013; Jacobsen and Burr, 2016a). Average width and wavelength of Aeolis Serpens were coupled with width-discharge and wavelength-discharge relationships, respectively, to estimate formative paleodischarges between 1710 m^3s^{-1} and 4015 m^3s^{-1} (Williams et al., 2013). Measurements of width and wavelength of stratigraphically younger, thin fluvial channel fills have been coupled with empirical relationships to estimate formative paleodischarges between 162 m^3s^{-1} and 427 m^3s^{-1} (Burr et al., 2010), which are an order of magnitude less than those of the stratigraphically older Aeolis Serpens. Measurements of width and wavelength from stratigraphic logs of exhumed fluvial channel deposits also yield decreasing formative discharges, from 89 m^3s^{-1} to 28 m^3s^{-1} (Kite et al., 2015b).

Overall, these quantitative analyses of the Aeolis Dorsa deposits support decreasing paleodischarge through time, consistent with estimates of paleodischarge elsewhere on Mars (Irwin et al., 2005; Howard and Moore, 2011; Williams and Weitz, 2014; Jacobsen and Burr, 2016a). These previous investigations have compared paleodischarge values for similar types of fluvial deposits. No investigation has, however, analyzed the stratigraphic transition from meander point bars to inverted channel fills (Figure III-2) in order to analyze these inferred changes in paleodischarge across this major transition in morphology and sedimentology. This analysis requires different empirical relationships for estimating paleodischarge. In turn, the use of this different relationship requires demonstration that these different relationships are mutually consistent.

Empirical relationships for estimating paleodischarge

Though quantitative analyses of Martian paleohydraulics commonly use empirical relationships derived from terrestrial fluvial systems (Table III-1) (Irwin et al., 2005; Williams et al., 2009; Burr et al., 2010; Jacobsen and Burr, 2016a), those empirical relationships have been criticized and become less favored compared to more advance statistical, analytical, or numerical models (Rhoads 1992; Darby and Van de Wiel 2003). Empirical relationships describe steady-state conditions based on temporally finite data, but variables controlling channel geometry are transient and may respond to external controls operating at scales beyond empirical datasets (Blum and Törnqvist 2000; Darby and Van de Wiel 2003). Similarly, empirical relationships represent conditions as a continuum, and do not include thresholds of flow and sediment processes within individual channels. Physical relationships (e.g., Darcy-Weisbach) used to estimate paleo-flow require knowledge of channel variables, such as slope, sediment load, and flow resistance, that may not be preserved or reliably estimated from examination of satellite images. Thus, empirical relationships represent the most viable technique for estimating paleodischarge when only one channel variable is preserved (e.g., Irwin et al., 2005; Williams et al., 2009; Burr et al., 2010; Jacobsen and Burr, 2016a).

To mitigate the limitations of empirical relationships, those relationships should be derived from robust datasets with variables that reflect causality. The most commonly used form-discharge relationship (i.e., equation 3.1 in Table III-1) was derived from data with no causal relationship between the width (i.e., W_{ac}, width of the active channel) and discharge variables (i.e., Q_{2yr}, discharge with a two-year recurrence interval) (Jacobsen and Burr, 2016a). Equation (3.1) is commonly scaled by a factor of 0.76, yielding equation (3.2), to account for a putative effect of reduced gravity on Mars relative to Earth (Irwin et al., 2005; Burr et al., 2010). However, results from analyses of submarine channels flowing in reduce-gravity environments suggest scaling of width-discharge relationships may not be necessary (Konsoer et al., 2013).

Hydraulic geometry relationships partly reflect causal processes in fluvial channels because they relate the formative bankfull discharge (i.e., Q_{bf}) to its component variables of bankfull width (i.e., W_{bf}), depth, and flow velocity (Leopold and Maddock, 1953; Eaton, 2013). Hydraulic geometry relationships have been derived from broader samples of channel sizes, including those in reduced-gravity environments, median grain sizes, and sedimentary environments (Eaton, 2013; Konsoer et al., 2013). Hydraulic geometry relationships have been algebraically inverted to yield width-discharge relationships (e.g., equation 3.2) that estimate bankfull discharge from a measurement of bankfull channel width (Jacobsen and Burr, 2016a). Equation (3.3) has been previously used to estimate paleodischarge in the Aeolis Dorsa region, but this equation was scaled for the putative effect of reduced gravity on Mars relative to Earth (Kite et al., 2015b). Analysis of a terrestrial analog fluvial channel suggest that width-discharge relationships from hydraulic geometry (e.g., equation 3.3) yield more accurate and more precise estimates of discharge than those from the more commonly used width-discharge relationship (i.e., equation 3.1) (Jacobsen and Burr, 2016a). Results from this previous analysis suggest that empirical relationships reflecting causality are more appropriate for estimating paleodischarge on Mars. This previous analysis also demonstrates the utility of using terrestrial analog rivers to assess the accuracy of empirical relationships before applying such relationships to Martian features.

Empirical relationships between channel wavelength and discharge have also been used to estimate paleodischarge on Mars (Burr et al., 2010; Irwin et al., 2015; Kite et al., 2015b). Equation (3.4) relates the discharge with a recurrence interval of 1.5 years (i.e., $Q_{1.5yr}$) with the channel wavelength (λ), measured as the distance between meander inflection points (Carlston, 1965; Williams, 1988; Burr et al., 2010). However, the causality of wavelength-discharge relationships is unknown (Knighton, 1998, p. 215). The relationship between wavelength and discharge may be related to morphodynamic interactions between flow, sediment, and bed topography (Whiting and Dietrich, 1993). Elucidating the uncertain causality of this relationship is beyond the scope of this investigation and, therefore, relationship (3.4) is not used here.

Empirical relationships for estimating paleochannel width

Morphometric relationships are a type of empirical relationship that relate one planform variable to another planform variable (Williams, 1988). The morphometric

relationship between channel radius of curvature and channel width (i.e., equation 3.5 in Table III-1) was derived from a large data set of fluvial channels and is consistent with many studies that find the ratio of radius of curvature (R_c) and channel width (W_{bf}) to be between 2 and 3 (Williams, 1988; Knighton, 1998). This ratio represents a balance between flow resistance and sediment dynamics around the meander bend. Ratios less than 2 are associated with increased flow resistance, eddying, and enhanced deposition in the downstream limb of the meander (Bagnold, 1960; Page and Nanson, 1982). Conversely, ratios greater than 3 are associated with increased shear stress in the downstream limb of the meander bend and limited deposition (Knighton, 1998).

Whereas morphometric relationship (3.5) in Table III-1 was originally derived from dimensions of fluvial channels, here we investigate the accuracy of coupling this relationship with the dimensions of meander point bars. This application of relationship (3.5) is not novel, as it was previously applied to fluvial deposits in the Aeolis Dorsa region and Eberswalde Crater, Mars (Williams et al., 2013; Irwin et al., 2015). However, these previous investigations were concerned with assessing the preservation and accuracy of paleochannel widths, as measured from exhumed, eroded, and topographically inverted fluvial deposits, instead of the current task of assessing the accuracy of the relationship.

Replacing the channel dimension with a fluvial deposit dimension in equation (3.5) is appropriate because the channel-forming discharge influences both dimensions (Miall, 1996; Knighton, 1998). However, the systematic uncertainty associated with this variable replacement has not been analyzed. Thus, before we estimate paleodischarge, we examine morphometric relationship (3.5) as it is applied to point bar deposits of terrestrial analog fluvial channels.

Analyses of terrestrial analog channels to assess empirical relationships

Analysis of a terrestrial analog river can be used to assess the accuracies of discharge estimates from width-discharge relationships (Jacobsen and Burr, 2016a). Here, we analyze three analog channels to evaluate the accuracy of coupling morphometric relationship (3.5) with the radius of curvature to meander point bars.

The Quinn River, NV, is one of the most analogous fluvial systems to the fluvial deposits of the Aeolis Dorsa because, despite being on Earth, it meanders in the virtual absence of vegetation. The Quinn River (Figure III-3a) flows through silt and clay-rich floodplain sediments deposited by Late-Pleistocene Lake Lahontan (Matsubara et al., 2014). These cohesive sediments provide sufficient bank stability to maintain meander dynamics, and similar paleolacustrine clays have been identified elsewhere on Mars (e.g., Williams and Weitz, 2014). Sediment deposition is facilitated by the river's elevated salinity, which promotes flocculation of mud particles, deposition of mud pebbles, and formation of mud bedforms (Matsubara et al., 2014). High-resolution plan view images and topography, in-situ measurements of flow, and modeling of bankfull discharge (Matsubara et al., 2014; Matsubara and Howard, 2014) make the Quinn River is one of the best-documented channels for examining the accuracy of morphometric relationship (3.5).

Rivers on the North Slope of Alaska, including the Meade and Usuktuk Rivers (Figure III-3b), are potentially analogous to the paleochannels in the Aeolis Dorsa region because they meander through permafrost floodplains (Matsubara et al., 2014). Permafrost, like paleolacustrine clays, is thought to provide sufficient bank stability to maintain meander dynamics in the absence of vegetation (Fairén et al., 2013). Field observations of channel banks in Alaska found dense networks of roots, which limit the appropriateness of these channels as terrestrial analogs (Matsubara et al., 2014). Nonetheless, the Meade and Usuktuk Rivers provide additional opportunities to examine the accuracy of morphometric relationship (3.5) because they are well covered by high-resolution plan view images and topography.

Methods

Morphometric analysis of terrestrial analog channels

To apply morphometric relationship (3.5) to these two terrestrial analog systems, visual and topographic data of the Quinn River, NV, and Meade and Usuktuk Rivers, AK, were analyzed in ArcMap geographic information system software. Visual images included 1-meter spatial resolution, orthorectified images from the National Agriculture Imagery Program (NAIP) and United States Geologic Survey (USGS). Topographic data of Alaskan rivers included a digital elevation model (DEM) with 5-meter spatial resolution derived from interferometric synthetic aperature radar data available from the USGS. A DEM of the Quinn River, NV, was derived from light detection and ranging (LiDAR) data, has 1-meter spatial resolution, and was produced by the National Center for Airborne Laser Mapping.

We systematically measured channel widths and radii of curvature of point bars along the Quinn River, Meade River, and Usuktuk River. These remote measurements were taken in the vicinity of in-situ analyses that examined bank materials and analogous materials to those in the Aeolis Dorsa region (Matsubara et al., 2014). Channel width was measured as the distance between the cut bank and the crest of the innermost point bar (Figure III-4). Channel widths were measured every 100 meters along channel length for the Quinn River and every 500 meters of channel length along the Alaskan Rivers. Width measurements made between channel inflection points were grouped as one set of width measurements and the average of each set was calculated. These measurements were repeated four times to calculate standard deviation of the mean (SDOM) as an assessment of measurement error.

Radius of curvature was calculated by delineating the crest of point bar ridges (Figure III-4), which appear as semi-concentric arcs in visual and topographic data. Delineations were fitted with circles by matching the highest-curvature portions of ridge delineations to the curvature of circles with known radii. Point bar ridges within the same meander bend were grouped as one set of measurements and the average of each set was calculated. Delineating ridges and fitting circles were repeated four times to calculate the SDOM. After data collection, average widths and average radii were

plotted together and compared with the expected trend of radii and widths from morphometric relationship (3.5).

Morphometric and paleodischarge analyses of Martian fluvial deposits

We conducted morphometric and paleodischarge analyses in two areas of the Aeolis Dorsa region, Area 35 and Area 40 (Figure III-1b). These regions were chosen for their well-developed meander deposits (Jacobsen and Burr, 2016a) and the availability of high-resolution plan view and topographic data. Visual and topographic data of Areas 35 and 40 were analyzed in ArcMap software. Data included visual images with <1-meter spatial resolution taken by the High Resolution Imaging Science Experiment (HiRISE) (McEwen et al., 2007) and 1-meter spatial resolution digital elevation models (DEM) derived from Softcopy Exploitation Toolkit (SOCET SET), a software and hardware package made by BAE Systems (Kirk et al., 2008).

Measurement of radii of curvature involved examining the lower stratum, consisting of meandering fluvial deposits, and delineating semi-concentric point bar ridges (Figure III-4). Ridge delineations were fit with circles by matching the highest-curvature portions of ridge delineations to the curvature of circles with known radii. Delineating point bar ridges, fitting circles, and deriving radii were repeated four times to calculate the SDOM. Radii measurements that correspond to a single fluvial feature were averaged and coupled with morphometric relationship (3.5) to estimate paleochannel width of the lower stratum of meandering fluvial deposits. These estimates of paleochannel width were then coupled with the width-discharge relationship (3.3) to estimate paleodischarge for the lower stratum.

Widths of the younger fluvial channel fills were measured as the distance across flat upper surfaces (Figure III-2c and III-4). Measurements were repeated four times to calculate SDOM. Width measurements were complemented by measurements of wavelength, which were used to assess preservation of the channel fills (Burr et al., 2010). The ratio of wavelength to width is 10 to 14 for terrestrial channels (Knighton, 1998), and, assuming the same ratio for Mars, we interpreted channel fills with ratios greater than 14 as eroded (Figure III-2c) (Burr et al., 2010). Average widths of the fluvial channel fills were coupled with the width-discharge relationship (3.3) in order to estimate paleodischarge. Widths and paleodischarges for the upper stratum of fluvial channel fills were then compared to the widths and paleodischarges of the lower stratum of meandering fluvial deposits to test the hypothesis of decreasing hydrologic activity across the stratigraphic transition. For analyses of each strata, measurement error was propagated through empirical relationships and combined with the standard error of equations (3.5) and (3.3) by following standard methods (Taylor, 1997).

Results

Morphometric results from terrestrial analog channels

Channel widths and radii of curvature of meander point bars were measured for 61 meander bends along the Quinn River, NV. Average radii of curvature ranged from

21 to 114 meters with SDOM between 1.5 and 43 meters. Average width ranged from 13 to 21 meters (SDOM between 0.24 and 2.4). A comparison of these data (Figure III-5a) and morphometric relationship (3.5) suggests that two thirds of the data plot within the interval of expected variation (i.e., 40% Standard Error of the Equation, SEE). However, one-third of the points plot above this interval. Possible explanations for these larger radii are provided in the discussion section.

We measured channel widths and point bar radii of curvature for 38 meander bends of the Usuktuk River. Average radii of curvature ranged from 130 to 600 meters (SDOM between 12 and 115) and average channel width ranged from 87 to 203 meters (SDOM between 1.8 and 41). Data from the Usuktuk plot mostly within the morphometric relationship and interval of the SEE (Figure III-5b), although several data points plot below it. Possible explanations for these smaller radii are provided in the discussion section.

Channel widths and radii of curvature of point bars were measured for 23 meander bends along the Meade River. Average radii ranged from 363 to 1366 meters (SDOM between 20 and 254) and average channel width ranged from 169 to 360 meters (SDOM between 3.7 and 23). Most radii and width data from the Meade River plot within the expected interval of variation.

Morphometric and paleodischarge results from Aeolis Dorsa, Mars

We measured 13 sets of stratigraphically lower meandering fluvial deposits and stratigraphically higher fluvial channel fills in Area 35. For the meandering fluvial deposits, average radii of curvature were between 72 and 214 meters with SDOM between 38 and 76. These radii coupled with morphometric relationship (3.5) yielded estimates of paleochannel widths between 32 (±12) and 84 (±33) meters (Figure III-6a). Coupling these estimates of paleochannel widths with width-discharge relationship (3.3) yielded paleodischarges between 65 (±29) and 392 (±175) m^3s^{-1} (Figure III-7a).

In general, these estimated widths and paleodischarges for the older unit of meandering fluvial deposits in Area 35 are greater than those for the younger fluvial channel fills. For the fluvial channel fills, average widths were between 13 and 50 meters with SDOM between 1.2 and 13 (Figure III-6a). These widths coupled with width-discharge relationship (3.3) yielded paleodischarge estimates between 12 (±3.5) and 148 (±44) m^3s^{-1} (Figure III-7a). Wavelength-to-width ratios of the thin fluvial channel fills were between 12 and 56, with only one measurement between the terrestrial range of 10 and 14.

We measured 9 sets of fluvial features across the transition from meandering fluvial deposits to fluvial channel fills in Area 40. Average radii of curvature for the older meandering fluvial deposits were between 112 and 468 meters with SDOM between 5.2 and 294 (Figure III-6b). These radii, when coupled with morphometric relationship (3.5), yielded estimates of paleochannel width between 47 (±20) and 169 (±120) meters. Estimated widths yielded paleodischarges from 135 (±63) to 1437 (±1485) m^3s^{-1} (Figure III-7b) when coupled with width-discharge relationship (3.3).

As in Area 30, estimated widths and paleodischarges of the meandering fluvial deposits in Area 40 are larger than those measured from the younger fluvial channel fills (Figures III-6 and III-7). Average widths of the fluvial channel fills were between 12 and 76 meters with SDOM between 1.4 and 6.4 (Figure III-6b). These widths coupled with width-discharge relationship (3.3) yielded paleodischarge estimates between 11 (±3.3) and 328 (±96) m^3s^{-1} (Figure III-7b). Wavelength-to-width ratios of the fluvial channel fills were between 12 and 38, and only one ratio was within the range for terrestrial channels (i.e., 10 to 14).

Discussion

Anomalous point bar radii and implications for Martian results

Our results show that the majority of radii and channel widths from the Nevada and Alaska channels plot within the interval of expected variation of the morphometric relationship (Figure III-5), supporting the validity of applying this morphometric relationship to analogous channels in the Aeolis Dorsa. However, approximately one-quarter (30/122) of data points plot either above or below the expected interval (Figure III-5), and those data suggest cofounding factors not accounted for in the empirical relationships. For one-third of the Quinn River data (Figure III-5a) plot above the expected interval of relationship (3.5) suggesting that some morphodynamic process produces larger than expected radii.

Anomalously high point bar radii may be explained by heterogeneity of the Quinn River floodplain sediment and associated heterogeneity of bank strength. Inspection of plan view visual images suggest that some portions of the Quinn River are bound by reworked fluvial sediments, as evidenced by floodplain meander scars, whereas other portions of the Quinn are bound by paleolacustrine silts and clays (Figure III-8a). Comparison of plan view images with morphometric data indicates that larger-than-expected radii correspond to locations where cut banks are composed of paleolacustrine deposits (Figure III-9). The coincidence of larger radii and paleolacustrine sediments suggests that these sediments are well lithified and limit lateral migration of the Quinn River and this suggestion is supported by in-situ observations and modeling (Matsubara and Howard, 2014). Instead of migrating laterally, the downstream limb of the meander translates downstream and expands the radii of curvature.

Larger-than-expected radii of curvature along the Quinn River suggest important implications for Martian morphometric analyses. Of particular concern is the potential to overestimate paleochannel width through the use of morphometric relationship (3.5). Coupling morphometric relationship (3.5) with the radius of curvature measured (i.e., 103 m) in Figure III-8a would yield a channel width estimate of 44 (±18) meters, an overestimate of channel width by a factor of ~2. Resistant and stable channel banks have been interpreted for the fluvial deposits in Aeolis Dorsa, but how bank conditions alter channel morphometry has not been considered. Though at the moment, it is not possible to infer bank strengths of Martian paleochannels, an examination of plan view images shows asymmetric meander patterns (Figure III-8b & III-10). This asymmetry is

consistent with heterogeneity of floodplain conditions, akin to those observed along the Quinn River (Figure III-8a). Results from our analysis of the Quinn River suggest that radii of curvature for meander deposits in Aeolis Dorsa may have had larger-than-expected radii for a given paleochannel width. If so, use of morphometric relationship (3.5) with radii measurements would yield overestimates of paleochannel width, which would erroneously increases the dissimilarity of paleodischarge between older and younger strata (Figure III-7).

Widths and radii from the Usuktuk River plot below the expected interval of variation for relationship (3.5), suggesting that another morphodynamic process leads to smaller than expected radii. Inspection of these anomalously low radii and plan view images reveals exposed bedforms and channel bars (Figure III-8c). These exposed bedforms and channel bars imply enhanced deposition, an effect previously observed in channels with small radii of curvature (Bagnold, 1960; Page and Nanson, 1982). Enhanced deposition along the Usuktuk River may be the effect of a high sediment load sourced from the abundant aeolian deposits composing the floodplain (Matsubara et al., 2014; and references therein).

This example from the Usuktuk River shows the potential to underestimate paleochannel width through the use of morphometric relationship (3.5). Coupling morphometric relationship (3.5) with the average radius of curvature measured (i.e., 149 m) in Figure III-8b yields an estimate of channel width of 61 (±24). This application of morphometric relationship (3.5) would underestimate channel width by a factor of 0.42. Underestimated paleochannel widths of fluvial meander deposits in Aeolis Dorsa would increase the dissimilarity of hydrologic activity between older and younger strata (Figure III-6 and III-7). However, since small meander bends are not observed in Aeolis Dorsa and banks along the Alaskan Rivers are affected by vegetation, we consider the potential to underestimate paleochannel width less relevant to interpretations of Martian results than the potential to overestimate width, as shown in the example from the Quinn River.

Erosion of fluvial deposits and implications for paleodischarge estimates

All but two fluvial channel fills have wavelength-to-width ratios greater than 14 (Figures III-6 and III-7). These results are similar to a previous analysis of wavelength-to-width ratios that found three well-preserved, fluvial channel fills (Burr et al., 2010). These high wavelength-to-width ratios suggest that the younger fluvial channel fills have experienced significant erosion, as is evidenced by the narrowing of some deposits to sharp-crested ridges (Figure III-2c & III-8d). Erosion of fluvial channel fills implies that their widths have been underestimated, exaggerating the dissimilarity of hydrologic activity between older and younger fluvial deposits (Figures III-6 and III-7). Analysis of wavelength-to-width ratios and interpretations of erosion assume that wavelength-to-width ratios are similar on Earth and Mars though a theoretical evaluation of this assumption has not been made. Nonetheless, significant erosion of the younger deposits is expected because this unit, and the Aeolis Dorsa region as a whole, has experienced erosion leading to exhumation and topographic inversion (Pain et al., 2007; Burr et al., 2009). Furthermore, the unit of fluvial channel fills is stratigraphically higher than other

fluvial deposits in the Aeolis Dorsa region, implying that the unit has been exposed to erosive processes longer than subjacent units.

Challenges of interpreting eroded fluvial environments

Results from analyses of stacked fluvial deposits in Areas 35 and 40 suggest that paleochannel widths and paleodischarges were greater for the older meandering fluvial deposits and less for the younger fluvial channel fills. These results support the regional hypothesis that hydrologic activity decreased over time. However, this interpretation is equivocal in light of results from terrestrial analog channels, particularly the potential to overestimate paleochannel width when using morphometric relationship (3.5), as demonstrated by analysis of the Quinn River (Figures III-5a and III-8a). Overestimation of paleochannel widths in the older stratum of meandering fluvial deposits would erroneously support the hypothesis (i.e., false positive). Furthermore, support for the hypothesis is less definitive given wavelength-to-width ratios that indicate erosion, and therefore underestimation, of widths and paleodischarges of the younger fluvial channel fills.

Results from our analysis of terrestrial analog channels suggest Martian paleohydraulic analyses should consider the properties of channel boundary condition, namely bank strength, that confound empirical relationships. The examples above demonstrate that erroneous estimates of paleochannel widths are possible when these considerations are not made. The morphometric and width-discharge relationships used here were developed from analyses of fluvial channels (Williams, 1988; Eaton, 2013), but these relationships have also been applied to alluvial and deltaic deposits on Mars (Fassett and Head, 2005; Williams and Weitz, 2014; Irwin et al., 2015). The confounding variables associated with alluvial and deltaic environments (e.g., slope, backwater currents), and how these environments differ from fluvial channels, require analysis if estimates of paleodischarge are to be considered reliable and helpful for remote evaluations of habitability at future landing sites (Fassett and Head, 2005; Williams and Weitz, 2014; Irwin et al., 2015; Golombek et al., 2016).

Exhumation and topographic inversion of diverse fluvial deposits are relevant factors beyond the Aeolis Dorsa region, such as Hadriacus Cavi, Arabia Terra, and NW Hellas (Barton et al., 2016; Davis et al., 2016; Gullikson et al., 2016) and at candidate rover landing sites, including Jezero crater, Ebersewalde crater, and SW Melas Chasma (Fassett and Head, 2005; Williams and Weitz, 2014; Irwin et al., 2015; Golombek et al., 2016). Wavelength-to-width ratios indicate that younger fluvial channel fills in Aeolis Dorsa have been eroded, leading to erroneously low channel widths and paleodischarges. Circumventing the problem of erosion depends on the robustness and applicability of morphometric relationships and ratios (e.g., wavelength-to-width) to Martian fluvial features. Further assessment of these relationships and ratios through theoretical investigations, modeling, and analyses of terrestrial analog systems will improve their ability to assess preservation and reconstruct channel dimensions.

Conclusions

Without validation through analyses of terrestrial analogs, terrestrial-based empirical relationships may be applied indiscriminately to Martian fluvial deposits. Results from our analyses of terrestrial analog channels suggest morphodynamic effects caused by confounding factors, including highly resistant channel banks and high sediment loads. If these confounding factors are not considered, application of empirical relationships (e.g., equation 3.5), will yield erroneous results. Although our results suggest decreasing paleochannel width and paleodischarge across a major stratigraphic transition in the Aeolis Dorsa region, these results are ambiguous because stable channel banks, a confounding factor in our terrestrial analysis, have been interpreted for meandering fluvial deposits on Mars. The contrast in paleodischarge across the stratigraphic transition in Aeolis Dorsa is made less definitive by high wavelength-to-width ratios suggesting erosion of fluvial channel fills. These results suggest that Martian paleohydraulic analyses be complemented by analyses of stratigraphy and sedimentary environments to increase the evidence for interpreting hydrologic change. Theoretical investigations of Martian fluvial conditions (e.g., reduced gravity) and their effects on channel morphometry may be helpful for inferring the pre-eroded dimensions of Martian fluvial paleochannels and deposits. Without additional information to constrain erosion and confounding factors, interpretations of paleohydrology and habitable aqueous environments may be erroneous.

References

Bagnold, R.A., 1960, Some aspects of the shape of river meanders: Professional Paper USGS Numbered Series 282-E, Washington, D.C.

Barton, M.L., Skinner, J.A., and Fortezzo, C.M., 2016, Occurrence and Morphology of Channel-Form Features in Stratified Deposits of Hadriacus Cavi, Mars, in *Lunar Planet. Sci.*, XXXXVII, Abstract 2833.

Bradley, B.A., Sakimoto, S.E.H., Frey, H., and Zimbelman, J.R., 2002, Medusae Fossae Formation: New perspectives from Mars Global Surveyor: Journal of Geophysical Research: Planets, v. 107, no. E8, p. 2–1, doi: 10.1029/2001JE001537.

Burr, D.M., Enga, M.-T., Williams, R.M.E., Zimbelman, J.R., Howard, A.D., and Brennand, T.A., 2009, Pervasive aqueous paleoflow features in the Aeolis/Zephyria Plana region, Mars: Icarus, v. 200, no. 1, p. 52–76, doi: 10.1016/j.icarus.2008.10.014.

Burr, D.M., Jacobsen, R.E., and Lefort, A., 2016, Thermal Detection of an Extensive Buried Fluvial Unit in the Aeolis Dorsa Region, Medusae Fossae Formation, Mars, in *Lunar Planet. Sci.*, XXXXVII, Abstract 1392.

Burr, D.M., Williams, R.M.E., Wendell, K.D., Chojnacki, M., and Emery, J.P., 2010, Inverted fluvial features in the Aeolis/Zephyria Plana region, Mars: Formation mechanism and initial paleodischarge estimates: Journal of Geophysical Research: Planets, v. 115, no. E7, p. E07011, doi: 10.1029/2009JE003496.

Carlston, C.W., 1965, The relation of free meander geometry to stream discharge and its geomorphic implications: American Journal of Science, v. 263, no. 10, p. 864–885.

Davis, J.M., Balme, M., Grindrod, P.M., Williams, R.M.E., and Gupta, S., 2016, Extensive Noachian fluvial systems in Arabia Terra: Implications for early Martian climate: Geology, p. G38247.1, doi: 10.1130/G38247.1.

Eaton, B.C., 2013, 9.18 Hydraulic Geometry: Empirical Investigations and Theoretical Approaches, *in* Shroder, J.F. ed., Treatise on Geomorphology, Academic Press, San Diego, p. 313–329.

Fairén, A.G., Davies, N.S., and Squyres, S.W., 2013, Equatorial Ground Ice and Meandering Rivers on Mars, in *Lunar Planet. Sci.*, XXXXIV, Abstract 2948.

Fassett, C.I., and Head, J.W., 2005, Fluvial sedimentary deposits on Mars: Ancient deltas in a crater lake in the Nili Fossae region: Geophysical Research Letters, v. 32, no. 14, p. L14201, doi: 10.1029/2005GL023456.

Fassett, C.I., and Head, J.W., 2008, The timing of martian valley network activity: Constraints from buffered crater counting: Icarus, v. 195, no. 1, p. 61–89, doi: 10.1016/j.icarus.2007.12.009.

Gibling, M.R., 2006, Width and Thickness of Fluvial Channel Bodies and Valley Fills in the Geological Record: A Literature Compilation and Classification: Journal of Sedimentary Research, v. 76, no. 5, p. 731–770, doi: 10.2110/jsr.2006.060.

Golombek, M.P., Grant, J.A., Farley, K.A., Williford, K., Chen, A., Otero, R.E., and Ashley, J.W., 2016, Downselection of Landing Sites Proposed for the Mars 2020 Rover Mission, in *Lunar Planet. Sci.*, XXXXVII, Abstract 2324.

Goudge, T.A., Fassett, C.I., Head, J.W., Mustard, J.F., and Aureli, K.L., 2016, Insights into surface runoff on early Mars from paleolake basin morphology and stratigraphy: Geology, p. G37734.1, doi: 10.1130/G37734.1.

Grant, J.A., Wilson, S.A., Mangold, N., Calef, F., and Grotzinger, J.P., 2014, The timing of alluvial activity in Gale crater, Mars: Geophysical Research Letters, v. 41, no. 4, p. 2013GL058909, doi: 10.1002/2013GL058909.

Greeley, R., and Guest, J.E., 1987, Geologic map of the eastern equatorial region of Mars: IMAP USGS Numbered Series 1802-B, Washington, D.C.

Gullikson, A.L., Anderson, R.B., and Williams, R.M.E., 2016, Mapping Sinuous Ridges in Northwest Hellas, Mars, in *Lunar Planet. Sci.*, XXXXVII, Abstract 2376.

Harrison, S.K., Balme, M.R., Hagermann, A., Murray, J.B., and Muller, J.-P., 2010, Mapping Medusae Fossae Formation materials in the southern highlands of Mars: Icarus, v. 209, no. 2, p. 405–415, doi: 10.1016/j.icarus.2010.04.016.

Hoke, M.R.T., Hynek, B.M., Di Achille, G., and Hutton, E.W.H., 2014, The effects of sediment supply and concentrations on the formation timescale of martian deltas: Icarus, v. 228, p. 1–12, doi: 10.1016/j.icarus.2013.09.017.

Howard, A.D., 2007, Simulating the development of Martian highland landscapes through the interaction of impact cratering, fluvial erosion, and variable hydrologic forcing: Geomorphology, v. 91, no. 3–4, p. 332–363, doi: 10.1016/j.geomorph.2007.04.017.

Howard, A.D., and Moore, J.M., 2011, Late Hesperian to early Amazonian midlatitude Martian valleys: Evidence from Newton and Gorgonum basins: Journal of Geophysical Research: Planets, v. 116, no. E5, p. E05003, doi: 10.1029/2010JE003782.

Howard, A.D., Moore, J.M., and Irwin, R.P., 2005, An intense terminal epoch of widespread fluvial activity on early Mars: 1. Valley network incision and associated deposits: Journal of Geophysical Research: Planets, v. 110, no. E12, p. E12S14, doi: 10.1029/2005JE002459.

Irwin, R.P., Craddock, R.A., and Howard, A.D., 2005, Interior channels in Martian valley networks: Discharge and runoff production: Geology, v. 33, no. 6, p. 489–492, doi: 10.1130/G21333.1.

Irwin, R.P., Lewis, K.W., Howard, A.D., and Grant, J.A., 2015, Paleohydrology of Eberswalde crater, Mars: Geomorphology, v. 240, p. 83–101, doi: 10.1016/j.geomorph.2014.10.012.

Jacobsen, R.E., and Burr, D.M., 2016a, Greater contrast in Martian hydrological history from more accurate estimates of paleodischarge: Geophysical Research Letters, p. 2016GL070535, doi: 10.1002/2016GL070535.

Jacobsen, R.E., and Burr, D.M., 2016b, Sedimentology in plan view: how terrestrial analogs can inform and caution remote interpretations of ancient fluvial and alluvial environments on Mars, *Geological Society of America Southeastern Regional Meeting*, Columbia, SC.

Jacobsen, R.E., and Burr, D.M., 2015, Wet-to-Dry Hydrological Transition Encapsulated in Fluvial Stratigraphy of Aeolis Dorsa, Mars, in *Lunar Planet. Sci.*, XXXXVI, Abstract 1011.

Kerber, L., and Head, J.W., 2010, The age of the Medusae Fossae Formation: Evidence of Hesperian emplacement from crater morphology, stratigraphy, and ancient lava contacts: Icarus, v. 206, no. 2, p. 669–684, doi: 10.1016/j.icarus.2009.10.001.

Kirk, R.L., Howington-Kraus, E., Rosiek, M.R., Anderson, J.A., Archinal, B.A., Becker, K.J., Cook, D.A., Galuszka, D.M., Geissler, P.E., Hare, T.M., Holmberg, I.M., Keszthelyi, L.P., Redding, B.L., Delamere, W.A., et al., 2008, Ultrahigh resolution topographic mapping of Mars with MRO HiRISE stereo images: Meter-scale slopes of candidate Phoenix landing sites: Journal of Geophysical Research (Planets), v. 113, p. E00A24, doi: 10.1029/2007JE003000.

Kite, E.S., Howard, A.D., Lucas, A.S., Armstrong, J.C., Aharonson, O., and Lamb, M.P., 2015a, Stratigraphy of Aeolis Dorsa, Mars: Stratigraphic context of the great river deposits: Icarus, v. 253, p. 223–242, doi: 10.1016/j.icarus.2015.03.007.

Kite, E.S., Howard, A.D., Lucas, A., and Lewis, K.W., 2015b, Resolving the era of river-forming climates on Mars using stratigraphic logs of river-deposit dimensions: Earth and Planetary Science Letters, v. 420, p. 55–65, doi: 10.1016/j.epsl.2015.03.019.

Knighton, D., 1998, Fluvial forms and processes: a new perspective, pp. 383, Hodder Arnold, London.

Konsoer, K., Zinger, J., and Parker, G., 2013, Bankfull hydraulic geometry of submarine channels created by turbidity currents: Relations between bankfull channel characteristics and formative flow discharge: Journal of Geophysical Research: Earth Surface, v. 118, no. 1, p. 216–228, doi: 10.1029/2012JF002422.

Lefort, A., Burr, D.M., Beyer, R.A., and Howard, A.D., 2012, Inverted fluvial features in the Aeolis-Zephyria Plana, western Medusae Fossae Formation, Mars: Evidence for post-formation modification: Journal of Geophysical Research: Planets, v. 117, no. E3, p. E03007, doi: 10.1029/2011JE004008.

Leopold, L.B., and Maddock, T., 1953, The hydraulic geometry of stream channels and some physiographic implications: United States Geological Survey PP – 252, Washington, D.C.

Mandt, K.E., de Silva, S.L., Zimbelman, J.R., and Crown, D.A., 2008, Origin of the Medusae Fossae Formation, Mars: Insights from a synoptic approach: Journal of Geophysical Research: Planets, v. 113, no. E12, p. E12011, doi: 10.1029/2008JE003076.

Mandt, K., Silva, S. de, Zimbelman, J., and Wyrick, D., 2009, Distinct erosional progressions in the Medusae Fossae Formation, Mars, indicate contrasting environmental conditions: Icarus, v. 204, no. 2, p. 471–477, doi: 10.1016/j.icarus.2009.06.031.

Matsubara, Y., and Howard, A.D., 2014, Modeling planform evolution of a mud-dominated meandering river: Quinn River, Nevada, USA: Earth Surface Processes and Landforms, v. 39, no. 10, p. 1365–1377, doi: 10.1002/esp.3588.

Matsubara, Y., Howard, A.D., Burr, D.M., Williams, R.M.E., Dietrich, W.E., and Moore, J.M., 2014, River meandering on Earth and Mars: A comparative study of Aeolis Dorsa meanders, Mars and possible terrestrial analogs of the Usuktuk River, AK, and the Quinn River, NV: Geomorphology, doi: 10.1016/j.geomorph.2014.08.031.

McEwen, A.S., Eliason, E.M., Bergstrom, J.W., Bridges, N.T., Hansen, C.J., Delamere, W.A., Grant, J.A., Gulick, V.C., Herkenhoff, K.E., Keszthelyi, L., Kirk, R.L., Mellon, M.T., Squyres, S.W., Thomas, N., et al., 2007, Mars Reconnaissance Orbiter's High Resolution Imaging Science Experiment (HiRISE): Journal of Geophysical Research: Planets, v. 112, no. E5, p. E05S02, doi: 10.1029/2005JE002605.

Miall, A., 1996, The Geology of Fluvial Deposits: Sedimentary Facies, Basin Analysis, and Petroleum Geology: Springer, Berlin, Heidelberg.

Osterkamp, W.R., and Hedman, E.R., 1982, Perennial-streamflow characteristics related to channel geometry and sediment in Missouri River basin: Professional Paper USGS Numbered Series 1242, Washington D.C.

Page, K., and Nanson, G., 1982, Concave-bank benches and associated floodplain formation: Earth Surface Processes and Landforms, v. 7, no. 6, p. 529–543, doi: 10.1002/esp.3290070603.

Pain, C.F., Clarke, J.D.A., and Thomas, M., 2007, Inversion of relief on Mars: Icarus, v. 190, no. 2, p. 478–491, doi: 10.1016/j.icarus.2007.03.017.

Parsons, R.A., Moore, J.M., and Howard, A.D., 2013, Evidence for a short period of hydrologic activity in Newton crater, Mars, near the Hesperian-Amazonian transition: Journal of Geophysical Research: Planets, v. 118, no. 5, p. 1082–1093, doi: 10.1002/jgre.20088.

Schultz, P.H., and Lutz, A.B., 1988, Polar wandering of Mars: Icarus, v. 73, no. 1, p. 91–141, doi: 10.1016/0019-1035(88)90087-5.

Scott, D.H., and Tanaka, K.L., 1986, Geologic map of the western equatorial region of Mars: IMAP USGS Numbered Series 1802-A, Washington, D.C.

Scott, D.H., and Tanaka, K.L., 1982, Ignimbrites of Amazonis Planitia Region of Mars: Journal of Geophysical Research: Solid Earth, v. 87, no. B2, p. 1179–1190, doi: 10.1029/JB087iB02p01179.

de Silva, S.L., Bailey, J.E., Mandt, K.E., and Viramonte, J.M., 2010, Yardangs in terrestrial ignimbrites: Synergistic remote and field observations on Earth with applications to Mars: Planetary and Space Science, v. 58, no. 4, p. 459–471, doi: 10.1016/j.pss.2009.10.002.

Smith, D.E., Zuber, M.T., Frey, H.V., Garvin, J.B., Head, J.W., et al., 2001, Mars Orbiter Laser Altimeter: Experiment summary after the first year of global mapping of Mars: Journal of Geophysical Research: Planets, v. 106, no. E10, p. 23689–23722, doi: 10.1029/2000JE001364.

Tanaka, K.L., Skinner, J.A., Dohm, J.M., Irwin III, R.P., Kolb, E.J., Fortezzo, C.M., Platz, T., Michael, G.G., and Hare, T.M., 2014, Geologic Map of Mars: U.S. Geological Survey Scientific Investigations Map, scale 10.3133/sim3292.

Taylor, J., 1997, Introduction to error analysis, the study of uncertainties in physical measurements, Univ. Sci. Books, Sausalito, Calif.

Ward, A.W., 1979, Yardangs on Mars - Evidence of recent wind erosion: Journal of Geophysical Research, v. 84, p. 8147–8166, doi: 10.1029/JB084iB14p08147.

Whiting, P.J., and Dietrich, W.E., 1993, Experimental constraints on bar migration through bends: Implications for meander wavelength selection: Water Resources Research, v. 29, no. 4, p. 1091–1102, doi: 10.1029/92WR02356.
Williams, G.P., 1988, Paleofluvial estimates from dimensions of former channels and meanders: Flood Geomorphology, John Wiley, New York, p 321-334.
Williams, R.M., Chidsey Jr, T.C., and Eby, D.E., 2007, Exhumed paleochannels in central Utah—Analogs for raised curvilinear features on Mars, in *Central Utah–Diverse Geology of a Dynamic Landscape, Utah Geol. Assoc. Publ. Ser.*, vol. 36, edited by G. C. Willis et al., pp. 221–235, Utah Geol. Assoc., Salt Lake City.
Williams, R.M.E., Irwin III, R.P., Burr, D.M., Harrison, T., and McClelland, P., 2013, Variability in martian sinuous ridge form: Case study of Aeolis Serpens in the Aeolis Dorsa, Mars, and insight from the Mirackina paleoriver, South Australia: Icarus, v. 225, no. 1, p. 308–324, doi: 10.1016/j.icarus.2013.03.016.
Williams, R.M.E., Irwin III, R.P., and Zimbelman, J.R., 2009, Evaluation of paleohydrologic models for terrestrial inverted channels: Implications for application to martian sinuous ridges: Geomorphology, v. 107, no. 3–4, p. 300–315, doi: 10.1016/j.geomorph.2008.12.015.
Williams, R.M.E., and Weitz, C.M., 2014, Reconstructing the aqueous history within the southwestern Melas basin, Mars: Clues from stratigraphic and morphometric analyses of fans: Icarus, v. 242, p. 19–37, doi: 10.1016/j.icarus.2014.06.030.
Zimbelman, J.R., and Griffin, L.J., 2010, HiRISE images of yardangs and sinuous ridges in the lower member of the Medusae Fossae Formation, Mars: Icarus, v. 205, no. 1, p. 198–210, doi: 10.1016/j.icarus.2009.04.003.
Zimbelman, J.R., and Scheidt, S.P., 2012, Hesperian Age for Western Medusae Fossae Formation, Mars: Science, v. 336, no. 6089, p. 1683–1683, doi: 10.1126/science.1221094.

Appendix III

Table III-1. Empirical relationships of estimating discharge and channel width

Equation	No.	Applicable range	Correl. coeff.	Std. error	Reference
$Q_{2yr} = 1.9W_{ac}^{1.22}$	(3.1)	$0.8 < W_{ac} < 430$ m	0.81	109%	Osterkamp & Hedman, 1984
$Q_{2yr} = 1.44W_{ac}^{1.22}$	(3.2)	$0.8 < W < 430$ m	0.81	109%	Irwin et al., 2005
$Q_{bf} = 0.10W_{bf}^{1.866}$	(3.3)	$2.3 < W_{bf} < 1975$ m	0.91	29%	Eaton, 2013
$Q_{1.5yr} = 0.011\lambda^{1.54}$	(3.4)	$145 \leq \lambda \leq 15{,}545$ m	0.93	11%	Carlston, 1965
$W_{bf} = 0.71R_c^{0.89}$	(3.5)	$2.6 \leq R_c \leq 3{,}600$ m	0.94	40%	Williams, 1986

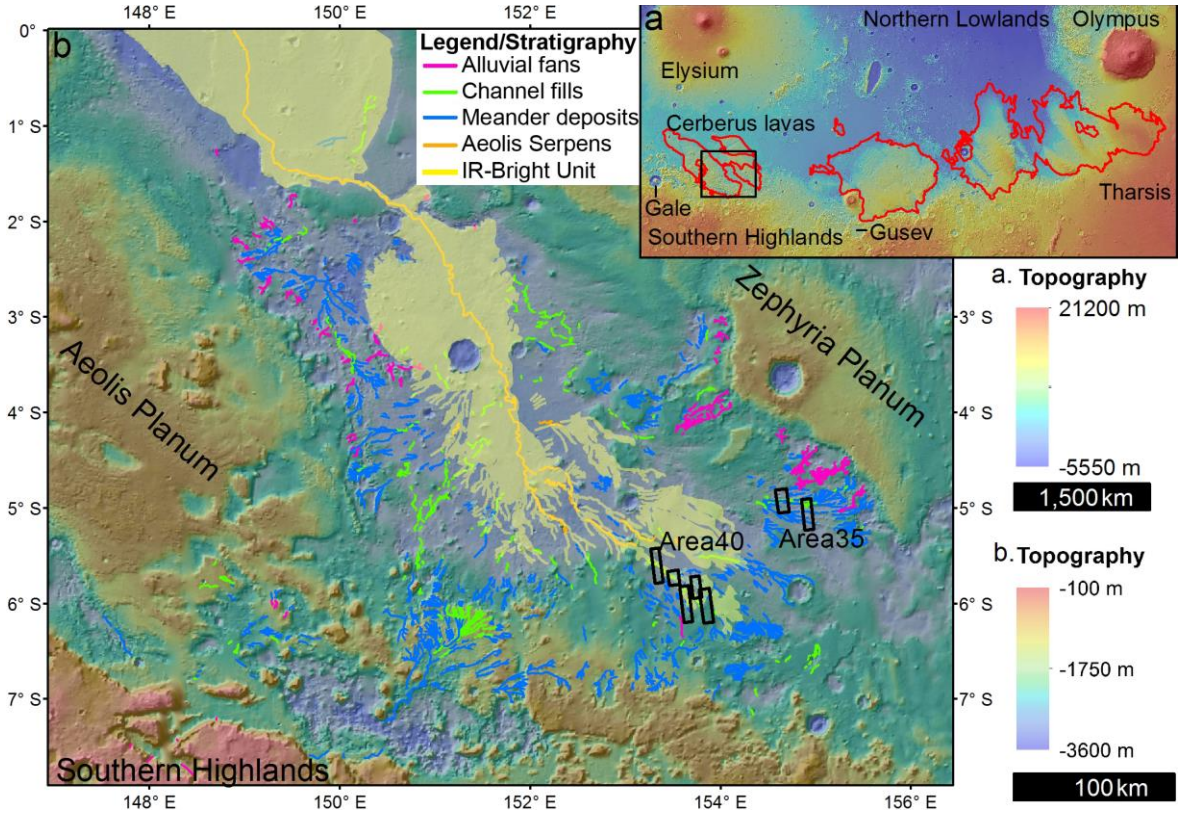

Figure III-1: (a) The Aeolis Dorsa region (black outline) is located at the transition between the southern highlands and the Cerberus lava plains. The region is also surrounded by the two westernmost deposits of the Medusae Fossae Formation, outlined in red (Scott and Tanaka, 1986; Greeley and Guest, 1987), although a wider distribution of deposits have been observed (Bradley et al., 2002; Harrison et al., 2010). **(b)** The Aeolis Dorsa region contains diverse fluvial features, which have been delineated by morphology and appearance in nighttime infrared (IR) data (Jacobsen and Burr, 2015; Burr et al., 2016). Areas with stacked fluvial deposits include Areas 35 and 40 in southeastern Aeolis Dorsa. Black outlines show areas of high-resolution visual images. Topographic color and hillshade are derived from Mars Orbiter Laser Altimeter data (Smith et al., 2001).

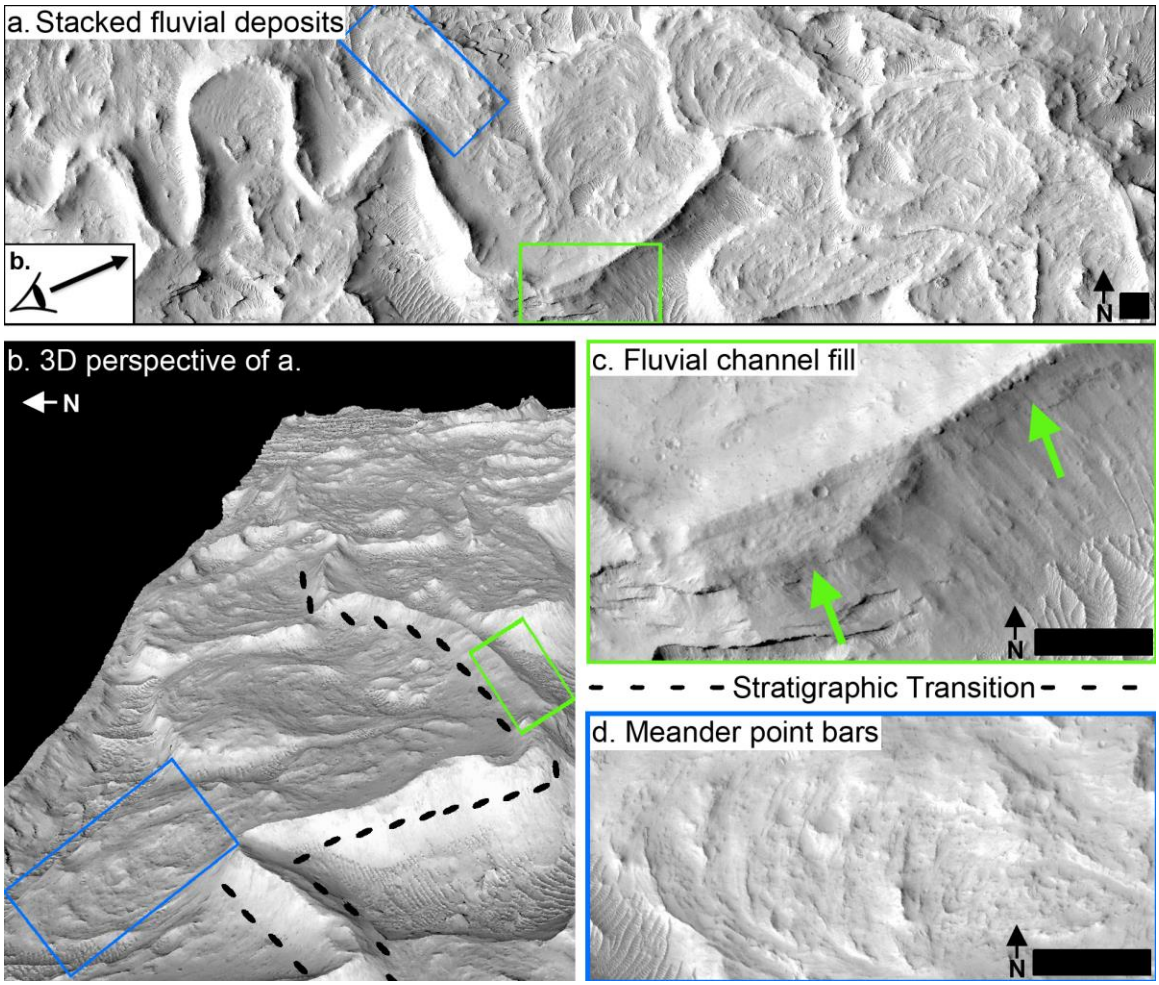

Figure III-2: (a) Stacked fluvial deposits in Area 35 include younger fluvial channel fills (an example is outlined in green and shown in (c) superimposed on top of older meander point bars (example outlined in blue and shown in (d). **(b)** 3D perspective of (a) derived from HiRISE visual and topographic data shows the stacked fluvial deposits and the stratigraphic transition (dashed line). **(c)** The plain upper surface (left arrow) is indicative of exhumed and inverted fluvial channel fills, but these widths of these deposits may be eroded (right arrow) by aeolian abrasion or impact cratering. **(d)** Ridges and swales suggest a paleochannel was laterally migrating towards the northwest, but the width of this paleochannel is not apparent and must be inferred from morphometric analysis. Scale bars are 100 meters. Vertical exaggeration of (b) is 2.5x.

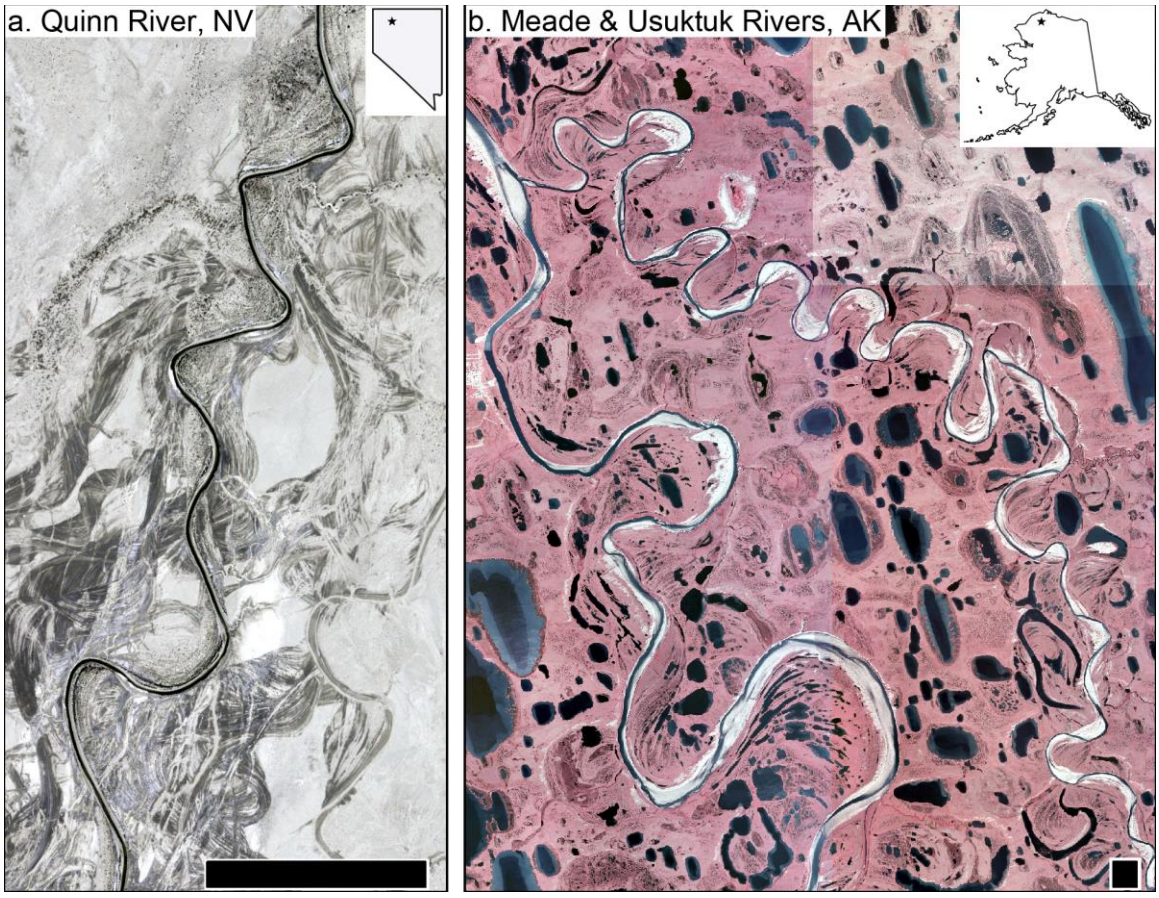

Figure III-3: Three terrestrial analog rivers from two fluvial systems provide a variety of scales and conditions to assess morphometric relationship (3.5), Table III-1. **(a)** The Quinn River, NV, meanders through clay-rich floodplains, nearly devoid of vegetation making it one of the most analogous fluvial systems to the Aeolis Dorsa. **(b)** The Meade River (left) and Usuktuk River (right) meander through permafrost floodplains on the North Slope of Alaska. This false-color visual-infrared image mosaic highlights vegetation (pink color), which limits the analogy of these channels to paleochannels in Aeolis Dorsa. Scale bars at the lower right of each image are 500 meters.

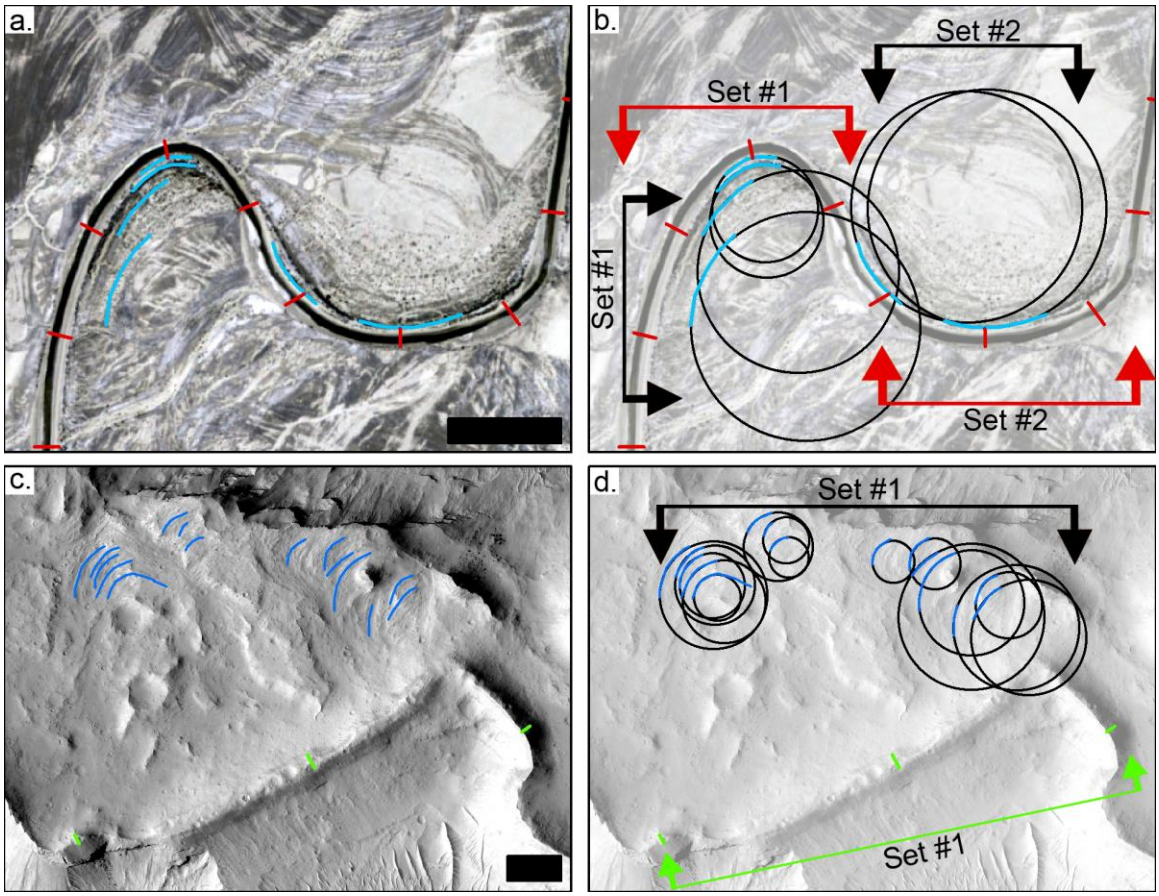

Figure III-4: Examples of morphometric measurements along the Quinn River, NV, and stacked deposits in Aeolis Dorsa. **(a)** Widths (red lines) were measured as the distance between opposing banks or the distance between the cut bank and innermost point bar. Arcs (blue lines) were delineated over point bar ridges and fitted with circles (b), from which radii were measured. **(b)** Calculating average widths and radii involved separating meander bends at inflection points, which separated one set of measurements from another. Average widths and average radii for each set were calculated and compared with morphometric relationship (3.5). **(c)** Widths (green lines) were measured as the distance across the upper surface of the channel fills and arcs (blue lines) were delineated over point bar ridges. **(d)** Radii of curvature of point bar ridges were derived from circles fit to arcs. The average radii of a set of point bar ridges was then used to estimate paleochannel width, and then compared to the average width of the superposing channel fill. Scale bars are 100 meters.

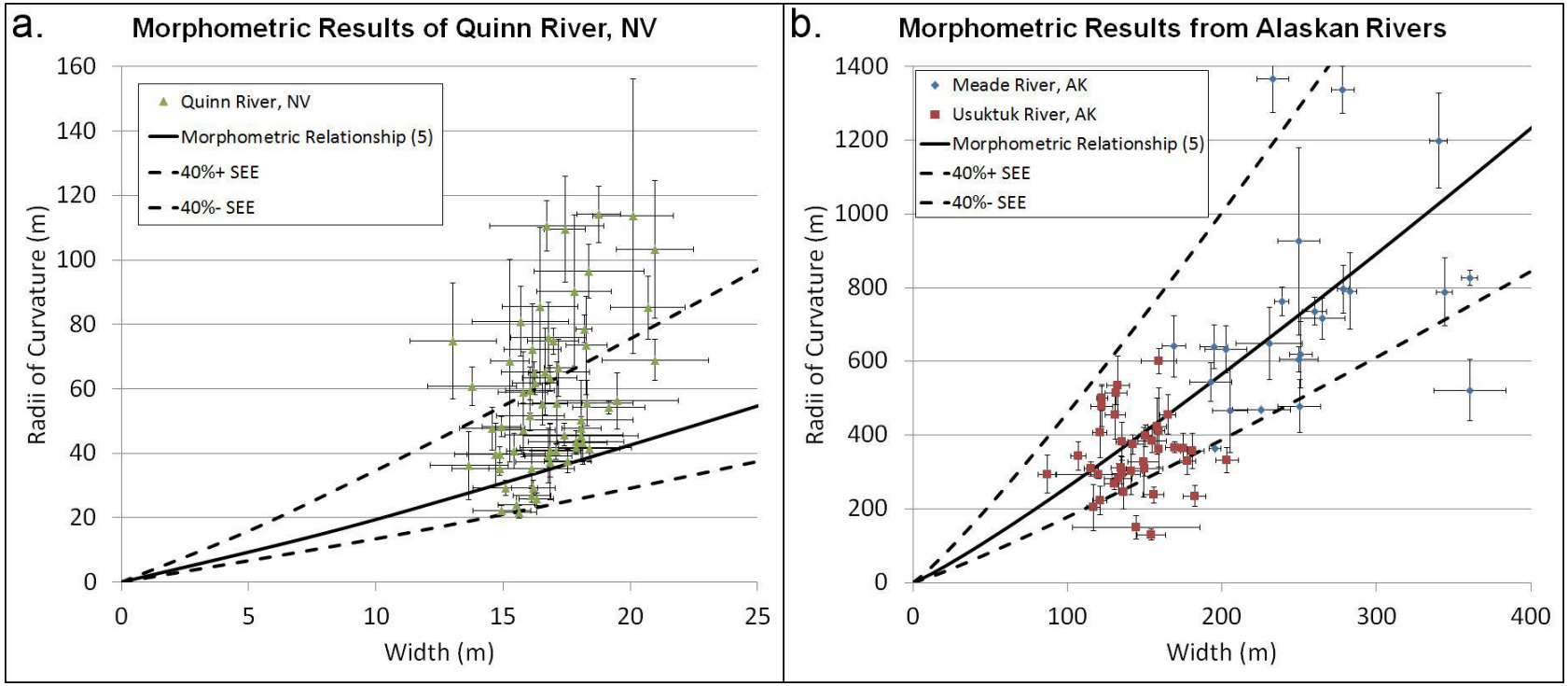

Figure III-5: Results from morphometric analyses of terrestrial analog channels show approximate fits to morphometric relationship (3.5), but several data points for each river fall outside the expected interval of natural variation (40% Standard Error of the Equation, SEE). **(a)** One-third of data points from the Quinn River have high radii of curvatures relative to morphometric relationship (3.5). **(b)** Several data points from the Usuktuk River have low radii of curvatures relative to the relationship. Error bars are measurement errors calculated from Standard Deviations of the Means (SDOM) of four repeated measurements of channel width and point bar radii of curvature.

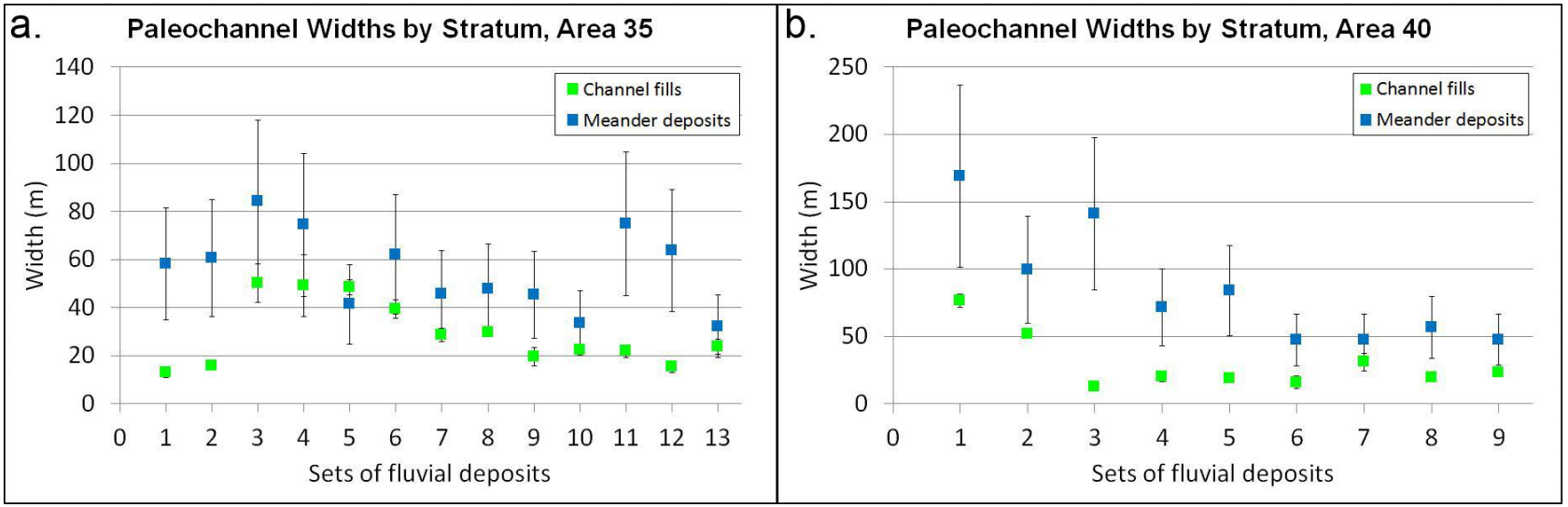

Figure III-6: Results from morphometric analyses of fluvial deposits in Aeolis Dorsa. **(a)** Area 35 preserves 13 sets of older meandering fluvial deposits and younger fluvial channel fills. In general, the paleochannels of the older stratum have larger paleochannel widths. **(b)** Area 40 preserves 9 sets of older and younger fluvial sets. Here, the older stratum also yields larger estimates of paleochannel widths than the younger stratum. Error bars represent measurement error (SDOM) and the standard error of morphometric relationship (3.5). Set 6 for Areas 35 and set 1 for Area 40 have channel fills with wavelength-to-width ratios between 10 and 14, suggesting preservation of channel fill widths; whereas other channel fills have higher ratios, suggesting erosion.

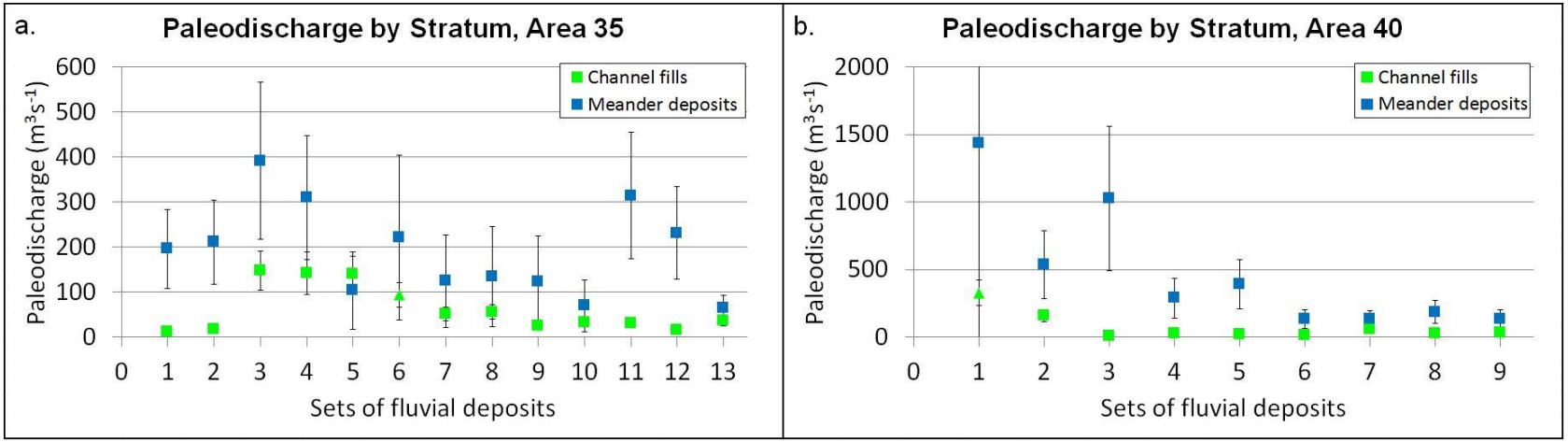

Figure III-7: Results from paleodischarge analyses in Aeolis Dorsa, Mars. In both areas, the older stratum of meandering fluvial deposits have larger paleodischarges than the younger stratum of fluvial channel fills. Error bars represent propagation of measurement error (SDOM) and the standard error of empirical relationships (3.5) and (3.3). Set 6 for Areas 35 and set 1 for Area 40 have channel fills with wavelength-to-width ratios between 10 and 14 suggesting preservation of channel fill widths, but other channel fills have higher ratios, suggesting erosion.

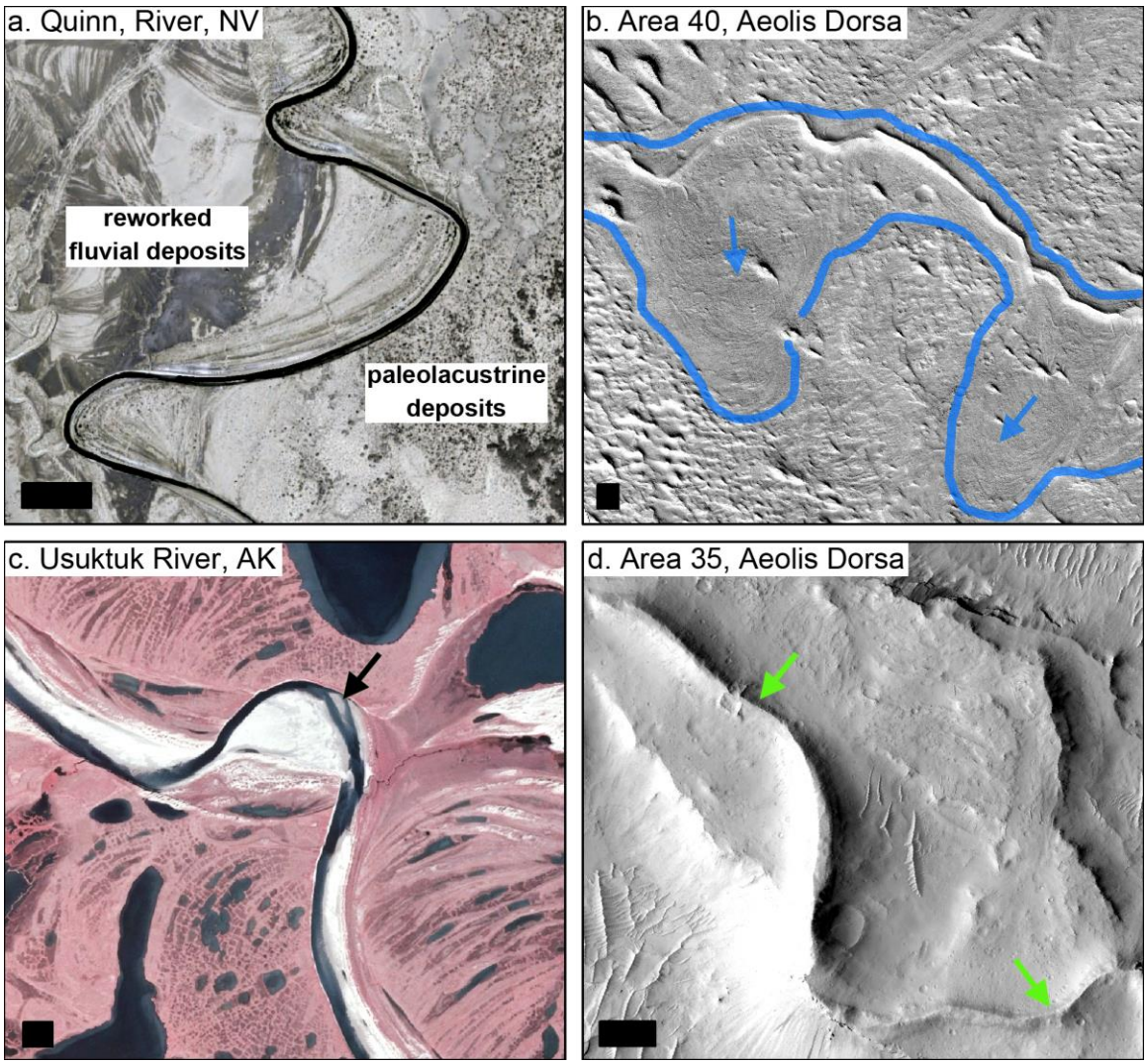

Figure III-8: Analyses of terrestrial analogs reveal morphodynamic processes and ambiguities of results from Martian analyses. **(a)** Where the Quinn cuts into higher standing paleolacustrine deposits lateral migration is inhibited and the channel translates downstream. Reworked fluvial deposits appear to provide enough bank stability to maintain meander dynamics, but not inhibit lateral migration. **(b)** Some meander deposits in the Aeolis Dorsa region form asymmetric migration patterns, i.e., preferentially migrating in one direction along the channel axis (arrows), suggesting possible heterogeneity in floodplain sediments, akin to those observed along the Quinn River. **(c)** Low radii of curvature for the Usuktuk River correspond to meander bends with enhanced sediment deposition, large channel bars (arrow), and shoot cut-offs. **(d)** High wavelength-to-width ratios (~56 for feature shown) indicate that younger fluvial channel fills have been eroded and that paleochannel widths have been underestimated. Arrows show channel fill eroded to a sharp-crested ridge. Scale bars on all images are 100 meters.

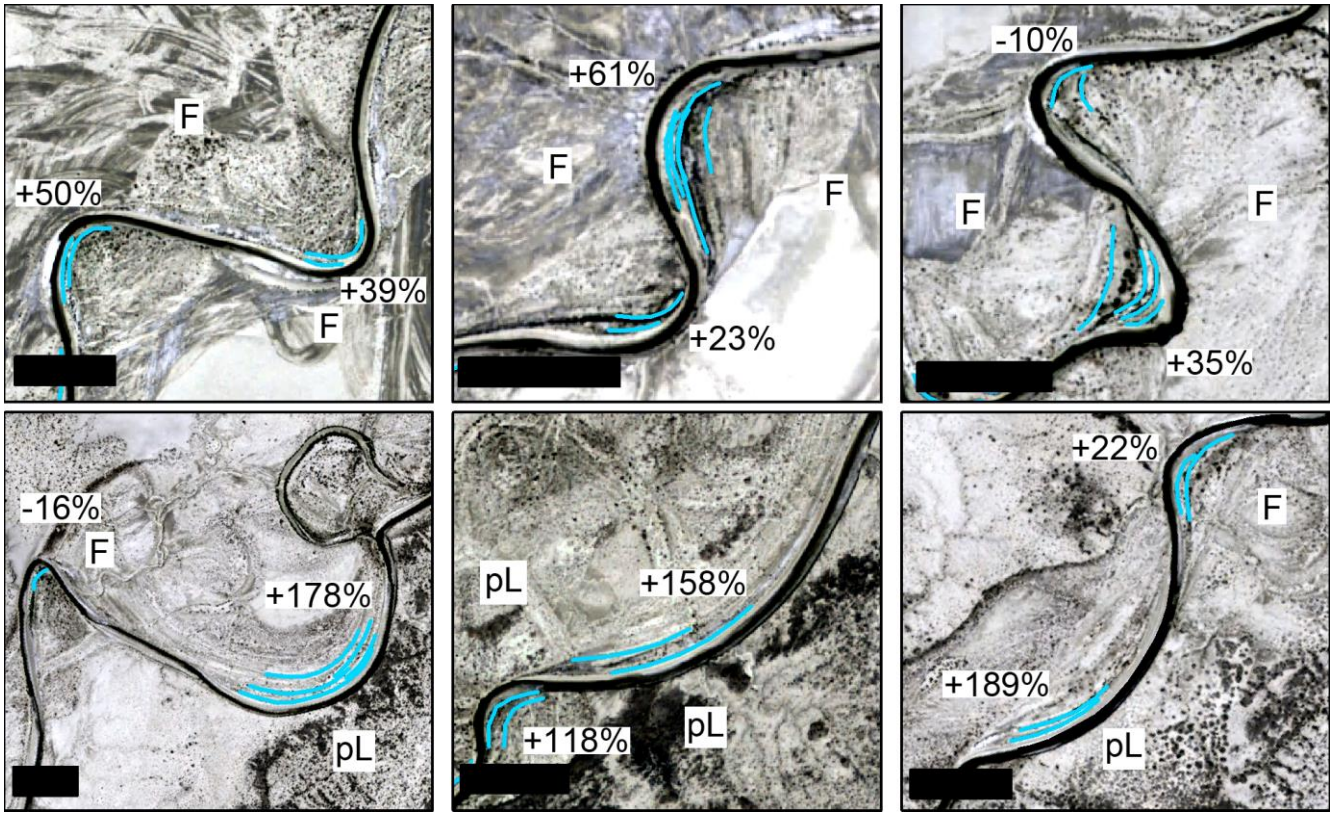

Figure III-9: Comparison of meander bends along the Quinn River with and without banks of paleolacustrine sediment. The upper row of images shows portions of the Quinn River with floodplains composed of reworked fluvial deposits (F). Percentages next to meander bends represent overestimate (+) or underestimate (-) of channel widths derived from morphometric relationship (3.5) and the average point bar radius of curvature. Estimate errors are close to or within the ±40% standard error of the equation for relationship (3.5). The lower row of images shows portions of the Quinn River interacting with paleolacustrine deposits (pL). Where banks are composed of paleolacustrine sediment, the channel translates downstream in the downstream limb, increasing point bar radii of curvature, leading to large overestimates (>+100%) of width derived from morphometric relationship (3.5).

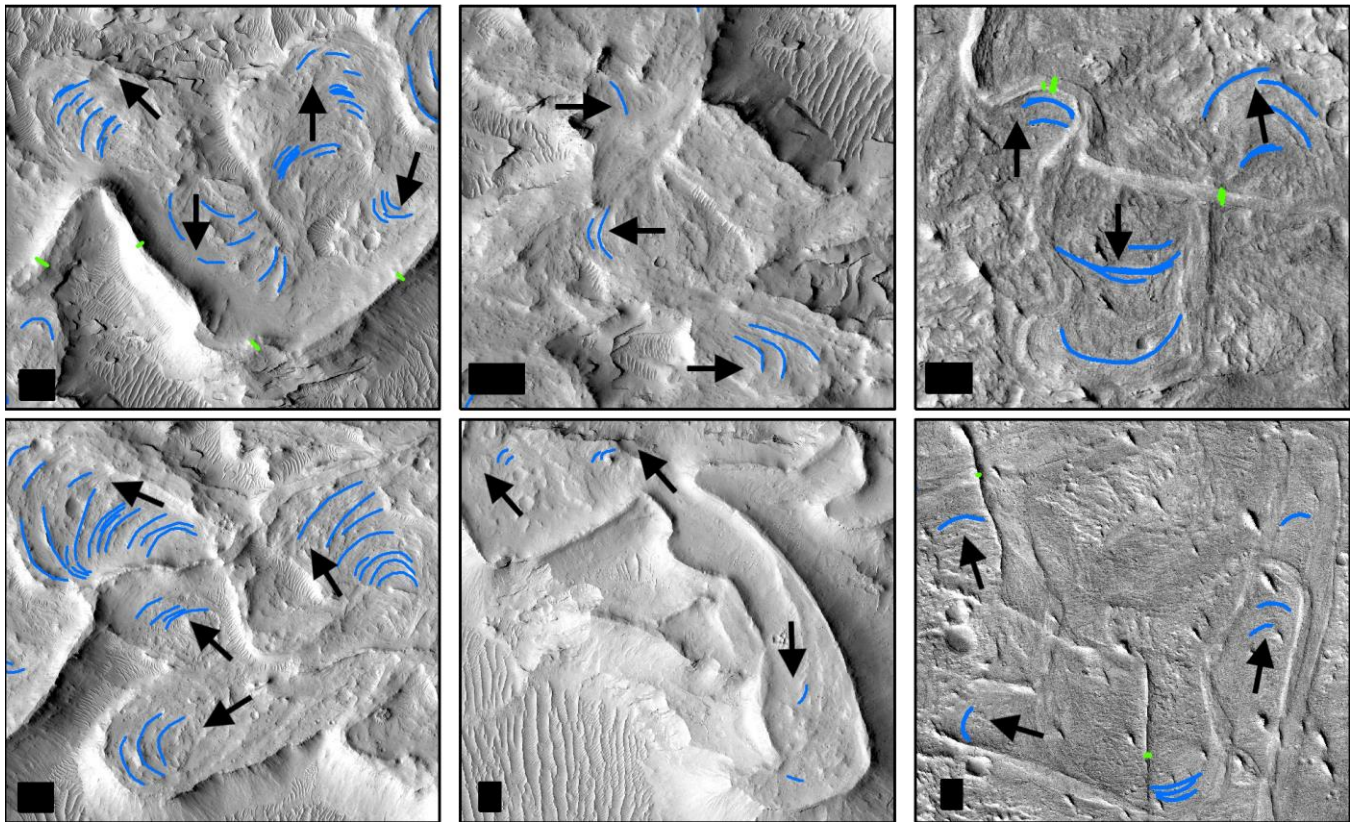

Figure III-10: Directionality and symmetry of meandering fluvial deposits in the Aeolis Dorsa region. The upper row of images shows meander deposits (blue lines) that alternate in opposite directions (bipolar), and have similar size meander deposits forming in each direction (symmetric). The lower row of images show meander deposits forming in multiple directions (multi-modal) and with various amplitudes, i.e., migrating unequal lengths (asymmetric). These diverse morphologies of meander deposits suggest heterogeneity of floodplain conditions and systematic error using morphometric relationships.

Conclusion

Several conclusions and new research questions can be made from this dissertation. These conclusions refine our understanding of the wet-to-dry hydrologic transition in terms of its regional consistency, its magnitude of change, and the confounding factors that effect the interpretation of the transition. New research questions aim to understand the wet-to-dry transition within the geologic and climatic system of ancient Mars.

Results from Chapter 1 show that the Aeolis Dorsa deposits preserve a consistent stratigraphic transition from widespread fluvial deposits representing relatively frequent hydrologic activity, to alluvial fan deposits formed by late, relief-forming tectonic deformation, and intermittent hydrologic activity. This stratigraphic transition correlates with and lends support for the wet-to-dry transition preserved elsewhere on Mars. Outstanding research areas about the hydrologic history of the Aeolis Dorsa include the timing of initial and terminal hydrologic activity. Timings for initial and terminal activity are necessary for augmenting the Martian geologic timeline with activity recorded in the Aeolis Dorsa region. Also, we do not know the time-stratigraphic evolution of the Aeolis Dorsa deposits. Were regional-scale fluvial sediments deposited together or were sediments deposited diachronously? This question is relevant to modeling regional patterns of precipitation, such as roaming zones of precipitation (Hoke and Hynek, 2009; Scanlon et al., 2013). Examinations of terrestrial analog deposits suggest geomorphic attributes used to interpret meandering fluvial deposits and stable hydrologic systems, but attributes do not provide information about paleo-temperatures. Were fluvial systems in the Aeolis Dorsa region sourced from paleoclimates with elevated mean annual temperatures, or were these features the products of brief, peak annual temperatures? This question is relevant to paleoclimate modeling and reconciling the debate between "warm/wet" and "cold/icy" Martian paleoclimates (Wordsworth et al., 2015; Hynek, 2016).

Results from Chapter 2 validate terrestrial-based empirical relationships for paleohydraulic analyses on Mars (Jacobsen and Burr, 2016). Width-discharge relationships, derived from hydraulic geometry, are shown to yield more accurate and more precise estimates of paleodischarge than the most commonly used relationship from the Missouri River Basin. Applying the width-discharge relationships to a suite of Martian features yields new paleodischarge estimates that increase the contrast between early and late episodes of Martian hydrologic activity. Whereas these relationships provide more accurate and more precise estimates of paleodischarge, width-discharge relationships for channels of alluvial fans and deltas have not been validated. These environment-specific relationships are critical for accurately characterizing the paleohydrology and habitability of potential rover landing sites (Fassett and Head, 2005; Williams and Weitz, 2014; Irwin et al., 2015; Golombek et al., 2016).

Results from Chapter 3 show that multiple terrestrial-based empirical relationships may be used to reconstruct paleochannel dimensions and estimate paleodischarge although not accurately or precisely in all cases. Results also show that explanations for apparent changes in geomorphology with stratigraphy are equivocal.

Changes in geomorphology are not necessarily the effects of changing paleodischarge, but may be the effects of confounding factors, such as changes in channel boundary conditions or erosion of fluvial deposits. These results emphasize the importance and complexity of interpreting geomorphology of an eroded extraterrestrial environment.

References

Fassett, C.I., and Head, J.W., 2005, Fluvial sedimentary deposits on Mars: Ancient deltas in a crater lake in the Nili Fossae region: Geophysical Research Letters, v. 32, no. 14, p. L14201, doi: 10.1029/2005GL023456.

Golombek, M.P., Grant, J.A., Farley, K.A., Williford, K., Chen, A., Otero, R.E., and Ashley, J.W., 2016, Downselection of Landing Sites Proposed for the Mars 2020 Rover Mission, in *Lunar Planet. Sci.*, XXXXVII, Abstract 2324.

Hoke, M.R.T., and Hynek, B.M., 2009, Roaming zones of precipitation on ancient Mars as recorded in valley networks: Journal of Geophysical Research: Planets, v. 114, no. E8, p. E08002, doi: 10.1029/2008JE003247.

Hynek, B., 2016, RESEARCH FOCUS: The great climate paradox of ancient Mars: Geology, v. 44, no. 10, p. 879–880, doi: 10.1130/focus102016.1.

Irwin, R.P., Lewis, K.W., Howard, A.D., and Grant, J.A., 2015, Paleohydrology of Eberswalde crater, Mars: Geomorphology, v. 240, p. 83–101, doi: 10.1016/j.geomorph.2014.10.012.

Jacobsen, R.E., and Burr, D.M., 2016, Greater contrast in Martian hydrological history from more accurate estimates of paleodischarge: Geophysical Research Letters, p. 2016GL070535, doi: 10.1002/2016GL070535.

Scanlon, K.E., Head, J.W., Madeleine, J.-B., Wordsworth, R.D., and Forget, F., 2013, Orographic precipitation in valley network headwaters: Constraints on the ancient Martian atmosphere: Geophysical Research Letters, v. 40, no. 16, p. 4182–4187, doi: 10.1002/grl.50687.

Williams, R.M.E., and Weitz, C.M., 2014, Reconstructing the aqueous history within the southwestern Melas basin, Mars: Clues from stratigraphic and morphometric analyses of fans: Icarus, v. 242, p. 19–37, doi: 10.1016/j.icarus.2014.06.030.

Wordsworth, R.D., Kerber, L., Pierrehumbert, R.T., Forget, F., and Head, J.W., 2015, Comparison of "warm and wet" and "cold and icy" scenarios for early Mars in a 3-D climate model: Journal of Geophysical Research: Planets, v. 120, no. 6, p. 2015JE004787, doi: 10.1002/2015JE004787.

Vita

On July 30th, 1988, Robert Eric Jacobsen and Georgia Annette Jacobsen welcomed into the world Robert Eric Jacobsen II. Robert was raised in Salida, CA, and enjoyed playing legos, video games, and with his younger sister Ariel Alysse. At an early age, Robert became fascinated with maps as he tracked his family's progress on road trips to southern California. This evolved into a fascination with geography and eventually his place in the universe. At the same time, Robert struggled to read, but was aided by his dedicated teachers and parents. Robert began to enjoy achieving in all his subjects so much that he attended Modesto High School for the International Baccalaureate program. Robert was challenged academically, but made lifelong friends through that program. Before graduating, Robert was diagnosed with Crohn's disease. In the wake of this disease, Robert began to reconsider his purpose in life and to explore new passions, including photography and the art of storytelling. These changes led him to Colorado College to study geology under the Block Plan. There, Robert struggled academically and socially, but there he met his Lord and Savior Jesus Christ. Through college Robert discovered the excitement of scientific research, his love of western films, and his place between the empirical and the spiritual. All of these led Robert to Knoxville, TN, and the University of Tennessee for doctoral research. There, Robert struggled to find balance in life and a direction for his dissertation, but he would eventually tell the stories of fossil rivers, now resurrected on the surface of Mars. Knoxville also brought him friends from all over the world and a strong desire to listen to others living around and between the spheres of science and religion. After finishing his doctorate, Robert will struggle, foster new relationships, and find peace in creative and unexpected ways.